AFCRL-67-0690

INTERPRETATION AND APPLICATION OF TRANSIENT AND IMPULSE RESPONSE APPROXIMATIONS IN ELECTROMAGNETIC SCATTERING PROBLEMS

2415-1

David L. Moffatt

The Ohio State University

ElectroScience Laboratory

(formerly Antenna Laboratory)
Department of Electrical Engineering
Columbus, Ohio 43212

Contract Number F19628-67-C-0239
Project Number 5635
Task Number 563502
Work Unit Number 56350201

Scientific Report No. 1
27 March 1968

Contract Monitor: John K. Schindler
Microwave Physics Laboratory

Prepared
for
AIR FORCE CAMBRIDGE RESEARCH LABORATORIES
OFFICE OF AEROSPACE RESEARCH
UNITED STATES AIR FORCE
BEDFORD, MASSACHUSETTS

228

NOTICES

When Government drawings, specifications, or other data are used for any purpose other than in connection with a definitely related Government procurement operation, the United States Government thereby incurs no responsibility nor any obligation whatsoever, and the fact that the Government may have formulated, furnished, or in any way supplied the said drawings, specifications, or other data, is not to be regarded by implication or otherwise as in any manner licensing the holder or any other person or corporation, or conveying any rights or permission to manufacture, use, or sell any patented invention that may in any way be related thereto.

Qualified requestors may obtain additional copies from the Defense Documentation Center. All others should apply to the Clearinghouse for Federal Scientific and Technical Information.

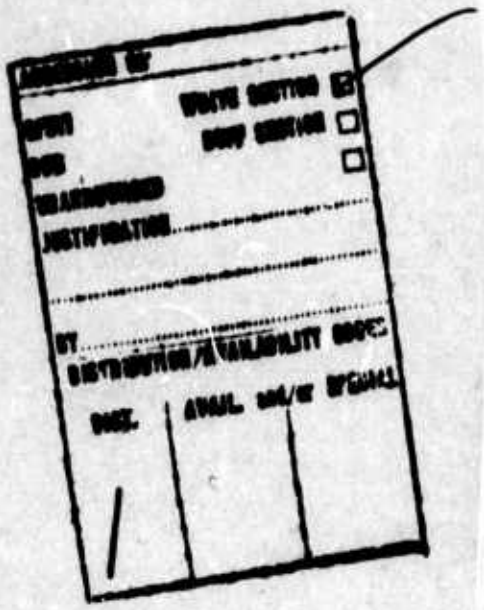

INTERPRETATION AND APPLICATION OF TRANSIENT AND IMPULSE RESPONSE APPROXIMATIONS IN ELECTROMAGNETIC SCATTERING PROBLEMS

David L. Moffatt

Ohio State University
Columbus, Ohio

27 March 1968

AFCRL-67-0690

INTERPRETATION AND APPLICATION OF TRANSIENT AND IMPULSE RESPONSE APPROXIMATIONS IN ELECTROMAGNETIC SCATTERING PROBLEMS

2415-1

David L. Moffatt

The Ohio State University

ElectroScience Laboratory

(formerly Antenna Laboratory)
Department of Electrical Engineering
Columbus, Ohio 43212

Contract Number F19628-67-C-0239
Project Number 5635
Task Number 563502
Work Unit Number 56350201

Scientific Report No. 1
27 March 1968

Contract Monitor: John K. Schindler
Microwave Physics Laboratory

Prepared
for
AIR FORCE CAMBRIDGE RESEARCH LABORATORIES
OFFICE OF AEROSPACE RESEARCH
UNITED STATES AIR FORCE
BEDFORD, MASSACHUSETTS

FOREWORD

This Report, OSURF 2415-1, was prepared by the ElectroScience Laboratory (formerly Antenna Laboratory), Department of Electrical Engineering, The Ohio State University at Columbus, Ohio. Research was conducted under Project 5635 of the Air Force Cambridge Research Laboratories, Office of Aerospace Research, United States Air Force, Bedford, Massachusetts. Dr. John K. Schindler, CRDG, was the Microwave Physics Laboratory Program Monitor and the research was conducted under Contract F19628-67-C-0239.

It is a pleasure to acknowledge the assistance and cooperation of Professor E. M. Kennaugh in the preparation of this report. The author is also indebted to the staff of the ElectroScience Laboratory. Helpful discussions with Professor Jack H. Richmond, Professor Leon Peters, Jr. and Mr. Robert J. Garbacz are hereby acknowledged.

The material contained in this report is also used as a dissertation submitted to the Department of Electrical Engineering, The Ohio State University as partial fulfillment for the degree Doctor of Philosophy.

ABSTRACT

A linear system analysis is applied to electromagnetic scattering problems. The relationship between the incident and scattered fields is reduced to a one-dimensional linear system by suitable restrictions, and modeled as a linear two-port with time-invariant parameters. The two-port is characterized by a real, time-dependent impulse response function and a transform-related complex, frequency-dependent phasor response. Two fundamental approaches for obtaining approximate solutions to electromagnetic scattering problems are seen. Estimates of either the frequency-dependent phasor response or the time-dependent impulse response can be attempted. The material in this study is concerned with the latter approach.

The concept of impulse and transient response approximations in electromagnetic scattering problems and the general properties of such waveforms are reviewed in Chapter I. It is demonstrated that the impulse and transient response waveforms provide a primary conceptual model for electromagnetic scattering which permits the integration of all existing frequency data, calculated or measured, and is simple in form. The model is directly related to the geometrical and physical properties of the scattering object; does not change drastically for small perturbations of parameters; and can be used to predict the response of the object to any type of incident plane wave. Analytical and experimental methods for obtaining estimates of the response waveforms are discussed, and a systematic procedure for securing such estimates is suggested.

Estimates of the impulse and transient response waveforms of a perfectly conducting prolate spheroid are obtained in Chapter II. Two results are derived. The first is restricted to axial incidence and utilizes the geometrical similarity of the sphere and spheroid to obtain the response waveforms of the spheroid. The second result is for arbitrary orientation of the spheroid and arbitrary linear polarization of the incident field. Calculations from both results are compared with measured data on a 2:1 axial ratio spheroid.

Derivation of the response waveforms of the prolate spheroid target requires, as input data, the Rayleigh scattering coefficient of the target. The Rayleigh coefficients of prolate and oblate spheroids for arbitrary orientation, axial ratio, and material properties; and for arbitrary linear polarization of the incident field are given in Appendix I. Time domain interpretations of high frequency asymptotic estimates of the creeping wave on conducting spheres and cylinders are considered in Appendix II. The non-causal nature of creeping wave estimates for the sphere is noted and suggestions for obtaining a causal response waveform are made.

CONTENTS

CHAPTER I
INTRODUCTION

Theoretical and experimental studies of the interaction of electromagnetic waves and finite material objects have received the attention of numerous investigators for several decades. One therefore finds in the literature[1] * an imposing array of sophisticated mathematical techniques for calculating such interactions and an equally impressive collection of calculated and measured data on the interactions for specific objects. These data are usually presented in the form of curves or patterns of the radar cross section of the object. With the exception of spherical objects, however, the theoretical contributions are characterized by restrictions on the orientation and material properties of the object and on the frequency, polarization and character of the incident electromagnetic field. In the same vein, experimental studies reported in the literature cannot hope to be all inclusive and inevitably involve some of the same limitations.

---

* Contributions prior to 1957 are covered by earlier Georgia Institute of Technology bibliographies also given in Reference 1.

One might summarize the present state of the art in prediction of the radar cross section of an object as follows; if the object is very large in terms of the wavelength, then several approximate or asymptotic theories of varying degree of complexity and accuracy are available for cross section calculations. The major difficulty encountered in this portion of the spectrum is in estimating how large a particular object must be in terms of the wavelength in order to achieve a given accuracy in the cross section calculation using a specific approximation. If the object is very small in terms of wavelength then again several approximate theories are available. In this case no particular difficulty is encountered in the accuracy of the calculations but the maximum object size which can be handled is rather strictly limited. Such limitations are imposed by either the geometrical shape and constitutive parameters of the object or by the storage capacity of present digital computers.

Exceptions exist of course, but in general one can achieve a reasonable estimate of the radar cross section of an object at the extremities of the spectrum. In what is somewhat loosely referred to as the resonance region[2] of an object, however, no such reasonable estimate is readily obtainable. In certain cases, i. e., for a specific object geometry, material properties and orientation, the extension of a particular high or low frequency approximate or

asymptotic theory into the resonance region has been achieved. No general extension can be implied from these results however, and in fact would appear to fail by the very nature of the assumed fields.

It would serve no purpose here to detail all of the approximate theories referred to above. The point to be made is that for the general finite, non-spherical object a significant portion of the spectrum usually cannot be analyzed by existing asymptotic or approximate scattering theories. Unfortunately, this gap in the spectrum is often of most practical interest for cross section calculations. Three additional comments are in order. First, it is customary with most approximate methods to assume a plane monochromatic incident field. Treatment of an arbitrary type signal often becomes a much more complex problem. Second, the approximate methods in vogue at present are not capable of systematically integrating calculated and measured data from various portions of the spectrum into a single model with a wider applicability. Thus, for example, good estimates of high and low frequency scattering properties of an object are not combined to improve the estimate of its resonance region behavior. Finally, the geometrical shape of an object is not simply related to the form of the predicted scattered field. Consequently, minor perturbations of the object geometry often require a tedious new solution rather than a minor modification of an existing solution.

It is the opinion of the author that no measurement or calculation program, regardless of its scope, can hope to satisfy the present and future requirements in radar reflectivity without the establishment of a primary conceptual model whereby all the existing theories and measurements on a given object and on objects of similar geometry can be integrated. Such a conceptual model should also incorporate an applicability to all types of signaling waveform including the ultra-short pulse of current interest.

The subject of this study is the interpretation and application of such a primary conceptual model for electromagnetic scattering. This model permits the integration of all existing frequency data, calculated or measured, and is simple in form. It is directly related to the geometrical shape and constitutive parameters of the object; does not change drastically for small perturbations of parameters; and can be used to predict the response of the object to any type of incident plane electromagnetic wave. This primary conceptual model, the impulse and related transient response waveforms of a scattering object, was first proposed by Kennaugh and Cosgriff[3] in 1957. In their paper, one facet of the impulse response concept, namely the use of high and low frequency approximations to secure approximate resonance region data, was exploited. Since that time, Kennaugh and his colleagues at The Ohio State University ElectroScience Laboratory have published

results dealing with various aspects and applications of the theory[4-16]. A review of these accomplishments; a description of the general properties of the solutions to transient electromagnetic scattering problems; and a discussion and illustration of various methods for approximating the appropriate waveforms was published by Kennaugh and Moffatt[13] in 1965. To the best of the author's knowledge, only three other publications dealing specifically with the impulse response waveform of a finite three dimensional scattering object have appeared. Betten[17] in 1962 discussed the experimental determination of the impulse response waveform of an object and the synthesis of an equivalent network. He also suggested a rather elaborate identification scheme utilizing cross correlation of object waveforms. Brown[18] in 1962 presented an approach to the solution of pulse scattering by finite obstacles which utilized the identification and separate treatment of the individual terms in a wavefront expansion of the transforms of the field vectors. This latter work, while mathematically quite elegant, adds little if any insight to the estimation of impulse response waveforms for finite objects. Finally, in 1963 Barabanenkov, et al. [19] derived, apparently independently, the impulse response waveform produced by the physical optics approximation as obtained by Kennaugh and Cosgriff in 1957.

In this study, the first chapter develops the necessary groundwork for investigating solutions to transient electromagnetic scattering problems. The general properties of such solutions are reviewed and definitions of the pertinent transient waveforms are given. Analytical and experimental techniques for obtaining approximate estimates of the impulse and transient response waveforms are discussed.

In Chapter II, the electromagnetic backscattering by a perfectly conducting prolate spheroid is analyzed, using estimates of the impulse response and related transient response waveforms. Two results are derived. The first is restricted to axial incidence and utilizes the geometrical similarity of the sphere and spheroid to obtain an impulse response for the spheroid in terms of known approximate waveforms for the sphere. The second result, based in part on the results of the axial solution, is for arbitrary axial ratio and orientation of the spheroid and for arbitrary linear polarization of the incident electromagnetic field. Calculations from both results are compared with measured data for a 2:1 axial ratio spheroid and previously calculated data for a 10:1 axial ratio spheroid.

Two Appendices are included in this study. In the first Appendix, the Rayleigh scattering coefficients of prolate and oblate spheroids are obtained. The results hold for arbitrary orientation, axial ratio, and

material properties of the spheroid and for arbitrary linear polarization of the incident wave. These results are utilized in Chapter II in deriving response waveforms of the prolate spheroid.

The second Appendix contains a time domain intepretation of certain high frequency asymptotic estimates of the creeping wave on cylinders and spheres. The non-causal nature of particular asymptotic estimates is demonstrated and suggestions for obtaining a causal response waveform are made.

A. The Concept of Impulse and Transient Response Waveforms in Electromagnetic Scattering Problems

Two basic assumptions are made which hold throughout this investigation. It is assumed that between the input terminals of the radiating system producing an incident field and the output terminals of the receiving system detecting the scattered field only linear processes with time-invariant parameters are involved. The scattering process is viewed as a cause and effect relationship whereby a transducer operates on the input or cause at the input terminals to produce the output or effect at the output terminals. With the assumptions given above, the transducer is a linear, time-invariant operator and is uniquely determined from the knowledge of a single function; the impulse response. Specifically, the cause is the incident

electromagnetic field in which the scatterer is immersed and the effect is the scattered electromagnetic field defined conventionally as the difference between the total and incident fields. It is further assumed that the input and output terminals are both in the far-field of the scattering object.

Thus, as shown in Fig. 1, the scattering process is modeled by a passive linear two-port with time-invariant parameters. The input is $E(t')$, the output $F(t')$, and the two-port has an impulse response function $F_I(t')$. The input and output are related through the convolution integral as

$$F(t') = \int_{t_1'}^{\infty} F_I(\tau)\, E(t'-\tau)\, d\tau \qquad (1)$$

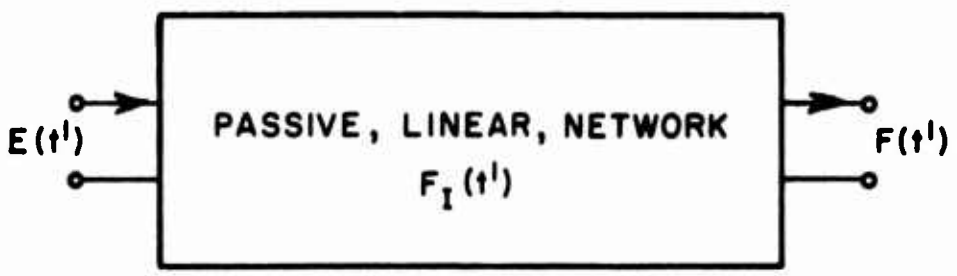

Fig. 1--Two port representation of scattering problem.

In order to define the various quantities in Eq. (1) and to explain the scalar treatment of the electromagnetic fields, it is necessary to introduce a coordinate reference frame. This coordinate frame is shown in Fig. 2. The incident plane electromagnetic field polarized in the x direction

$$\underline{E}^i = \hat{x}\, E(t - z/c) \quad , \tag{2}$$

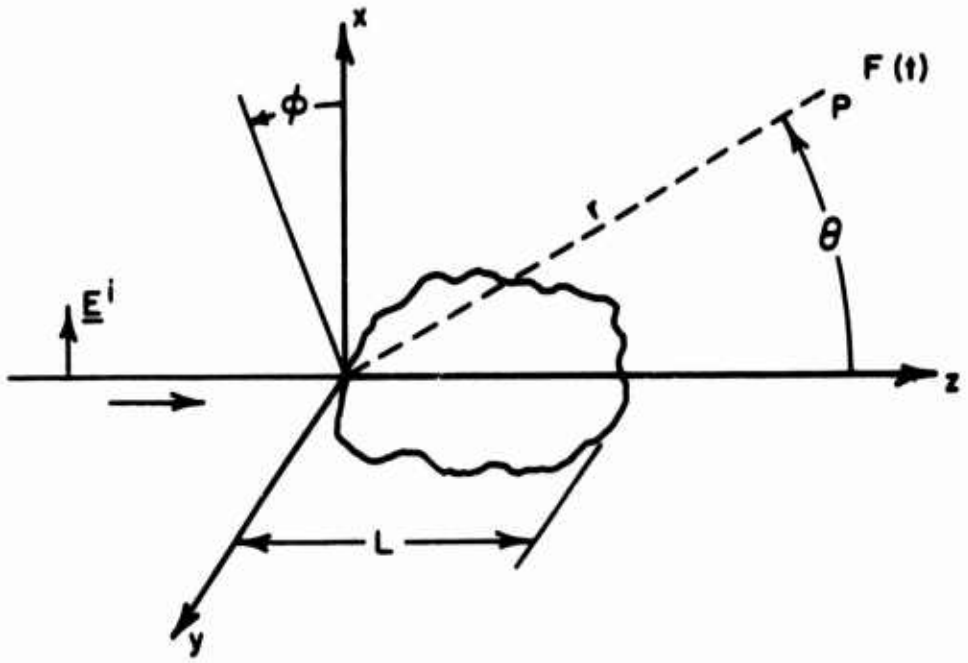

Fig. 2--Coordinates of scattering problem.

evaluated at z = 0 has an intensity E(t). With this plane wave incident on the scattering object as shown in Fig. 2, a scattered field is produced. At an arbitrary location P in the far-field of the scattering object, a normalized transverse component of the scattered field has an intensity F(t). In order to remove the time delay between scatterer and observer, a new time scale t' = t-r/c is introduced. The input E(t') is simply E(t) with t replaced by t'. For the output F(t'), t-r/c is replaced by t' in F(t). The impulse response waveform $F_I(t')$ is the response when the input E(t') is impulsive, i. e., $E(t') = \delta(t')$. The lower integration limit t_1' in Eq. (1) is the initial value of t' at which the impulse response waveform $F_I(t')$ departs from zero. This limit is, in general, not zero since the initial contribution need not arrive at a time t = r/c. If L is the maximum object dimension then $t_1' > -L/c$ in the half-space z > 0 and $t_1' > 0$ in the half space z < 0. The two-port has a frequency-dependent phasor response G(jω) which is related to the radar cross-section of the scatterer as

$$\sigma(\omega) = \pi |G(j\omega)|^2 \qquad (3)$$

The frequency-dependent phasor response G(jω) and the time-dependent impulse response waveform $F_I(t')$ form a Laplace transform pair.

$$(4) \qquad G(j\omega) = c\int_0^{\infty} F_I(t')\, e^{-j\omega t'}\, dt'$$

$$F_I(t') = \frac{1}{2\pi jc}\int_{-\infty}^{\infty} G(j\omega)\, e^{t'j\omega}\, d\omega \quad ,$$

or using s notation ($s = j\omega$)

$$(5) \qquad G(s) = c\int_0^{\infty} F_I(t')\, e^{-st'}\, dt'$$

$$F_I(t') = \frac{1}{2\pi jc}\int_{-j\infty}^{j\infty} G(s)\, e^{t's}\, ds \quad .$$

Equations (3) and (4) define the normalization mentioned above. It should be noted that the scattering object in Fig. 2 is located in the half-space $z > 0$ of the coordinate frame. A more detailed development of the normalized impulse response waveform $F_I(t')$ is found in Kennaugh and Moffatt[13] .

Certain points should be stressed concerning the two-port in Fig. 1. Its time-dependent impulse response $F_I(t')$ is dependent on the orientation of the scattering object, the observation angles (but not range) and the particular transverse component of the scattered field selected. The electromagnetic scatterer properties are uniquely determined by $F_I(t')$, but one cannot extrapolate this statement without proof to imply that $F_I(t')$ uniquely determines the physical properties of the scatterer. It seems doubtful that two

geometrically or materially different scatterers could (for fixed source and receiver locations and polarizations), have exactly the same phasor response over the entire spectrum, but a unique determination of the physical properties of the scatterer has not been proven.

The impulse response waveform $F_I(t')$ is the time-dependent electromagnetic field intensity produced at the output terminals when the input $E(t')$ is an impulsive plane electromagnetic wave, i. e., $E(t') = \delta(t')$. Once $F_I(t')$ is known, the response waveform for any incident waveform is determined by Eq. (1). Two other particular response waveforms are of interest in this study and need to be defined. The step response

$$(6) \qquad F_U(t') = \int_{t_1'}^{\infty} F_I(\tau)\, u(t'-\tau)\, d\tau \quad ,$$

and the ramp response

$$(7) \qquad F_R(t') = \int_{t_1'}^{\infty} F_I(\tau)\,(t'-\tau)\, u(t'-\tau)\, d\tau = \int_{t_1'}^{t'} F_U(\tau)\, d\tau \quad .$$

The Laplace transform relations in Eqs. (4) and (5) state that $F_I(t')$ and $G(j\omega)$ can each be derived from the other. But $G(j\omega)$ is known exactly for only one finite three dimensional shape; the sphere, and even for this shape the transformation to obtain $F_I(t')$ cannot be achieved exactly. Thus, a study of the scattering problem in the time

domain consists essentially of the development of a reasonable estimate for the impulse response waveform $F_I(t')$. In exactly the same way, the study of scattering problems in the frequency domain has been, as discussed in the introduction to this chapter, the development of reasonable estimates to the phasor response $G(j\omega)$, but usually for either the high or low extremities of the spectrum. A number of distinct advantages to the time domain approach, as well as some disadvantages, will be enumerated in the course of this study. It is hoped that the time domain approach can be presented with sufficient clarity and simplicity, and its utility demonstrated on a sufficiently complex problem, that future investigators will move freely between the domains to exploit the maximum potential of either approach.

It would be premature at this point to discuss the relative advantages and disadvantages of a frequency domain versus time domain approach to an electromagnetic scattering problem. What is hoped to be demonstrated is that one can incorporate into the time domain model most of the advantages of a frequency domain approach while at the same time exploiting certain unique features of the time-dependent waveform model. Consideration at the moment is to be restricted to simply the solution of a given electromagnetic scattering problem involving a single isolated object. In the opinion of the author, the

following remarks justify consideration of the time domain approach and at the same time indicate the basic premises upon which such an approach is based.

1. It is to be generally expected that, compared to the complicated complex phasor response G(s) of a given object as a function of frequency, the real, time-dependent waveform F_I(t') will be relatively simple. In the context of this study, the scatterer can be represented by a distributed constant, linear, time-invariant two-port network. As such, its impulse response waveform should be relatively simple compared to the transcendental response functions characterizing distributed systems in the frequency domain.

2. The impulse and transient response waveforms of a scattering object must be related in a rather direct way to the geometry and constitutive parameters of the object. It will be shown, for example, that the area beneath the ramp response waveform is proportional to the Rayleigh coefficient; and hence, to the volume of the scatterer. More fundamentally, however, as the impulsive or transient illumination moves across the object, only that portion of the object which has been illuminated can possibly

contribute to the scattered field waveform. Therefore, up until the time when the transient illumination has passed completely over the object, there is a direct correlation between the response waveform at a given time and a specific portion of the object. Furthermore, since we are dealing with a physically realizable system which cannot be a predictor, two objects which present initially identical geometrical and physical properties over a given region must yield identical response waveforms up to the time corresponding to complete illumination of this region, regardless of their geometrical and physical properties beyond this point.

3. In principle at least, it is possible to incorporate into an estimate of the waveform $F_I(t')$ all of the best features of various approximate or asymptotic estimates of $G(s)$ while at the same time utilizing certain unique features of the time-dependent waveform. If one has certain estimates of $G(s)$ whose validity is restricted to particular portions of the spectrum, it is far from clear how consideration of these estimates can be used to approximate a $G(s)$ corresponding to the remainder of the spectrum. In the time domain however, the estimates of $G(s)$ become time-limited portions of the waveform, and it is known that these pieces must combine with other pieces to

produce a single waveform. Certain conditions on this total waveform are known from low-frequency derived moment conditions. Even very crude estimates of how the pieces are combined must add some new knowledge concerning G(s).

4. The convolution integral in Eq. (1) relating the response waveform to the interrogating signal provides an additional understanding of the relationship between the contributions of G(s) from various portions of the spectrum and the response waveform $F_I(t')$. Let the input signal be a monochromatic continuous wave. The graphical interpretation of convolution is that of reversing one of the signals with respect to time and then sliding one over the other. At any given time, the response is given by the integral of the product of the two waveforms over that time interval where they coincide. For the monochromatic input, this consists of sliding a sinusoid of a given period across the reversed waveform $F_I(-t')$. It follows that at relatively low frequencies, the response can be influenced little by the minute details of the waveform; therefore the response at low frequencies is basically dependent on the general size and shape of the waveform. As the input frequency increases, more and more of the waveform detail is important and slowly varying portions of the waveform less important since the contributions

from these are effectively cancelled by the positive and negative portions of the sinusoid. Two conclusions can be drawn from these remarks[13]: (1) The general shape and size of the impulse response waveform $F_I(t')$ is dictated by the low-frequency response of the object and (2) The fine structure and detail of the waveform is controlled by the high-frequency response of the object. Thus if one constructs an estimate of $F_I(t')$ using the moment conditions, it is to be expected that such a model would fit relatively well at low frequencies, but would require modifications and corrections to predict the response well at high frequencies.

5. The use of experimental data in deriving estimates of $G(s)$ or $F_I(t')$ is an important consideration. The most straightforward but probably least effective method for utilizing such data is simply the comparison of theoretical results based on a model obtained wholly from analytical considerations with such data. If only a limited amount of experimental results are available, such comparisons are not conclusive and often not indicative of the changes required in the model. From the discussion in (4) above, it is apparent that one should be able to construct a crude model of the response waveforms from a limited number of low-frequency measurements, and

that systematic procedures for incorporating such data with theoretical estimates of $F_I(t')$ should be feasible.

This study does not fully develop the methods and techniques mentioned in (5) above, and it will be found that the model of $F_I(t')$ developed in Chapter II for the prolate spheroid target is obtained without consideration of experimental data; such data only being used to compare with calculations from the model. However, we shall discuss how such experimental data might be more effectively used and the possible directions of future research in this area.

B. General Properties of the Impulse and Transient Response Waveforms

The frequency-dependent phasor response $G(j\omega)$ and the corresponding time-dependent impulse response waveform $F_I(t')$ are both governed by Maxwell's equations. Therefore $F_I(t')$ must be a causal function, i. e., a backscattering response cannot appear at the output terminals before the time $t' = 0$. The square integrable criterion

$$\frac{1}{\pi}\int_0^\infty |G(j\omega)|^2 \, d\omega < \infty \quad , \tag{8}$$

can be applied provided, as pointed out by Paopulis[20], all constants and positive powers of $j\omega$ are first removed from $G(j\omega)$. Note that it does not necessarily follow that approximate or asymptotic estimates

of $G(j\omega)$ will also lead to causal time functions. It will be shown in Appendix II that certain high-frequency asymptotic estimates of $G(j\omega)$ lead to non-causal time functions.

The definition in Eq. (3) shows that $G(j\omega)$ must have the dimension of length. From Eqs. (4), (6), and (7) respectively, it is seen that the impulse response $F_I(t')$ is dimensionless; the step response $F_U(t')$ has the dimension time; and the ramp response $F_R(t')$ the dimension time squared. It is most convenient to choose a time scale measured in units of the transit time for some characteristic dimension of the scatterer. If ℓ is such a characteristic length then the transit time

$$t_o = \ell/c \,, \tag{9}$$

is set equal to unity. This can be interpreted as choosing a time scale such that c is unity and a distance scale such that a free space wave traverses the length ℓ in unit time.

The low frequency scattering properties of any finite, three dimensional object provide interesting and useful conditions on the impulse and transient response waveforms. At sufficiently low frequencies, it is known that the phasor response, $G(s)$, of a scattering object can be expanded in a Taylor series about the origin $s = 0$ as

$$(10) \qquad G(s) \simeq \sum_{n=0}^{\infty} a_n s^n \quad ,$$

where Rayleigh's theory dictates that the coefficients a_0 and a_1 in such an expansion are zero while the coefficient a_2 is proportional to the scatterer volume. Note that the coefficient a_2 depends upon the shape, orientation, and constitutive parameters of the scatterer as well as the polarization of the incident and scattered fields. Expanding $e^{-st'}$ in the definition integral in Eq. (5) in a Taylor series about the origin $s = 0$ there results,

$$(11) \qquad \int_0^{\infty} F_I(t')\,dt' = a_0 = 0$$

$$\int_0^{\infty} t' F_I(t')\,dt' = a_1 = 0$$

$$\int_0^{\infty} t'^2 F_I(t')\,dt' = \frac{2a_2}{c}$$

$$\int_0^{\infty} t'^n F_I(t')\,dt' = \frac{(-1)^n n!\, a_n}{c} \quad .$$

These are moment conditions on the impulse response waveform $F_I(t')$. An integration by parts of the second and third expressions in Eq. (11) shows that the first three moment conditions can be interpreted as requiring that the net area beneath the impulse and

step response waveforms be zero and that beneath the ramp response waveform proportional to the so-called Rayleigh coefficient, a_2, of the scatterer. A word is in order concerning this proportionality factor which has caused some difficulty in the past. With the definition in Eq. (11), the Rayleigh term (for small ω) is

$$(12) \qquad G(j\omega) = \frac{-a_2(2\pi)^2 c^2 \ell^2}{\ell^2 \lambda^2} = \frac{-a_2(2\pi)^2}{t_o^2}\left(\frac{\ell}{\lambda}\right)^2 ,$$

where ℓ is some characteristic dimension of the scattering object. If the Rayleigh coefficient, K, is <u>defined</u> by

$$(13) \qquad G(j\omega) = K\left(\frac{\ell}{\lambda}\right)^2 ,$$

then

$$(14) \qquad K = \frac{-a_2(2\pi)^2}{t_o^2} ,$$

and

$$(15) \qquad \int_0^\infty F_R(t')\,dt' = \frac{-K\,t_o^2}{(2\pi)^2 c} .$$

Note that the moment conditions in Eq. (11) were not obtained from the final value theorem of the Laplace transform theory

$$(16) \qquad \lim_{s \to 0} sG(s) = \lim_{t' \to \infty} F_I(t') ,$$

which theorem simply yields the result that in the limit of large time the response must decay to zero. This latter result is clearly reasonable on physical grounds.

The expansion for G(s) in Eq. (10) is not unique unless a phase center is defined. Since the first non-zero term is the coefficient of s^2, the choice of phase center does not change the first three moments. However, to employ moments higher than the third both the choice of phase center and the origin of coordinates on the t' scale must be specified. The first two moment conditions are applicable to any finite, three dimensional object. For a great many targets, the Rayleigh term (coefficient of s^2) can also be estimated making the third moment applicable. The higher order coefficients can only be obtained for particular objects, therefore the usefulness of the higher order moment conditions ($n > 2$) is restricted to a small class of targets. An exception to this exists for the case of objects which have a center of symmetry. * Stevenson[21] has demonstrated that for this class of targets the coefficient of the s^3 term is identically zero when the phase center for the expansion is chosen at the center of

---

* An object has a center of symmetry, 0, if it is symmetrical to a transformation consisting of rotation by π radians about an axis through 0 and then reflection in a plane perpendicular to the axis of rotation and containing 0.

symmetry. Therefore for this class of objects, the fourth moment condition can be utilized. If the phase center is chosen at the center of symmetry and the origin of the t' axis at the point where the incident impulsive wave first encounters the body then

$$(17) \qquad \int_0^\infty t'^3 F_I(t')\,dt' = \frac{12 L a_2}{c} \quad ,$$

where L is twice the linear distance from the center of symmetry to the t' origin and is a negative quantity. Equation (17) may also be written as

$$(18) \qquad \int_0^\infty t' F_R(t')\,dt' = \frac{2 L a_2}{c} \quad .$$

The moment conditions given in Eq. (11) implicitly assume that all the moments of the time-dependent impulse response waveform exist[22]. It is clear that for the n^{th} moment to exist, $F_I(t')$ for large t' must vanish at least as fast as $1/t'^{n+1}$. In the latter portion of this section a discussion of the proper analytical models for $F_I(t')$ and $G(s)$ makes it clear that insofar as the approximations of interest for these functions are concerned, the assumption of the existence of the moments is not unreasonable.

A well known high frequency estimate of G(s) is the physical optics approximation. It can be shown[23] that this approximation predicts the following form for the step response waveform $F_U(t')$ for conducting objects if the observation location is constrained to the E or H planes of the incident field.

E plane, direct polarized component

$$(19) \qquad F_U(t', \theta, \beta) = \frac{1}{\pi c^2} \int\int_{s^{ill}} \delta\left[t' - \frac{\underline{\rho} \cdot (\hat{g} - \hat{\xi})}{c}\right] \hat{\xi} \cdot \hat{n}\, ds$$

E plane, cross polarized component

$$(20) \qquad F_U(t', \theta, \beta) \equiv 0$$

H plane, direct polarized component

$$(21) \qquad F_U(t', \theta, \beta) = \frac{-1}{\pi c^2} \int\int_{s^{ill}} \delta\left[t' - \frac{\underline{\rho} \cdot (\hat{g} - \hat{\xi})}{c}\right] \hat{g} \cdot \hat{n}\, ds$$

H plane, cross polarized component

$$(22) \qquad F_U(t', \theta, \beta) = \frac{-\sin\beta}{\pi c^2} \int\int_{s^{ill}} \delta\left[t' - \frac{\underline{\rho} \cdot (\hat{g} - \hat{\xi})}{c}\right] \hat{x} \cdot \hat{n}\, ds \quad .$$

In the above equations (as shown in Fig. 3), $\hat{g}$ is a unit vector in the direction of propagation of the incident field; $\hat{\xi}$ is a unit vector in the direction of propagation of the scattered field; $\hat{n}$ is the unit outward normal from the scatterer surface; and $\underline{\rho}$ is the position vector of a

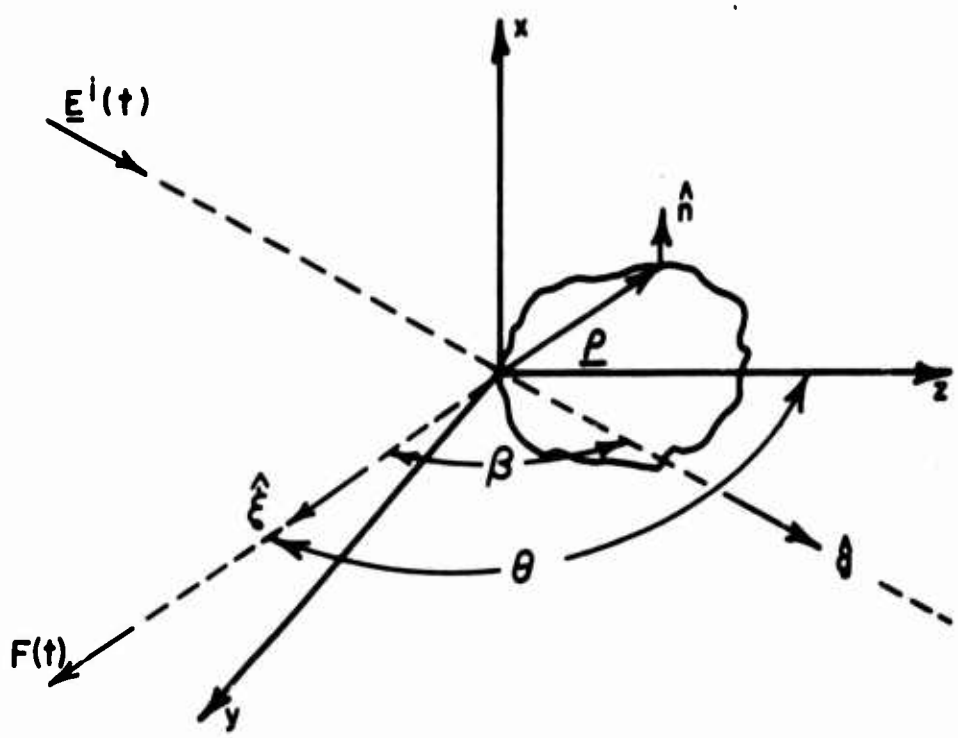

Fig. 3--Coordinates of scattering problem.

point on the scatterer surface. β is the angle between the unit vectors $\hat{g}$ and $\hat{\xi}$ ($\beta \leq \pi$) and s^{ill} is the illuminated surface of the scatterer. For the backscattering case ($\beta = \pi$) specializing to the orientation in Fig. 2

$$(23) \qquad F_U(t') = -\frac{1}{2\pi c}\frac{dA(z)}{dz} \quad , \qquad z = ct'/2$$

and

$$(24) \qquad F_I(t') = -\frac{1}{4\pi}\frac{d^2A(z)}{dz^2} \quad , \qquad z = ct'/2 \quad .$$

The function A(z) measures the area of the scatterer surface between the x, y plane and a cutting plane at z projected orthogonally on the x, y plane. A detailed derivation of Eq. (24) is given in Reference 13. The bistatic results in Eqs. (19), (21), and (22) have also been interpreted in terms of area functions[23] . It can be shown[13] that the physical optics result in Eq. (24) always satisfies the zero moment condition [first of Eq. (11)] but does not in general satisfy the higher order moments.

Similar time domain interpretations can be made of other high-frequency approximations, usually however only with reference to a particular scattering object. If the inverse transformation [Eq. (4)] can be achieved in closed form then an analytical result is obtained. If the inverse transformation cannot be achieved, a Fourier synthesis procedure can be used to obtain an estimate of the time-dependent waveform. The Fourier synthesis procedure is adequately described in Reference 13. In essence, given the phasor response G(s) at a sufficient number of harmonically related frequencies, estimates of the time-dependent response waveforms can be generated.

It will be instructive at this point to examine certain of the approximate impulse and transient response waveforms which have been obtained for specific objects. The interest here is in noting the salient features and characteristics of the waveforms. It is stressed

that these are far or radiation field response waveforms and the conclusions drawn from them are restricted to that region. The backscattering impulse, step, and ramp response waveforms of a perfectly conducting sphere[13] are shown in Fig. 4. The sphere radius is a and the time scale is in units of the sphere diameter transit time ($t_o = 2a/c$). In this figure, as well as those presented in the remainder of this study, the delta-function pulse of weight α is denoted by a vertical arrow with α by the arrow head. For the impulse response waveform, the incident waveform is a positive delta function pulse of weight unity. The impulse response waveform consists of a negative impulse of weight a/c followed by a positive jump of 0. 5 and a secondary negative maximum at approximately t' equal 2. $57t_o$. Beyond this secondary negative peak the waveform damps rapidly, becoming negligible in comparison to the earlier portions for times greater than approximately 6 transit times for the sphere diameter. The secondary negative peak at $t' \simeq 2.57t_o$ corresponds to the arrival of a diffracted front. Both the negative impulse and 0. 5 jump at $t' = 0$ are correctly predicted by approximate high frequency solutions. The response waveforms of the conducting sphere, particularly the diffracted or creeping wave peak at $t' = 2.57t_o$, will be discussed in Appendix II. One should note that the exact nature of the creeping wave maximum is not resolved in Fig. 4. It is important to discern

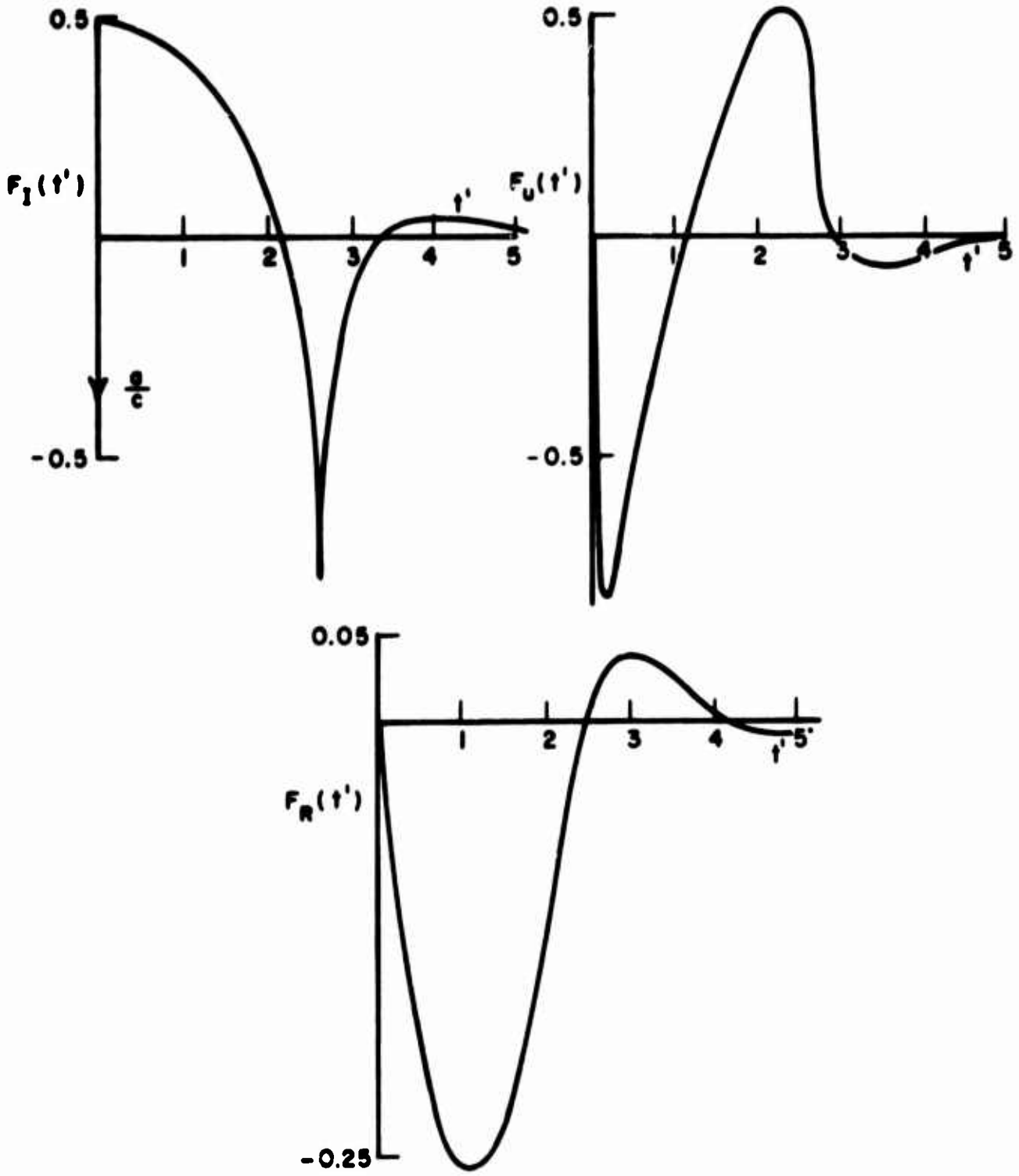

Fig. 4--Approximate impulse, step, and ramp response waveform of conducting sphere. Backscatter.

two main points from the waveforms shown in Fig. 4. The first is that the successive integrations to obtain the step and ramp response waveforms from the impulse response result in a considerable smoothing of the latter waveforms. Thus distinct singularities and peaks present in the impulse response waveform are effectively masked in the corresponding ramp response and one can conclude that a reasonable approximation to the ramp waveform is more simply obtained that an impulse response approximation. Clearly, each waveform contains all the information; for example the secondary peak in the sphere impulse response becomes at most a subtle change in slope in the ramp waveform, but an estimate of the ramp waveform which ignored the change in slope would still be a reasonable approximation over a range of lower frequencies. The second point of interest is the effective time-limited nature of the response waveforms. For times greater than 5 or 6 t_o, the response waveforms have decayed to a negligible value. Regardless of the exact nature of this decay, it is evident that an approximation to the waveform which fits well for $t' < 6\ t_o$ and which vanishes for large times would, for all practical purposes, provide a satisfactory model.

The response waveforms shown in Fig. 4 were obtained by a Fourier synthesis procedure using calculated values of G(s) from the Mie series. In Fig. 5, the approximate impulse response waveforms of several other objects are shown. The waveforms in Fig. 5 were obtained from a combination of high-frequency estimates of G(s) and the lower order moment conditions. In the case of the cone-sphere[8] (Fig. 5b) and the prolate spheroid[10] (Fig. 5d), the sphere results in Fig. 4 were also utilized. The reader's attention is called to the correction in the response waveform shown for the flat-based right circular cone in Fig. 5a. The response waveform for this object given in Reference 13 inadvertently reversed the time behavior of the doubly-diffracted term from the base.

Some additional characteristics of the impulse response waveform can be deduced from the waveforms shown in Fig. 5. There is clearly a general relationship between the object geometry and the response waveform; i. e. , the various singularities and peaks in the response waveform occurring at given times can be directly associated with a corresponding geometrical feature of the object. Furthermore, the estimated character of the singularity or peak can also be deduced from the geometrical feature. For example, the response waveform associated with the diffraction from smooth convex surfaces (the secondary peak in the sphere impulse response of Fig. 4) has the

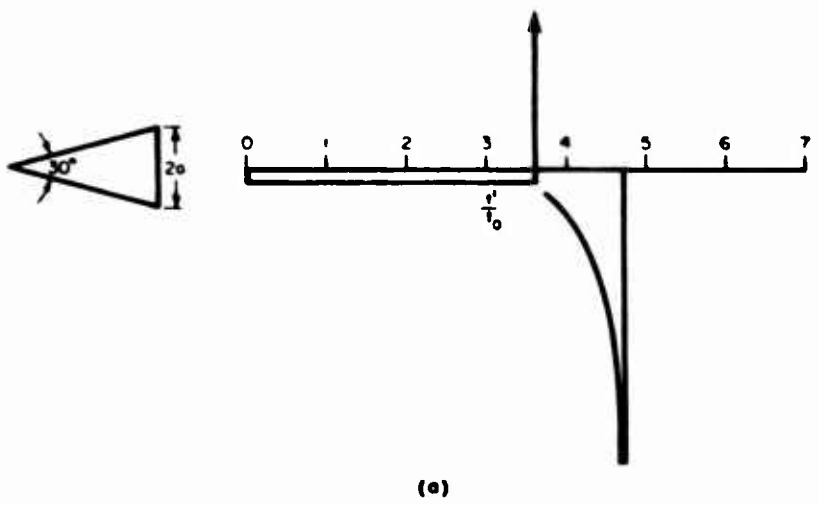

(a)

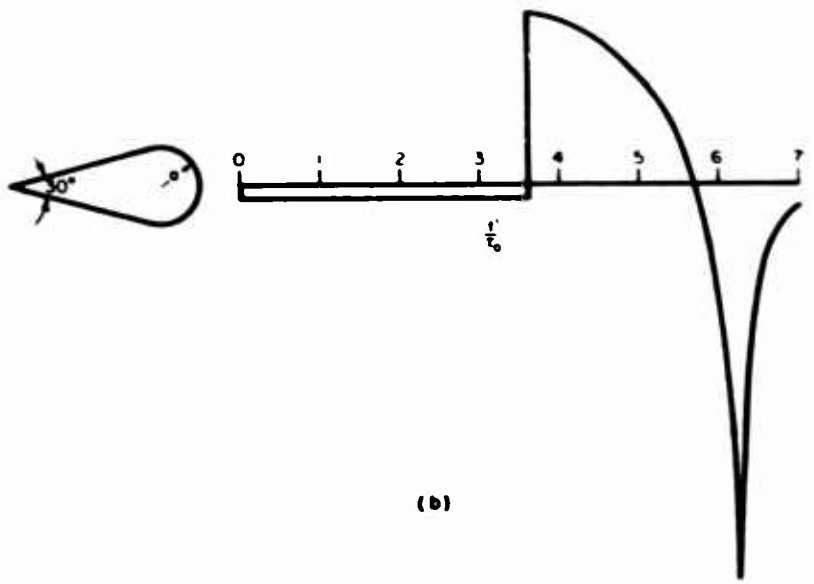

(b)

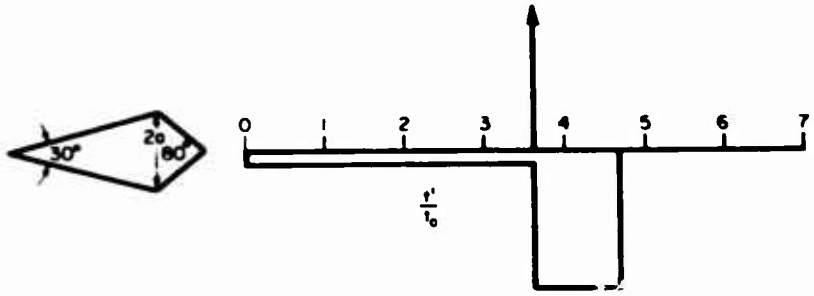

(c)

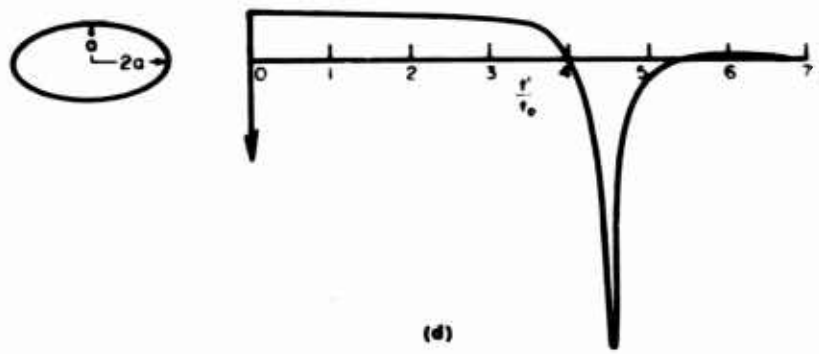

(d)

Fig. 5--Approximate impulse response waveforms. Backscatter.
a. Conducting flat-based right circular cone.
b. Conducting cone-sphere.
c. Conducting double cone.
d. Conducting 2:1 prolate spheroid.

same general form for the sphere, spheroid and cone-sphere. In a similar fashion, it is seen from Fig. 5 that single diffraction from edges has a delta function character and double diffraction a $1/\sqrt{t' - T}$ behavior. It is clearly evident in Fig. 5 that objects which initially present identical geometrical and physical properties to the incident transient excitation must also have identical response waveforms for an initial time period. The impulse response waveforms for the cone, cone-sphere and double cone in Fig. 5 are identical until a time corresponding to the arrival of the incident impulsive wave at a change in geometry. Consider a more explicit example. Compare two cone-sphere targets (as in Fig. 5b) identical in every respect except for an axial needle protruding from the sphere in one case. For an incident impulsive wave along the cone axis toward the cone tip, the impulse response waveforms of these targets would be identical for all t' less than $\approx 6.3t_o$. For times larger than this, the two response waveforms may differ markedly. We emphasize the fact that, as the impulsive wave moves over the object in the illuminated region or the transient currents excited by the incident wave move beyond the shadow, a change in the geometry or composition of the object cannot be anticipated. The excitation, propagating with a finite velocity, must reach the perturbation before a change in the response waveform can occur. Thus if one were attacking the scattering problem of the perturbed target, the early portion of the waveform

would be known and the analysis could be concentrated on the effect of the perturbing geometry. A question clearly exists as to exactly when the forcing function, i. e. , the incident impulsive wave, ceases to influence the transient currents induced on the target. From a geometrical optics viewpoint, the forcing function would shut off at the shadow boundary. More realistically, the impulsive wave probably continues to influence the induced current somewhat beyond the shadow boundary but confined to the neighborhood of the boundary. Therefore in the case where a change in the geometry or composition occurs close to the shadow boundary, some uncertainty would exist in predicting exactly when the response waveform should depart from the unperturbed case. This causality feature of the response waveform with respect to a given geometrical feature of the target is extremely useful in devising estimates of the waveform. That is, in most cases the location in time if not the character of the response due to a specific feature can be determined.

The most important question in the application of the time domain concepts discussed thus far in this chapter is: What is a valid general analytical model for the time-dependent response waveform $F_I(t')$, or alternatively for the frequency-dependent phasor response $G(s)$, in a scattering problem? In the context of this study, the scattering object is a two-port transducer and the two-port is a linear,

distributed-constant system. Thus G(s) must be some combination of rational and transcendental functions of s. Unfortunately, the literature on the analysis of distributed constant systems via transform methods is quite limited compared to that on lumped constant idealizations. Two points should be made; first, the impulse response of a lumped constant system is only an approximation (at sufficiently high frequencies the system is distributed), but one which is sufficiently good for the frequency ranges of practical interest, secondly, some circuit concepts developed by transform methods with reference to lumped constant systems may have to be modified for application to a distributed constant system.

It must be stressed that in the context of this study, what is sought is an approximate analytical model capable of producing a reasonable estimate of $F_I(t')$ or $G(s)$ in the range of practical interest. For example, the dc and optical properties of the scatterer are not really of interest here; and consequently, the estimate of $G(s)$ need not be valid at these limits of the spectrum. Such a band-limited approximation for $G(s)$, or alternatively for $F_I(t')$, is further justified when one considers the effective bandwidths of practical radar systems. The question becomes therefore: What is a sufficiently general physical model of the scattering process in such a band-limited approximation? Clearly, the necessary complexity of the physical model depends to some extent on the specific scattering

object and one cannot rigorously justify the assumption of any particular model for the general object. However, the representative waveforms shown in Figs. 4 and 5 do illustrate some of the characteristics the general model must be able to reproduce. Specifically, it can be seen that over limited time ranges, the model must be capable of generating an increasing rather than decreasing function with time and also admit to at least approximations of various types of singularities. Finally, for moderately large times the model must produce a rapid damping.

Consider first the large time behavior of the impulse response waveform. It is known[24] that in any passive or stable active lumped-constant network, the force-free behavior decays exponentially* so that a short time following the transient interval only the forced behavior survives. In the present case of a distributed constant system, this generalization cannot be made precisely because of the presence of the transcendental functions of s. However, given sufficient elements, one can synthesize an approximation to the distributed constant system using lumped elements. Clearly this lumped constant approximation, regardless of the number of elements needed to secure a reasonable estimate, must decay exponentially for large time. For an

---

* In the general case one has a summation of exponentials, but for large time the minimum decay rate dominates and the response approaches an exponential decay.

approximate model for $F_I(t')$ an exponential decay for large time is assumed, i. e. , beyond some finite value of t' which will vary with the scatterer, an exponential decay of the waveform is enforced. Physically, this exponential decay is associated with radiation and dissipation effects. If the inverse transformation of Eq. (5) is written as

$$(25) \qquad F_I(t') = \frac{1}{2\pi jc} \int_{\gamma - j\infty}^{\gamma + j\infty} G(s)\, e^{t's}\, ds \qquad \gamma > -\alpha$$

then α is the minimum exponential decay rate of the impulse response waveform for large values of t' . The results in Figs. 4 and 5 indicate that α is reasonably large for practical scatterers.

It is also known[24] that for lumped constant systems with simple poles the most general representation of the impulse response waveform is a linear combination of terms of the type

$$(26) \qquad f(t) = \sum_{n=1}^{N} A_n\, e^{a_n t}\, u(t) \qquad .$$

This in fact is the most general time function having a rational Laplace transform when the $\mathrm{Re}(a_n) < 0$. It is immediately clear that one would require N large to approximate the response waveforms in Figs. 4 and 5 with a function of this type, except for large t' . However, if the real part of the a_n are unrestricted and a delay

factor is introduced then a linear combination of terms of this type should be capable of achieving reasonable estimates of the time response waveforms with just a few terms. A possible analytical model for the impulse response waveform is

$$(27) \qquad F_I(t') = \sum_{m=1}^{M} A_m \delta(t'-t_m) + \sum_{k=1}^{K} \sum_{n=1}^{N} B_{nk} e^{b_{nk}t'} [\, u(t'-T_k) - u(t'-T_{k+1}) \,] \qquad T_{K+1} = \infty \ .$$

The model in Eq. (27) consists of weighted delta function singularities at selected instants plus sections of sums of exponential functions and a final exponential decay. Note that there are no restrictions on the real part of the b_{nk} except in the final time interval, i. e., $t' > T_k$. In this final time interval

$$(28) \qquad Re(b_{nK}) < 0 \ ,$$

to ensure an exponential decay of the response waveform for large time.

Excluding the delta function singularities and the exponential decay for large time, the analytical model in Eq. (27) is a superposition of bounded, time-limited waveforms in sub-intervals or sections. The number of sub-intervals into which the response waveform is separated is finite for any scatterer, and judging from

the response waveforms in Figs. 4 and 5 will usually be no more than 3 or 4. The point is that the number of sub-intervals (K-1), their relative location (T_k) and duration ($T_{k+1} - T_k$) is selected from an examination of the geometry of the target. Locations on the target where changes in the curvature or the derivatives of curvature, or the composition of the scatterer occur are natural join points of the sub-intervals. With this type of model it is clear that both experience and a knowledge of the known response waveforms for various objects (a catalog of known response waveforms) is an indispensable aid in making a judicious choice of the model for a given target.

It is not intended to imply in the compactly written analytical model in Eq. (27) that the same number of exponential terms necessarily be used in each sub-interval. The number of terms required in each sub-interval will depend on the complexity of the waveform, primarily at the end points of the interval. It is intended that the character of the response at the joins of the sub-intervals be determined from various approximate or asymptotic theories and the geometry of the shape. In this regard it is evident that the analytical model in Eq. (27) cannot, in its present form, faithfully reconstruct singularities such as those corresponding to double diffraction (Fig. 5a). However, such cusp type singularities are usually predicted by an asymptotic theory and are associated with abrupt discontinuities in

the curvature of an object. Such discontinuities are mathematical idealizations for real targets which exhibit less perfect curvature transitions. It is contended that a practical interpretation of the singularities resulting from such discontinuities is a bounded variation of the response waveform. Therefore an approximation to the singularity can be obtained with the analytical model proposed in Eq. (27).

Neglecting the delta function singularities, this analytical model of the impulse response waveform is a superposition of bounded, time-limited waveforms with various delays plus a final exponential decay. In the s domain, the model corresponds to a combination of entire functions[25], i. e., functions which have no singularities in the finite portion of the plane; and rational functions. Such a function, i. e., one made up of entire and rational functions, is known as meromorphic in the unextended plane. The analytical model for the phasor response is

$$(29) \qquad G(s) = \sum_{m=1}^{M} A_m e^{-t_m s} + \sum_{k=1}^{K} \sum_{n=1}^{N} \frac{B_{nk}}{b_{nk} - s} \left[e^{(b_{nk} - s) T_{k+1}} - e^{(b_{nk} - s) T_k} \right] .$$

The analytical time domain model in Eq. (27) and the corresponding phasor response in Eq. (29) have not been based on an assumed physical model for the distributed constant system but rather on the known impulse response waveforms of certain representative scatterers. It is clearly not imperative that the analytical model be linked to a particular physical model; but such a correlation is advantageous as a partial justification of the model. Franks[26] has shown that the finite impulse sequence

$$(30) \qquad f(t) = \sum_{m=1}^{M} A_m \delta(t - t_{rn}) \quad ,$$

given as the first part of Eq. (27) corresponds to the impulse response of a network consisting of delay lines lumped loaded with resistors. He has also shown that the impulse response of delay lines with general lump loading can have the bounded, time-limited behavior corresponding to entire functions in the s domain. Franks suggested a segmental impulse response involving an exponential sum approximation in each interval similar to the second part of Eq. (27) for such a network. In his case however, it was stipulated that the real part of the b_{nk} be less than zero. However, the purpose of Frank's approximation was for the realization of a segmental impulse response which consisted of segments of time functions having rational Laplace transforms between critical break points corresponding to

lengths of delay line. If one replaces the delay line with finite lengths of uniform transmission line, then the segments of time functions will no longer have rational transforms. The general representation in Eq. (26) for time functions with rational transforms is no longer adequate and a less restrictive representation is required. A possible interpretation of the physical model corresponding to the approximate analytical representation in Eq. (27) consists of a finite length of uniform transmission line lump loaded at various intervals. As a practical physical model to approximate the scattering of an electromagnetic field by a finite three dimensional object, such a representation does not seem unreasonable.

Some final comments on the analytical model in Eq. (27) are necessary. The impulse response waveform $F_I(t')$ must be real, therefore a necessary relationship between the coefficients in the exponential sums exists. If the b_{nk} are complex, they must exist as conjugate pairs and the corresponding B_{nk} are equal in magnitude. If these B_{nk} have the same sign they are real, if they have the opposite sign they are imaginary. If the b_{nk} are purely real then the B_{nk} are also purely real. In some cases it may prove advantageous in terms of determining the b_{nk} and B_{nk} in a particular interval to write the exponential in a shifted form

(31) $B_{nk}\, e^{b_{nk}(t'-T_k)}$

in order to isolate B_{nk} when t' equals T_k.

At best, the preceeding discussion has perhaps achieved a reasonable rationalization for the use of the analytical model. A rigorous demonstration that the analytical model has the physical interpretation suggested has not been given, nor has it been demonstrated that these models are necessarily a valid approximate representation of an actual scattering problem. At this point in the development of impulse response methods in scattering problems, however, it is felt that such rigorous demonstrations are not necessary. There is evidence[13] that the analytical model in Eq. (27) yields adequate representations of the response waveforms for certain objects. That is, the published estimates of the response waveforms for particular targets[13], which have been verified by comparisons of the corresponding phasor responses with measured or calculated data, were achieved with the implicit assumption of the analytical model suggested here. Thus while a more rigorous basis for the analytical model is desirable, it is not a prerequisite for further applications of the impulse response approach.

C. Analytical and Experimental Approximations of Impulse and Transient Response Waveforms

The purpose of this Section is to discuss in a general manner the development of approximate impulse and transient response waveforms. To place the discussion in proper perspective, it is perhaps advisable to begin with some comments regarding electromagnetic scattering studies. If the ultimate goal of such research is an "understanding" of the scattering by various objects, then the most direct route to this "understanding" lies via the development of the time domain approach rather than the development of theoretical solutions per-se. The point is that the ultimate refinement of a given theoretical solution lends little insight to the general problem. Using the time domain approach, it is possible to secure estimates of the response of a variety of object shapes in a limited amount of time. A most important consideration is the applicability of experimental data. Despite the vast literature on electromagnetic scattering[1], one is hard pressed to find examples where experimental data have been used in a direct way to help construct a theoretical estimate. The handbook approach, followed almost without exception, has been to devise an estimate of the phasor response based purely on theoretical considerations and then compare calculations from this model with experimental data. Our criticism is not of experimental

data, but rather of the fact that such data have been generated haphazardly without any useful integration of the results. With the ever increasing complexity and number of objects of practical interest, the utilization of experimental data must be extended beyond simply a confirmation of theoretical estimates or the compilation of patterns on a specific shape.

The time domain approach appears to offer the first practical way in which to build one's knowledge and understanding of scattering by the systematic improvement of a basic model. Thus, experimental measurements as well as computer derived solutions[27] can be used in a direct way to refine the theoretical model discussed in the previous section. It is to this systematic procedure that the discussion in this section is directed.

It is postulated that the fundamental building block in the development of a general approach for obtaining the response waveforms of an object is the ramp response waveform $F_R(t')$. There are several reasons which make an initial estimate of the ramp response waveform a logical starting point. It was pointed out in the previous section that one could estimate the ramp response waveform using fewer parameters than would be required for estimates of the corresponding step or impulse response waveforms. If the estimated ramp response waveform has a finite integral over all t' then the first two moment

conditions are automatically satisfied. Forcing this finite integral to be proportional to the Rayleigh coefficient (Eq. (15)) then satisfies the first three moment conditions. Finally, it has been shown[13] that whereas many values of the phasor response are required to synthesize an estimate of the impulse response waveform, as few as five values of the phasor response can be used to generate an estimate of the ramp response waveform. The required input data are low frequency harmonics with the fundamental wavelength approximately 10 times the maximum linear dimension of the object. Note that the necessary phasor response data could be obtained from experimental measurements as well as theoretical calculations; consequently, an experimentally derived first estimate of the ramp response waveform is also feasible[13] . Regardless of the method used to generate this first estimate, the corresponding estimate of the phasor response will be a low-frequency, i. e. , Rayleigh and low resonance region approximation.

In most previous applications of the time response concepts, direct estimates of the impulse response waveform have been attempted employing segmental exponential sum approximations similar to Eq. (27). In specific cases, sinusoids or polynomials in t' have been used in place of an exponential sum in some sub-intervals. In general, the physical optics approximation is used to predict the short time behavior of the response waveform. Later portions of the waveform

are selected either from a knowledge of the character of the response corresponding to specific geometrical features of the object or simply from a rough guess as to its probable form. These various pieces of the waveform are then joined with sufficient undetermined parameters to permit the known moment equations to be satisfied. Exactly this type of approach is used in Chapter II to obtain an estimate of the impulse response waveform of a prolate spheroid target; the extension being to a general orientation of the spheroid and an arbitrary linear polarization of the incident plane wave.

The approach outlined above for obtaining estimates of the impulse response waveform of an object is clearly inadequate. The fact that such a procedure has led to significant contributions to electromagnetic scattering theory is probably the strongest possible recommendation for further study in the time domain. The most obvious difficulty with the method above is that a successful estimate of the impulse response waveform is almost wholly dependent on the ingenuity of the analysist in deducing the character of the response waveform for other than short times. The moment conditions can also lead to problems in that enforcing the moments results in a system of simultaneous nonlinear equations. Even a very simple model for the response waveform can lead to an extremely difficult system of equations. Thus in many cases it is necessary to devise

a model such that a soluble system of equations is obtained, and this usually requires some sacrifice in the desired character of the waveform. The approach also lacks the property of finality in that if an additional exponential term is added in any one sub-interval, then all of the coefficients must be redetermined. The final criticism is that there is no established procedure for selecting the distribution of parameters in the various sub-intervals which are to be determined from known conditions or the waveform. It seems apparent that a need exists for studies on techniques for securing estimates of the response waveforms of distributed constant systems. It is not intended to pursue such an investigation in this research beyond the point of indicating some possible lines of attack. The reader should note that one feature of the segmental impulse response waveform will probably be retained, ultimately, in any derived estimate of the response waveform of a given object. The singularities, discontinuities, and peaks in the impulse response waveform are directly associated with the arrival of reflected and diffracted fronts from specific geometrical and physical features of the object. Since the arrival time of these fronts can usually be accurately predicted, procedures for estimating the response waveforms of the object must, at one point, successfully exploit this knowledge.

In considering alternative methods for estimating the response waveforms, one is naturally led to a consideration of the techniques developed for time domain synthesis and time domain identification in network and control system studies. The literature, as was noted in the case of linear system analysis via transform methods, is predominantly devoted to a consideration of lumped constant idealizations. Horowitz[28] has discussed a number of these techniques. Two main points are noted; emphasis is on expansion of the impulse response waveform in a finite series of orthogonal functions, and an error criterion, usually the integral square-error or the weighted integral square-error is used to judge the accuracy of the approximation.

Both time domain synthesis and time domain identification are concerned with the following problem. How does one find a frequency-dependent response $H_a(s)$ whose inverse transform approximates a given time function $f(t)$? As previously stated, $H_a(s)$ is usually assumed to be a rational function of s. Clearly, the problem at hand is somewhat different. Simply stated it is; how does one find a time-dependent impulse response waveform whose transform approximates the phasor response of a system over the range of practical frequencies, given certain conditions on the waveform and estimates of its value at particular times? There are common areas of the problems,

however, which enable one to consider application of some of the techniques described in the literature.

It was concluded previously that the initial estimate of the time-dependent waveform should be made on the ramp response waveform of the target. From a mathematical viewpoint it would seem that the ramp response waveform should be expanded in a set of functions, complete and orthogonal on the range 0 to ∞. The reason for this is that if it is assumed that the ramp response waveform $F_R(t')$ is square integrable

$$(32) \qquad \int_0^\infty |F_R(t')|^2 \, dt' < \infty \quad ,$$

and is expanded in an orthogonal series which is complete

$$(33) \qquad F_R(t') \simeq \sum_{n=0}^{N} A_n \phi_n(t') \quad ,$$

then

$$(34) \qquad \lim_{N\to\infty} \int_0^\infty \left| F_R(t') - \sum_{n=0}^{N} A_n \phi_n(t') \right|^2 dt' = 0 \quad .$$

Also, if $F_R(t')$ is continuous then

$$(35) \qquad \lim_{N\to\infty} \sum_{n=0}^{N} A_n \phi_n(t') = F_R(t') \quad .$$

In a great many cases it is reasonable to expect $F_R(t')$ to be continuous, since a jump discontinuity in $F_R(t')$ would mean a doublet in the impulse response waveform. The coefficients in such an expansion have the property of finality, an obvious advantage. The problem of course is in obtaining the coefficients A_n in the expansion. Formally, if the ϕ_n are assumed to be an orthonormal set then

$$A_n = \int_0^\infty F_R(t')\ \phi_n(t')\, dt' \qquad (36)$$

Note that one could therefore express estimates of the ramp response waveform obtained by any method in the form of Eq. (33).

Kautz[29] has described the conversion of polynomial sets which are orthogonal over a finite interval into exponential sets orthogonal over the semi-infinite interval $0 \leq x < \infty$. An advantage of this technique is that whereas simply transforming sets orthogonal over a finite interval into sets orthogonal over the semi-infinite interval leads to poles in the s plane equally spaced along the negative real axis,* the exponential set permits an arbitrary location of the poles. Assuming a set ϕ_n, orthonormal over the semi-infinite interval Kautz forms

---

* An exception is the Laguerre polynomials, orthogonal over the semi-infinite interval with weight e^{-2at}, which lead to a simple multiple order pole at $s = -a$[29].

$$(37)\qquad \phi_1(t') = \mathrm{Re}C_{11}\, e^{-s_1 t'}$$

$$\phi_2(t') = \mathrm{Re}C_{21}\, e^{-s_1 t'}$$

$$\phi_3(t') = \mathrm{Re}C_{31}\, e^{-s_1 t'} + \mathrm{Re}C_{32}\, e^{-s_2 t'}$$

$$\phi_4(t') = \mathrm{Re}C_{41}\, e^{-s_1 t'} + \mathrm{Re}C_{52}\, e^{-s_2 t'} + \mathrm{Re}C_{53}\, e^{-s_3 t'}$$

etc. ,

where the $s_k = \alpha_k + j\beta_k$ are arbitrary. From the orthonormal condition on the ϕ_n it is shown that the coefficients $C_{\nu\ell}$ can be determined and relatively simple computational techniques are given involving partial fraction expansions of the Laplace transform of the ϕ_n. From Eq. (36), taking as an example the third coefficient

$$(38)\qquad A_3 = \mathrm{Re}\int_0^\infty C_{31}\, e^{-s_1 t'}\, F_R(t')\,dt' + \mathrm{Re}\int_0^\infty C_{32}\, e^{-s_2 t'}\, F_R(t')\,dt' .$$

But from Eq. (5),

$$(39)\qquad \int_0^\infty e^{-st'}\, F_R(t')\,dt' = \frac{1}{c}\,\frac{G(s)}{s^2} .$$

Thus Eq. (38) becomes

$$(40)\qquad A_3 = \mathrm{Re}\,\frac{C_{31}}{c}\,\frac{G(s_1)}{s_1^2} + \mathrm{Re}\,\frac{C_{32}}{c}\,\frac{G(s_2)}{s_2^2} ,$$

or in general[29], A_n is replaced by the sum

$$(41) \qquad A_\nu = \sum_{\ell=1}^{n} \mathrm{Re}\, \frac{C_{\nu\ell}}{c} \; \frac{G(s_\ell)}{s_\ell^2} \quad .$$

Now if all the poles are chosen to lie equally spaced along the $j\omega$ axis ($s_k = j\beta_k$) then this configuration corresponds to a Fourier series in the time domain, and each orthonormal function of the set consists of a single sine or cosine term. Note that $G(j\beta_k)$ is the phasor response of the scatterer at the angular frequency β_k, a measurable quantity. For the special pole configuration leading to a Fourier series, the result is simply an alternative Fourier synthesis procedure. However, the pole locations (s_k) are arbitrary and one could choose unequally spaced imaginary poles or any desired combination of real and complex poles. For example, the above procedure could be used when calculated or measured values of the phasor response were available at nonharmonically related frequencies.* When only imaginary poles are utilized Kautz[29] (for equally spaced poles) suggests a predistortion of the response waveform

$$(42) \qquad F_R(t') = e^{+at'} F_R(t') \quad .$$

---

* A procedure for this situation was also suggested in Reference 30.

That is, the ramp response waveform is divided by $e^{-at'}$ before expansion and then multiplied by $e^{-at'}$ afterwards. This has the effect of multiplying the error bound as a function of time by $e^{-at'}$ [29]. Thus far it is clear that an analytical estimate of the ramp response waveform can be put in the form of an orthonormal expansion and that an initial orthonormal expansion estimate of the ramp response waveform can be obtained from calculated or measured data on the phasor response. It is also known[13] that such data should be predominantly low-frequency.

An attractive feature of an orthonormal expansion is that it automatically minimizes the rms error[29]. That is, if $F_R(t')$ is the actual ramp response waveform and $F_{RA}(t')$ an orthonormal approximation such as Eq. (33) then

$$(43) \qquad \epsilon^2 = \int_0^\infty [F_R(t') - F_{RA}(t')]^2 \, dt' \quad ,$$

becomes

$$(44) \qquad \epsilon^2 = \int_0^\infty F_R^2(t') \, dt' - \sum_{n=0}^{N} A_n^2 \quad .$$

From Parseval's theorem[20], Eq. (43) interpreted in the S domain is

$$(45) \qquad \epsilon^2 = \frac{1}{j\pi c^2} \int_0^{j\infty} \left| \frac{G(s) - G_A(s)}{s^2} \right|^2 ds \quad ,$$

where $G(s)$ corresponds to $F_R(t')$ and $G_A(s)$ to $F_{RA}(t')$. Equation (45) may also be written as

$$(46) \qquad \epsilon^2 = \frac{1}{\pi c^2} \int_0^\infty \left\{ \left[\frac{\Delta_r(j\omega)}{\omega^2} \right]^2 + \left[\frac{\Delta_i(j\omega)}{\omega^2} \right]^2 \right\} d\omega \quad ,$$

where

$$\Delta(j\omega) = \Delta_r(j\omega) + j\Delta_i(j\omega) = G(j\omega) - G_A(j\omega) \quad .$$

Regardless of how the approximation of the ramp response is obtained, an estimate of the rms error can be obtained from phasor response data. How good an estimate of the rms error one can obtain clearly depends on the extent and nature of the phasor response data. In any practical situation, at most a band limited knowledge of the phasor response may be known and Eq. (46) becomes

$$(47) \qquad \tilde{\epsilon}^2 = \frac{1}{\pi c^2} \int_0^{\omega_f} \left\{ \left[\frac{\Delta_r(j\omega)}{\omega^2} \right]^2 + \left[\frac{\Delta_i(j\omega)}{\omega^2} \right]^2 \right\} d\omega \quad ,$$

where ω_f is the cut-off frequency of the band-limited phasor response. Note that if in the range $0 \le \omega \le \omega_f$, the maximum value of $\Delta(j\omega)/\omega^2$ occurs at ω_p then

$$(48) \qquad \tilde{\epsilon}^2 \le \frac{1}{\pi c^2} \left| \frac{\Delta(j\omega_p)}{\omega_p^2} \right|^2 \omega_f \quad .$$

Both $F_R(t')$ and $F_{RA}(t')$ must be causal time functions, therefore Eq. (47) may be written as[20] *

$$(49) \qquad \tilde{\epsilon}^2 \simeq \frac{2}{\pi c^2} \int_0^{\omega_f} \left[\frac{\Delta_r(j\omega)}{\omega^2}\right]^2 d\omega \simeq \frac{2}{\pi c^2} \int_0^{\omega_f} \left[\frac{\Delta_i(j\omega)}{\omega^2}\right]^2 d\omega \quad ,$$

and in the notation of Eq. (48),

$$(50) \qquad \tilde{\epsilon}^2 \leq \frac{2}{\pi c^2} \left[\frac{\Delta_r(j\omega_p)}{\omega_p^2}\right]^2 \omega_f = \frac{2}{\pi c^2} \left[\frac{\Delta_i(j\omega_p)}{\omega_p^2}\right]^2 \omega_f \quad .$$

In a great many practical cases, only data on the radar cross section are available. One possible method for securing an error estimate, not of the waveforms themselves but of the waveforms convolved with themselves, can be given.

It can be shown that if a ramp response waveform is convolved with itself, i. e., the autocorrelation of the ramp waveform, the resultant waveform is given by

$$(51) \qquad F_{RR}(t') = \frac{1}{c} \mathcal{L}^{-1} \left\{ \left| \frac{G(j\omega)}{\omega^2} \right|^2 \right\} = \frac{1}{\pi c} \mathcal{L}^{-1} \left\{ \frac{\sigma(j\omega)}{\omega^4} \right\} \quad .$$

---

* Equation (49) actually only holds for $\omega_f = \infty$, but for the present case, i. e., $G(s)/s^2$, it is felt to be a reasonable approximation for finite ω_f.

Thus forming the error measure

$$(52) \qquad \epsilon_o^2 = \int_0^\infty [F_{RR}(t') - F_{RRA}(t')]^2 \, dt' \quad ,$$

and

$$(53) \qquad \tilde{\epsilon}_o^2 \simeq \frac{1}{\pi c} \int_0^{\omega_f} \left[\frac{\sigma(j\omega) - \sigma_A(j\omega)}{\omega^4} \right]^2 d\omega \quad .$$

Data on the phasor response or radar cross section are usually given as a function of an electrical length, say $k\ell$. The equivalent expression for Eq. (53) is

$$(54) \qquad \tilde{\epsilon}_o^2 = \frac{2}{\pi c} \int_0^{2(k\ell)_f} \left[\frac{\sigma(2k\ell) - \sigma_A(2k\ell)}{(2k\ell)^4} \right]^2 d(k\ell) \quad ,$$

where $t_o = 2\ell/c$ is set equal to unity. Note that the error estimates given above are applicable to any approximation of the ramp response waveform. They are not confined to orthogonal expansions of the response. Also, similar expressions involving the step and impulse response waveforms of the target can be obtained with the restriction that these waveforms be real, causal, and square integrable. It is possible therefore to obtain an estimate of the rms error for a given approximation and deduce from this when further modifications of the model are not justified. Such a gauge is important in that there are

really three approximation problems to be solved, sequentially the ramp, step and impulse response waveforms of the object, and one must economize the treatment of the preliminary steps.

Simply stated, the suggested approach to the approximation problem is as follows: From a combination of theoretical estimates and experimental data, a basic model of the ramp response waveform is obtained. This is a low-frequency model and the number of parameters involved should be minimized consistent with obtaining an rms error of possibly 5 to 10 percent. The model is then interpreted as a step response waveform (differentiation), additional parameters added and an rms error of again 5 to 10 percent achieved. Note at this point that two simultaneous conditions must be satisfied by the added parameters. A specified minimum error in the step waveform is sought but at the same time the ramp response error must be maintained. Proceeding to the impulse response waveform, additional parameters are once again included. At this point it is desired to build into the model all available information. That is, approximate or asymptotic high frequency estimates of the reflected and diffracted fields, natural points of discontinuity or rapid change of the response corresponding to geometrical or physical features of the object, high frequency experimental data, etc. There are now three conditions to satisfy, the ramp, step and impulse response error.

Realistically, it must be recognized that how meaningful these errors are depends upon the extent of the phasor response data available. A band-limited estimate of the area beneath the real and imaginary parts of the phasor response as a function of frequency clearly requires much more data than to estimate the area beneath these same curves divided by the frequency squared. The point is that a reasonable estimate of the integral in Eq. (49) might be obtained from a few properly distributed values of $\Delta_r(j\omega)$ or $\Delta_i(j\omega)$, but the corresponding integrals for the step and impulse error would require an increasing density of known values. The upper bound on the error given in Eq. (50) is somewhat conservative. Lacking sufficient data to estimate Eq. (49) directly, a more reasonable estimate than Eq. (50) would be to assume the average $\Delta_r(j\omega)/\omega^2$ or $\Delta_i(j\omega)/\omega^2$ to be independent of frequency. That is, given Q values of $\Delta_r(j\omega)/\omega^2$, let

$$\Delta = \frac{1}{Q} \sum_{n=1}^{Q} \frac{\Delta_r(j\omega_n)}{\omega_n^2} \quad , \tag{55}$$

then

$$\tilde{\epsilon}^2 \simeq \frac{2\Delta^2 \omega_f}{\pi c^2} \quad . \tag{56}$$

Since the ramp waveform is a low frequency estimate, a weighted sum

$$\Delta_w = \frac{1}{Q} \sum_{n=1}^{Q} \{1 - e^{-(\omega_f - \omega_n)}\} \frac{\Delta_r(j\omega_n)}{\omega_n^2} \quad , \tag{57}$$

might also be used. The choice depends upon both the cut-off frequency ω_f and the distribution of the data within this bandwidth.

If one is to use an orthonormal expansion to estimate the response waveform, the major problem is to select the proper set of orthogonal functions. Strictly speaking, this involves the pole locations of the orthonormal expansion and hence the natural resonances of the transient. That is, the optimum location of the poles is at the natural resonances of the scattering object. The flexibility of the orthogonal exponentials of Kautz[29], described earlier, have an advantage in this regard since the pole locations may be arbitrarily specified. However, unless all the specified poles have negative, non-zero real parts, the orthogonal functions do not have the necessary decaying behavior with large time and a predistortion would be required. The set of orthonormal Laguerre polynomials have a decaying behavior for large time, but correspond to a single multiple order real pole[29]. It can be shown that if a given time function is expanded in a set of orthonormal Laguerre polynomials, the coefficients in the expansion are a linear combination of the coefficients of a power series expansion of the corresponding frequency domain function about the real pole. Thus such an expansion eliminates the possibility of directly determining the expansion coefficients in terms of measured phasor response data. It is not possible, at this point,

to recommend one particular set of orthogonal functions for expansion of the response waveforms. There are numerous possibilities[29], and perhaps the most expedient procedure would be to compare expansions for several known ramp response waveforms[13] . Note that the objective is not a selected set for each individual scatterer but rather one particular set which has a reasonable applicability to numerous objects. Assuming that a particular orthonormal set has been selected, logical procedures for estimating the ramp response waveforms of an object can be postulated.

An initial estimate of the ramp response waveform can be secured in several ways; the Fourier synthesis procedure using experimental data and an analytical approach combining the physical optics approximation and the second moment condition as mentioned previously. It is not expedient to adopt the latter approach, precisely because of the necessity for selecting a specific functional form for the model. There is no reason, however, why one cannot simply sketch a curve for the ramp waveform utilizing exactly the same information, i. e. , physical optics, the geometry of the object, and the second moment. Such a possibility has been suggested previously[13] . Envisoned is some type of analog interplay with a digital computer whereby one could very rapidly, by trial and error, secure a ramp waveform similar to that predicted by physical optics over

most of the illuminated region of the target, which had the proper net area, and which agreed with experimental data. It must be stressed that the anticipated estimate of the ramp waveform is a simple, continuous curve with at most possibly three significant zero crossings.* Thus either from a Fourier synthesis of experimental data or the above described sketched estimate, a first model for the ramp response waveform is secured. The model is simply a curve in graphical form, and is not described analytically. This model can now be approximated by an orthonormal expansion, the integrations in Eq. (36) being approximated using digital computer techniques. The fact that a time-limited model for the ramp response waveform is used makes this approach feasible. One also sees the advantage of using one orthonormal set for at least a class of objects; the orthonormal functions need only to be calculated once, over an initial time range, at suitable increments.

The second moment condition introduces a constraint on the coefficients. Let $\Phi_n(s)$ be the Laplace transform of $\phi_n(t)$, from Eqs. (15) and (36)

---

* A complicated (in terms of geometrical or physical properties) target may have a ramp waveform with more than three significant zero crossings, but a first estimate of this waveform would probably not recognize this fact.

$$(58) \qquad \sum_{n=0}^{N} A_n \Phi_n(0) = \frac{-K\, t_o^2}{(2\pi)^2\, c}$$

Other constraints may also be introduced, for example

$$(59) \qquad G(S_i) = c\, S_i^2 \sum_{n=0}^{N} A_n \Phi_n(S_i)$$

relating calculated or measured data at a specific frequency to the expansion coefficients, or

$$(60) \qquad F_R^m(t_i') = \sum_{n=0}^{N} A_n \phi_n^m(t_i') \qquad m = 0, 1, 2, \cdots ,$$

whereby the ramp response or its derivatives is constrained to a specific value at a fixed time. It is not clear at this point which constraints should be utilized, aside from that in Eq. (58), or at what point in the development they should be introduced. Note that the type of constraint in Eq. (60) is an obvious way to introduce into the model both a knowledge of the arrival time of diffracted fronts and asymptotic estimates of their value. When constraints on the orthonormal expansion are introduced, minimization of the rms error in Eq. (43) requires the use of a Lagrange multiplier. A generalized method for the case of several constraints of the form of Eq. (60), yielding the Lagrange multipliers and the new expansion coefficients has been given[29].

A systematic procedure for progressing beyond the ramp response waveform, i. e. , to the step and impulse response, is more difficult to formulate. The first estimate of the step response (adding M terms to the ramp model)

$$(61) \qquad F_U(t') = \sum_{n=0}^{N+M} A_n \phi'_n(t')$$

has M undetermined coefficients. The constraint in Eq. (58) must now be imposed on the N+M coefficients. It need not have been imposed explicitly on the N coefficients of the initial ramp waveform since the sketched or synthesized ramp response satisfied the second moment. The form of solution with the constraint requires that the M added coefficients be calculated without the constraint and then a new set of N+M coefficients be computed. Therefore M adjustments on the step response waveform can be made. That is, the corrected step waveform is

$$(62) \qquad F_U(t') = \sum_{n=0}^{N+M} \bar{A}_n \phi'_n(t') \,,$$

where

$$\bar{A}_n = A_n + \lambda \Phi_n(0)$$

and

$$\lambda = \frac{-\sum_{n=0}^{N+M} A_n \Phi_n(0)}{\sum_{n=0}^{N+M} \Phi_n^2(0)}$$

The problem is in calculating the M new coefficients without the constraint. It is these coefficients which are to add the necessary additional detail to the step waveform. Given sufficient phasor response data to estimate the rms error in the step response waveform in Eq. (61), the new parameters could be adjusted to reduce this error. Lacking such data, two alternatives are seen. The first is to incorporate certain theoretical estimates of the step response detail into a revised sketch of the waveform and then proceed as with the ramp model to calculate the coefficients. New coefficients would then be computed as in Eq. (62). The second alternative is to incorporate additional constraints of the form in Eq. (60), calculate the additional unconstrained coefficients from the ramp model, and then solve for the new coefficients subject to the constraints. When more than one constraint is introduced, a system of linear equations must be solved to determine the Lagrangian multipliers. Essentially the same problems and alternatives exist in going to the impulse response waveform. In this case one should not attempt to incorporate

into the model delta function or higher order singularities in the waveform, since these can be added independently.

An attempt has been made, in the preceding pages, to outline a systematic general procedure for estimating the canonical response waveforms in a transient electromagnetic scattering problem. The effective integration of analytical and experimental data into a single model is stressed, along with an orderly, predictable method for determining the parameters of the model. The use of orthonormal expansions of the response waveform estimates has been suggested, and certain advantages of such an approach discussed. The feasibility of the approach has not been demonstrated, and hinges primarily on the availability of a set of functions, orthogonal and complete on the semi-infinite interval $(0, \infty)$, which will permit a reasonable estimate of the ramp waveform with just a few terms. Two sets, orthogonal exponentials and Laguerre polynomials, satisfying the orthogonality and completeness criteria have been suggested, but their applicability has not been shown. No claim is made that the suggested attack on the problem represents an optimum procedure, and it is evident that future research should investigate not only orthonormal expansions but other possible approaches.

One rather important conclusion can be drawn from the discussion in this section. For any given combination of theoretical estimates and experimental data, the best hope for achieving a waveform estimate which closely approximates the true object response lies with the ramp response waveform. Corresponding estimates of the step and impulse response waveforms will be less exact, if derived from limited theoretical and experimental data.

CHAPTER II
THE ELECTROMAGNETIC BACKSCATTERING BY A PERFECTLY CONDUCTING PROLATE SPHEROID

The investigation of scalar and vector boundary value problems in general ellipsoidal coordinates, and more particularly in the degenerate cases of prolate and oblate spheroidal coordinate systems, has been a favorite of the mathematical analysist for almost nine decades. Flammer[32] in his "Spheroidal Wave Functions" gives an excellent historical survey of the main contributions to the development of the spheroidal wave functions and the applications of these functions to various boundary value problems. More recently, Sleator[33] has reviewed the analytical and experimental contributions to the acoustical and electromagnetic scattering by prolate and oblate spheroids. It is vividly evident in this latter work that despite the long history of interest in the subject, very few numerical results have been obtained for the vector problems. The reasons for this are discussed by both Flammer and Sleator, and are briefly reviewed below. The point, however, is that a good approximate general solution to the plane wave scattering by spheroids has not been obtained

even in a formal sense. Those approximate solutions which are amenable to computation, even with modern high speed digital computers, are limited either to a particular range of the spectrum or to specific orientations of the spheroid.

Recently, solutions for the scattering from conducting spheroids have been reported by Andreasen[34] , Oshiro[35] , and by Waterman[36]. These results, while differing somewhat in specifics, are essentially all applications of the "point matching" approach to electromagnetic scattering problems. As such, there is a practical limitation imposed by the size of present electronic computers and the costs involved on the maximum spheroid size which can be handled successfully. Estimates of the maximum size which can be handled vary, and much depends upon what one considers reasonable in terms of computer running time. For example, Waterman[36] reports a running time of two hours on an IBM 7030 computer to compute the scattering pattern of a 2:1 prolate spheroid with a minor circumference of 10 wavelengths. In any event, such solutions must be supplemented by approximate high frequency methods to cover the entire spectrum. A most useful application of these "point matching" solutions for spheroid targets would be the computation of sufficient phasor response data at harmonically related low frequencies to generate the ramp response waveform for specific orientations via Fourier synthesis.

In this Chapter, an approximate general solution for the electromagnetic backscattering by a perfectly conducting prolate spheroid is derived using time domain concepts. The formulas obtained hold for arbitrary orientation and axial ratio of the spheroid and for arbitrary linear polarization of the incident plane electromagnetic wave. These results have the extremely attractive feature that calculations using the derived formulas are quite simple, involving nothing more complicated than exponential functions.

The major difficulty in obtaining a rigorous solution of the plane wave scattering by spheroids is that the vector wave equation is not separable in either oblate spheroidal or prolate spheroidal coordinates[32]. Specifically, what goes wrong for the prolate spheroid can be seen from a consideration of the simplest case, that of a plane electromagnetic wave incident along the major axis of a perfectly conducting prolate spheroid. This is the problem which was considered by Schultz[37] . As shown by Schultz[37] , the incident field can be expanded in an infinite series of vector spheroidal wave functions. An expansion for the scattered field as the sum of two infinite series of vector spheroidal wave functions can also be devised, and such an expansion properly is a solution of the vector Helmholtz equation, has zero divergence, and satisfies the radiation condition at infinity. However, in attempting to satisfy the boundary conditions at the

spheroid surface it is found that the field cannot be resolved into components such that individual terms in the series can satisfy the boundary conditions. This difficulty arises for two reasons: (1) the angle functions have different indices in the expansion of the incident and scattered fields, and (2) the scale factors involved in the definition of the vector spheroidal functions appear explicitly in the expansions. In the classical solution of the sphere, the angular dependence is the same term by term in the expansions of the incident and scattered fields. Therefore one can utilize the orthogonality of the angular functions to obtain equations relating the coefficients of the expansions of the incident and scattered fields. For the spheroid, this cannot be done, i. e. , the known and unknown coefficients cannot be related for a finite number of summation indices. It is at this point that the rigor of Schultz's solution is lost since an infinite system of equations for the infinite set of coefficients must be truncated to obtain a solution for the expansion coefficients of the scattered field.

Although, as related by Sleator[33] , certain advances have been made in the approximate or asymptotic theories for high and low frequencies, the returns from the numerous studies of the problem have been woefully meager. The situation is summarized (prior to the "point matching" results) by Sleator[33] as follows:

> "Since the work of Schultz[37] and the computations based on this by Siegel, et al.[38] , virtually no progress has been made in the solution of the vector problem in the resonance region. All existing techniques either break down completely or become prohibitively difficult or tedious in this region, and the need for a totally new approach becomes more and more apparent. "

It is to this new approach that the work in this Chapter is directed. The new approach is an application of the time domain concepts discussed in Chapter I. The application of these concepts is in its infancy, i. e. , a new approach to electromagnetic scattering problems is being developed, and the approach is via a "model" rather than a sophisticated extension and application of a well-known technique. Consequently the treatment will be mathematically simple and the philosophy of an engineering approximation liberally applied. The goal of this study is the development of a general model for the electromagnetic backscattering by a perfectly conducting prolate spheroid for arbitrary orientation and axial ratio and arbitrary linear polarization of the incident field. What is sought is an estimate of the response waveform of the target capable of yielding a reasonable approximation of the scattered field for a variety of orientations,

polarizations, and frequencies. A precise determination of the model for one fixed combination of these parameters is not intended.

The first section of this Chapter briefly reproduces a solution for the axial impulse response waveform of the spheroid published by Moffatt and Kennaugh[11] in 1965. The reason for the inclusion of this result is two-fold; first, much of the study for the general case is predicated on retaining the essential character of the axial waveform, and second, the axial result is intimately related to the response waveform of a sphere, an understanding of which is essential for later discussions of the spheroid waveforms.

With this background a basic general model for the impulse response waveform of the spheroid is then derived and calculated results from this model compared with measured data on a 2:1 axial ratio spheroid and calculated data (axial) for a 10:1 spheroid. The Chapter concludes with a discussion of these results and the applicability of the basic model for spheroids with other axial ratios.

In Appendix II, that portion of the sphere impulse response waveform corresponding to the creeping wave is examined in some detail. This digression to the sphere is used to illustrate the basic nature of the creeping wave contribution in the time-domain. The creeping wave contributions predicted by high-frequency asymptotic

solutions are analyzed and certain inconsistencies resulting from their non-causal nature discussed.

A. The Axial Impulse Response Waveform

Consider the perfectly conducting sphere and the related perfectly conducting prolate spheroid with an n to 1 axial ratio shown in Fig. 6. The spheroid has a semiminor axis equal to the sphere radius

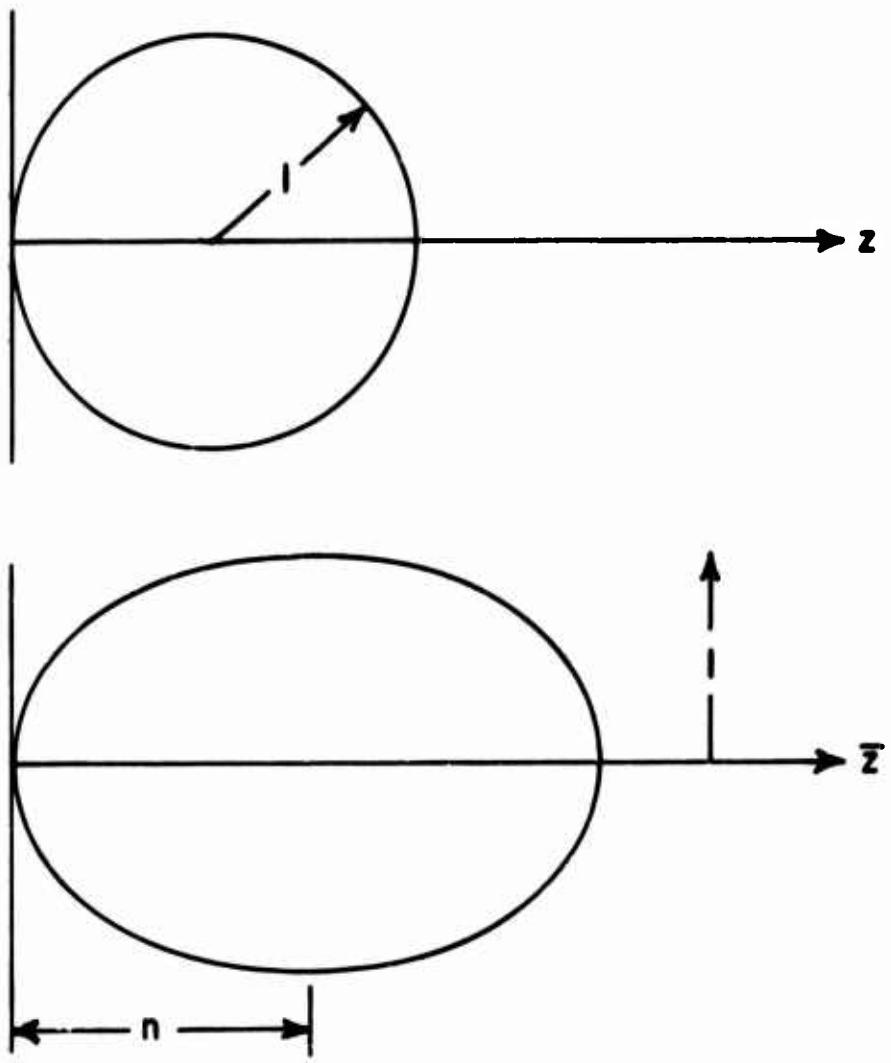

Fig. 6--Sphere and prolate spheroid geometries.

which is taken as unity. Let the sphere and spheroid be illuminated by a ramp type excitation propagating in the z and $\bar{z}$ directions respectively.

(63) $$E(t') = t'\,u(t')$$

$$E(\bar{t}') = \bar{t}'\,u(\bar{t}') \quad ,$$

where $t' = t - z/c$ and $\bar{t}' = t - \bar{z}/c$.

Now if the axial ratio of the spheroid is unity, clearly the response waveforms will be identical for the sphere and spheroid. This, of course, is true for any excitation. As the axial ratio of the spheroid is increased (n > 1) differences in the sphere and spheroid response waveforms will occur. The basis for the approximate spheroid response waveform derived in this section is the assumption that the ramp response waveform of the spheroid can be obtained by simply a change in the time scale of the sphere ramp response waveform. Since the step and impulse response waveforms may be obtained by successive differentiations of the ramp response waveform, a change in time scale for the ramp response waveform results in a change in amplitude as well as time scale for the step and impulse response waveforms. To a first approximation at least, the ramp response waveform of the spheroid undergoes only a time scale change as can be shown in two ways.

For the sphere, using Eq. (24) of Chapter I, the response waveforms predicted by the physical optics approximation are

$$(64)\qquad F_R(t') = \left[-\frac{t_o t'}{2} + \frac{t'^2}{4}\right]\left[u(t') - u(t'-t_o)\right]$$

$$F_U(t') = \left[-\frac{t_o}{2} + \frac{t'}{2}\right]\left[u(t') - u(t'-t_o)\right]$$

$$F_I(t') = -\frac{t_o}{2}\,\delta(t') + \frac{1}{2}\left[u(t') - u(t'-t_o)\right] \quad ,$$

and those for the spheroid are

$$(65)\qquad \bar{F}_R(\bar{t}') = \left[-\frac{t_o \bar{t}'}{2n} + \frac{\bar{t}'^2}{4n^2}\right]\left[u(\bar{t}') - u(\bar{t}'-nt_o)\right]$$

$$\bar{F}_U(\bar{t}') = \left[-\frac{t_o}{2n} + \frac{\bar{t}'}{2n^2}\right]\left[u(\bar{t}') - u(\bar{t}'-nt_o)\right]$$

$$\bar{F}_I(\bar{t}') = -\frac{t_o}{2n}\,\delta(\bar{t}') = \frac{1}{2n^2}\left[u(\bar{t}') - u(\bar{t}'-nt_o)\right] \quad ,$$

where $t_o = 2a/c$, and a bar has been used to denote the spheroid waveforms. If, in the expression for the ramp response waveform of the sphere the substitution $t' = \bar{t}'/n$ is made then the ramp response waveform of the spheroid is obtained. Obviously successive differentiation leads to the correct physical optics step and impulse responses. Note that the same change in time scale in the step or impulse response of the sphere does not yield the spheroid physical optics result. It is concluded therefore that insofar as the physical optics approximation

is concerned it is the ramp response waveform which undergoes only a time scale change.

A second argument for only a time scale change in the ramp waveform is provided by the moment conditions; specifically the second moment which relates the area beneath the ramp response waveform and the Rayleigh coefficient of the target. The approximate axial ramp response waveform of the spheroid according to this assumption is obtained by a linear deformation of the time axis in the illuminated region and a nonlinear deformation in the shadowed region. Corresponding ordinates on the ramp response waveforms for the sphere and spheroid are defined by equal cross sections in a plane perpendicular to the line of sight. Corresponding abscissa are defined by the shortest ray path to the given cross section following the line of sight to the shadow boundary and the scatterer surface beyond.

Thus setting

$$\bar{F}_R(\bar{t}') = F_R(t') \,, \tag{66}$$

and differentiating

$$\bar{F}_U(\bar{t}') = F_U(t') \frac{dt'}{d\bar{t}'} \tag{67}$$

$$F_I(t') = F_I(t') \left[\frac{dt'}{d\bar{t}'}\right]^2 + F_U(t') \frac{d^2t'}{d\bar{t}'^2} \,.$$

$$t' = \begin{cases} z & 0 \le t' \le t_o \\ t_o + \int_1^z \dfrac{2x\,dx}{\sqrt{2x - x^2}} & t_o \le t' \le t_o S \end{cases}$$

(68)

$$\bar{t}' = \begin{cases} \bar{z} & \bar{z}t_o \le \bar{t}' \le nt_o \\ nt_o + \dfrac{t_o}{n} \displaystyle\int_n^{\bar{z}} \frac{\sqrt{(x^2-2nx)(1-n^2) + n^2}}{\sqrt{2nx-x^2}}\,dx & nt_o \le \bar{t}' \le S't_o \,. \end{cases}$$

(69)

$$\frac{dt'}{d\bar{t}'} = \begin{cases} \dfrac{1}{n} & 0 \le t' \le t_o \\ \dfrac{1}{\sqrt{(z^2-2z)(1-n^2)+1}} & t_o \le t' \le t_o + S \,, \end{cases}$$

and

(70)

$$\frac{d^2t'}{d\bar{t}'^2} = \begin{cases} 0 & 0 \le t' \le t_o \\ \dfrac{(1-z)(1-n^2)\sqrt{2z-z^2}}{[(z^2-2z)(1-n^2)+1]^2} & t_o \le t' \le t_o + S \,, \end{cases}$$

where $S = \displaystyle\int_1^2 \frac{dx}{\sqrt{2x-x^2}}$, $S' = \frac{1}{n}\displaystyle\int_n^{2n} \frac{\sqrt{(x^2-2nx)(1-n^2)+n^2}}{\sqrt{2nx-x^2}}\,dx$.

An example of the spheroid ramp response waveform obtained in this way is shown in Fig. 7b for a prolate spheroid with a 2:1 axial ratio. The sphere ramp response waveform is shown in Fig. 7a. A graphical integration of the spheroid ramp response waveform shown in Fig. 7b

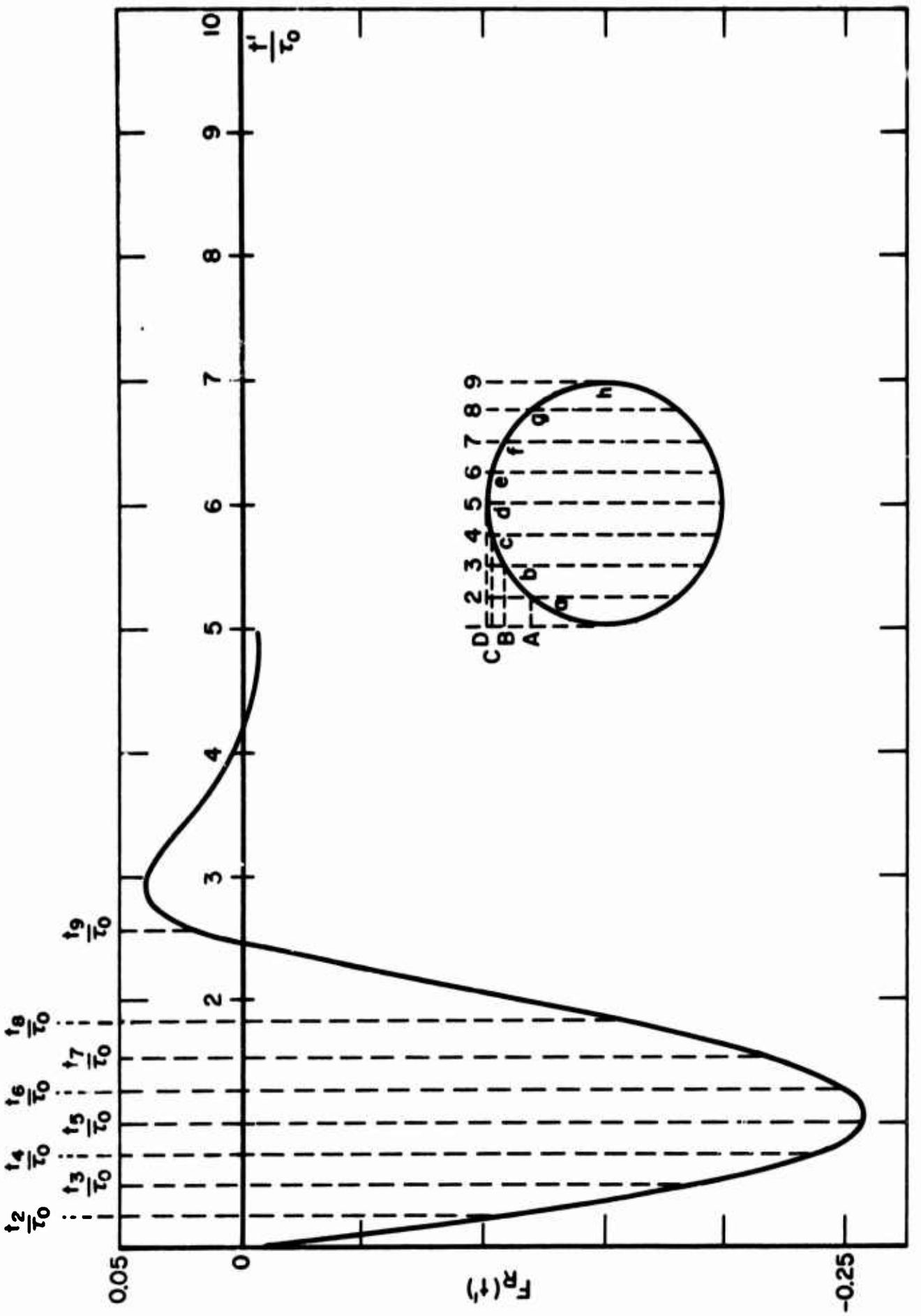

Fig. 7a--Normalized ramp response (axial) and associated geometry. Sphere.

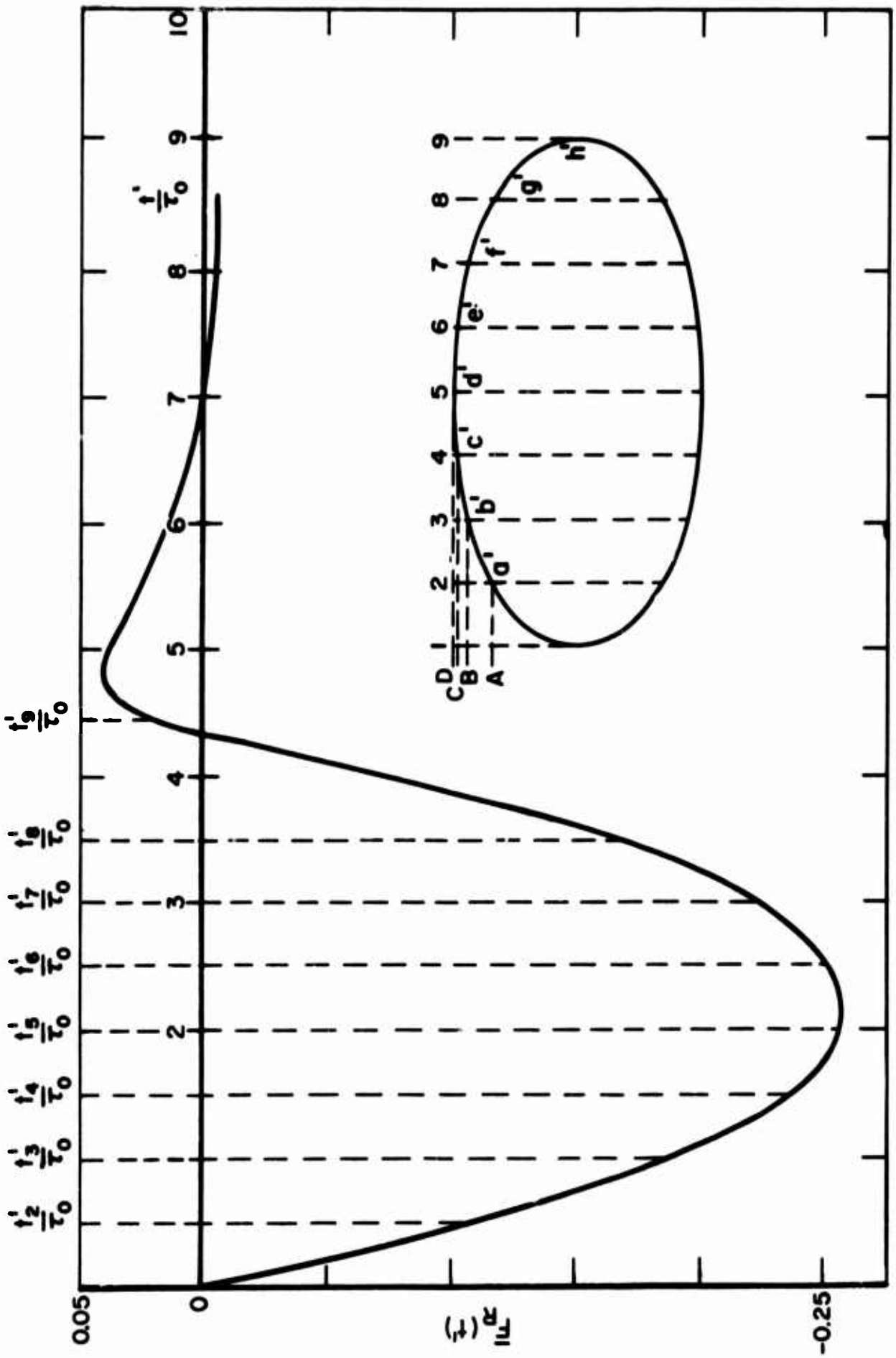

Fig. 7b--Normalized ramp response (axial) and associated geometry. Spheroid.

demonstrates that the second moment condition is approximately satisfied. A comparison of the Rayleigh coefficient obtained by graphical integration of the curve in Fig. 7b and that calculated in Appendix I shows an error of approximately 3 percent. Similar comparisons for axial ratios of 4, 6, 8, and 10 gave a minimum error of 1 percent (8:1) and a maximum error of 5 percent (4:1). No discernable trend of error versus axial ratio was observed. The ramp response waveform of the sphere (Fig. 7a) was obtained from the exact Mie solution using the Fourier synthesis procedure. The synthesis procedure is described in Reference 13. Thus both physical optics and the second moment condition (as do the two lower orders) support the assumption that the ramp response waveform of the spheroid is obtained from that of the sphere by a change in the time scale alone.

It is important to emphasize one point in the above results. The Fourier synthesis procedure used to obtain the approximate impulse, step and ramp response waveforms of the sphere does not yield analytical expressions for these waveforms, but only their magnitudes at selected values of time. The time increments are arbitrary so that the waveforms may be obtained to any accuracy desired (within the limitation of a finite pulse width), but only in the sense of a point by

point plot. Consequently the ramp, step and impulse response waveforms of the spheroid obtained by the above described method are also only point by point plots at arbitrary values of time.

A detailed development of the axial response waveforms of the spheroid is given in the 1965 publication by Moffatt and Kennaugh[11] . Shown in Fig. 8 (solid curve) is the impulse response waveform of a 2:1 axial ratio spheroid as obtained by a nonlinear transformation of the time scale for the ramp response waveform of the sphere. Also shown in Fig. 8 (dashed curve) is an analytical exponential sum approximation for the waveform. The Laplace transform of this exponential sum approximation was found to yield a satisfactory frequency-domain approximation for minor axis circumferences of the spheroid in wavelengths greater than 1. 5. For minor axis circumferences in wavelengths less than 1. 5 it was necessary to use convolution and an approximate integration of the derived ramp response waveform to obtain frequency domain data. A comparison of calculated and measured echo area for a 2:1 axial ratio spheroid is shown in Fig. 9. Data denoted as target motion are explained in Reference 11.

It has been shown that an approximate solution for the axial backscattering from a prolate spheroid may be obtained through a modification of the impulse response waveform of a spherical scatterer. Experimental verification of the results predicted was obtained for a

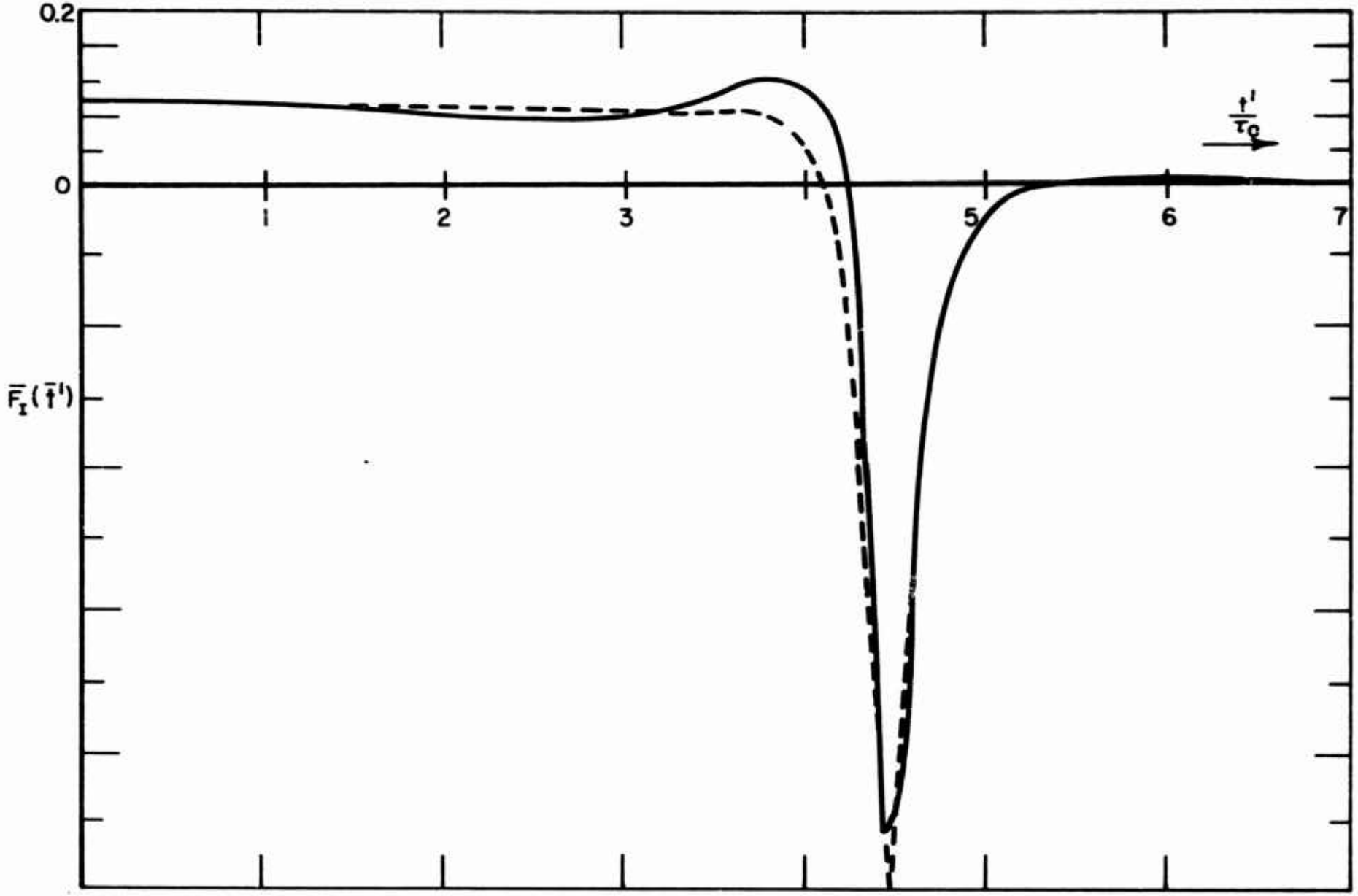

Fig. 8--Approximate impulse response waveform (axial) of 2:1 axial ratio prolate spheroid. Dashed curve is exponential sum approximation.

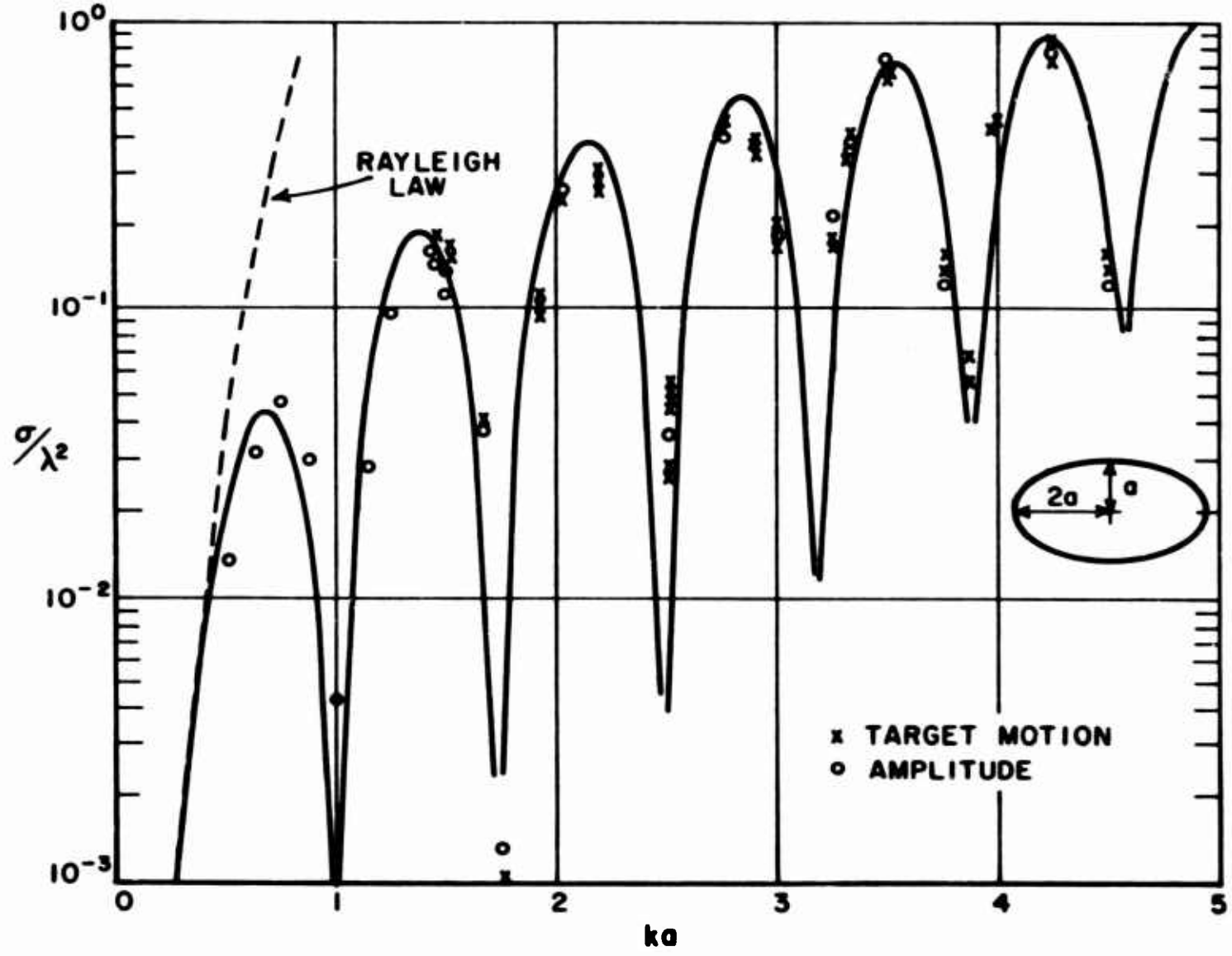

Fig. 9--Calculated (solid curve) and measured axial echo area of a 2:1 axial ratio conducting prolate spheroid.

prolate spheroid of 2:1 axial ratio. The method used employs a non-linear transformation of the time scale to obtain the ramp function response of the spheroid from that of the sphere. The method has not been applied to extremely large axial ratios and may require further corrections in such cases.

The model has a number of deficiencies which need to be studied further. First, for times after the impulsive excitation reaches the rear of the spheroid it was assumed that the time relations (Eqs. (69) and (70)) were the same as the first portion, corresponding to the excitation progressing on around the spheroid. This assumption, used primarily for lack of an alternative procedure, needs to be placed on a sound basis or a different technique devised. Second, it can be seen from Eqs. (67), (69), and (70), that the creeping wave peak predicted is independent of the spheroid axial ratio and equals, in all cases, that of the sphere; a questionable result. Both of these questions are related to the nature of the creeping wave on smooth convex surfaces. In Appendix II, some insight to this problem is gained from the time domain interpretation of asymptotic estimates of the creeping wave on spheres and circular cylinders. However, in this study the results in Appendix II have not been utilized to improve the axial model. In terms of the basic goal of this Chapter, that of a general model, two

results of this section are used. One, the fact that an exponential approximation of the creeping wave consisting of a join of two exponentials with finite slopes at the time of the creeping wave peak yielded reasonable results, and two, the fact that the magnitude of this creeping wave peak could, at least for a 2:1 axial ratio spheroid, be assumed to be independent of axial ratio.

B. A General Impulse Response Waveform Model

For the general problem, the prolate spheroid and the associated coordinates are shown in Fig. 10. The spheroid has a semiminor axis a and a semimajor axis b. The incident plane electromagnetic field is incident from a direction defined by the spherical angles θ and ϕ. Because of the rotational symmetry of the spheroid, the direction of propagation of the incident field can be restricted to lie in the y, z plane without loss of generality. With this restriction, two principal polarizations of the incident field are defined; T. E. , where the incident electric field vector is normal to the y, z plane, and T. M. , where the incident electric field vector lies in the y, z plane. Associated with each of the two principal polarizations is a path length corresponding to line of sight to the shadow boundary and a geodesic on the surface beyond. Note that these paths are measured from a

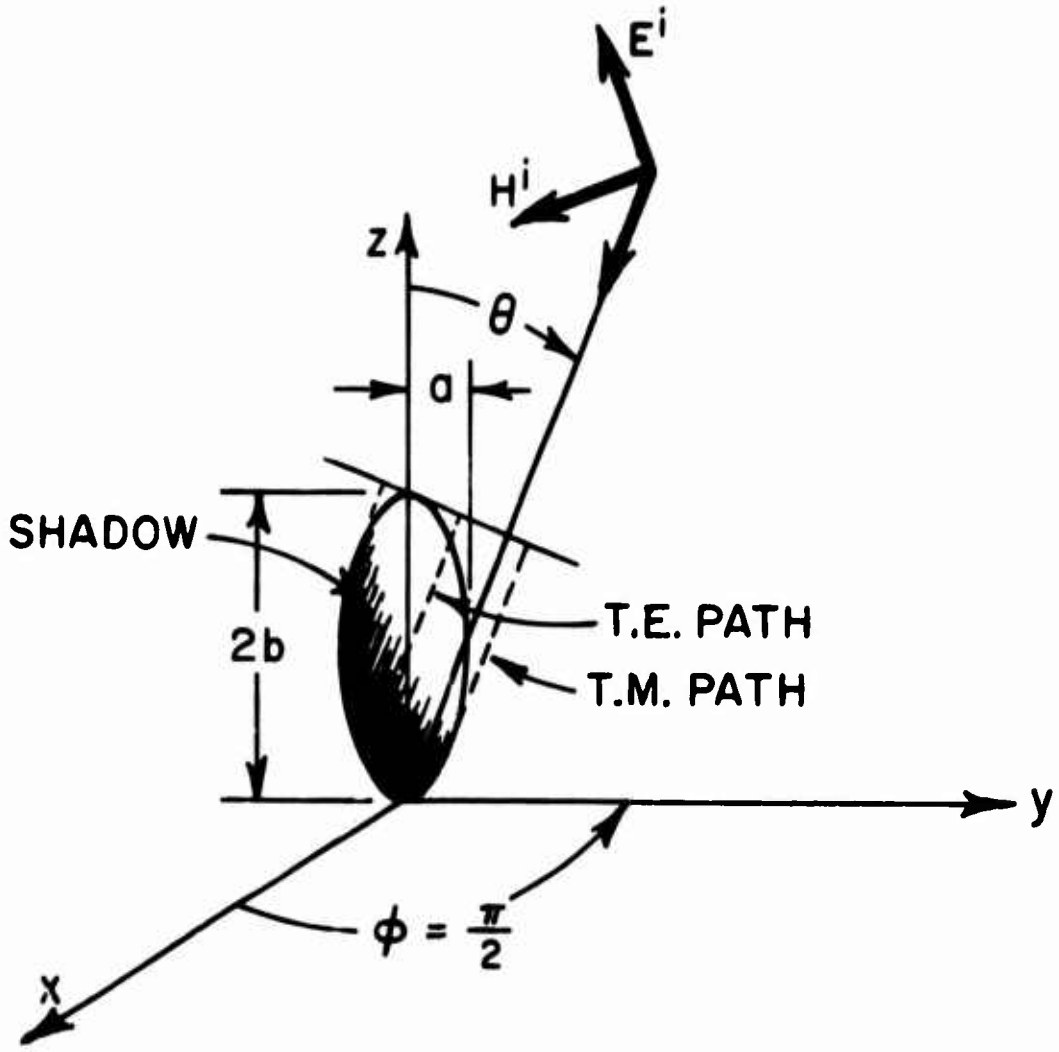

Fig. 10--The prolate spheroid and associated coordinates.

plane perpendicular to the line of sight, and located at the point where such a plane first touches the spheroid.

In an earlier study of the general prolate spheroid target[12] , the author derived an approximate spheroid model based on an approximation to the ramp response waveform of the target. The results of this initial study are of some interest; both as an example of how a very crude approximation in the time domain can yield reasonable

results in the frequency domain, and as a demonstration of the necessity for a well choosen impulse response model in order to achieve fine accuracy in the frequency domain. A general discussion of the derivation of transient and impulse response waveforms for a finite, three dimensional target was given in Chapter I; it is reiterated however that it is reasonable that the twice integrated function of a real variable be easier to approximate with fewer parameters than the function itself.

The above model for the prolate spheroid target was based upon an earlier study by Kennaugh[39] demonstrating that the ramp response waveform of a conducting sphere could be approximated quite well using very simple functions. In this approach, the ramp response waveform consists of the physical optics approximation to the shadow boundary and an amplitude proportional to the circumference of the section cut from the sphere surface by a plane moving along the line of sight with half the free space velocity beyond the shadow boundary. For those times after the plane moves beyond the sphere, this latter waveform is extended continuously and multiplied by an exponentially damped term whose magnitude is chosen to satisfy the second moment condition. The amplitudes of the above two sections are matched at the shadow boundary. The resulting approximation to the ramp response waveform of a conducting sphere of radius a is

$$(71) \qquad F_R(t') = \left[-\frac{t_o t'}{2} + \frac{t'^2}{4} \right] \left[u(t') - u(t'-t_o) \right]$$

$$- \frac{t_o^2}{4} \cos(t'-t_o) \left[u(t'-t_o) - u(t'-(1+\pi/2)t_o) \right]$$

$$- \frac{t_o^2}{4} e^{\sqrt{5}\,(t_o(1+\pi/2)-t')} \cos(t'-t_o)\, u(t'-(1+\pi/2)t_o) \quad .$$

Several salient features of this waveform should be noted. The first term in Eq. (71) is simply the physical optics approximation to the ramp response waveform. It was shown in Chapter I that this is simply proportional to the cross-sectional area intercepted by a transverse plane moving in the direction of the incident wave at half the free space velocity. The second term corresponds to the circumference of this cross-sectional area beyond the shadow. Note, however, that the times corresponding to these amplitudes are measured from the shadow along the surface of the sphere. Thus the circumference reaches zero at $t' = (1 + \pi/2)\, t_o$ rather than $2t_o$. As was shown by Kennaugh[39], this waveform is a rather good approximation to the ramp response waveform obtained by Fourier synthesis from the exact Mie solution and shown in Fig. 7a. As will be seen, however, such a waveform leads to certain difficulties where twice differentiated to obtain an impulse response waveform.

One can derive a similar approximation for the ramp response waveform of a prolate spheroid for the general off-axis case. Note that in this case a polarization-sensitive approximation is obtained because of the dependence of the second moment condition on the Rayleigh coefficient of the target, which is dependent on both the incident polarization and the orientation of the spheroid.* In order to secure a closed form expression for the ramp response waveform, certain simplifying approximations are made for the spheroid case. The first of these involves the point of termination, in time, of the physical optics approximation. For the sphere, the shadow boundary is always normal to the direction of propagation of the incident field. For the spheroid, however, this only occurs at axial and broadside ($\theta = 0$ and 90 degrees respectively in Fig. 10). At other orientations, the shadow boundary is not perpendicular to the line of sight. As a crude approximation, the shadow boundary was ignored and the physical optics approximation terminated at the peak transverse cross section encountered by the cutting plane. A second difficulty encountered is in the measurement of path lengths on the shadowed side of the spheroid. This is, for either polarization, a distance

---

* The Rayleigh dependence of prolate and oblate spheroids for arbitrary polarization and orientation and for arbitrary constitutive parameters is given in Appendix I.

along the perimeter of an ellipse, i. e., an incomplete elliptic integral. The circumference of the area cut from the surface by the cutting plane is also an ellipse. Again, in the interests of a simple closed form expression, the second portion of the waveform was crudely approximated by a shifted cosine wave whose period was determined by the creeping wave geodesic path, i. e., T. E. or T. M.. The ramp response waveform so obtained is given by

$$\overline{F}_R(t') = [-At' + Bt'^2/2]\left[u(t') - u\left(t' - \frac{A}{B}t_o\right)\right] - \frac{A^2}{2B}\cos\left[\beta\left(t' - \frac{A}{B}t_o\right)\right]\left[u\left(t' - \frac{A}{B}t_o\right) - u(t' - T_2 t_o)\right] - \frac{A^2}{2B}e^{\alpha(T_2 t_o - t')}\cos\left[\beta\left(t' - \frac{A}{B}t_o\right)\right]u(t' - T_2 t_o) \quad , \tag{72}$$

where

$$A = \frac{a\,b\,t_o}{2[b^2\cos^2\theta + a^2\sin^2\theta]} \quad ,$$

$$B = \frac{a^2\,b}{4[b^2\cos^2\theta + a^2\sin^2\theta]^{3/2}} \quad ,$$

$$\alpha = \left\{\frac{-\beta A^2/2B}{-\frac{A^3}{3B^2} - \frac{K}{2} - \frac{A^2}{2\beta B}} - \beta^2\right\}^{1/2}$$

and

$$\beta = \frac{\pi/2}{T_2 - \frac{A}{B}t_o} \quad .$$

The constants A and B are obtained from the physical optics approximation to the ramp response waveform. The constant α is determined from the second moment condition and K is the Rayleigh coefficient of the spheroid (Appendix I). The time T_2 is determined from the geometry of the spheroid and corresponds to a creeping wave path length, following the line of sight to the shadow boundary and a geodesic path on the spheroid beyond. Assuming that the circumference of the ellipse in the x, z plane may be expressed as

$$(73) \qquad C_{ir} = 2\pi \left| \sqrt{\frac{a^2 + b^2}{2}} \right| \quad ,$$

with negligible error, T_2 is given by

T. M. Polarization

$$(74) \quad T_2 = \frac{\sin\theta\cos\theta\,(b^2 - a^2)}{2\sqrt{a^2\cos^2\theta + b^2\sin^2\theta}} + \frac{1}{2}\sqrt{b^2\cos^2\theta + a^2\sin^2\theta}$$

$$+ \frac{\pi}{2}\sqrt{\frac{a^2 + b^2}{2}} + \frac{1}{2}\left| \frac{\sin\theta\cos\theta\,(b^2 - a^2)}{\sqrt{a^2\cos^2\theta + b^2\sin^2\theta}} - \sqrt{b^2\cos^2\theta + a^2\sin^2\theta} \right| ,$$

and

T. E. Polarization

$$(75)\quad T_2 = \frac{\sin^2\theta\cos^2\theta\ (b^2 - a^2)^2}{\sqrt{b^2\cos^2\theta + a^2\sin^2\theta}\,(b^2\sin^2\theta + a^2\cos^2\theta)} + \sqrt{b^2\cos^2\theta + a^2\sin^2\theta} + \frac{\pi}{2}\sqrt{\frac{c_1^2 + c_2^2}{2}}\ ,$$

where

$$C_1^2 = a^2\left[1 - \frac{\sin^2\theta\cos^2\theta(b^2 - a^2)^2}{a^2b^2} + \frac{\left\{\dfrac{\sin^2\theta\cos^2\theta(b^2 - a^2)(a^2 - b^2)}{a^2b^2\sqrt{b^2\cos^2\theta + a^2\sin^2\theta}}\right\}^2}{\dfrac{b^2\sin^2\theta + a^2\cos^2\theta}{a^2b^2}}\right]$$

and

$$C_2^2 = \frac{a^2b^2 - \sin^2\theta\cos^2\theta(b^2 - a^2)^2}{b^2\sin^2\theta + a^2\cos^2\theta} + \left[\frac{\sin^2\theta\cos^2\theta(b^2 - a^2)(a^2 - b^2)}{\sqrt{b^2\cos^2\theta + a^2\sin^2\theta}\,(b^2\sin^2\theta + a^2\cos^2\theta)}\right]^2.$$

In actual calculations in this study, the quarter circumference of an ellipse which appears in the T. M. case as

$$\frac{\pi}{2}\sqrt{\frac{a^2+b^2}{2}} \quad ,$$

and in the T. E. case as

$$\frac{\pi}{2}\sqrt{\frac{C_1^2+C_2^2}{2}} \quad ,$$

was computed using the polynomial approximation to the complete elliptic integral[40]

$$(76) \qquad C_{ir} = 4b\left\{1+a_1\left(\frac{a}{b}\right)^2+a_2\left(\frac{a}{b}\right)^4 + \left[b_1\left(\frac{a}{b}\right)^2+b_2\left(\frac{a}{b}\right)^4\right]\ell n\left(\frac{b}{a}\right)^2\right\} \quad ,$$

where $a_1 = 0.4630151$

$a_2 = 0.1077812$

$b_1 = 0.2452727$

$b_2 = 0.0412496$,

for an ellipse of major axis 2b and minor axis 2a. Note that for a unity axial ratio spheroid, Eq. (72) reduces to Eq. (71).

The ramp response waveform in Eq. (72) was used in Reference 12 by the author as the basic model for the conducting prolate spheroid. Calculations of the echo area of the spheroid using this model were compared with measured data on a 2:1 axial ratio spheroid. The comparison covered a frequency range from 1.5 to 5.0 minor axis circumferences in wavelengths in increments of 0.25 wavelenths and an aspect range of θ (Fig. 10) from 0° to 90° in increments of 10°, for both the T. E. and T. M. polarizations. Considering the crudeness of the ramp waveform model, the results of this comparison were quite good. An example of the type of agreement obtained is shown for an aspect angle θ of 40° in Figs. 11a and 11b for the T. E. and T. M. polarizations respectively. Note that the basic deficiency for both polarizations appears to be a constant shift of the maxima and minima of the calculated data with respect to the measured data. But, taking into account this shift, the calculated and measured periodicity and amplitudes are in fair agreement. It would serve no purpose here to duplicate all of the results obtained with this ramp response model. These are reported in detail in Reference 12 and the reader is referred to that publication.

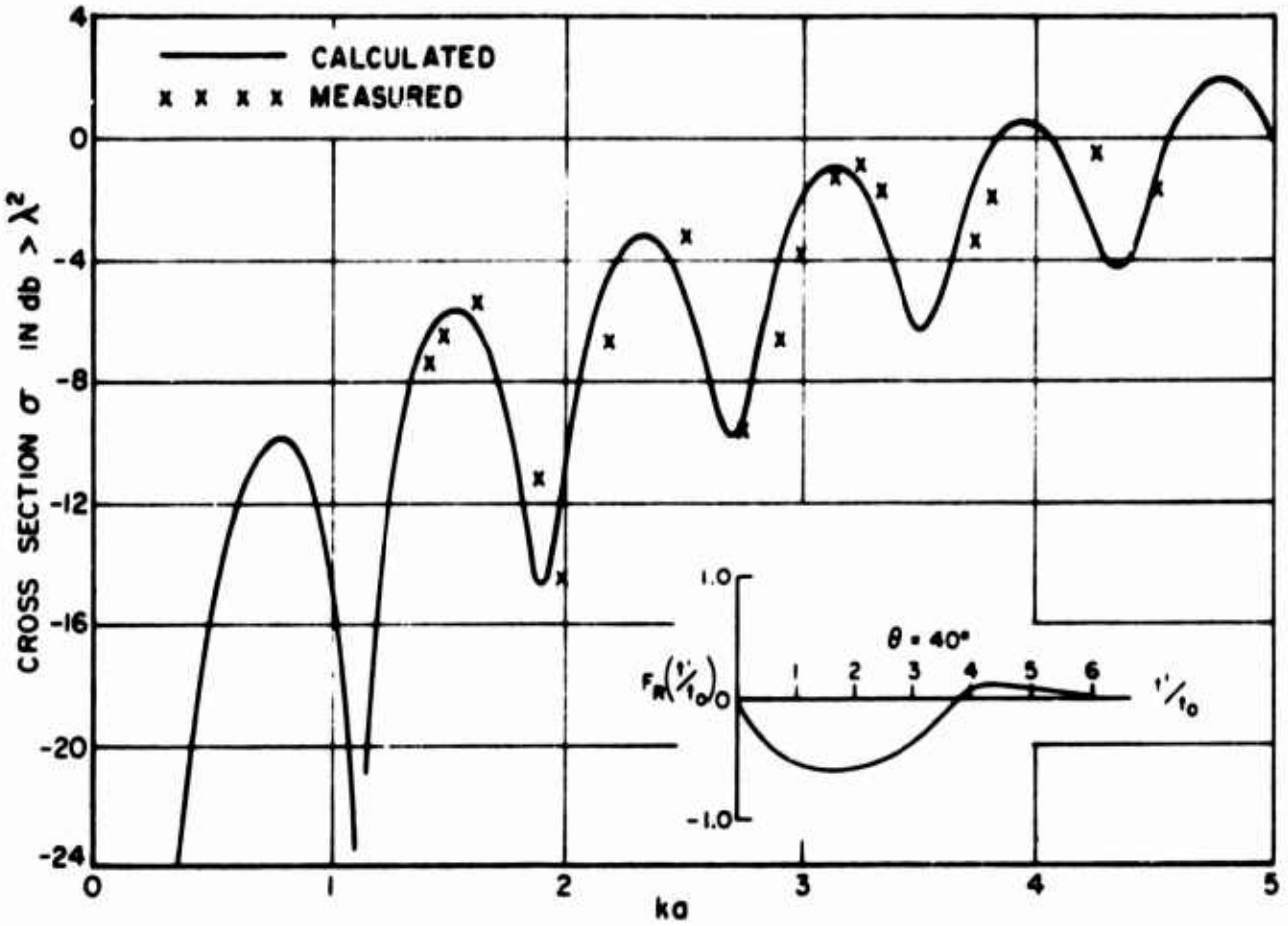

Fig. 11a--Calculated (solid) and measured echo area of a 2:1 axial ratio prolate spheroid. Ramp response model, T. E. polarization, $\theta = 40°$.

Aside from the specific calculations for the prolate spheroid targets, the results obtained with the crude ramp response model yielded two general conclusions. First, the study reported in Reference 12 was the initial attempt to extend the application of transient and impulse response approximations to a nonsymmetrical or off-axis target orientation. As such they were distinctly encouraging and lent real hope that other targets might be amenable to a similar attack.

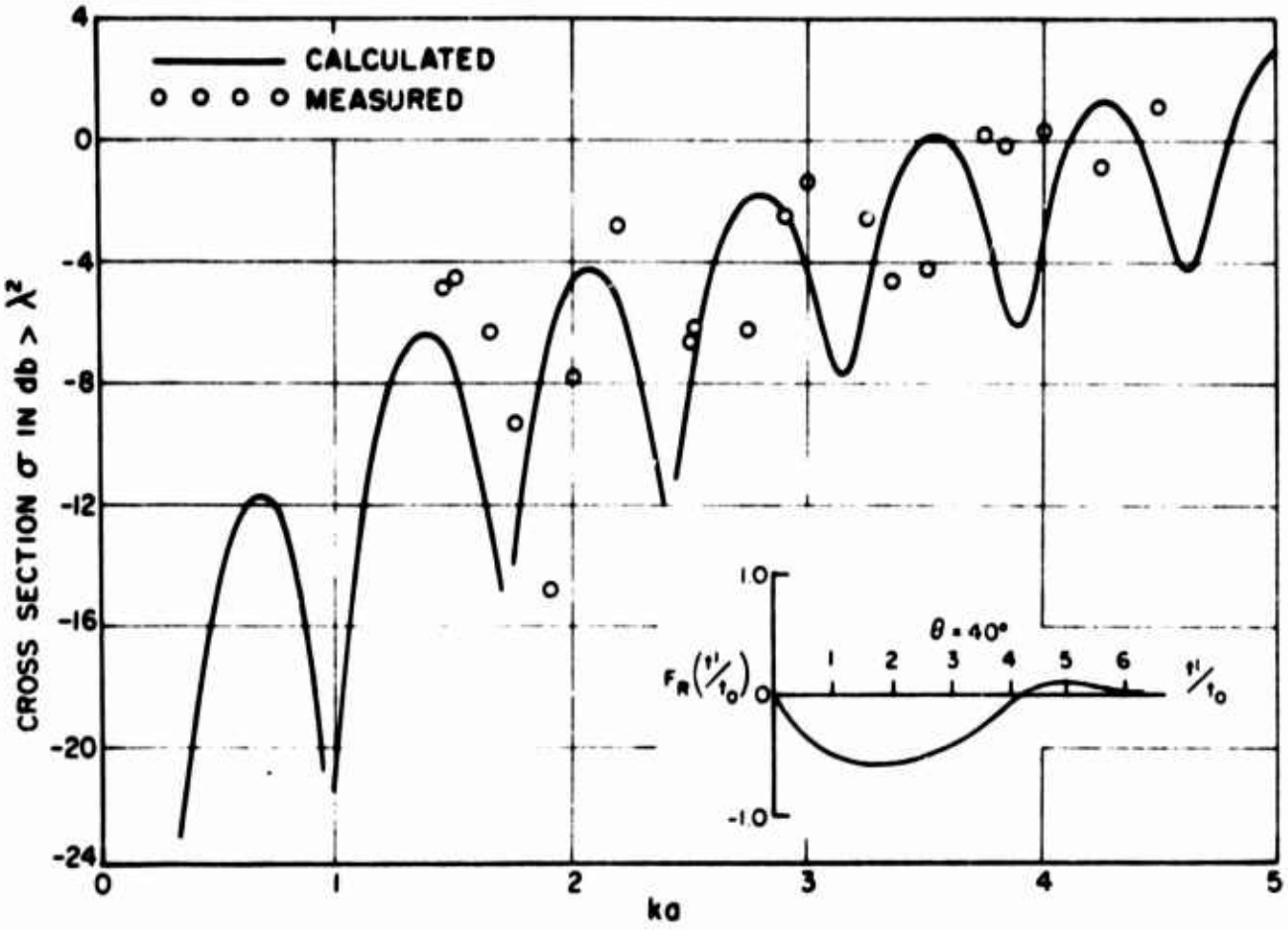

Fig. 11b--Calculated (solid) and measured echo area of a 2:1 axial ratio prolate spheroid. Ramp response model, T. M. polarization, $\theta = 40°$.

Second, it had been contended by E. M. Kennaugh and the author in 1965[13] that, with experience and intuition, one might ultimately be able to roughly sketch the ramp response waveform of a target from simply a consideration of physical optics, the target geometry and the low-frequency derived moment conditions. Noting that to this point, the above considerations were the only ones involved in deriving the ramp response waveform, it is felt that this premise

has been proved – and proved for a target which heretofore has stubbornly resisted even an approximate practical theoretical solution.

Two basic deficiencies can be noted with the ramp response waveform given in Eq. (72). These are most apparent from a consideration of the related impulse response waveform. Differentiating Eq. (72) twice with respect to time,

$$\begin{aligned}(77)\qquad \overline{F}_I(t') = -A\delta(t') + B\left[u(t') - u\left(t' - \frac{A}{B}t_o\right)\right] \\ + \frac{A^2\beta^2}{2B}\cos\left[\beta\left(t' - \frac{A}{B}t_o\right)\right]\left[u\left(t' - \frac{A}{B}t_o\right) - u(t' - T_2t_o)\right] \\ + \frac{A^2}{2B}(\beta^2 - \alpha^2)e^{\alpha(T_2t_o - t')}\cos\left[\beta\left(t' - \frac{A}{B}t_o\right)\right]u(t' - T_2t_o) \\ - \frac{A^2\alpha\beta}{B}e^{\alpha(T_2t_o - t')}\sin\left[\beta\left(t' - \frac{A}{B}t_o\right)\right]u(t' - T_2t_o)\quad .\end{aligned}$$

A rough sketch of the form of the impulse response waveform in Eq. (77) is shown in Fig. 12. From a knowledge of the axial impulse response waveform in Section A and the nature of the creeping wave in Appendix II, it is clear that the impulse response waveform in Eq. (77) has two primary faults. First, the erroneous jump occuring at $t' = A/B\ t_o$, and second the form of the response waveform at the creeping wave peak (T_2t_o). In the first case, there is no evidence that in the neighborhood of the shadow boundary a discontinuity should occur in the waveform. The axial model (Section A) predicts a smooth

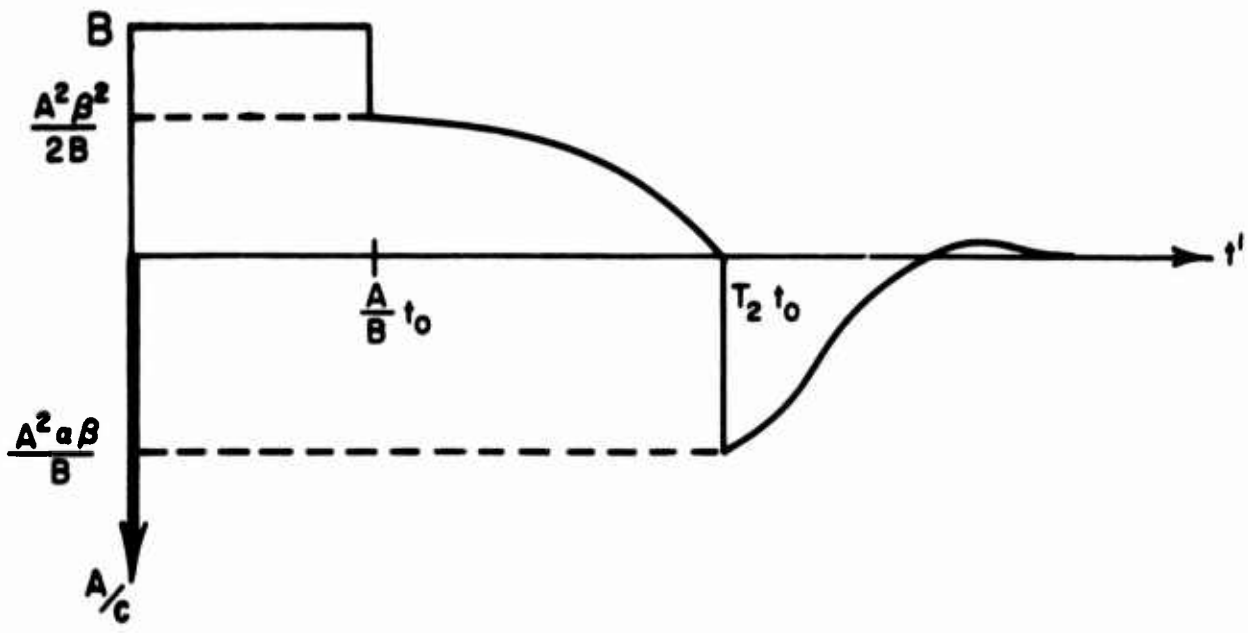

Fig. 12--Rough sketch of impulse response waveform predicted by basic ramp model.

continuous waveform in this region. The creeping wave portion of the waveform in Fig. 12 resembles, if anything, that to be expected from a cylinder (see Appendix II). In the earlier study[12], part of the discrepancy in the shifted periodicity of the calculated data with respect to the measured data was attributed to the approximation in Eq. (73) with regard to the creeping wave times. For a 2:1 axial ratio spheroid, Eq. (72) is approximately 6 percent in error. However, a later correction of this error using Eq. (76) did not significantly alter the positions of maxima and minima in the theoretical curves. It is now clear that the character of the creeping wave contribution in conjunction with the erroneous jump at the peak

cross-sectional area produced the error. This will be demonstrated with calculations on the improved impulse derived model. One should note that, in principle, it would be possible to correct the ramp response derived model. That is, a polynomial section rather than a shifted cosine could be used to eliminate the jump at the shadow boundary and at the same time force the waveform to assume the desired behavior in the neighborhood of the creeping wave maximum. However, the additional parameters required would exceed the known conditions on the waveform. This is the type of dilemma one encounters when starting with an analytical approximation of the ramp response waveform. Since this waveform is smoother than its first or second derivatives, it can be estimated with fewer parameters. But the type of functional dependence assumed is extremely critical, when twice differentiated, in the impulse response waveform. It will be seen, for example, that the impulse response waveforms of the new model differ markedly from that sketched in Fig. 12.

Turning directly to the derivation of a model which will have the desired features lacking above, it is advantageous to start with an assumed approximation for the impulse response waveform of the target, while at the same time retaining those features seen to be desirable in the ramp model. There seems no reason to doubt the validity of the physical optics approximation for short times, thus the

specular delta function and jump discontinuity will be given by the constants A and B respectively in Eq. (72). It is desired, with this model, to secure the secondary peak type behavior for the creeping wave maximum occuring at the time T_2 given in Eqs. (74) and (75). Evidence from the axial waveform in Section A, the asymptotic estimates in Appendix II, and, indirectly, the ramp response derived model discussed in this section, indicates this type of waveform for the creeping wave. The basic impulse response waveform for the spheroid is assumed to be of the form

$$F_{IH}(t') = -A\delta(t') + [B - C e^{\alpha t'}]\,[u(t') - u(t' - T_2 t_o)] + De^{-\alpha t'}\, u(t' - T_2 t_o) \quad , \tag{78}$$

where the subscript H denotes this to be the high frequency portion of the final impulse response waveform. Two conditions are imposed on this waveform

$$C << B \quad , \tag{79}$$

and

$$B - Ce^{\alpha T_2 t_o} = De^{-\alpha T_2 t_o} = P \quad , \tag{80}$$

where P is a constant. Note that this high frequency portion of the waveform has deliberately been made as simple as possible by chosing

the same exponential coefficient on either side of the creeping wave peak. The waveform is designated as high frequency because it is the relatively high frequency properties of the scatterer which it must satisfy, the low frequency conditions will be added later. From Eq. (80),

$$D = \frac{1}{C}\left[PB - P^2\right] \quad , \tag{81}$$

and

$$\alpha = \frac{1}{2T_2 t_o} \ln\left[\frac{D}{C}\left(\frac{B}{P} - 1\right)\right] \quad . \tag{82}$$

It is clear from Eqs. (81) and (82) that two constants in the waveform of Eq. (78), P and C, have not as yet been specified. With these two parameters, it is possible to effect a degree of control on the character of the creeping wave contribution. For example, with the peak creeping wave contribution, P, fixed, C controls the slope of the waveform prior to the peak. The basic assumption with this model is that the impulse response waveform of the spheroid, regardless of orientation or polarization, should be roughly similar in character to the waveform of the conducting sphere and the waveform derived in Section A for the spheroid axial case. Note particularly that no attempt has been made to utilize the low-frequency derived moment conditions to determine the constants P and C or to include additional parameters and enforce

higher moment conditions. Such an approach has been found to be ineffective, primarily because one cannot conveniently maintain simultaneously the desired character of the impulse waveform. Even for very simple waveforms, the integrations indicated by the moment conditions can lead to a very complicated set of simultaneous nonlinear equations.

Two possibilities exist for establishing, approximately, the peak, P, of the creeping wave contribution. The first is an evaluation of the asymptotic expression obtained in Appendix II. The second is to accept the assumption in Section A that the peak magnitude is invariant with axial ratio, and use the known magnitude of the sphere waveform. In either case, the derivation of the remaining low-frequency portion of the impulse response waveform for the spheroid is unchanged. It is proposed to superimpose a second waveform on that given in Eq. (78) whose sole purpose is to ensure the correct low-frequency behavior of the response. This waveform is an exponentially damped sinusoid which is written in the form

$$\overline{F}_{IL}(t') = E\{e^{-\phi_1 t'} - e^{-\phi_2 t'}\}\, u(t') \quad , \tag{83}$$

where E, ϕ_1, and ϕ_2 can be complex. Let the first three moments of the high-frequency waveform in Eq. (78) be denoted by I_1, I_2, and I_3 respectively, i. e.,

$$(84) \qquad \int_0^\infty \overline{F}_{IH}(t')\,dt' = I_1 \quad ,$$

etc. Setting the impulse response waveform of the spheroid to be

$$(85) \qquad \overline{F}_I(t') = \overline{F}_{IH}(t') + \overline{F}_{IL}(t') \quad ,$$

and imposing the zero, first, and second moment conditions on the waveform yields the set of simultaneous, nonlinear equations

$$(86) \qquad \begin{aligned} E[\phi_2 - \phi_1] &= -I_1 \phi_1 \phi_2 \\ E[\phi_2^2 - \phi_1^2] &= -I_2 \phi_1^2 \phi_2^2 \\ 2E[\phi_2^3 - \phi_1^3] &= (K - I)\,\phi_1^3 \phi_2^3 \quad . \end{aligned}$$

Solving Eq. (86), if

$$(87) \qquad \frac{4}{\left(\frac{I_2}{I_1}\right)^2 + \frac{K-I_3}{2I_1}} \leq \frac{I_2^2}{I_1^2 + \left(\frac{I_2}{I_1}\right)^2 + \frac{K-I_3}{2I_1}} \quad ,$$

then ϕ_1, ϕ_2, and E are real and given by

$$(88) \qquad \phi_2 = \frac{I_2/I_1}{2\left[\left(\frac{I_2}{I_1}\right)^2 + \left(\frac{K-I_3}{2I_1}\right)\right]} + \frac{1}{2}\left\{\frac{(I_2/I_1)^2}{\left[\left(\frac{I_2}{I_1}\right)^2 + \frac{K-I_3}{2I_1}\right]^2} - \frac{4}{\left(\frac{I_2}{I_1}\right)^2 + \frac{K-I_3}{2I_1}}\right\}^{1/2} \quad ,$$

$$\phi_1 = \frac{1}{\phi_2\left[\left(\frac{I_2}{I_1}\right)^2 + \frac{K-I_3}{2I_1}\right]} \quad , \tag{89}$$

and

$$E = -\frac{I_1 \phi_1 \phi_2}{\phi_2 - \phi_1} \quad . \tag{90}$$

If the inequality in Eq. (87) is not satisfied, then ϕ_1 and ϕ_2 become complex conjugates and are given by

$$\phi_{1r} = \phi_{2r} = \frac{I_2}{2I_1\left\{\left(\frac{I_2}{I_1}\right)^2 + \frac{K-I_3}{2I_1}\right\}} \quad , \tag{91}$$

$$\phi_{1i} = -\phi_{2i} = -\frac{1}{2}\left\{\frac{4}{\left(\frac{I_2}{I_1}\right)^2 + \frac{K-I_3}{2I_1}} - \frac{I_2^2}{I_1^2 + \left(\frac{I_2}{I_1}\right)^2 + \frac{K-I_3}{2I_1}}\right\}^{1/2} \quad , \tag{92}$$

and

$$E = -\frac{i}{2}\left\{\frac{I_1}{\phi_{1i}\left[\left(\frac{I_2}{I_1}\right)^2 + \frac{K-I_3}{2I_1}\right]}\right\} \quad , \tag{93}$$

where the subscripts r and i refer to the real and imaginary parts respectively. To complete the formulas, the moments of the high-frequency waveform in Eq. (78) are given by

$$I_1 = -A + BT_2 - \frac{Ce^{\alpha T_2}}{\alpha} + \frac{De^{-\alpha T_2}}{\alpha} \quad , \tag{94}$$

$$(95)\qquad I_2 = \frac{BT_2^2}{2} - \frac{CT_2 e^{\alpha T_2}}{\alpha} + \frac{Ce^{\alpha T_2}}{\alpha^2} + \frac{DT_2 e^{-\alpha T_2}}{\alpha} + \frac{De^{-\alpha T_2}}{\alpha^2} \quad ,$$

and

$$(96)\qquad I_3 = \frac{BT_2^3}{3} + \frac{T_2^2}{\alpha}\left[De^{-\alpha T_2} - Ce^{\alpha T_2}\right] + \frac{2T_2}{\alpha^2}\left[Ce^{\alpha T_2} + De^{-\alpha T_2}\right] + \frac{2}{\alpha^3}\left[De^{-\alpha T_2} - Ce^{\alpha T_2}\right] \quad .$$

Thus with the exception of the constants C and P, all of the parameters in the model of the impulse response waveform of the spheroid in Eq. (85) are determined.

Consider first the expressions for the creeping wave in the time domain obtained in Appendix II. Using the approximations valid in the neighborhood of the creeping wave peak and specializing to the time at the peak, Peters' expression reduces to

$$(97)\qquad F_I^{cw}(\alpha) = \frac{A\,3^{3/4}}{(2\pi)^{3/2}\beta^{1/4}} \int_{-\infty}^{\infty} \frac{e^{-\frac{2\beta^{3/2}}{3^{3/2}\sqrt{\tau-\alpha}}}\, u(\tau-\alpha)}{(\tau-\alpha)^{3/2}}\, d\tau \quad ,$$

and Keller's result to

$$(98)\qquad F_I^{cw}(\alpha) = -\frac{A\,3^{3/4}}{2\pi\sqrt{\pi}\,\beta^{1/4}} \int_{-\infty}^{\infty} \left\{ \frac{\beta^{3/2}}{3^{3/2}(\tau-\alpha)^{11/4}} - \frac{1}{4(\tau-\alpha)^{9/4}} \right\} e^{-\frac{2\beta^{3/2}}{3^{3/2}\sqrt{\tau-\alpha}}}\, u(\tau-\alpha)\, d\tau \quad .$$

A change of variable yields for Eq. (97)

$$(99) \qquad F_I^{cw}(\alpha) = \frac{A\, 3^{9/4}}{(2\pi)^{3/2}\,(\beta)^{7/4}} \quad ,$$

and for Eq. (98)

$$(100) \qquad F_I^{cw}(\alpha) = -\frac{\bar{A}\, 3^{9/2}\,\Gamma(7/2)}{2^{7/2}\,(\pi)^{3/2}\,\bar{\beta}^4} + \frac{\bar{A}\, 3^{9/2}\,\Gamma(5/2)}{4(\pi)^{3/2}\,2^{5/2}\,\bar{\beta}^4} \quad .$$

Peters' result applies strictly to the sphere in the form given and cannot be used for the spheroid. It will be of interest, however, to compare Eq. (99) with the estimated peak obtained by Fourier synthesis of the exact solution for the sphere. On the other hand Keller's formula is for a general spheroid, and while the constants given apply to the sphere, for the general spheroid only the constants $\bar{A}$ and $\bar{\beta}$ change in Eq. (100), as well of course as α. It will also be of interest to see how these results compare for the sphere.

A final comment is in order concerning the use of Keller's result in Eq. (100) to predict the creeping wave peak, P, for the arbitrarily oriented spheroid. As derived by Keller, the geometrical theory of diffraction expression is for axial incidence ($\theta = 0°$) only. A corresponding expression for the arbitrarily oriented spheroid has not been given. The contention here, however, is that for estimating the creeping wave peak at an arbitrary orientation, Eq. (100) could be used provided the constants $\bar{A}$ and $\bar{\beta}$ are chosen to correspond to the

ellipse cut from the spheroid by the plane defined by the incident electric field vector and the line of sight. This obviously is a gross distortion of the theory of geometrical diffraction, and the author intends in no way to implicate Keller or others in this assumption. It has been seen, however, with the ramp response waveform model, that very crude approximations in the time domain can lead to good frequency domain results. Moreover, it will be shown that an even cruder assumption concerning the creeping wave peak leads to what must be considered satisfactory results for a 2:1 axial ratio spheroid. In any event, with reference to the designated T. E. and T. M. polarizations, for the T. M. polarization a constant creeping wave peak is predicted with this approximation corresponding to the actual axial ratio of the spheroid. This is so because while the total path length changes (T_2 in Eq. (74)), the distance traveled along a geodesic path on the spheroid remains constant for all aspects. However, for the T. E. polarization, the ellipse cut by the above defined plane has an axial ratio which decreases with θ (Fig. 10), and is unity at $\theta = 90°$. The semiminor and semimajor axis of this ellipse are given by the constants C_1 and C_2 respectively in Eq. (75).

In Fig. 13, the creeping wave peak as calculated from Eq. (100) is shown for a range of axial ratios from 1 to 10. Peters' estimate of the creeping wave peak for a sphere (Eq. (99)) is also shown. In

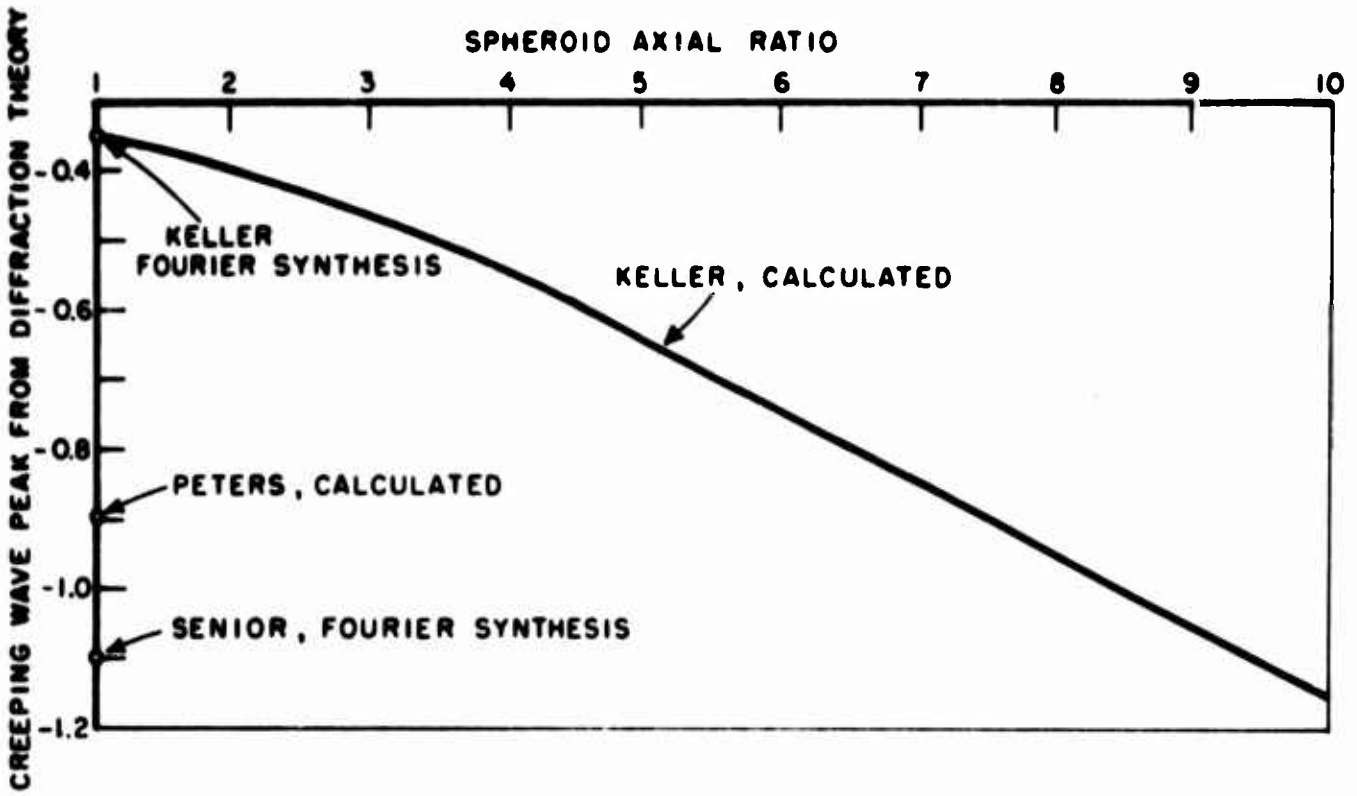

Fig. 13--Peak magnitude of the creeping wave response in the time domain predicted by Keller's spheroid diffraction theory (axial incidence) as a function of the spheroid axial ratio.

comparing these results for the sphere with those obtained from a Fourier synthesis of the exact solution, it must be remembered that optical contributions are also present in the synthesis picture, but are not included in the creeping wave estimates. With this in mind, the estimates of the creeping wave peak in Fig. 13 for a unity axial ratio seem reasonable, if not precise.

An even cruder estimate of the creeping wave peak is obtained by accepting the result in Section A that the creeping wave peak is independent of the spheroid axial ratio. In this case P takes the value -1.0 approximately, and is independent of both orientation and

polarization. The remaining problem, with either the above estimate of P or the geometrical result, is the choice of the constant C in Eq. (78). In order to achieve a basic waveform with the essential character of the sphere response, it is apparent that C must decrease with increasing axial ratio since the exponential in the second term of Eq. (78) should only be strongly effective as the creeping wave peak is approached. Clearly, one can generate an infinite variety of waveforms by varying C, but several checks on the magnitude of this parameter can be used. This parameter is not, therefore, a curve fitting device in the sense that C is varied until the best fit with independent measured or calculated echo area data is obtained. The first check on C is the form of impulse response waveform obtained; in essence a smoothly decreasing function such as that shown in Fig. 8 (dashed curve) for the exponential sum approximation is desired. Note that the exponential sum approximation in Reference 12 gives a clue as to the order of magnitude required for C at least for a 2:1 spheroid. C in this case roughly corresponds to the coefficient A_2 in Eq. (17) of Reference 12, which is of the order of 1×10^{-14}, a very small number. A third check on the assumed magnitude of C is provided by the coefficients calculated for the low-frequency waveform in Eq. (83). The low-frequency waveform is a correction waveform in the sense that it is added to enforce the moment conditions. However,

if the assumptions concerning the similarity of the spheroid waveform to the sphere are correct, and the choice of C reasonable, then very little correction should be needed. Thus if the magnitude of the coefficients in the low-frequency waveform are such as to seriously distort the waveform, then it is an indication that the assumed magnitude of C is in error.

The basic model proposed for the impulse response waveform of the prolate spheroid target, for the defined T. E. and T. M. polarizations and any orientation, is that given by Eq. (85). It is deceptively simple in form, and leads, through the Laplace transform, to a computationally simple frequency-dependent function. It remains to test the various hypothesis and assumptions inherent in the model both as to the form of the response waveforms generated and ultimately, of course, with respect to calculated echo areas for the target. These tasks are undertaken in the next Section.

C. Calculated and Measured Results for a 2:1 Axial Ratio Spheroid

Of the two suggested models for the general impulse response waveform of the spheroid, that one utilizing an invariant (with axial ratio, orientation, and polarization) creeping wave peak taken from the sphere is by far the easiest to implement. It is reasonable, therefore, to consider this model first. From the exponential sum

approximation to the spheroid impulse response waveform given in Reference 12, taking into consideration the fact that for the present model the jump magnitude (F) does not have an exponential decay, the constant C in Eq. (78) is set equal to 1×10^{-12}. The above choice for C was the first one made. The best proof of this, regardless of the resultant echo area calculations, is that neither the impulse response waveforms obtained for the spheroid nor the magnitude of the damped sinusoid correction are by any means exactly what was desired for all orientations and polarizations. It is also clear that much more sophisticated techniques for obtaining both P and C could be devised. For example, one could confine these parameters to a particular range of values and then minimize the area beneath the impulse and step response waveforms by some type of testing procedure. But such sophistication is accomplished at the expense of a more complicated model. One of the most distinctive features of the time domain approach is the results which can be obtained, in terms of predicting frequency domain behavior, with very crude models. This will be demonstrated presently for the spheroid model using exactly the gross approximations described above.

It is instructive first to consider the magnitudes of the various parameters in the impulse response waveform model described above as a function of both orientation and polarization. These parameters

are given in Tables I and II for the T. E. and T. M. polarizations respectively. The above tables list, reading from left to right; the aspect angle, specular magnitude (A), jump magnitude (B), time of creeping wave peak (T_2), Rayleigh coefficient (K), exponential decay (α), exponential coefficients C and D, real and imaginary parts of the correction exponentials (ϕ_1 and ϕ_2), and the coefficient of the correction term (E). The symbols in the table headings correspond to the symbols in Eqs. (78) and (83). In Table III, the corresponding moments of the basic model, i. e., without the added damped exponential of Eq. (83) are given, again for both T. E. and T. M. polarizations. Note that if the basic model were correct, I_1 and I_2 in Table III would be zero, and I_3 equal to the corresponding Rayleigh coefficient.

Consider first the T. E. polarization; from Table I and Table III it is seen that as the aspect angle increases from the axial case ($\theta = 0°$), the basic waveform (Eq. (78)) becomes first a better and then a poorer model and the correction waveform (Eq. (83)) becomes progressively larger with aspect angle after $\theta = 20°$. Note that the uncorrected moments of the basic model are not wholly compatible. That is, in terms of the zero and first moments (I_1 and I_2), the model is best at approximately $\theta = 20°$, in terms of the second moment (I_3), $\theta = 30°$ is the optimum model. In considering the magnitude of the correction coefficient (last column in Table I) it must be remembered

TABLE I
PARAMETERS OF IMPULSE WAVEFORM MODEL
T. E. CASE

θ	A	B	T_2	K	α	C	D	ϕ_{1r}	ϕ_{1i}	ϕ_{2r}	ϕ_{2i}	E
0	0. 25	0. 125	4. 42	-2. 75	6. 4	1×10^{-12}	-4.5×10^{12}	0. 094	-0. 12	0. 094	0. 12	+0. 0054
10	0. 256	0. 1295	4. 37	-2. 74	6. 52	1×10^{-12}	-4.518×10^{12}	0. 068	-0. 09	0. 068	0. 09	+0. 0025
20	0. 274	0. 1435	4. 23	-2. 71	6. 73	1×10^{-12}	-4.574×10^{12}	0. 049	-0. 14	0. 049	0. 14	-0. 0023
30	0. 3075	0. 170	4. 01	-2. 67	7. 10	1×10^{-12}	-4.68×10^{12}	0. 28	-0. 43	0. 28	0. 43	-0. 044
40	0. 3625	0. 218	3. 73	-2. 61	7. 64	1×10^{-12}	-4.872×10^{12}	0. 33	-0. 36	0. 33	0. 36	-0. 11
50	0. 4465	0. 2985	3. 42	-2. 56	8. 35	1×10^{-12}	-5.194×10^{12}	0. 35	-0. 37	0. 35	0. 37	-0. 21
60	0. 5715	0. 432	3. 11	-2. 50	9. 19	1×10^{-12}	-5.728×10^{12}	0. 38	-0. 40	0. 38	0. 40	-0. 39
70	0. 740	0. 635	2. 83	-2. 46	10. 12	1×10^{-12}	-6.548×10^{12}	0. 43	-0. 44	0. 43	0. 44	-0. 69
80	0. 917	0. 878	2. 64	-2. 43	10. 92	1×10^{-12}	-7.512×10^{12}	0. 47	-0. 48	0. 47	0. 48	-1. 10
90	1. 0	1. 0	2. 57	-2. 42	11. 25	1×10^{-12}	-8.0×10^{12}	0. 48	-0. 50	0. 48	0. 50	-1. 3

TABLE II
PARAMETERS OF IMPULSE WAVEFORM MODEL
T. M. CASE

θ	A	B	T_2	K	α	C	D	ϕ_{1r}	ϕ_{1i}	ϕ_{2r}	ϕ_{2i}	E
10	0. 256	0. 1295	4. 4	-2. 82	6. 47	1×10^{-12}	-4.518×10^{12}	0. 057	-0. 078	0. 057	0. 078	+0. 0019
20	0. 274	0. 1435	4. 33	-3. 01	6. 59	1×10^{-12}	-4.574×10^{12}	0. 057	-0. 17	0. 057	0. 17	-0. 0037
30	0. 3075	0. 170	4. 22	-3. 31	6. 76	1×10^{-12}	-4.682×10^{12}	0. 43	-0. 54	0. 43	0. 54	-0. 079
40	0. 3625	0. 218	4. 08	-3. 67	6. 98	1×10^{-12}	-4.872×10^{12}	0. 47	-0. 39	0. 47	0. 39	-0. 20
50	0. 4465	0. 2985	3. 92	-4. 06	7. 28	1×10^{-12}	-5.194×10^{12}	0. 46	-0. 38	0. 46	0. 38	-0. 38
60	0. 5715	0. 432	3. 75	-4. 42	7. 63	1×10^{-12}	-5.728×10^{12}	0. 46	-0. 39	0. 46	0. 39	-0. 68
70	0. 740	0. 635	3. 58	-4. 72	8. 04	1×10^{-12}	-6.548×10^{12}	0. 48	-0. 41	0. 48	0. 41	-1. 20
80	0. 917	0. 878	3. 47	-4. 91	8. 32	1×10^{-12}	-7.512×10^{12}	0. 50	-0. 43	0. 50	0. 43	-1. 80
90	1. 0	1. 0	3. 42	-4. 98	8. 48	1×10^{-12}	-8.0×10^{12}	0. 51	-0. 44	0. 51	0. 44	-2. 10

TABLE III
MOMENTS OF UNCORRECTED IMPULSE
WAVEFORM MODEL

θ	I_1	I_2	I_3	I_1	I_2	I_3
0	-0.056	-0.47	-5.7	-0.056	-0.47	- 5.7
10	-0.036	-0.38	-5.3	-0.032	-0.39	- 5.4
20	0.029	-0.12	-4.1	0.039	-0.13	- 4.4
30	0.14	0.3	-2.5	0.18	0.33	- 2.9
40	0.32	0.88	-0.5	0.42	1.00	- 0.66
50	0.60	1.6	1.6	0.82	2.10	2.40
60	1.0	2.6	3.6	1.5	3.70	6.40
70	1.6	3.7	5.6	2.4	5.9	11.00
80	2.3	4.8	7.2	3.6	8.2	16.00
90	2.6	5.3	7.9	4.1	9.3	19.00

that the duration of the waveforms is decreasing with increasing θ, thus the correction must effectively be made at smaller times. From the trend of the moments and the correction coefficient, it is concluded that a broadening of the creeping wave in the neighborhood of the peak for aspect angles greater than 30° and a narrowing of this waveform below 30° is required. In the neighborhood of the creeping wave peak, rather small changes in the slope of the waveform will have a substantial effect on the higher moments.

Turning to the T. M. polarization in Table II, a similar trend is observed. Here, however, the zero and first moments are smallest on axis ($\theta = 0°$) whereas the second moment is best at $\theta = 30°$. For the T. M. polarization, the moments of the uncorrected model are seen to be in error by a greater amount for aspects near 90° than were those for the T. E. case. Again, a required broadening of the creeping wave waveform is indicated with somewhat greater broadening necessary for the T. M. than for the T. E. polarization. It is of interest next to examine the ramp and impulse response waveforms predicted by this model, with the correction waveform added, and to compare the corresponding frequency-dependent function with experimental data. It is desired to compare the ramp response waveforms predicted by this model with the ramp waveforms obtained with the earlier ramp waveform model given in Eq. (72). This comparison is shown in Figs. 14 through 18 for both the T. E. and T. M. polarizations for aspect angles θ from 0° to 90° in increments of 10°. It is evident that except for small times, the ramp waveforms predicted by the two models differ substantially. The differences are primarily a longer endurance and higher magnitude for the impulse response derived model. Note also that the magnitude of the ramp derived model never exceeds the physical optics estimate whereas the impulse derived model does, particularly for aspects approaching broadside. On the basis of the ramp

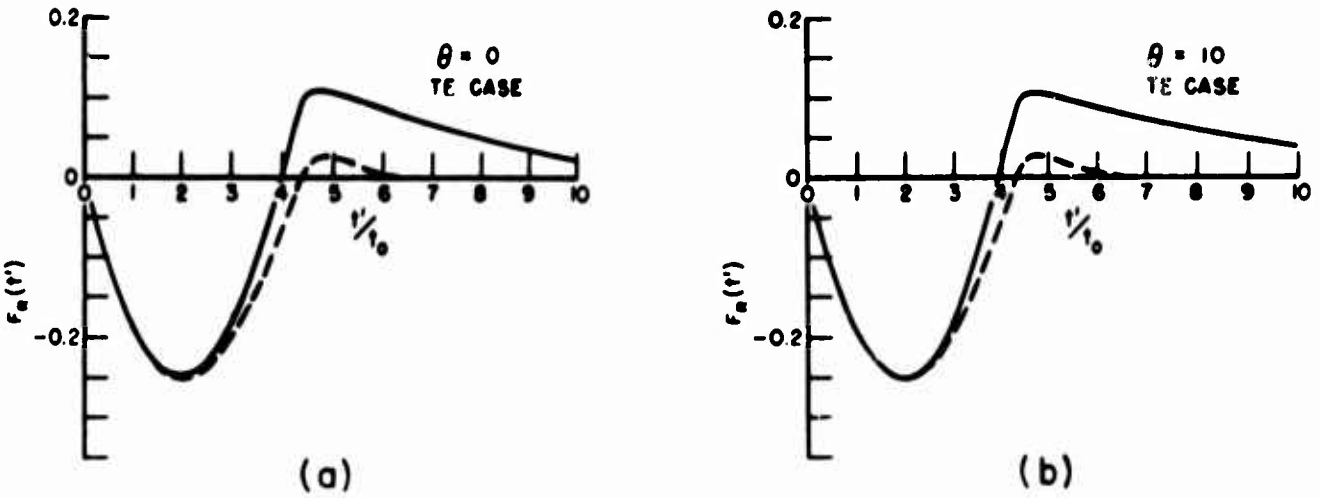

Fig. 14--Ramp response waveforms of 2:1 axial ratio spheroid obtained from ramp derived (dashed) and impulse derived models. T. E. polarization.
(a) $\theta = 0°$; (b) $\theta = 10°$; (c) $\theta = 20°$; (d) $\theta = 30°$

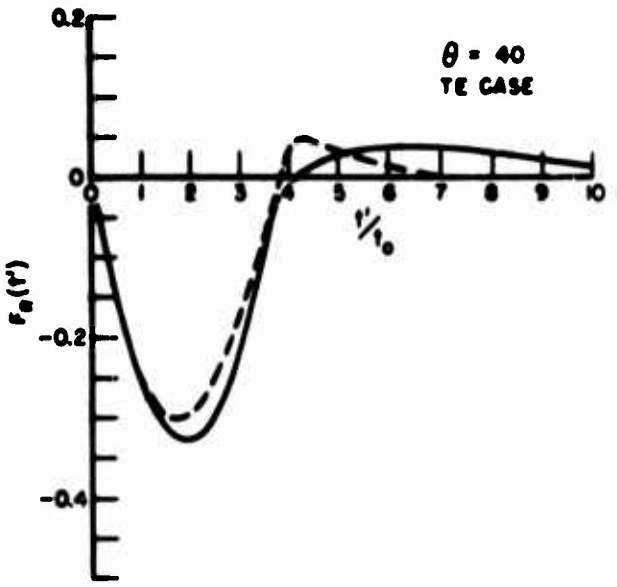

(a)

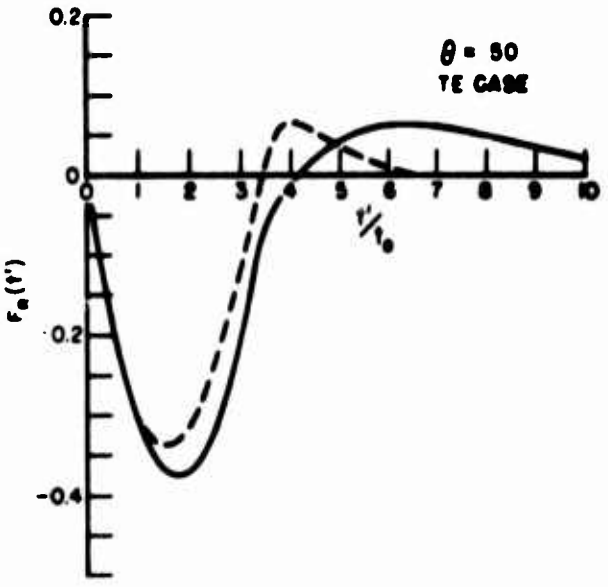

(b)

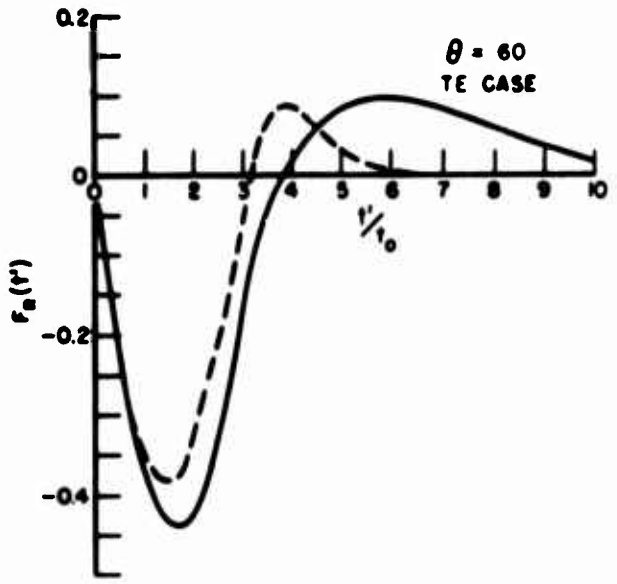

(c)

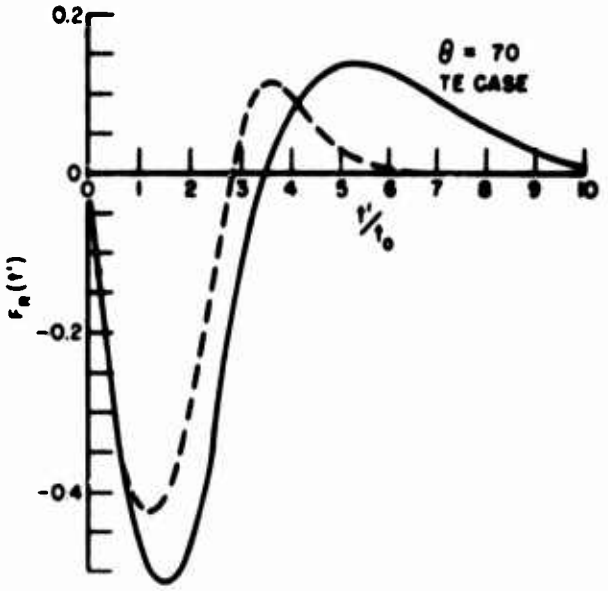

(d)

Fig. 15--Ramp response waveforms of 2:1 axial ratio spheroid obtained from ramp derived (dashed) and impulse derived models. T. E. polarization.
(a) $\theta = 40°$; (b) $\theta = 50°$; (c) $\theta = 60°$; (d) $\theta = 70°$

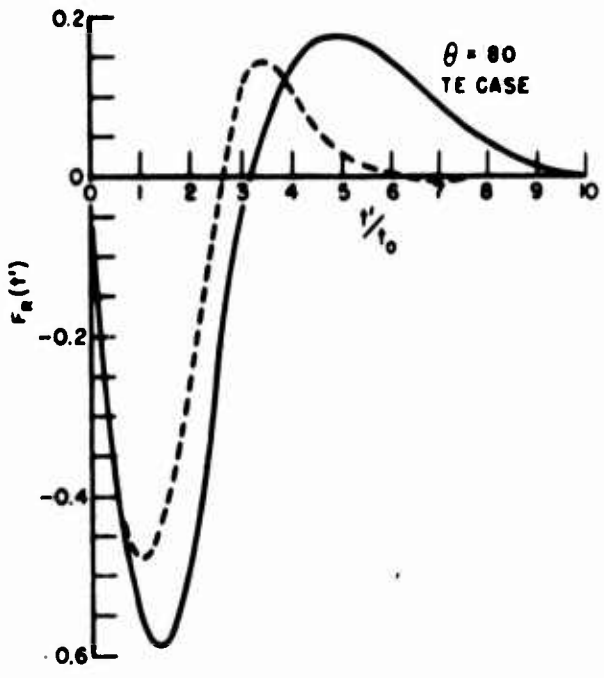

(a)

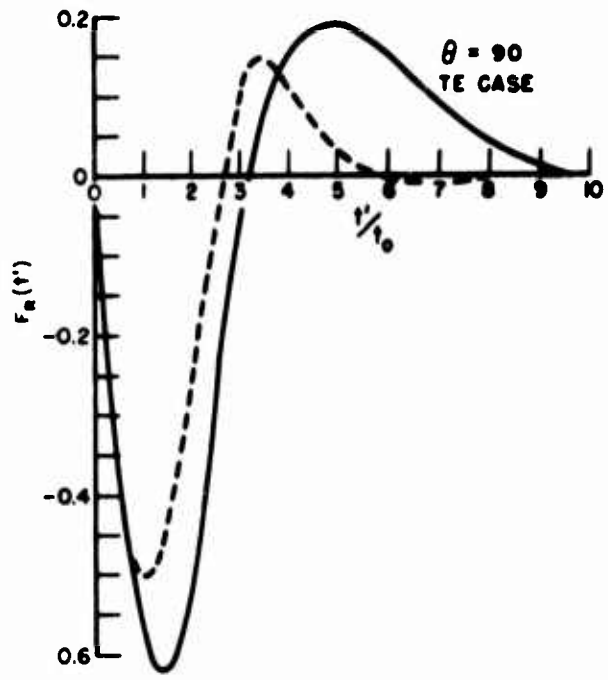

(b)

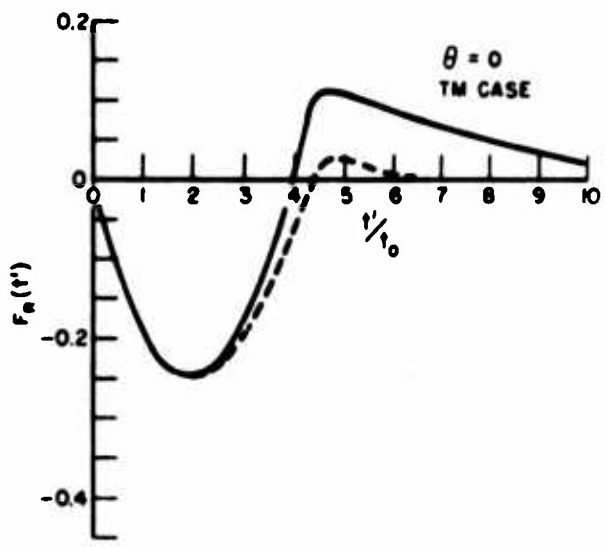

(c)

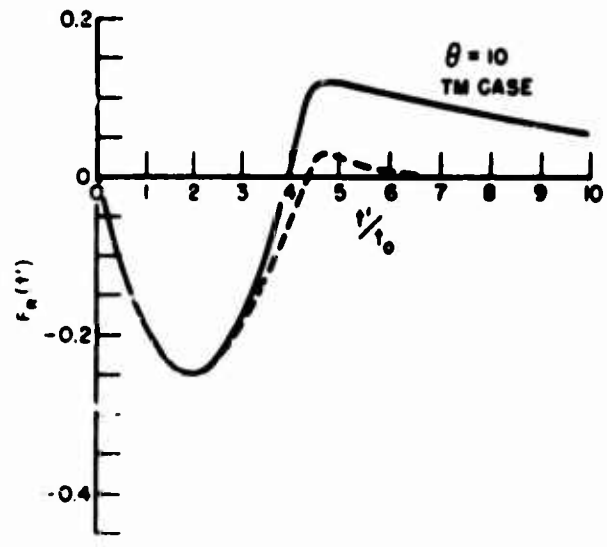

(d)

Fig. 16--Ramp response waveforms of 2:1 axial ratio spheroid obtained from ramp derived (dashed) and impulse derived models.
(a) $\theta = 80°$; (b) $\theta = 90°$, T. E. polarization
(c) $\theta = 0°$; (d) $\theta = 10°$, T. M. polarization

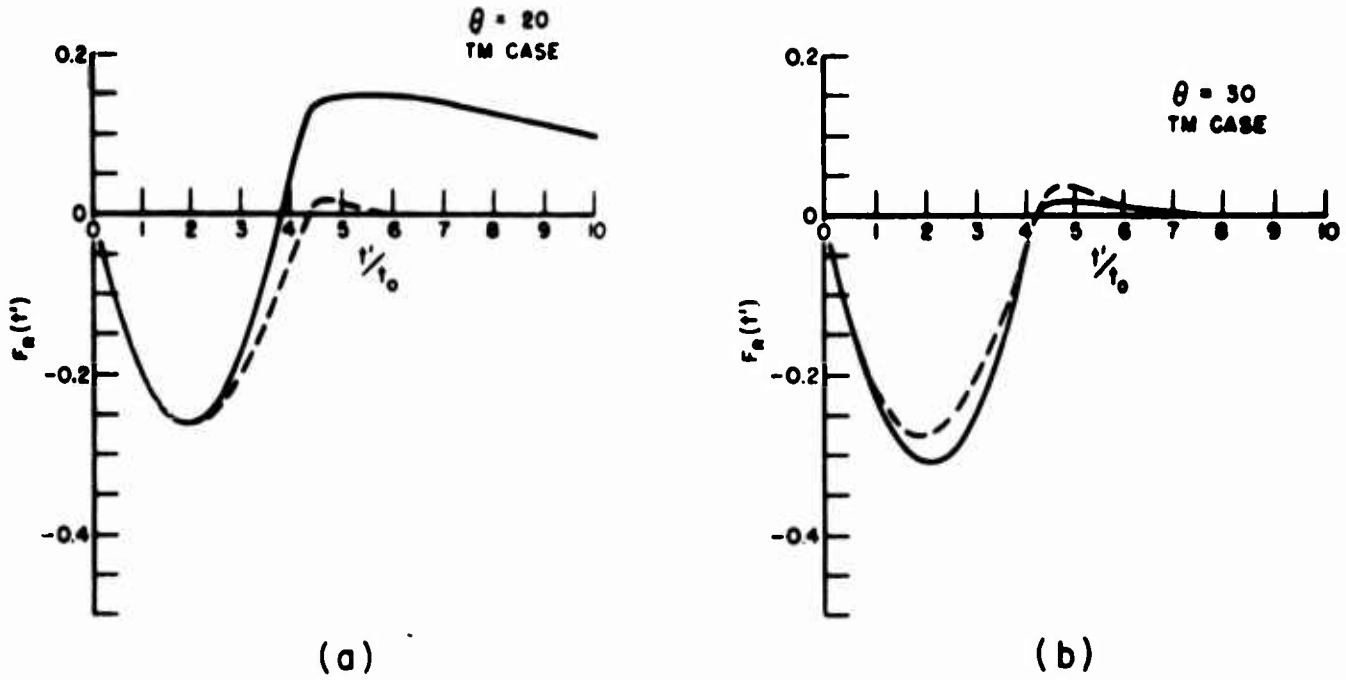

Fig. 17--Ramp response waveforms of 2:1 axial ratio spheroid obtained from ramp derived (dashed) and impulse derived models. T. M. polarization.
(a) $\theta = 20°$; (b) $\theta = 30°$; (c) $\theta = 40°$; (d) $\theta = 50°$

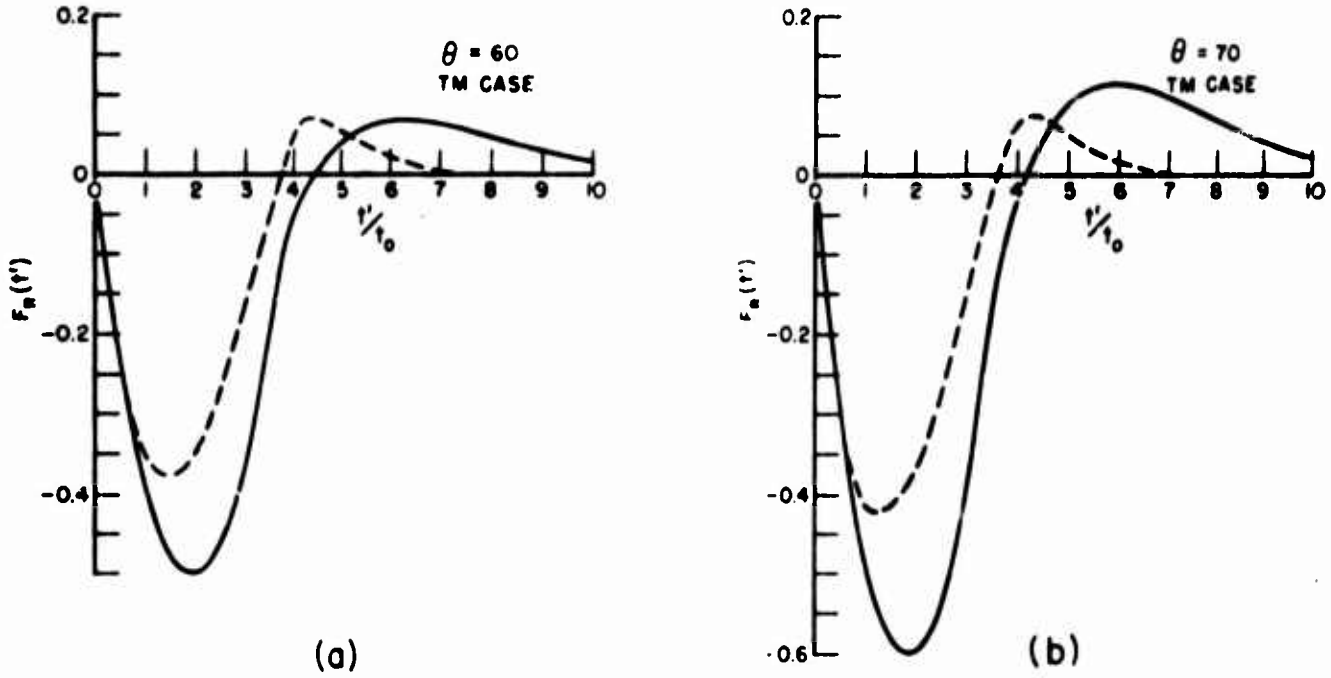

Fig. 18--Ramp response waveforms of 2:1 axial ratio spheroid obtained from ramp derived (dashed) and impulse derived models. T. M. polarization.
(a) $\theta = 60°$; (b) $\theta = 70°$; (c) $\theta = 80°$; (d) $\theta = 90°$

waveform for axial incidence derived in Section A, one would conclude that the ramp derived model is more nearly correct, at least for aspects near axial incidence. It is not possible to settle this question completely with the limited low-frequency data available (this point is discussed later). One could, however, with the techniques discussed in Chapter I; utilize additional experimental data or "point matching" solutions to estimate the mean square error of the waveforms. For the stated purpose of this study, that of obtaining an approximate general model, it is not necessary to resolve this question. It is noted however that some reservations concerning the ramp response waveforms must be retained and that the next investigation of the prolate spheroid target should begin with the ramp response waveform.

The impulse response waveforms predicted by the new (Eq. (85)) model are shown in Figs. 19 through 23. Two points are immediately evident from these waveforms. First, the model has succeeded in enforcing the type of creeping wave contribution felt to be necessary. Second, the damped sinusoid correction term while adjusting the creeping wave peaks to some extent has, in the process of enforcing the moment conditions, distorted the waveforms significantly for earlier times. This is vividly evident for either polarization as the aspect angle approaches 90°. Note that the specular component has been omitted from these figures. It is simply a negative delta function

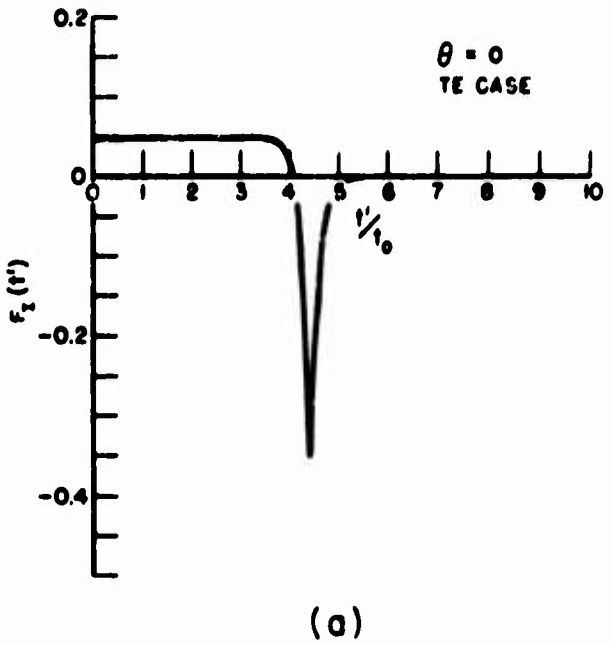

(a)

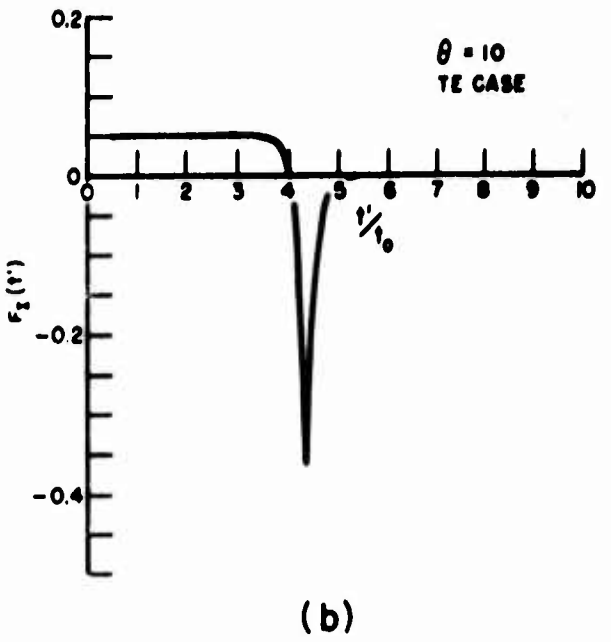

(b)

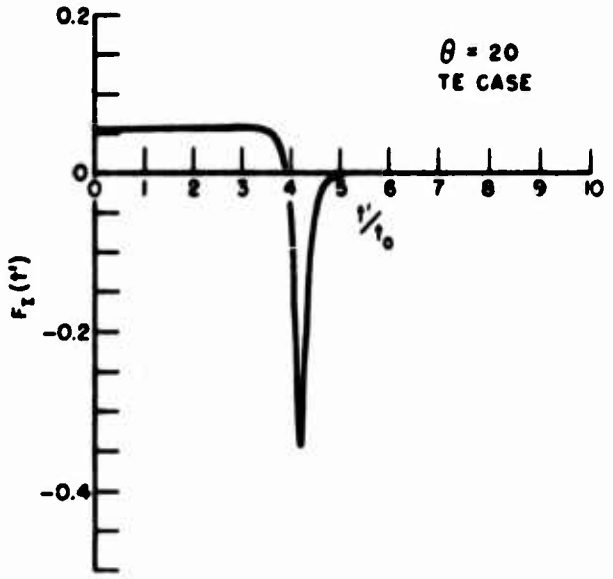

(c)

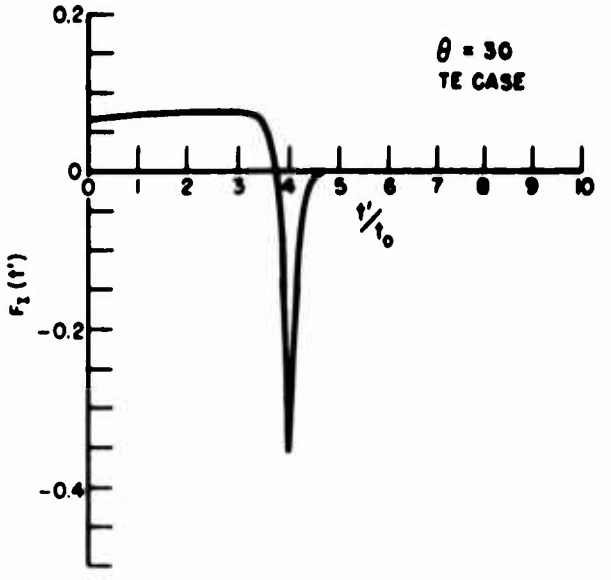

(d)

Fig. 19--Impulse response waveform of 2:1 axial ratio prolate spheroid obtained from impulse derived model. T. E. polarization.
(a) $\theta = 0°$; (b) $\theta = 10°$; (c) $\theta = 20°$; (d) $\theta = 30°$

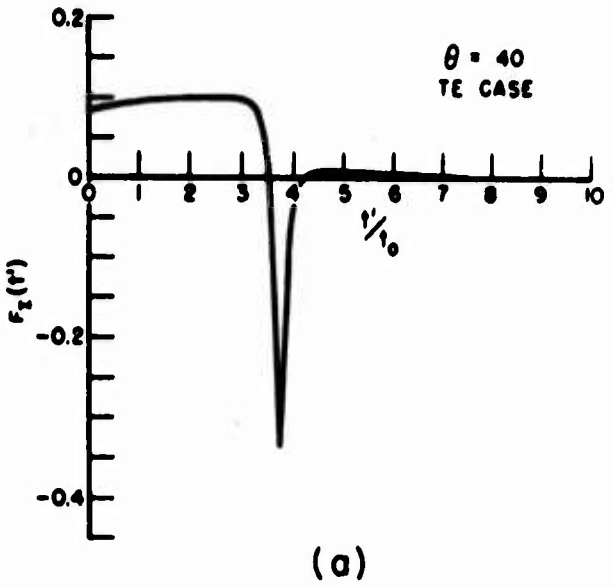

(a)

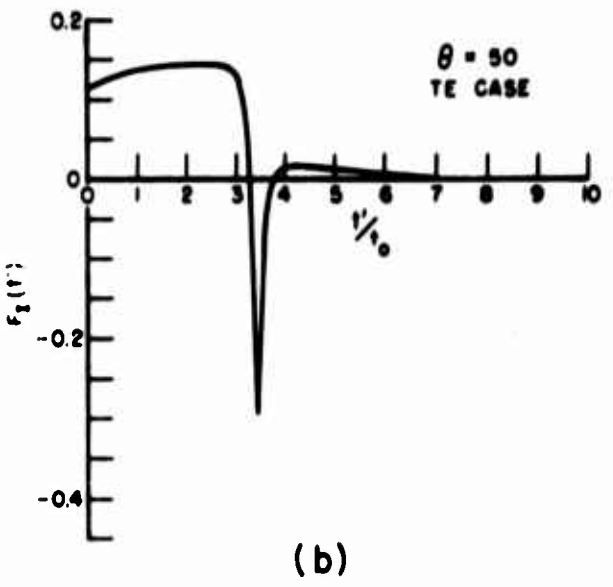

(b)

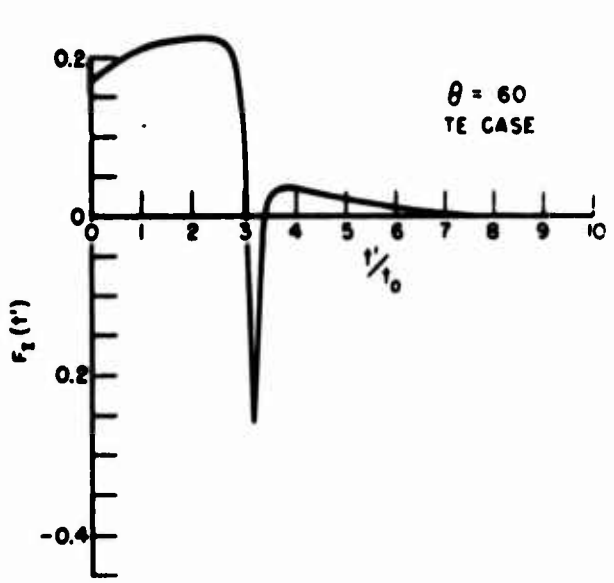

(c)

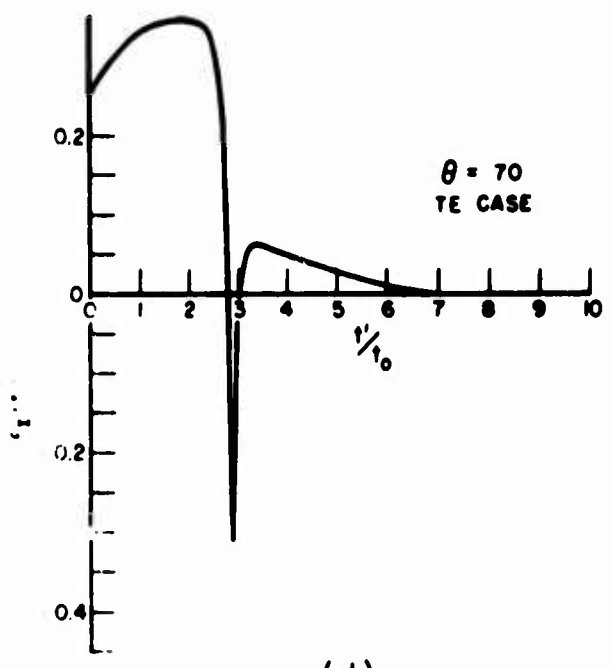

(d)

Fig. 20--Impulse response waveform of 2:1 axial ratio prolate spheroid obtained from impulse derived model. T. E. polarization.
(a) θ = 40° ; (b) θ = 50° ; (c) θ = 60° ; (d) θ = 70°

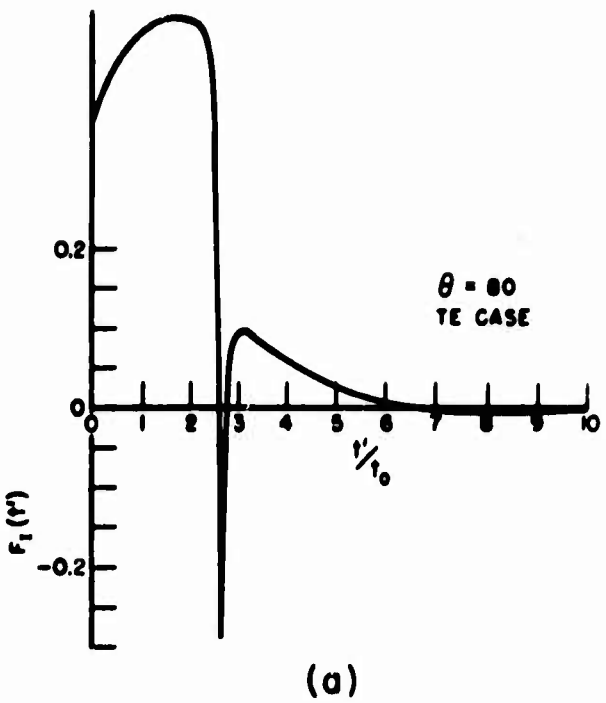

(a)

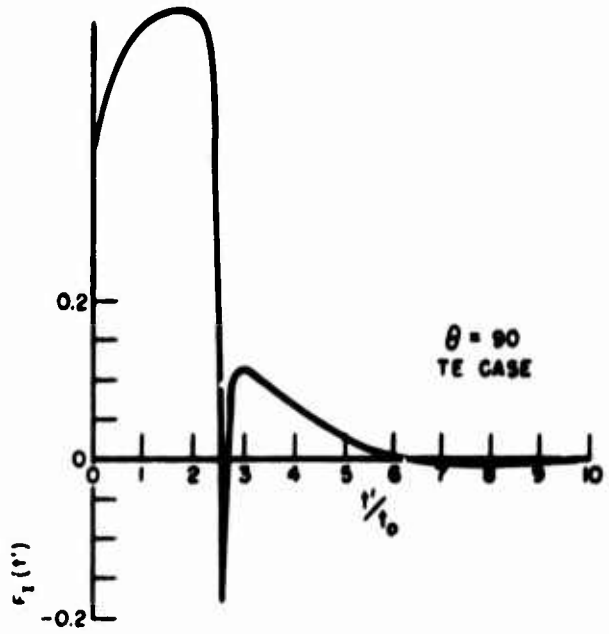

(b)

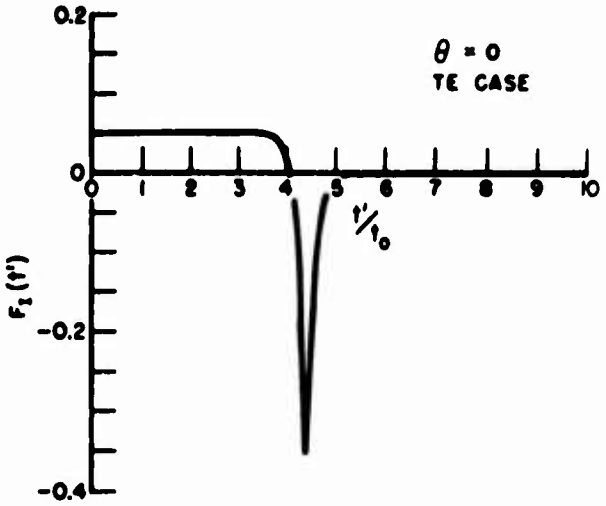

(c)

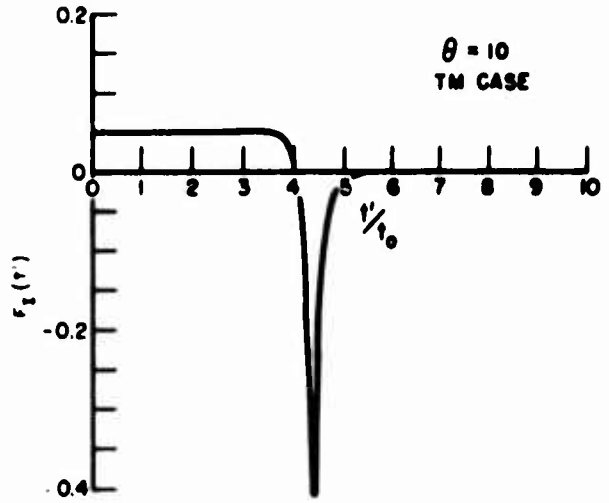

(d)

Fig. 21--Impulse response waveform of 2:1 axial ratio prolate spheroid obtained from impulse derived model.
(a) $\theta = 80°$; (b) $\theta = 90°$, T. E. polarization
(c) $\theta = 0°$; (d) $\theta = 10°$, T. M. polarization

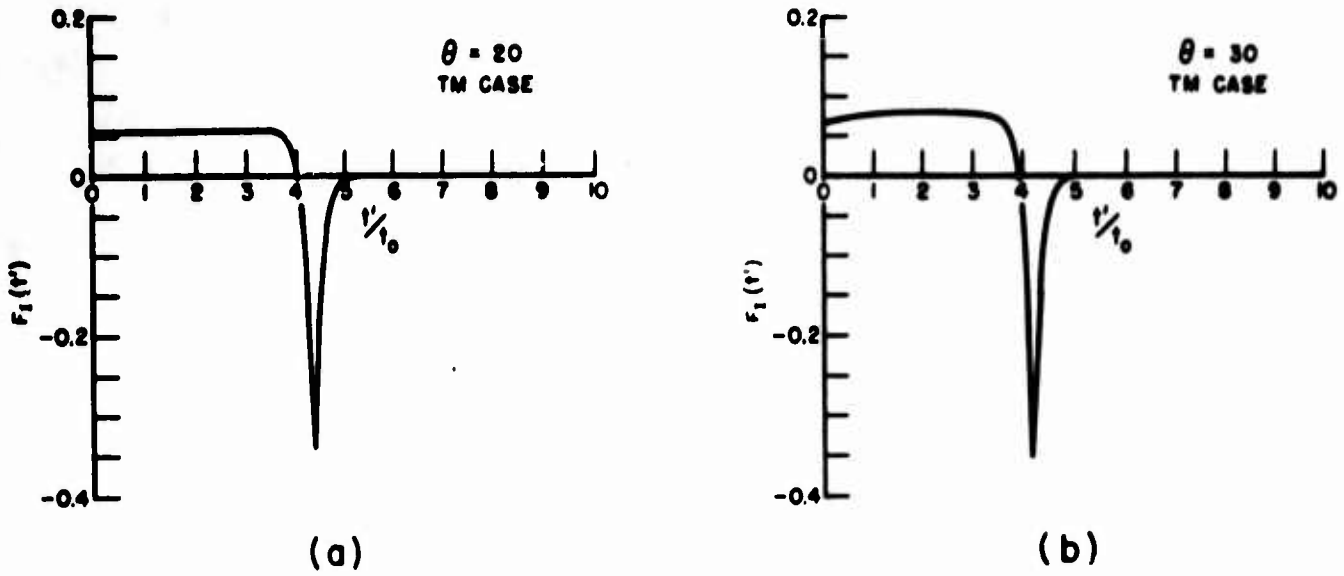

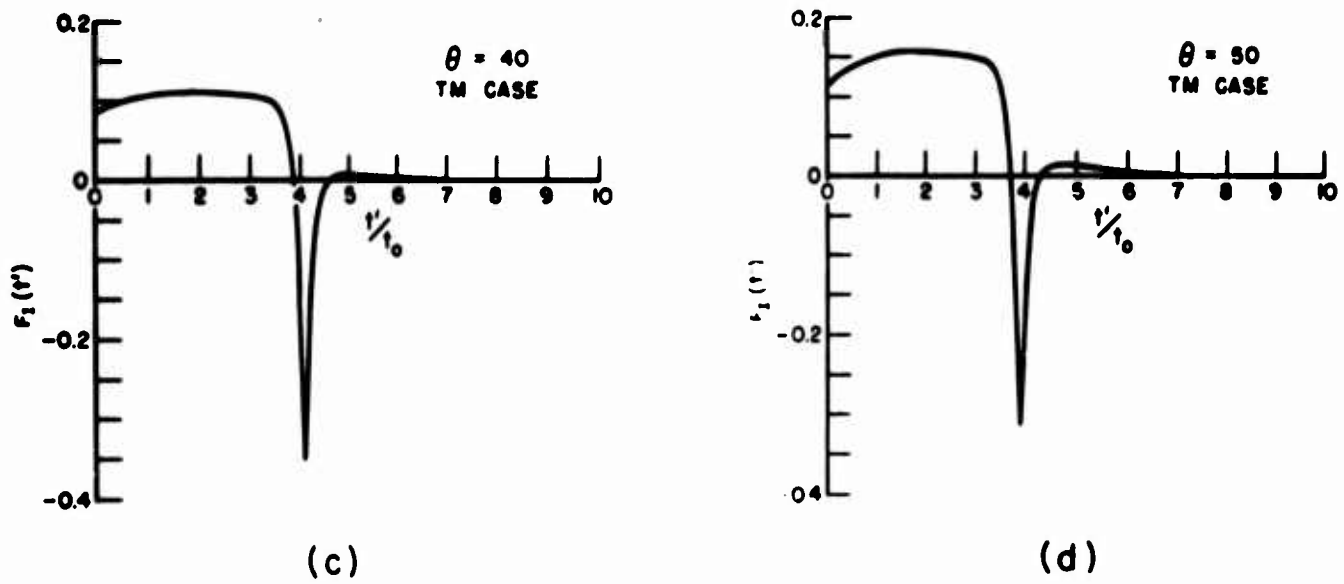

Fig. 22--Impulse response waveform of 2:1 axial ratio prolate spheroid obtained from impulse derived model. T. M. polarization.
(a) θ = 20° ; (b) θ = 30° ; (c) θ = 40° ; (d) θ = 50°

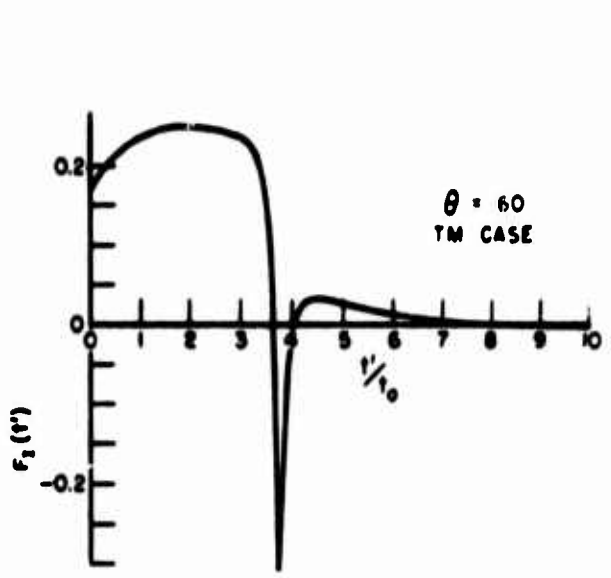

(a)

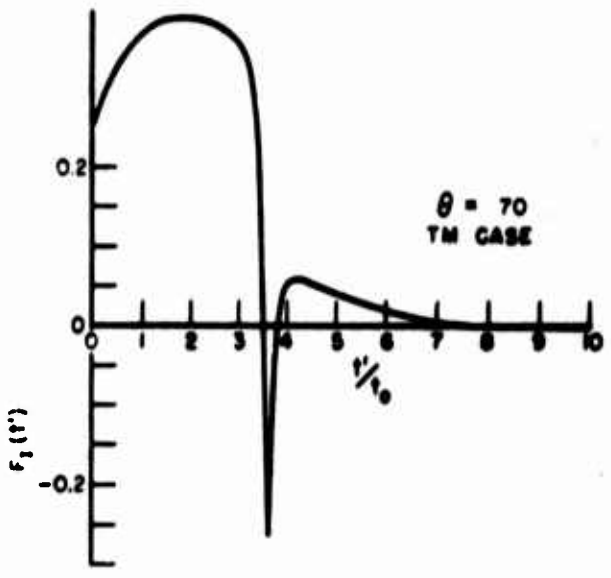

(b)

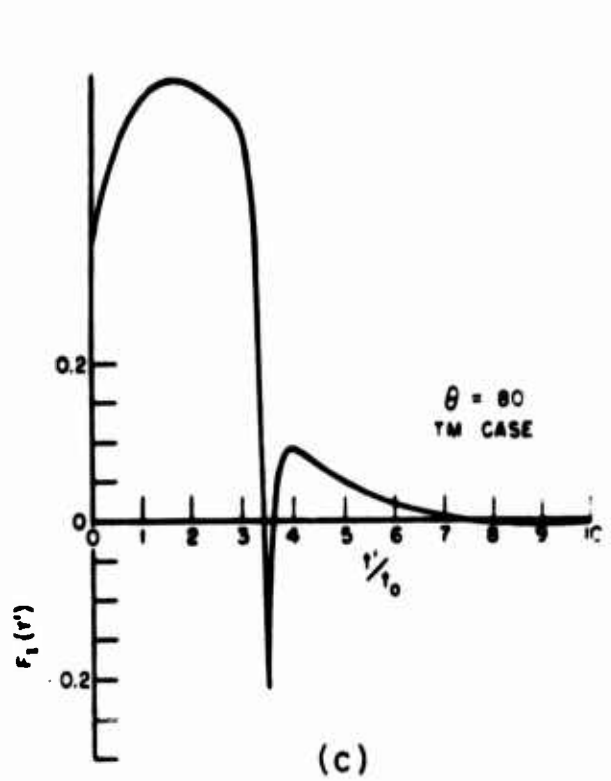

(c)

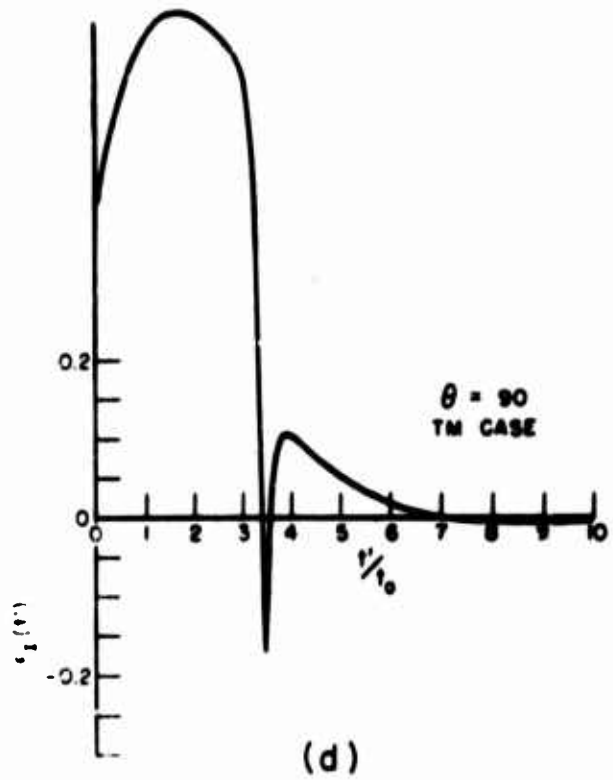

(d)

Fig. 23--Impulse response waveform of 2:1 axial ratio prolate spheroid obtained from impulse derived model. T. M. polarization.
(a) $\theta = 60°$; (b) $\theta = 70°$; (c) $\theta = 80°$; (d) $\theta = 90°$

of weight A/c at t' = 0 which is given in Tables I and II in the second column. The same conclusions observed earlier from an examination of the model parameters in Tables I, II, and III are confirmed by the impulse response waveforms. In each case it is seen that the correction sinusoid has increased the negative area beneath the waveforms. Unfortunately, the correction is not concentrated in the vicinity of the creeping wave peak and has, as is apparent, substantially distorted the waveforms for earlier times.

The final test of the model is a comparison of calculated and measured results for the backscattering from a prolate spheroid target. Extensive data have been measured on a 2:1 axial ratio prolate spheroid for both the T. E. and T. M. polarizations over 360° of aspect. The measured patterns corresponding to this data were reported in Reference 12 and will not be repeated here. In Reference 12 the accuracy of the measured results is estimated as $\pm$1.0 dB at a level of 20 dB less than a square wavelength. Two comparisons of calculated data from the model and experimental measurements are desired. The first is the echo area at a fixed orientation and polarization as a function of frequency, and the second is the echo area as a function of orientation for fixed frequency and polarization. The variable frequency comparisons will be more extensive. In Figs. 24 through 33, the predicted

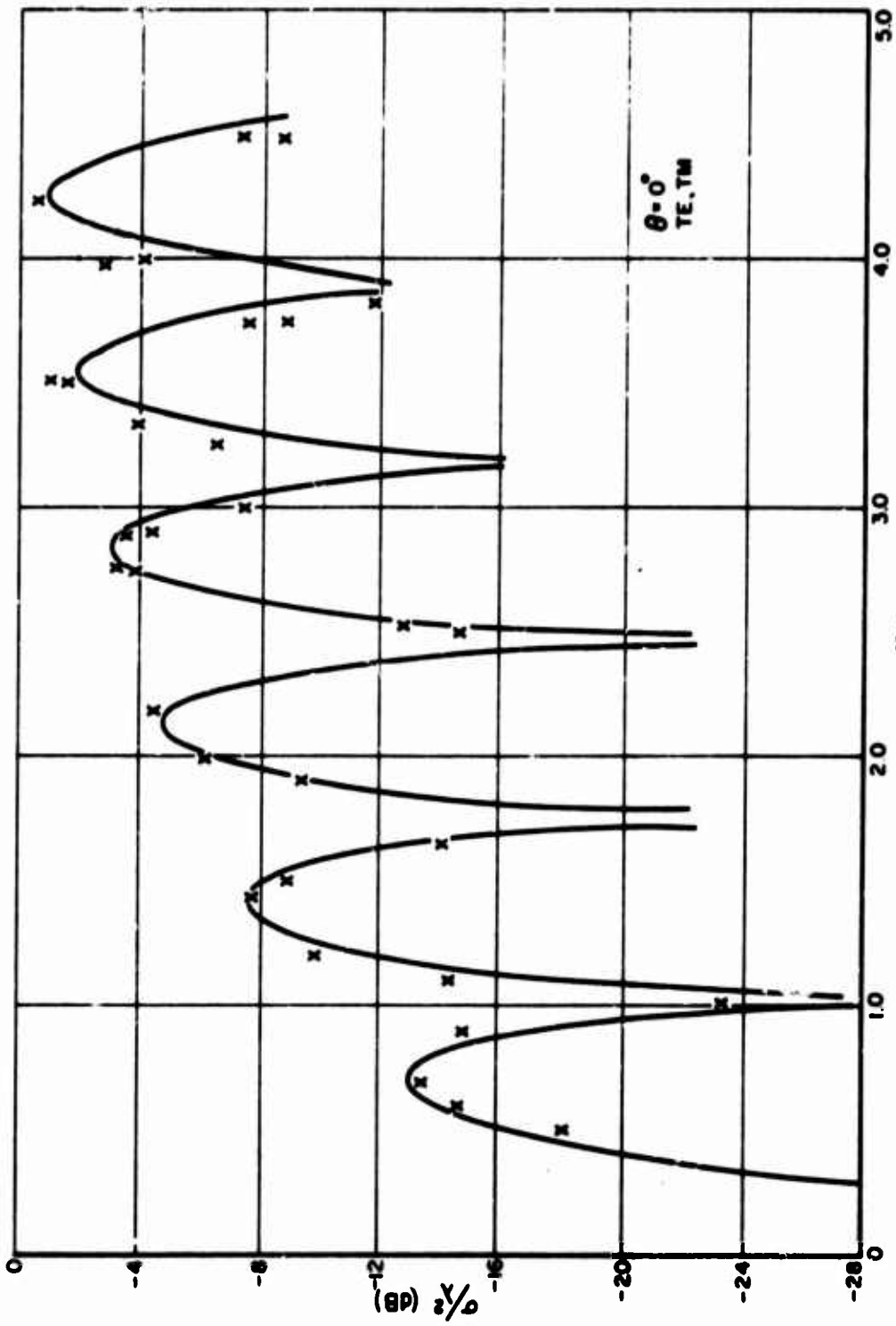

Fig. 24--Calculated (solid curve) and measured echo area of a 2:1 axial ratio prolate spheroid in dB > λ^2 as a function of minor axis circumference in wavelengths. $\theta = 0°$.

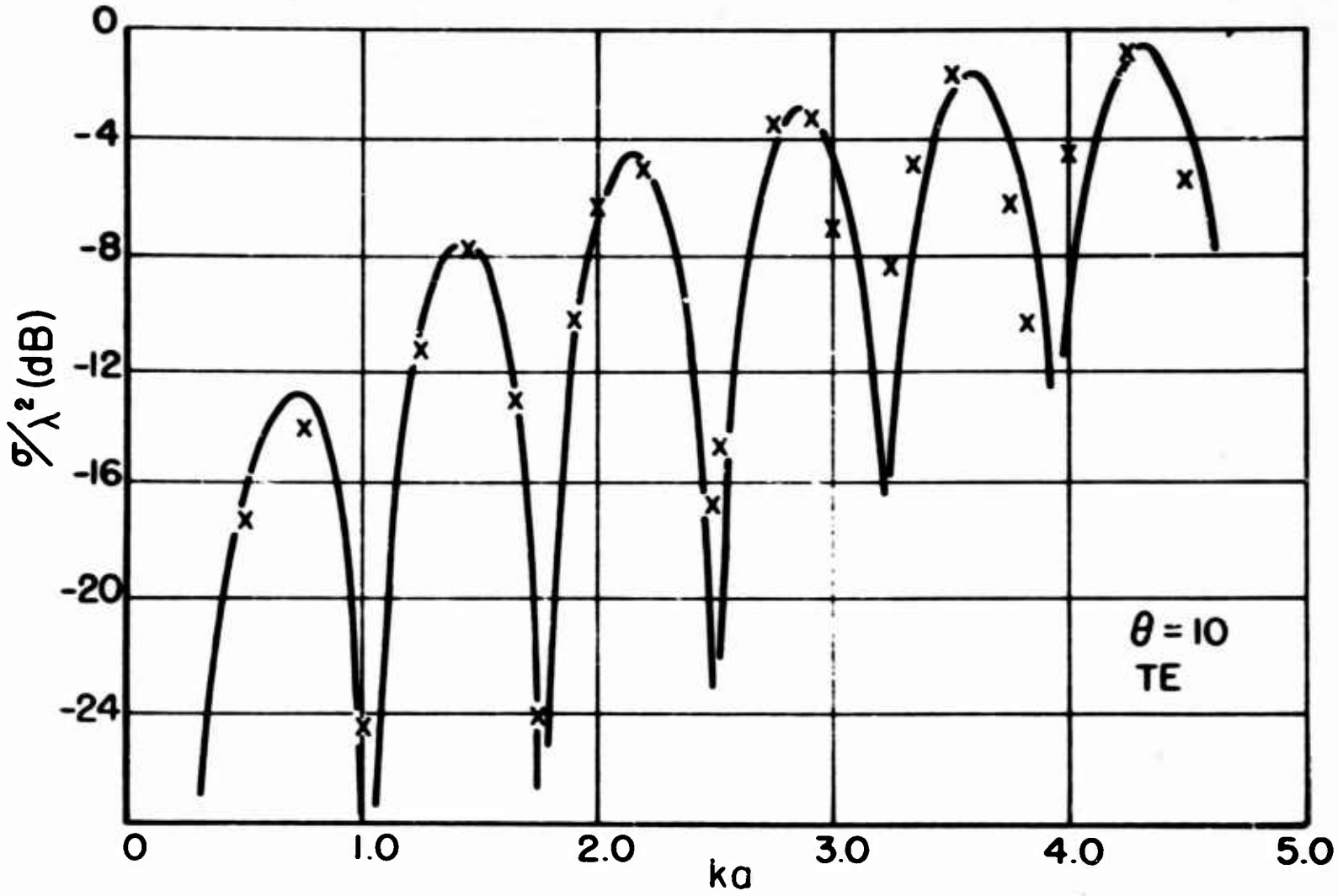

Fig. 25--Calculated (solid curve) and measured echo area of a 2:1 axial ratio prolate spheroid in dB > λ^2 as a function of minor axis circumference in wavelengths. $\theta = 10°$.
a. T. E. polarization.

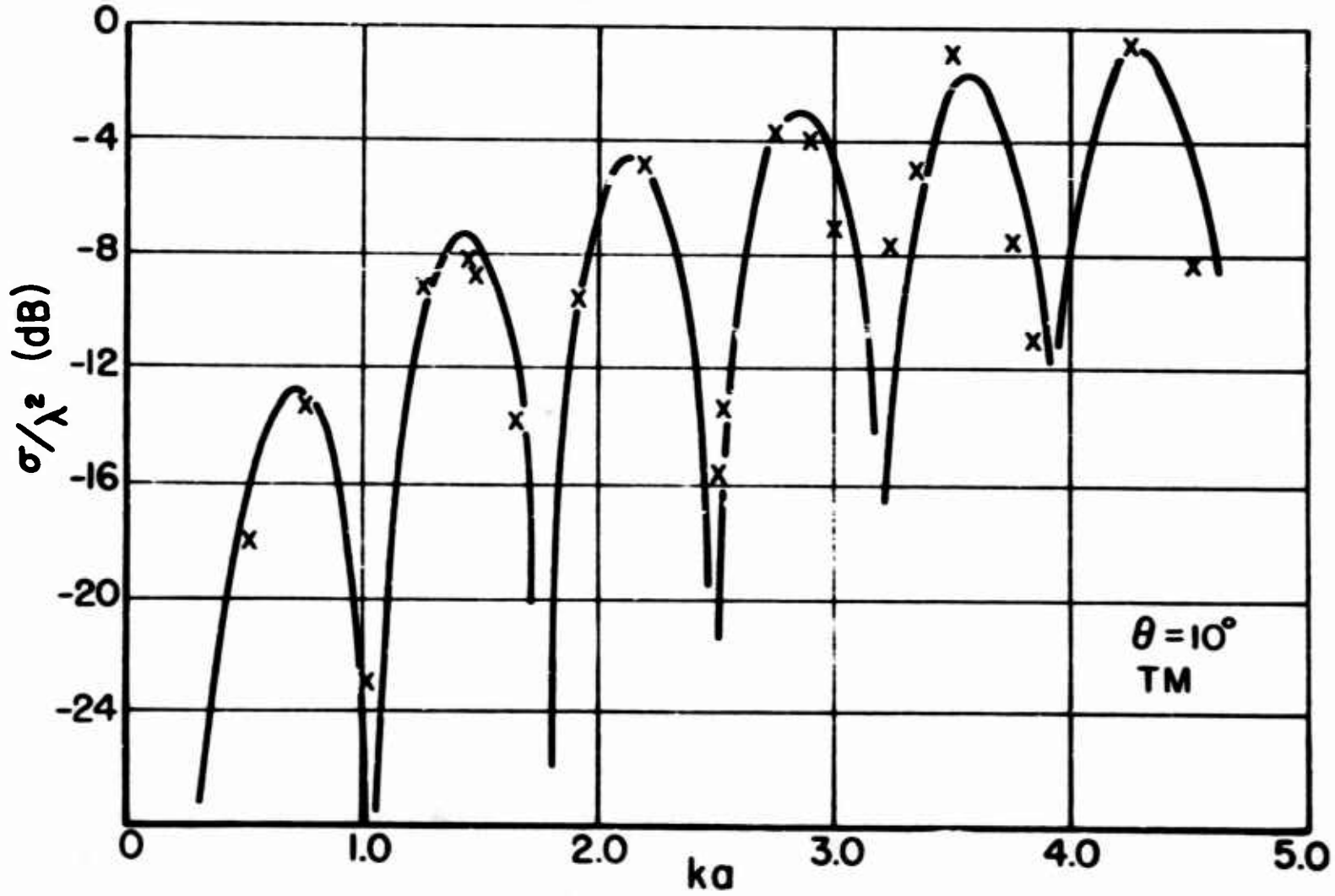

Fig. 25--Calculated (solid curve) and measured echo area of a 2:1 axial ratio prolate spheroid in dB > λ^2 as a function of minor axis circumference in wavelengths. $\theta = 10°$.
b. T. M. polarization.

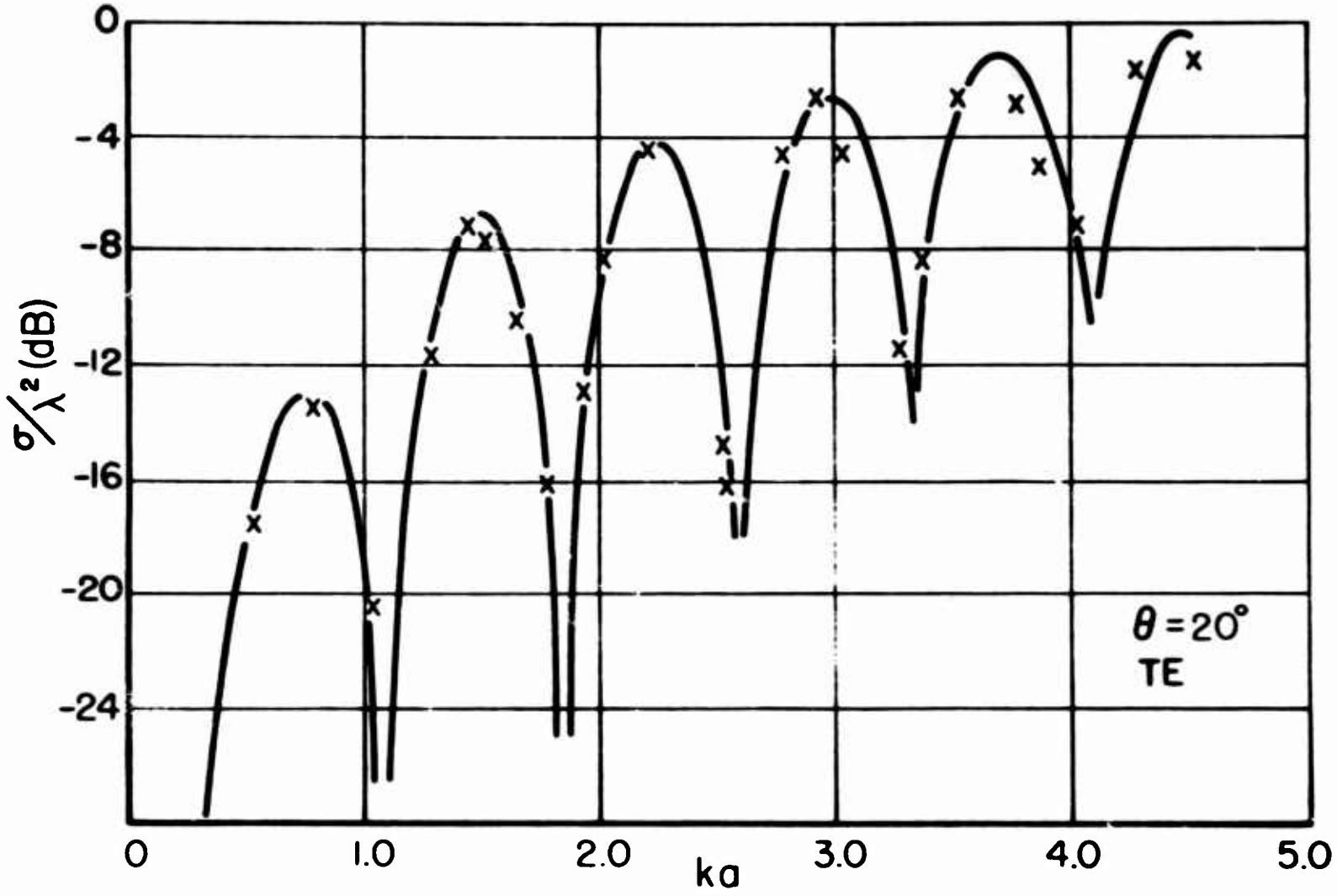

Fig. 26--Calculated (solid curve) and measured echo area of a 2:1 axial ratio prolate spheroid in dB > λ^2 as a function of minor axis circumference in wavelengths. $\theta = 20°$.
a. T. E. polarization.

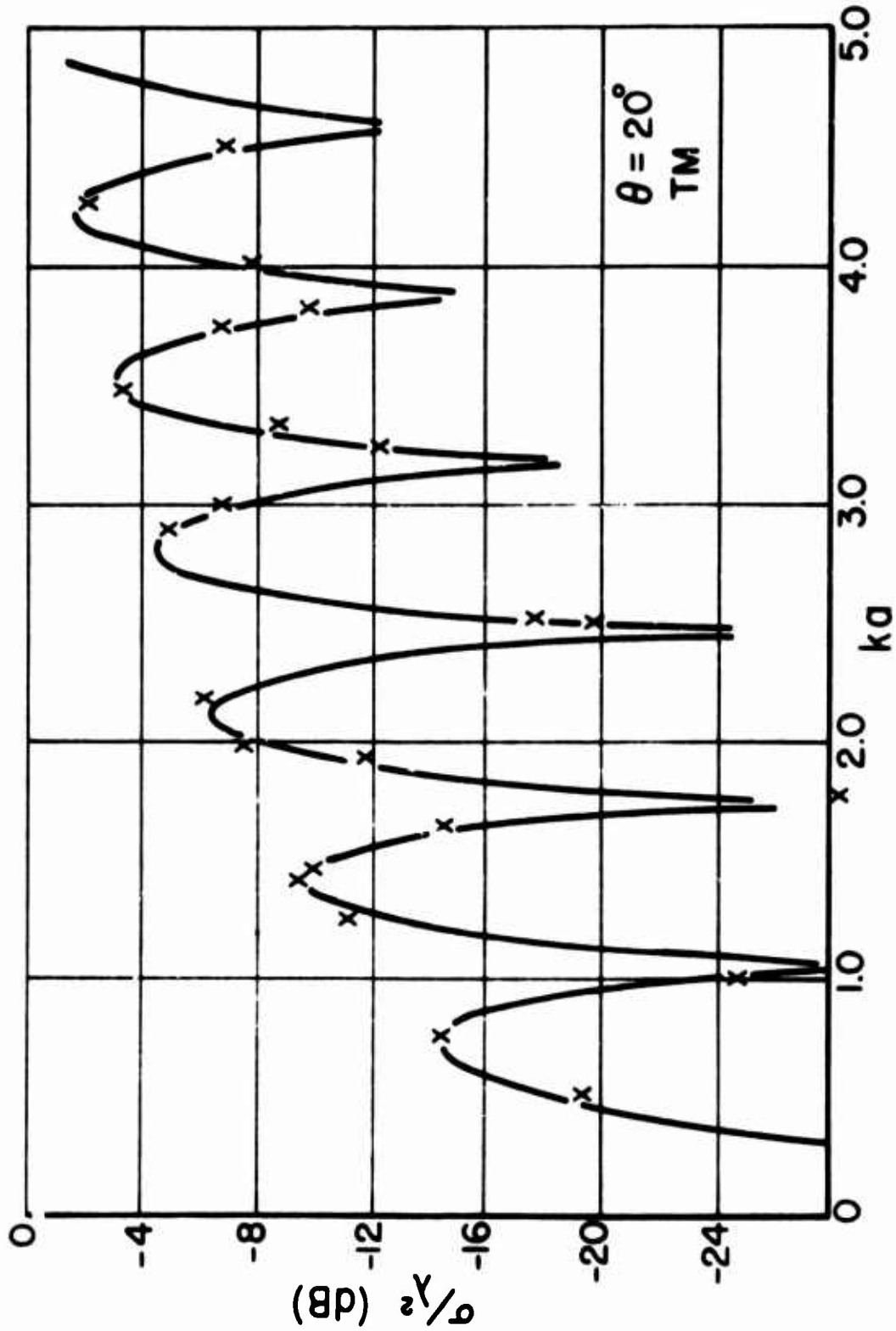

Fig. 26--Calculated (solid curve) and measured echo area of a 2:1 axial ratio prolate spheroid in dB > λ^2 as a function of minor axis circumference in wavelengths. $\theta = 20°$.
b. T. M. polarization.

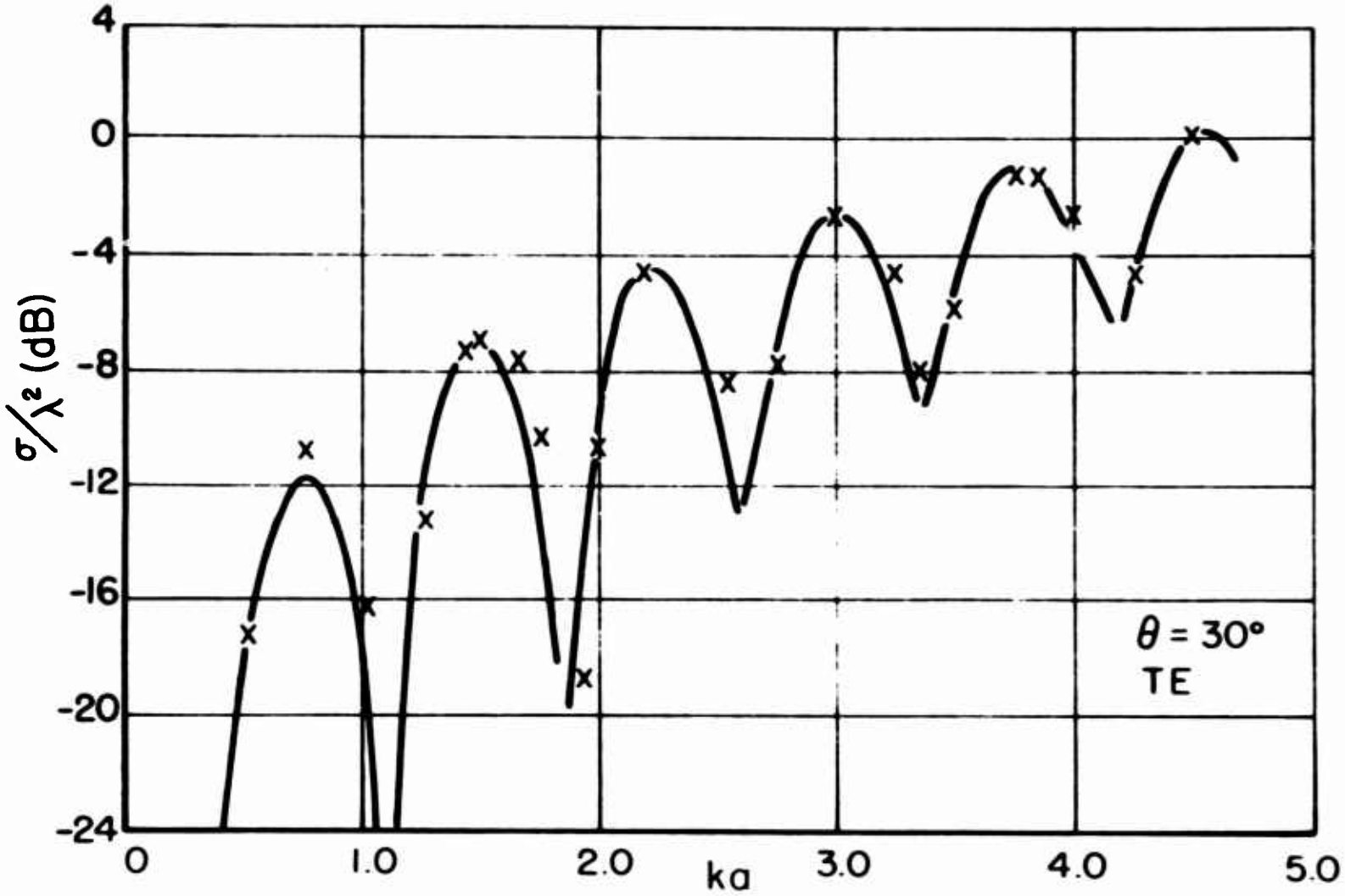

Fig. 27--Calculated (solid curve) and measured echo area of a 2:1 axial ratio prolate spheroid in dB > λ^2 as a function of minor axis circumference in wavelengths. $\theta = 30°$.
a. T. E. polarization.

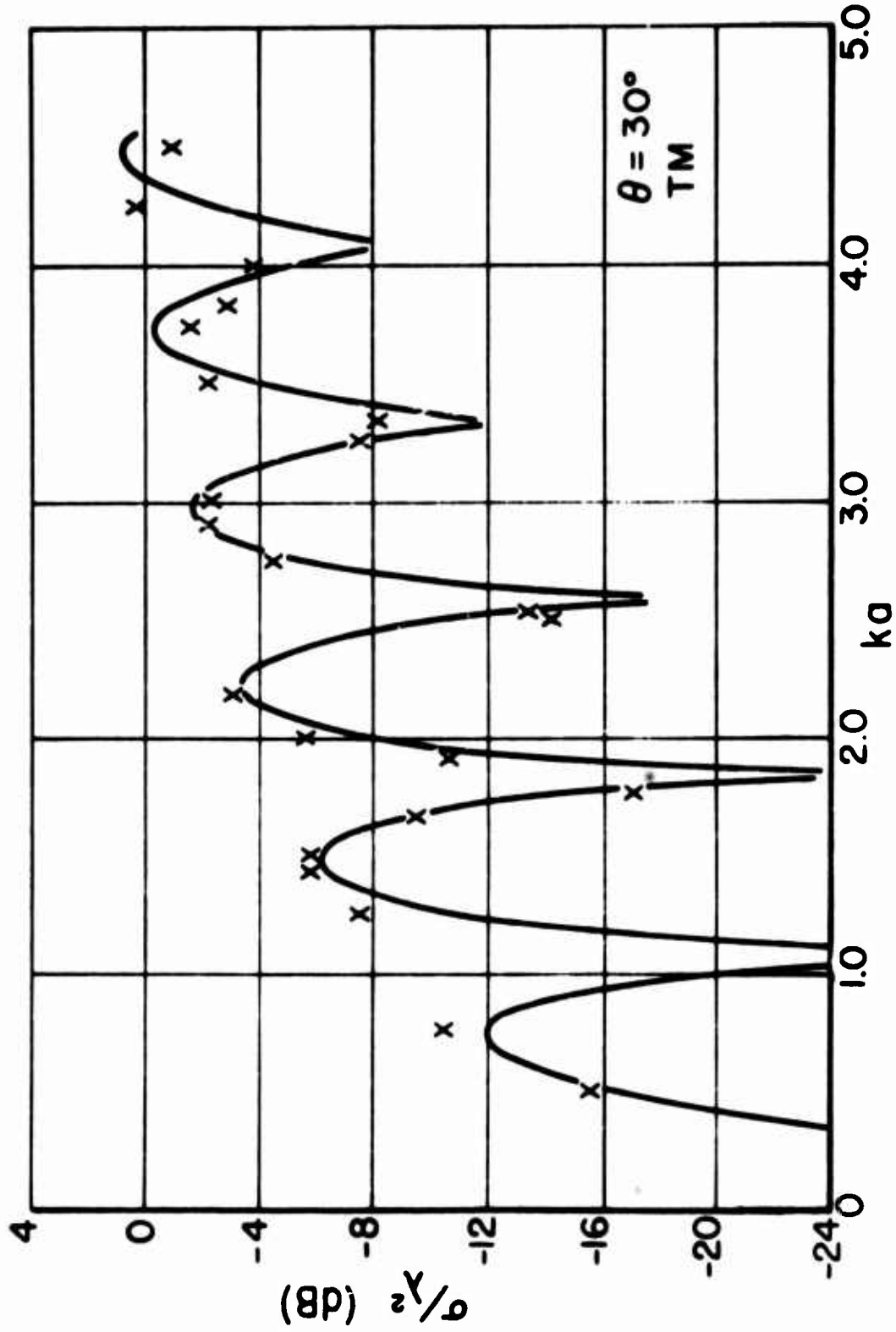

Fig. 27--Calculated (solid curve) and measured echo area of a 2:1 axial ratio prolate spheroid in dB > λ^2 as a function of minor axis circumference in wavelengths. $\theta = 30°$.
b. T. M. polarization.

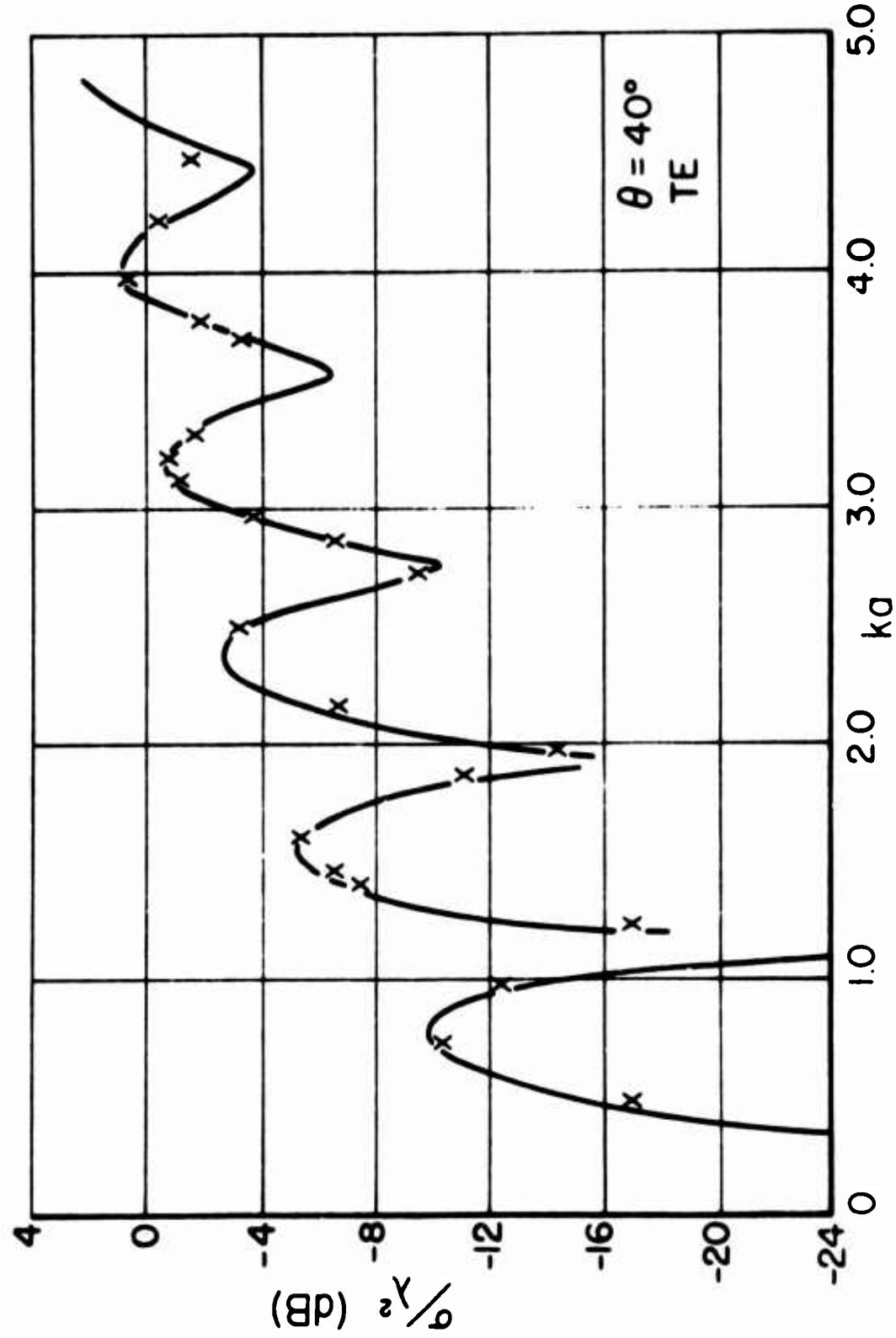

Fig. 28--Calculated (solid curve) and measured echo area of a 2:1 axial ratio prolate spheroid in dB > λ^2 as a function of minor axis circumference in wavelengths. $\theta = 40°$.
a. T. E. polarization.

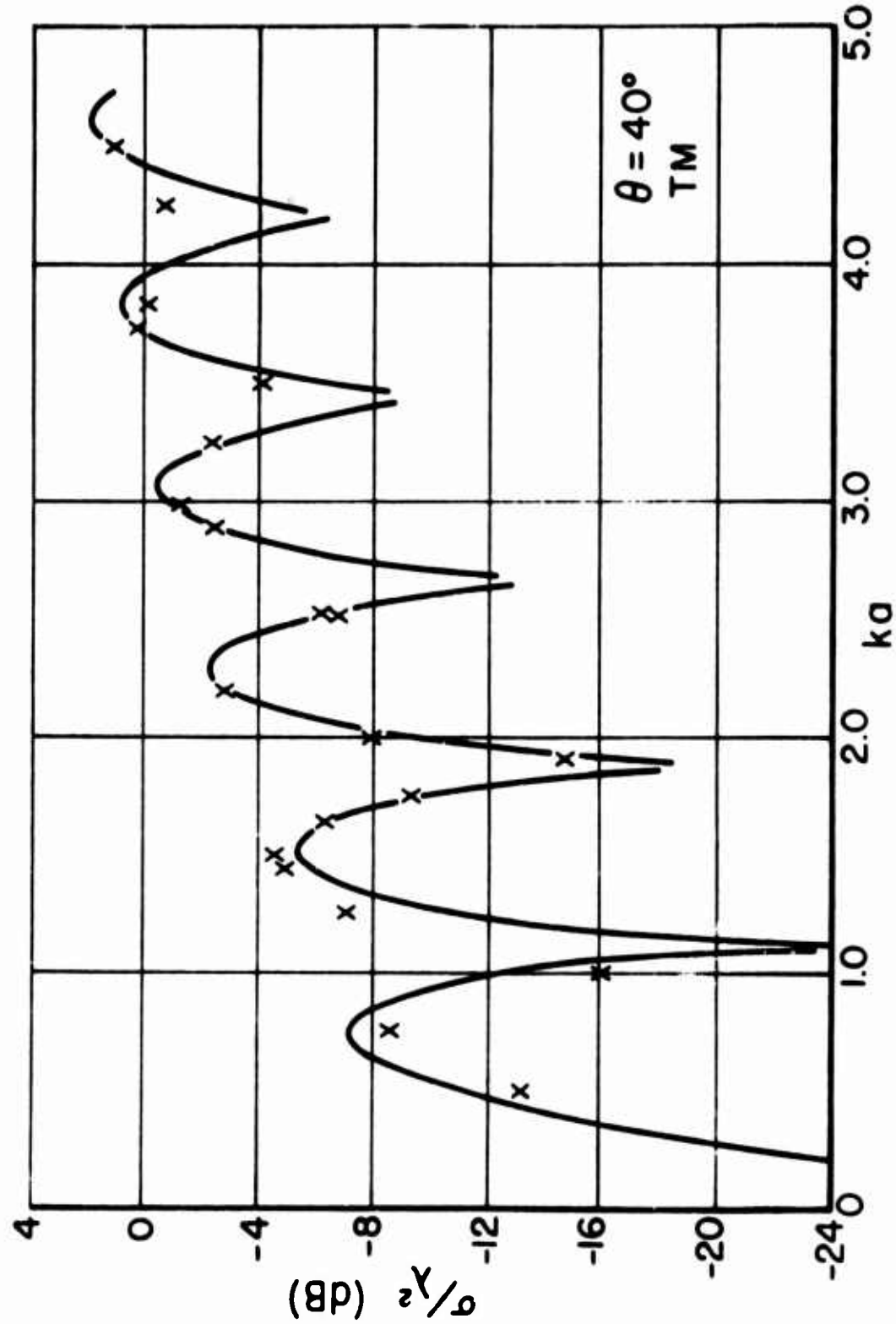

Fig. 28--Calculated (solid curve) and measured echo area of a 2:1 axial ratio prolate spheroid in dB > λ^2 as a function of minor axis circumference in wavelengths. $\theta = 40°$.
b. T. M. pol. polarization.

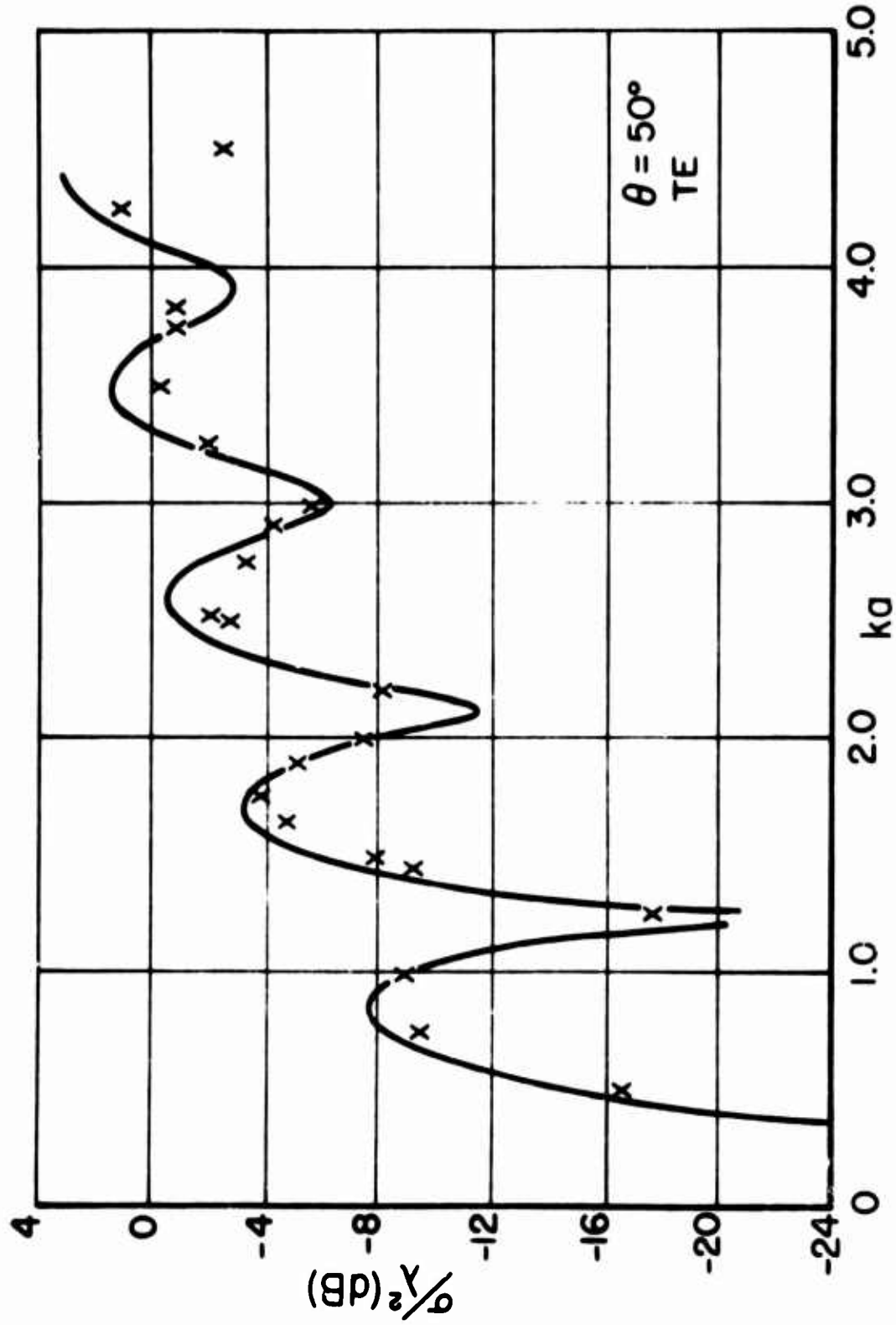

Fig. 29--Calculated (solid curve) and measured echo area of a 2:1 axial ratio prolate spheroid in dB > λ^2 as a function of minor axis circumference in wavelengths. $\theta = 50°$.
a. T. E. E. polarization.

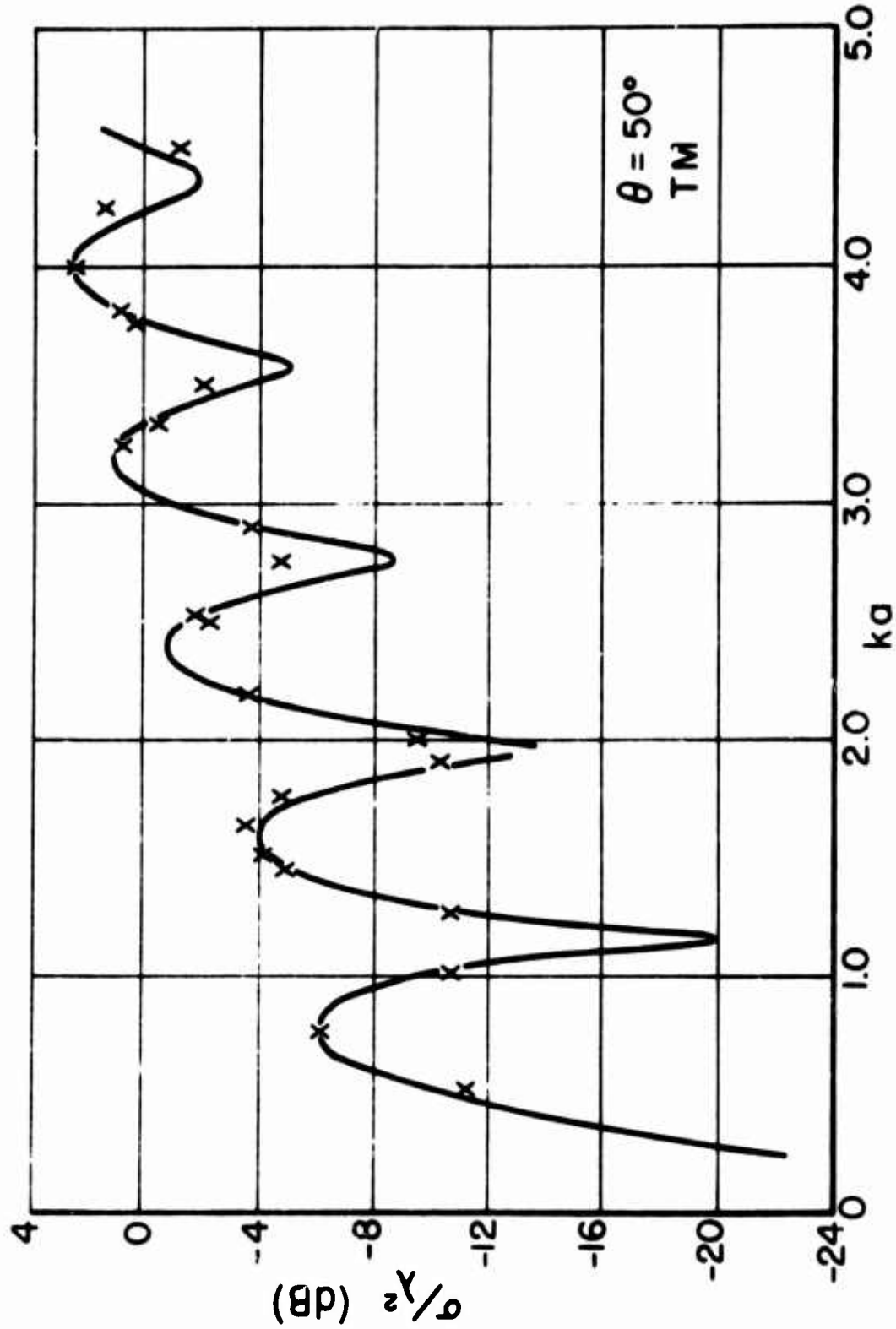

Fig. 29--Calculated (solid curve) and measured echo area of a 2:1 axial ratio prolate spheroid in dB > λ^2 as a function of minor axis circumference in wavelengths. $\theta = 50°$.
b. T. M. polarization.

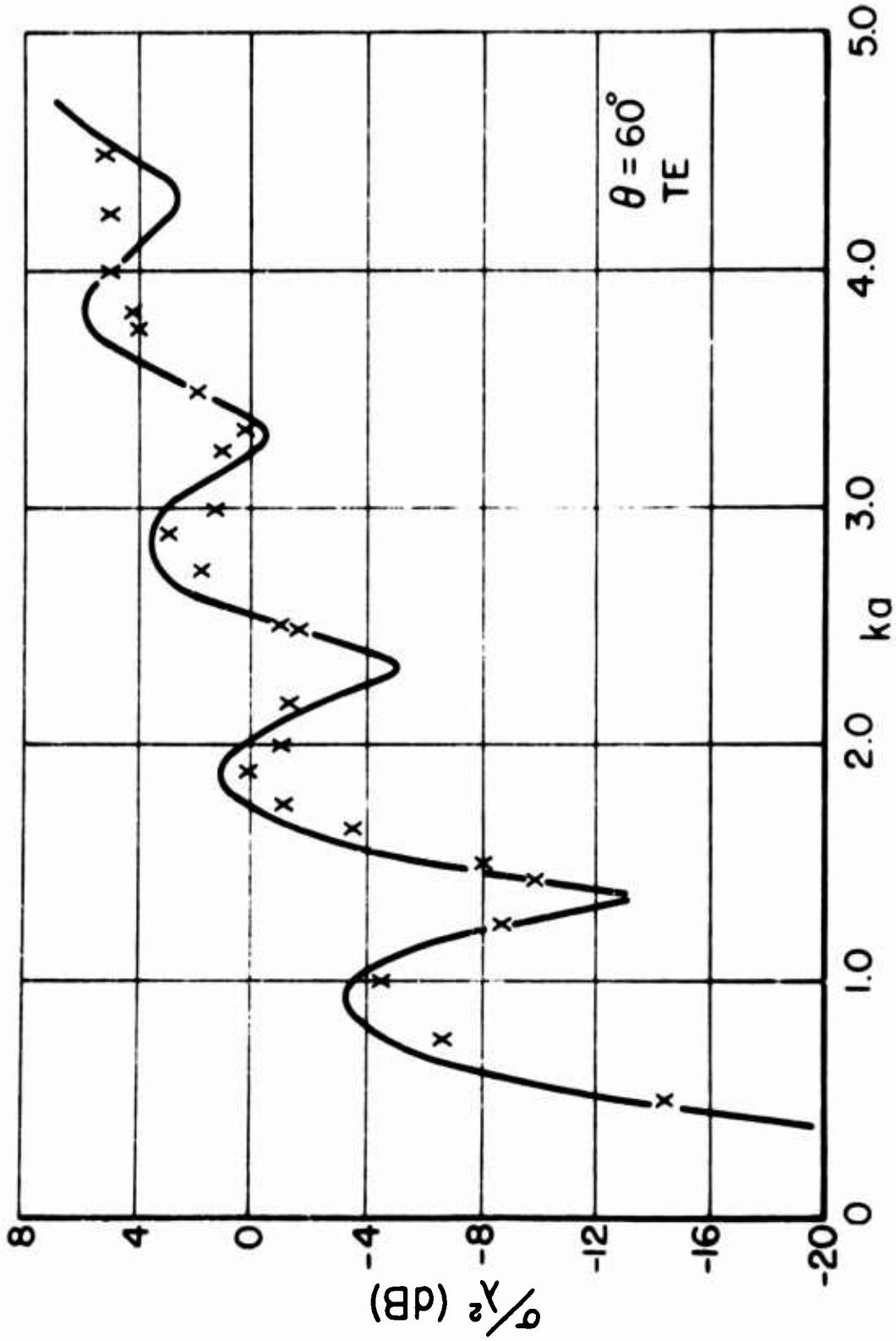

Fig. 30--Calculated (solid curve) and measured echo area of a 2:1 axial ratio prolate spheroid in dB > λ^2 as a function of minor axis circumference in wavelengths. $\theta = 60°$.
a. T. E. polarization.

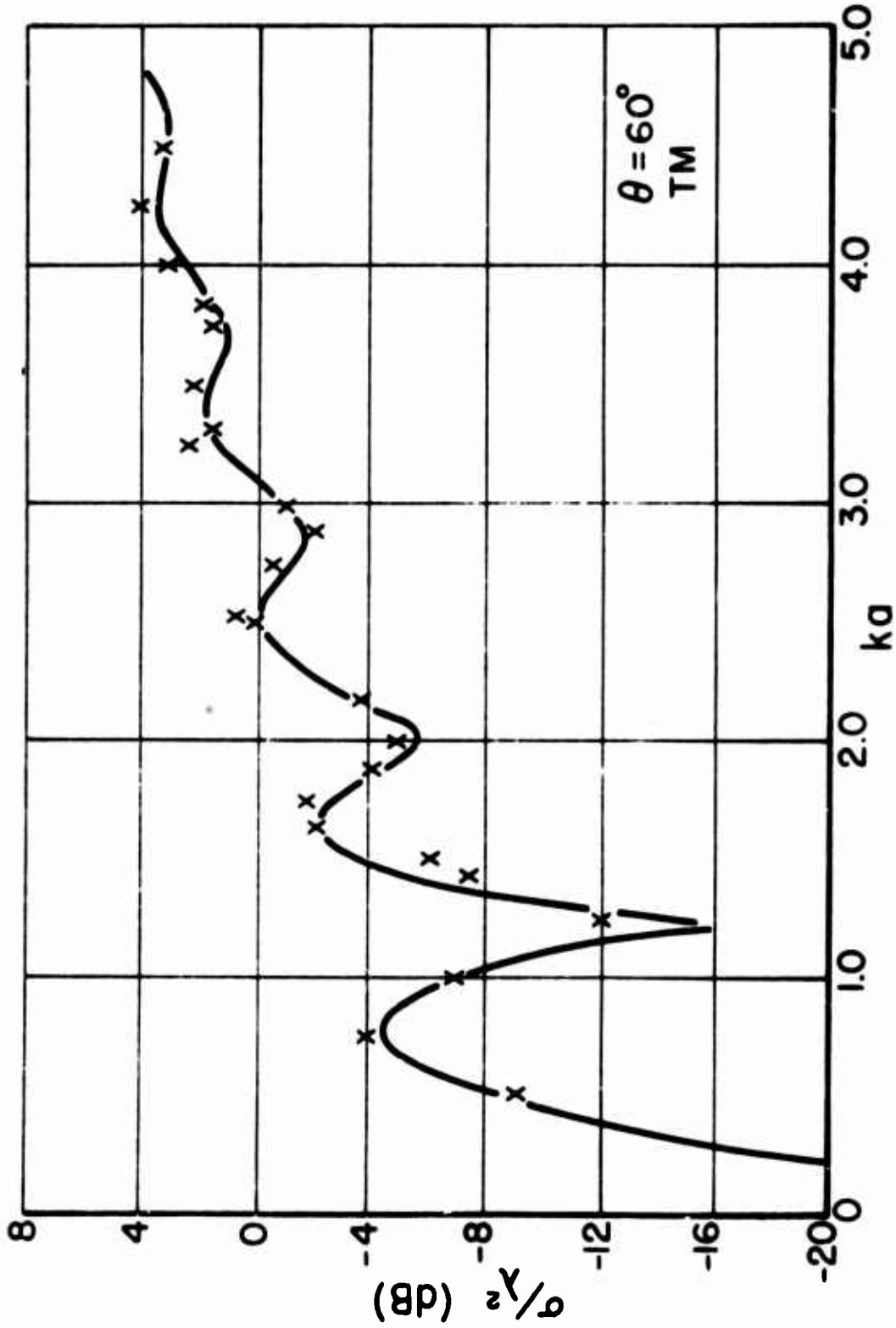

Fig. 30--Calculated (solid curve) and measured echo area of a 2:1 axial ratio prolate spheroid in dB > λ^2 as a function of minor axis circumference in wavelengths. $\theta = 60°$.
b. T. M. polarization.

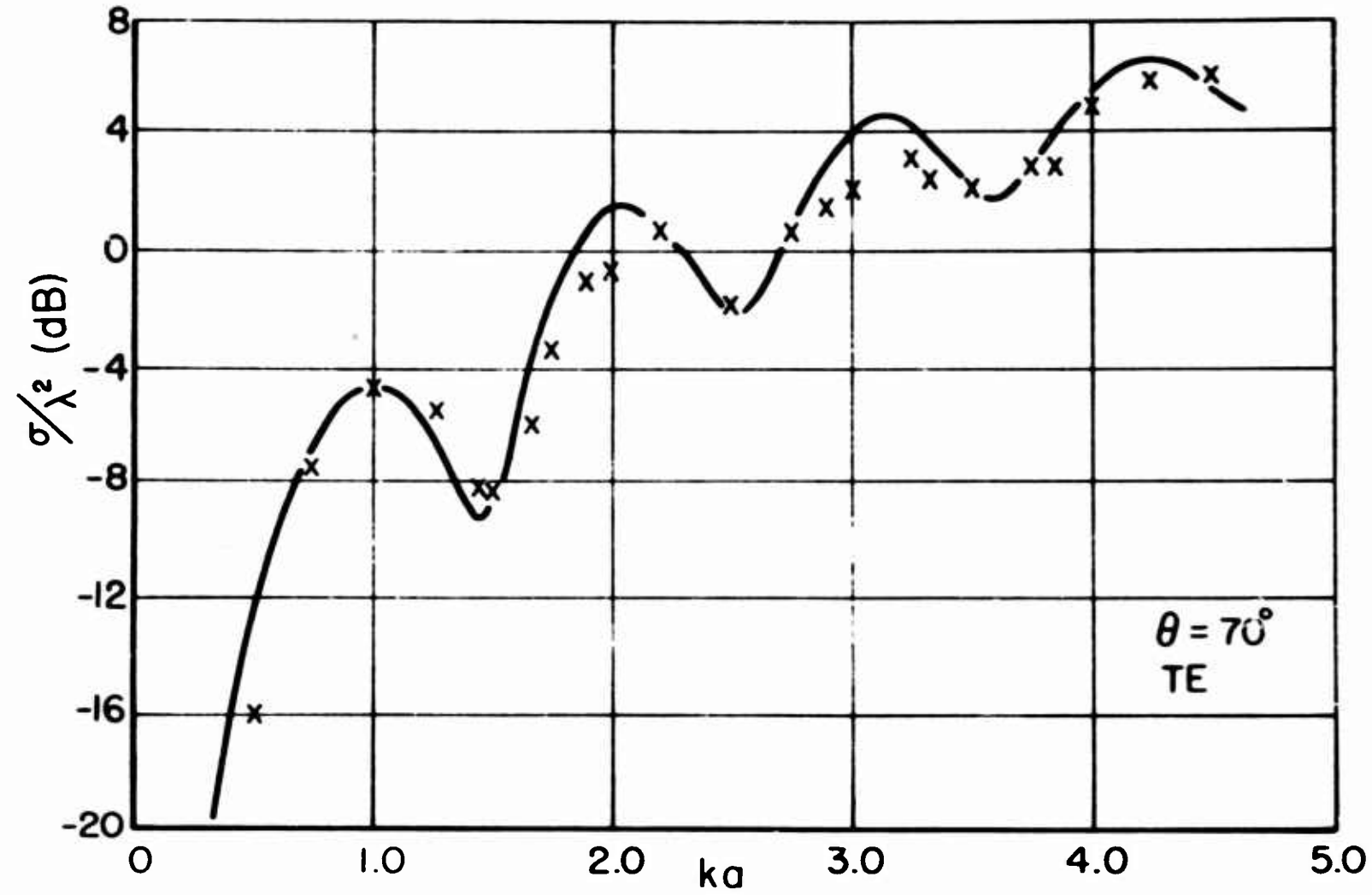

Fig. 31--Calculated (solid curve) and measured echo area of a 2:1 axial ratio prolate spheroid in dB > λ^2 as a function of minor axis circumference in wavelengths. $\theta = 70°$.
a. T. E. polarization.

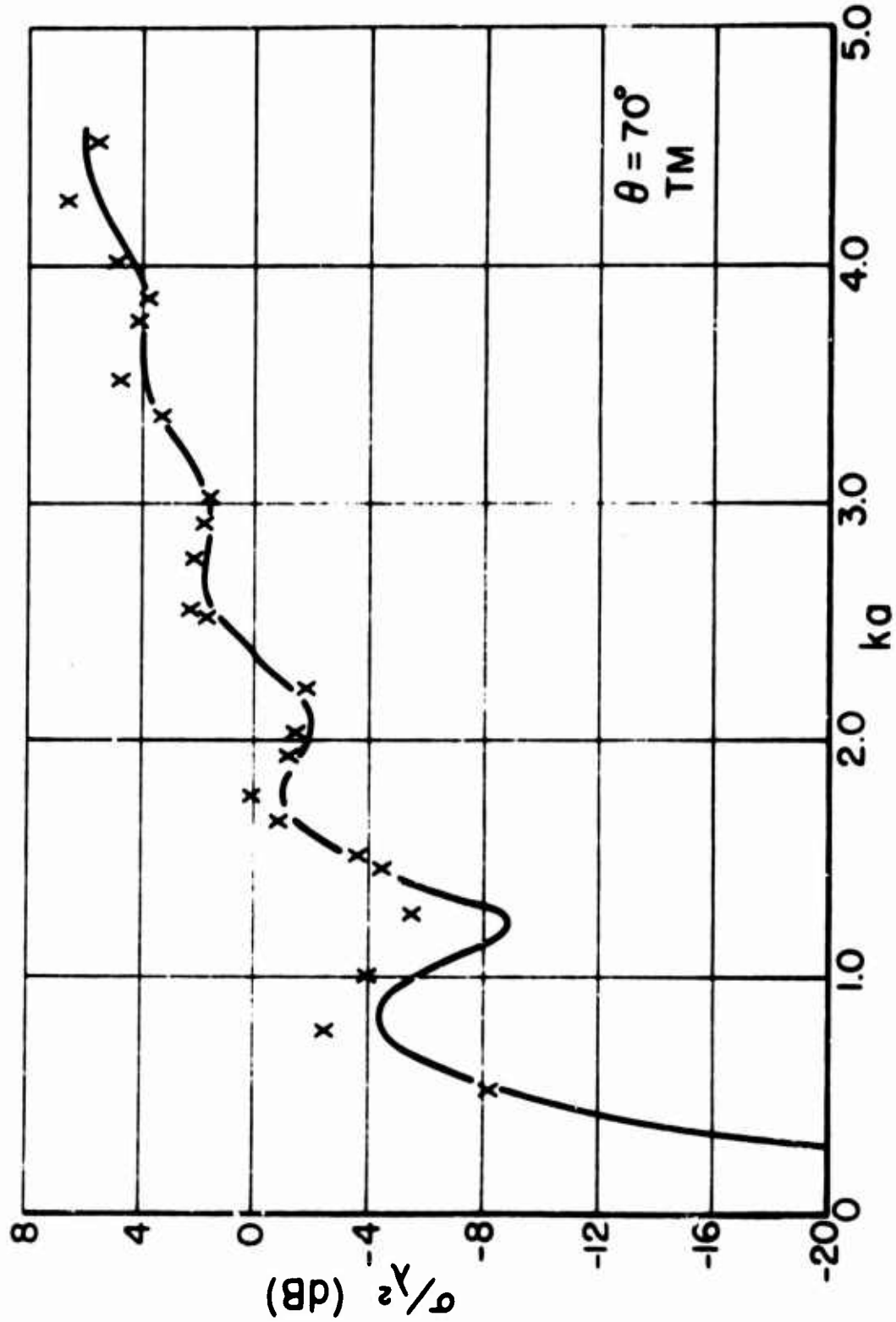

Fig. 31--Calculated (solid curve) and measured echo area of a 2:1 axial ratio prolate spheroid in dB > λ^2 as a function of minor axis circumference in wavelengths. $\theta = 70°$.
b. T. M. polarization.

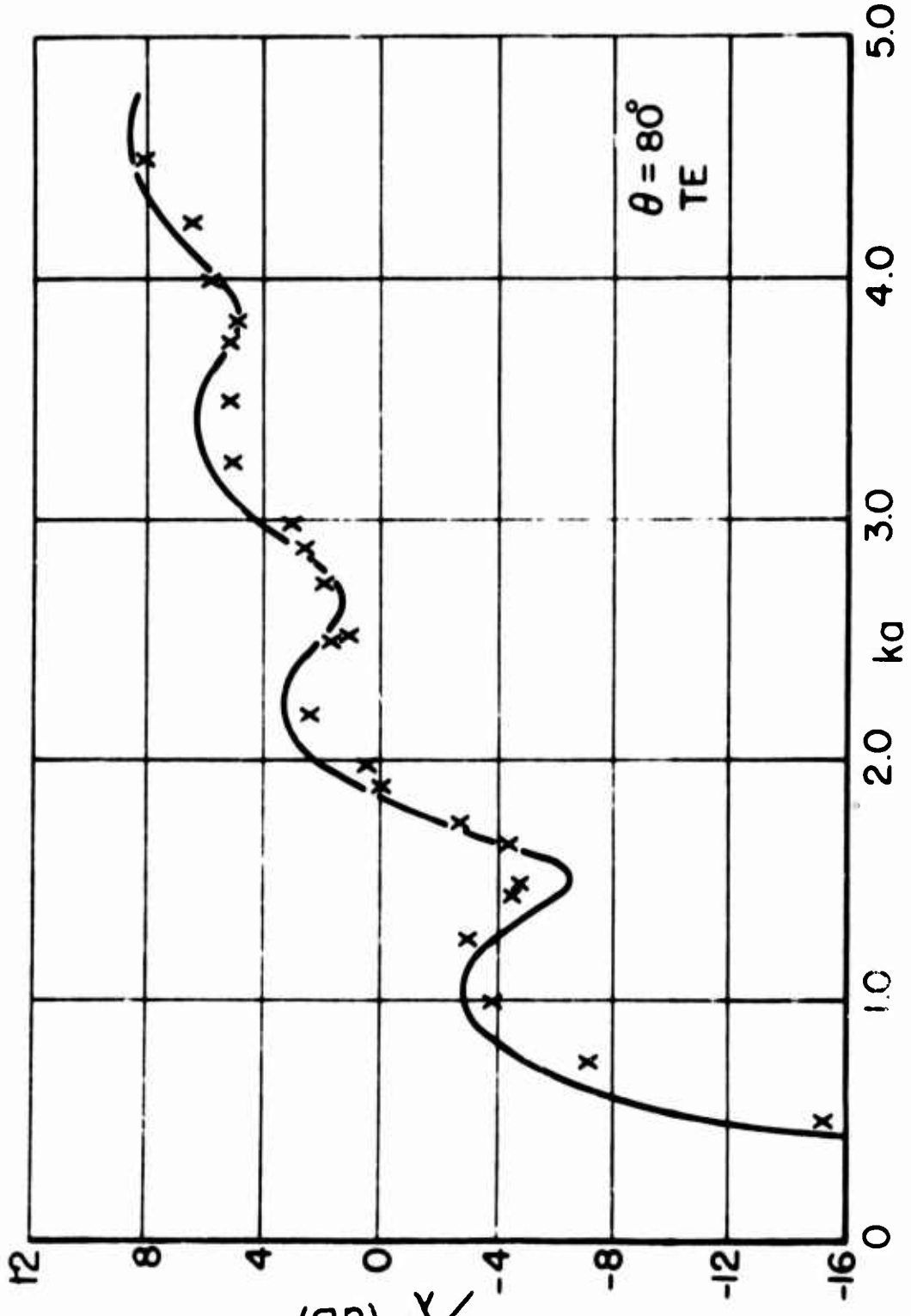

Fig. 32--Calculated (solid curve) and measured echo area of a 2:1 axial ratio prolate spheroid in dB > λ^2 as a function of minor axis circumference in wavelengths. $\theta = 80°$.
a. T. E. polarization.

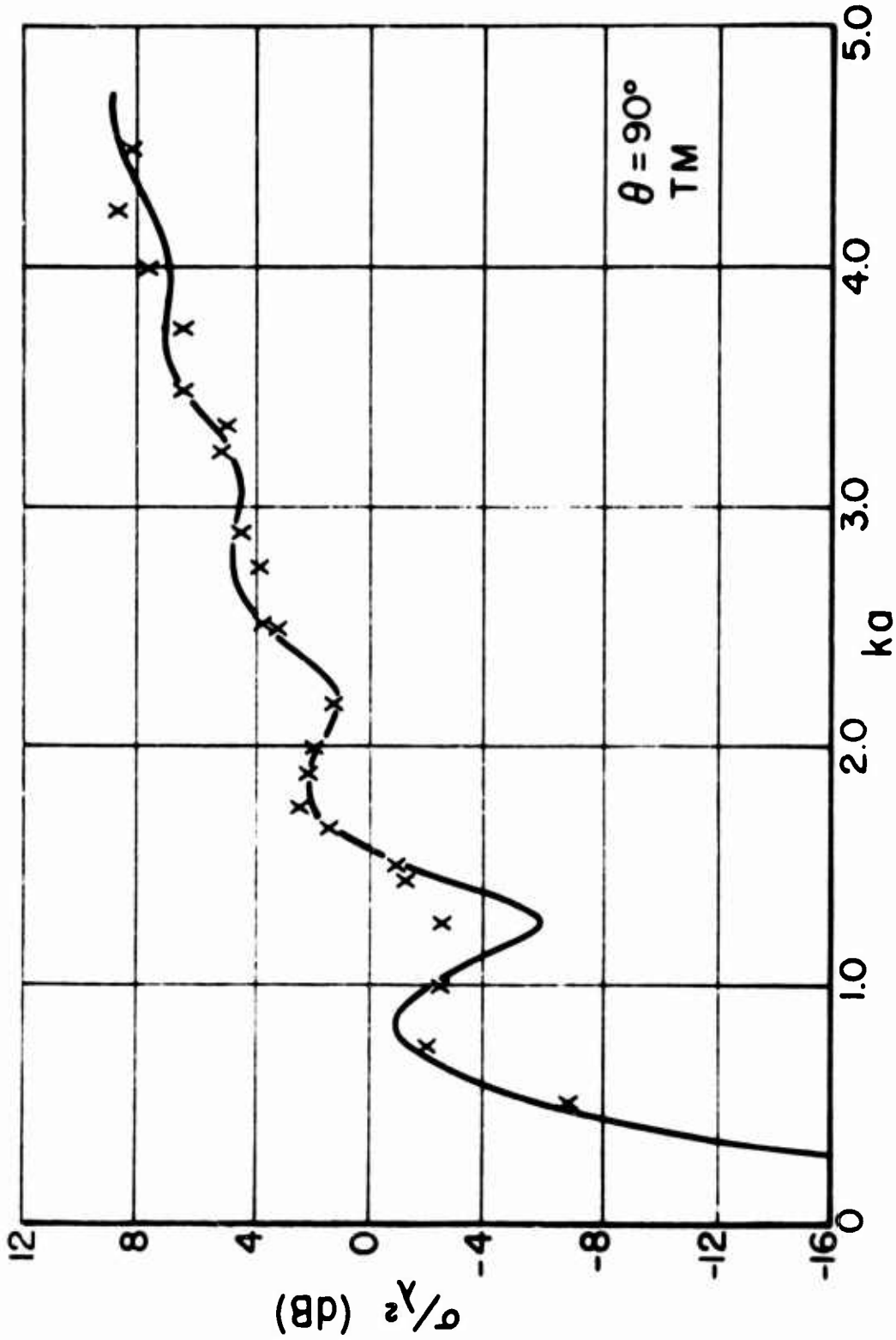

Fig. 32--Calculated (solid curve) and measured echo area of a 2:1 axial ratio prolate spheroid in dB > λ^2 as a function of minor axis circumference in wavelengths. $\theta = 80°$.
b. T. M. polarization.

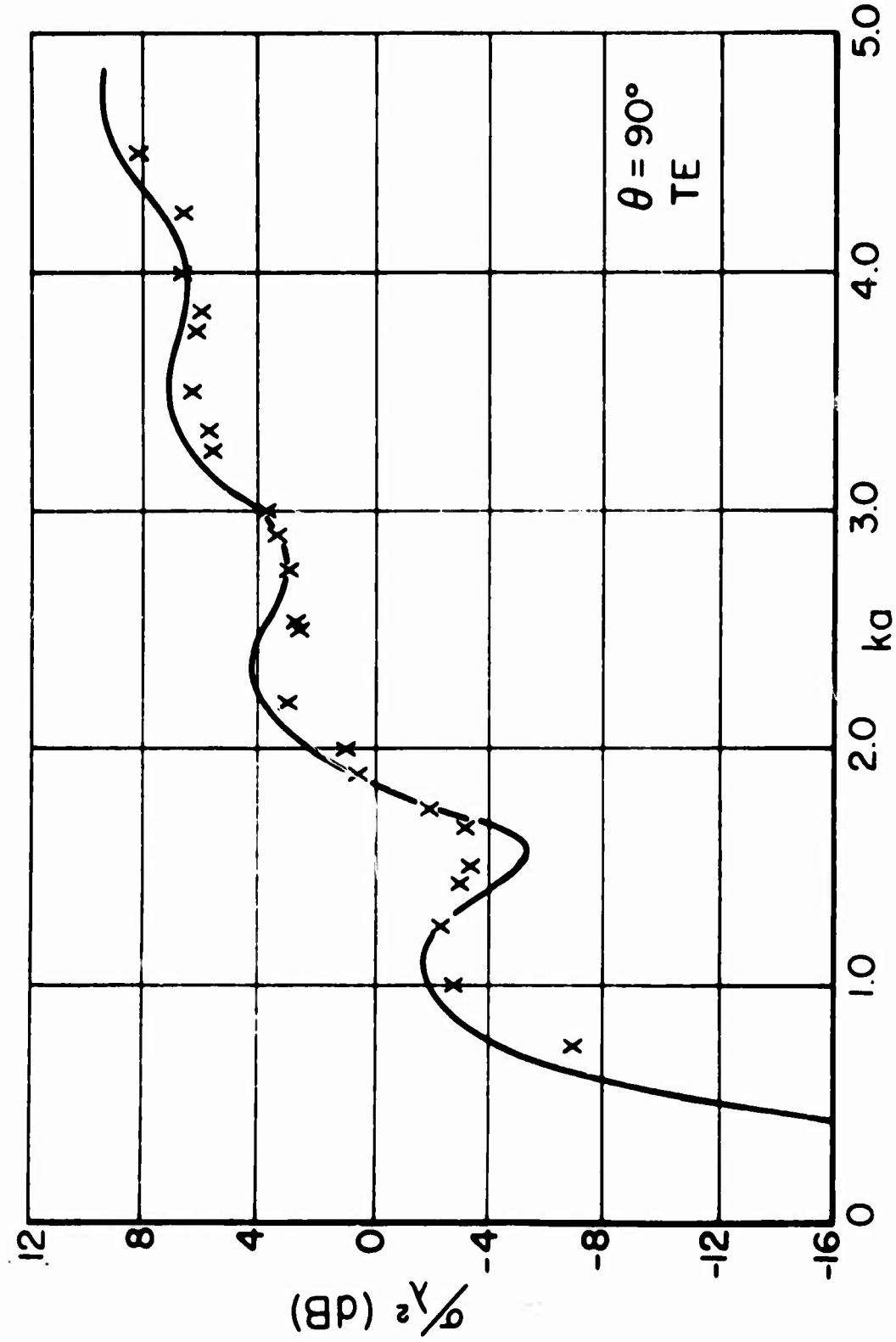

Fig. 33--Calculated (solid curve) and measured echo area of a 2:1 axial ratio prolate spheroid in dB > λ^2 as a function of minor axis circumference in wavelengths. $\theta = 90°$.
a. T. E. polarization.

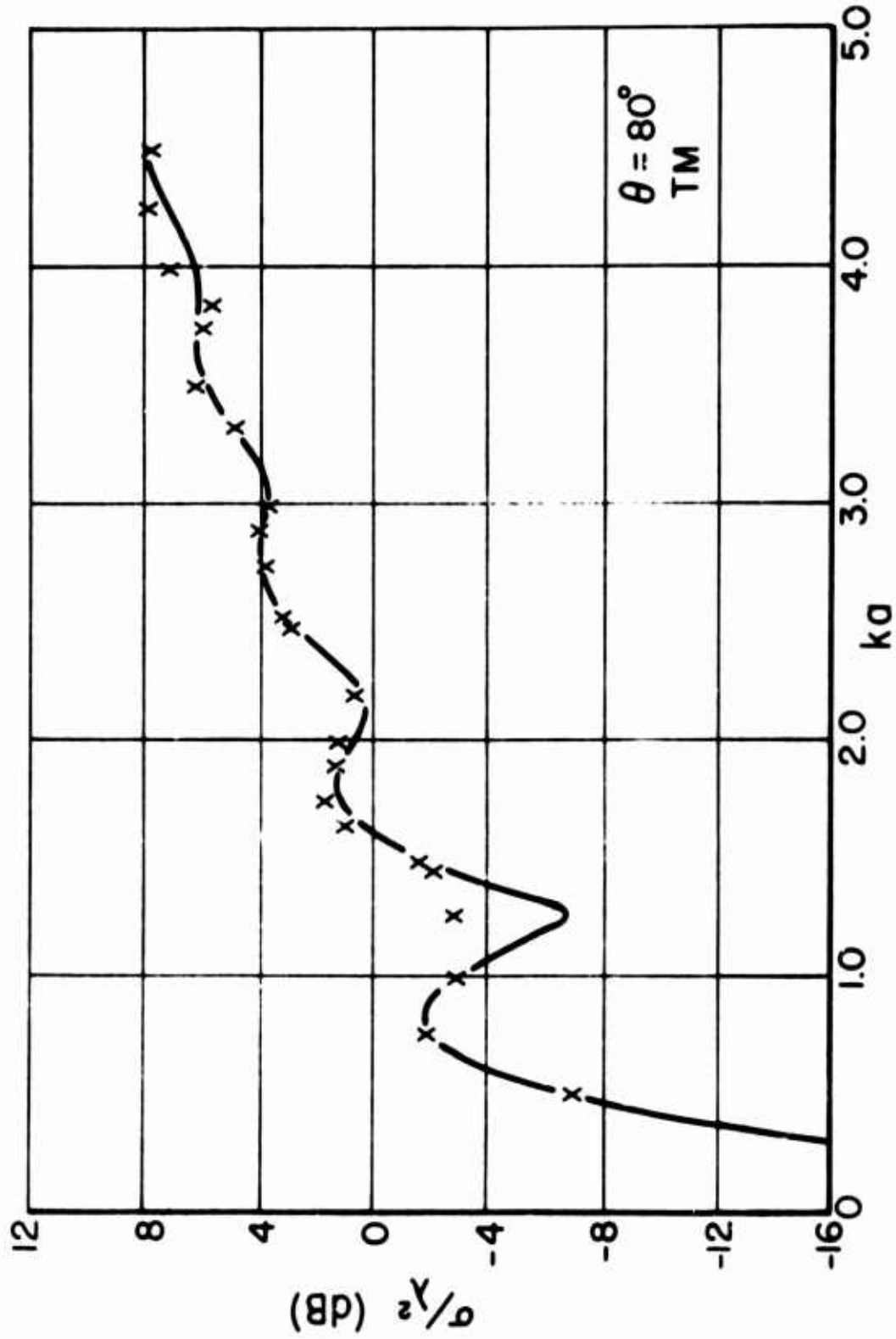

Fig. 33--Calculated (solid curve) and measured echo area of a 2:1 axial ratio prolate spheroid in dB > λ^2 as a function of minor axis circumference in wavelengths. $\theta = 90°$.
b. T. M. polarization.

and measured echc area of the 2:1 prolate spheroid are compared for aspect angles; θ, from 0° in increments of 10° to 90° as a function of the minor axis circumference of the spheroid in wavelengths. In each figure, the calculated data is the solid curve. Part a of each figure is for the T. E. polarization and part b for the T. M. polarization. It is evident from these figures that considering the crudeness of the theoretical model, substantial agreement with the measured data has been obtained. Minor disagreements are apparent, as in the location of maxima and minima for aspects of 0° and 10°, but the general indication is that the model rather accurately predicts the echo area of the 2:1 spheroid for arbitrary orientation and linear polarization.

The question concerning the ramp response waveforms of the ramp derived and impulse derived models is partially resolved by the comparison with measured echo data. It was found that for aspect angles less than 40° (for both polarizations) calculations from the ramp derived model were in somewhat better agreement with the measured data for minor circumferences less than one wavelength. For aspect angles greater than 40°, there was little to choose between the two models. In the limit of low frequencies the models agree, as dictated by the enforced moment conditions. For aspects less than 40° and minor axis circumferences less than one wavelength, the calculations shown in Figs. 24-28 are from the ramp derived model.

Turning to the second test, in Figs. 34 through 37, the measured and calculated echo and phase patterns of a 2:1 axial ratio spheroid for the T. M. polarization are shown for minor axis circumferences of 1. 5, 2. 0, 2. 5, and 3. 0 wavelengths respectively. In these figures the measured data are shown as the solid curve (part a of each figure is the echo data, part b the phase data). The phase data are referenced to the center of the spheroid. It is estimated that the echo area data have an error of $\pm$ 1. 0 dB at 20 dB below a square wavelength, and the phase data an error of $\pm$ 10 degrees. The agreement between calculated and measured data, while perhaps not as striking as for the variable frequency curves, is still reasonably good.

Calculations of the creeping wave peak predicted by Keller's geometrical theory of diffraction result were shown in Fig. 13 as a function of the spheroid axial ratio. Two points should be noted from this curve. First, Keller's result for the degenerate case of the sphere is in error, as is seen in Appendix II from the Fourier synthesis figures, and would have to be shifted in magnitude to be used. Second, for the 2:1 spheroid the change in creeping wave peak from the sphere case is so slight that a second model, for the case of a 2:1 spheroid, does not seem to be warranted. Suggestions for the use of the curve in Fig. 13 for higher axial ratio spheroids are given in the next Section. However, it is noted here that with estimates of the slope

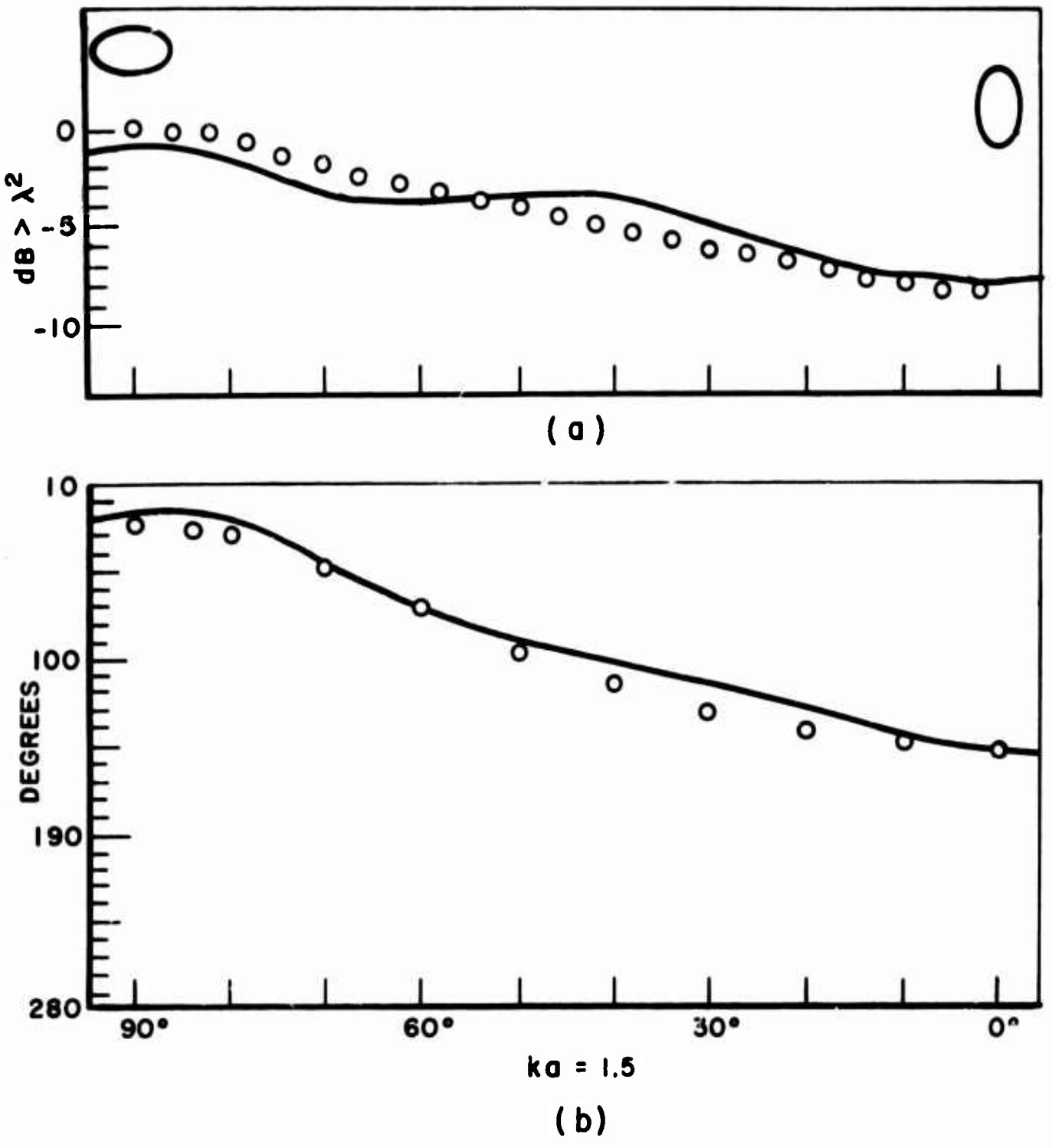

Fig. 34--Measured (solid) and calculated echo and phase patterns of a 2:1 axial ratio prolate spheroid. Minor axis circumference equal 1.5 wavelengths. (a) Echo area. (b) Phase.

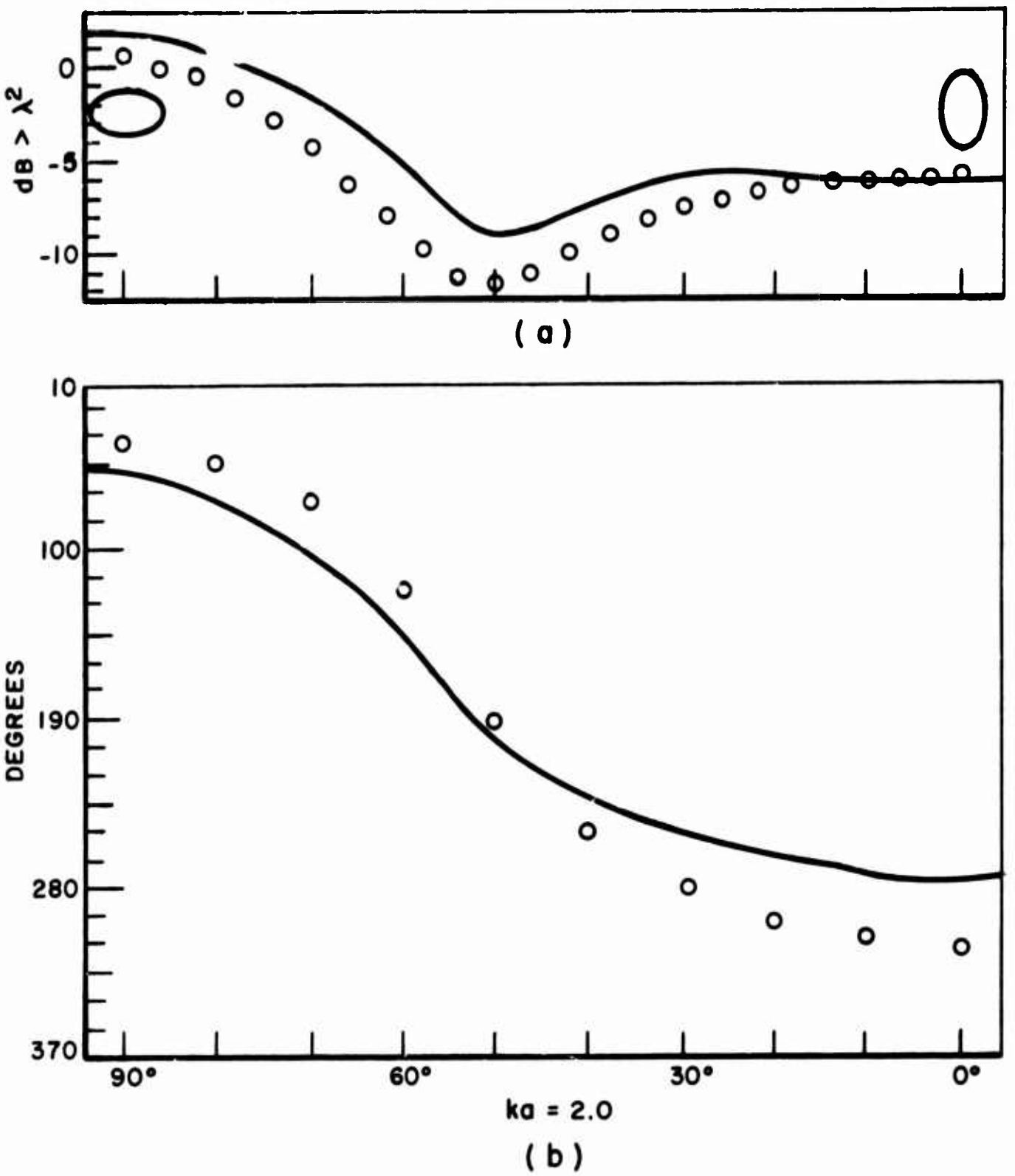

Fig. 35--Measured (solid) and calculated echo and phase patterns of a 2: axial ratio prolate spheroid. Minor axis circumference equal 2. 0 wavelengths. (a) Echo area. (b) Phase.

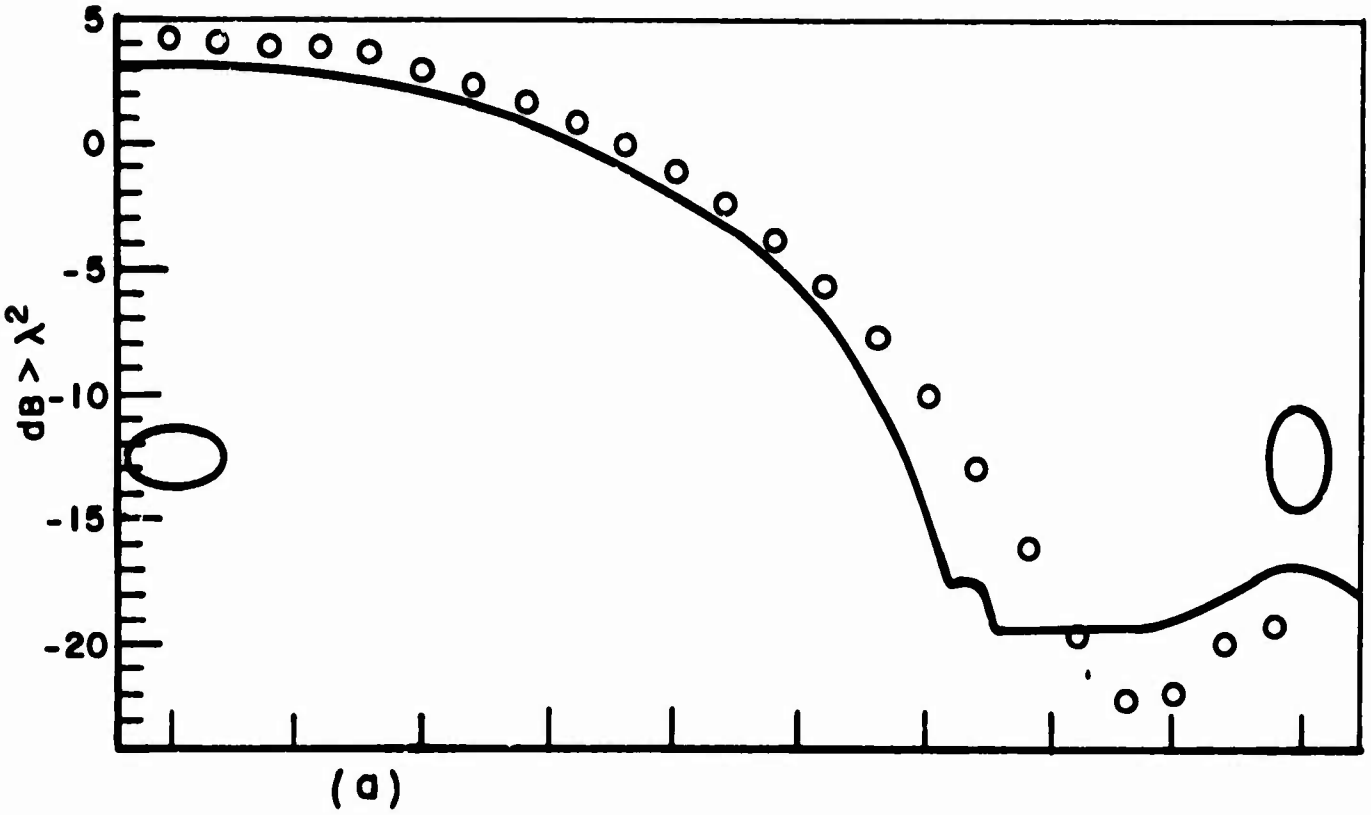

Fig. 36--Measured (solid) and calculated echo and phase patterns of a 2:1 axial ratio prolate spheroid. Minor axis circumference equal 2. 5 wavelengths. (a) Echo area. (b) Phase.

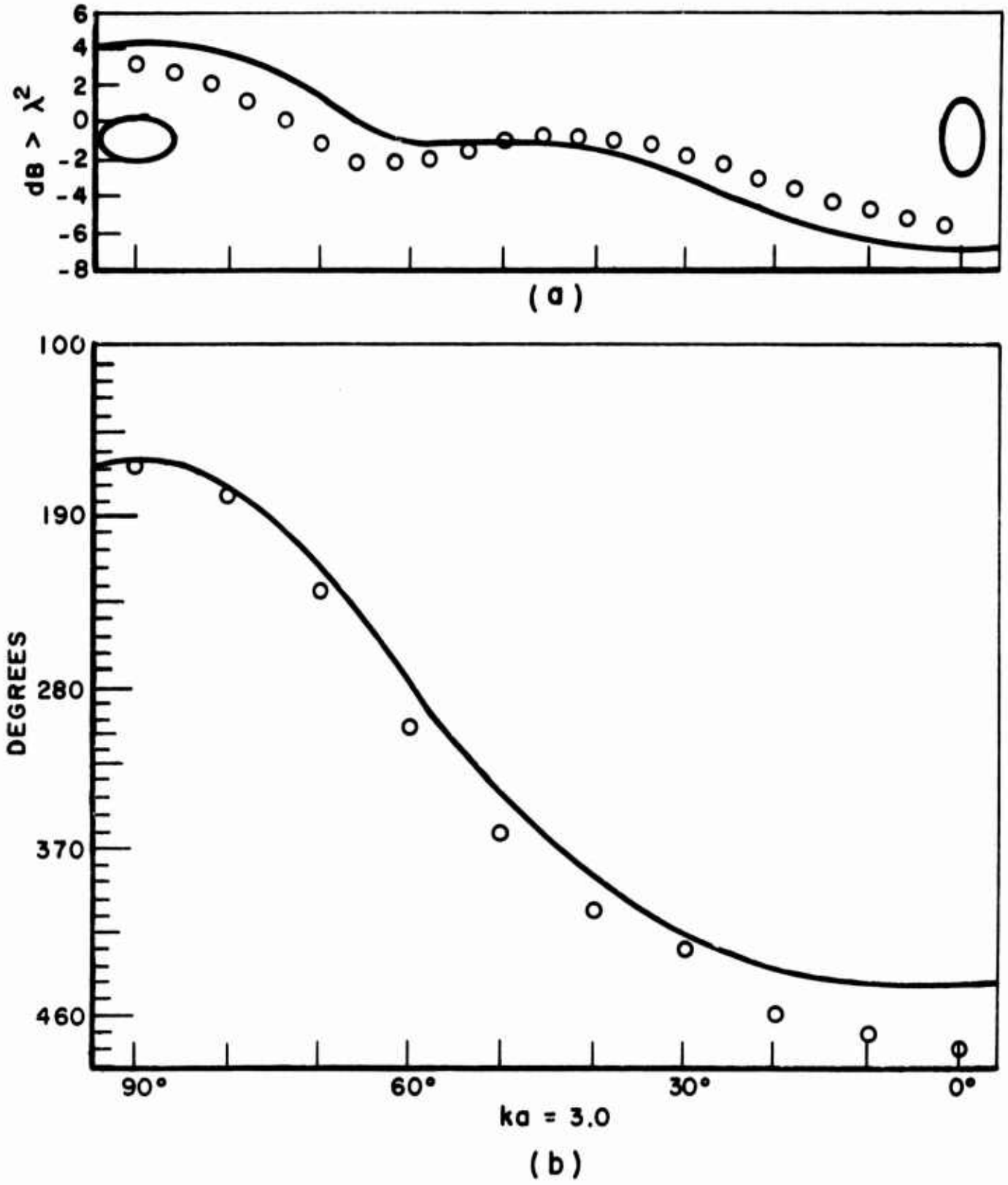

Fig. 37--Measured (solid) and calculated echo and phase patterns of a 2:1 axial ratio prolate spheroid. Minor axis circumference equal 3.0 wavelengths. (a) Echo area. (b) Phase.

of the creeping wave on either side of the peak from Keller's theory, additional parameters could be added to the impulse waveform model. Realistically, there seems little advantage in this added complexity until failures of the simpler model are noted or a more exact asymptotic estimate of the spheroid creeping wave is obtained.

Finally it is desired to list some results obtained from the impulse response waveform model of the 2:1 spheroid which may be of use to other investigators. The primary concern is not, as was noted in Chapter I, the details of the impulse response waveform of the derived model, but is instead the predicted ramp response waveform. A reasonable approximation to this ramp waveform can be generated by Fourier synthesis from the first nine harmonics of the phasor response, and a comparison of the ramp waveform predicted by other theories with those given here would be extremely useful. To this end, the predicted phasor response for both the T. E. and T. M. polarizations at aspects of 0° (10°) 90° for minor axis circumferences from 0.25 (0.25) 2.25 wavelengths are tabulated in Table IV. The phase reference for these data is at the point the incident wave first strikes the spheroid. Note in Table IV that the real and imaginary parts are normalized such that the cross section normalized by the shadow cross-sectional area πa^2 is given by the sum of the squares of the real and imaginary parts.

TABLE IV

$\sigma / \pi a^2 = |R^2 + I^2|$ T. E. POLARIZATION (Minor Axis Circumference in Wavelengths)

Aspect Angle θ in Degrees		0.25	0.50	0.75	1.00	1.25	1.50	1.75	2.00	2.25
0	R	0.176	-0.484	-0.886	-0.054	-0.621	-0.871	0.009	-0.731	-0.688
	I	-0.266	-0.811	0.133	-0.104	-0.668	0.319	-0.009	-0.482	0.348
10		0.181	-0.472	-0.927	-0.060	-0.564	-0.935	-0.022	-0.656	-0.783
		-0.264	-0.837	0.111	-0.069	-0.679	0.257	0.074	-0.520	0.294
20		0.195	-0.432	-1.046	-0.099	-0.410	-1.066	-0.188	-0.431	-0.973
		-0.258	-0.911	0.030	0.033	-0.667	0.048	0.273	-0.531	0.059
30		0.217	-0.351	-1.221	-0.235	-0.228	-1.106	-0.586	-0.195	-0.954
		-0.246	-0.990	-0.166	0.193	-0.542	-0.296	0.400	-0.296	-0.354
40		0.245	-0.430	-1.303	-0.724	-0.175	-0.939	-1.092	-0.336	-0.583
		-0.228	-1.059	-0.413	0.368	-0.278	-0.612	0.195	0.152	-0.511
50		0.275	-0.423	-1.401	-1.150	-0.378	-0.680	-1.349	-0.973	-0.448
		-0.204	-1.208	-0.697	0.230	0.015	-0.674	-0.311	0.308	-0.095
60		0.303	-0.391	-1.558	-1.603	-0.819	-0.608	-1.275	-1.589	-1.044
		-0.176	-1.477	-1.049	-0.027	0.187	-0.487	-0.725	-0.096	0.256
70		0.329	-0.268	-1.775	-2.108	-1.392	-0.819	-1.172	-1.848	-1.839
		-0.147	-1.858	-1.527	-0.366	0.209	-0.254	-0.855	-0.648	-0.028
80		0.348	-0.060	-1.967	-2.600	-1.951	-1.152	-1.201	-1.926	-2.344
		-0.124	-2.225	-2.060	00.734	0.147	-0.097	-0.838	-1.008	-0.409
90		0.356	0.057	-2.041	-2.823	-2.208	-1.322	-1.244	-1.952	-2.510
		-0.115	-2.380	-2.319	-0.915	0.105	-0.042	-0.817	-1.129	-0.609

TABLE IV (Contd.)

$\sigma / \pi a^2 = |R^2 + I^2|$ T. M. POLARIZATION (Minor Axis Circumference in Wavelengths)

Aspect Angle θ in Degrees		0.25	0.50	0.75	1.00	1.25	1.50	1.75	2.00	2.25
0	R									
	I									
10		0.170	-0.454	-0.929	-0.083	-0.603	-0.907	-0.009	-0.705	-0.739
		-0.271	-0.805	0.056	-0.010	-0.676	0.291	0.027	-0.502	0.325
20		0.177	-0.426	-0.997	-0.024	-0.553	-1.006	-0.080	-0.624	-0.877
		-0.275	-0.841	-0.039	0.173	-0.694	0.202	0.127	-0.545	0.238
30		0.216	-0.440	-1.085	-0.134	-0.474	-1.130	-0.241	-0.492	-1.042
		-0.268	-0.983	0.045	0.241	-0.696	0.041	0.262	-0.550	0.049
40		0.257	-0.414	-1.314	-0.317	-0.412	-1.256	-0.535	-0.376	-1.148
		-0.265	-1.073	-0.071	0.296	-0.672	-0.190	0.365	-0.454	-0.239
50		0.299	-0.715	-1.500	-0.563	-0.403	-1.358	-0.954	-0.388	-1.128
		-0.263	-1.240	-0.214	0.324	-0.626	-0.463	0.360	-0.243	-0.524
60		0.342	-0.842	-1.784	-0.861	-0.473	-1.460	-1.447	-0.626	-1.052
		-0.264	-1.528	-0.383	0.326	-0.591	-0.746	0.210	-0.003	-0.676
70		0.382	-0.980	-2.192	-1.198	-0.596	-1.603	-1.963	-1.068	-1.067
		-0.271	-1.962	-0.590	0.332	-0.600	-1.039	-0.048	0.160	-0.674
80		0.411	-1.076	-2.642	-1.521	-0.707	-1.760	-2.425	-1.548	-1.196
		-0.282	-2.442	-0.813	0.362	-0.639	-1.326	-0.326	0.221	-0.616
90		0.422	-1.105	-2.857	-1.668	-0.748	-1.830	-2.629	-1.770	-1.279
		-0.290	-2.670	-0.922	0.384	-0.660	-1.462	-0.458	0.228	-0.587

Calculated data on a prolate spheroid with a 10:1 axial ratio for axial incidence ($\theta = 0°$) have been given by Siegel, et al. [38]. These data are shown in Fig. 38 as the solid curve. Also shown in Fig. 38 are calculations for this target from the ramp response derived model. These data are designated by crosses. An impulsive response waveform model for this target was also given by Kennaugh and Cosgriff[3], and showed reasonable agreement with the calculated data. For such a large axial ratio spheroid, it is clear that the simple model in Eq. (78) is not a good approximation. As shown by the model in Reference 3, the creeping wave contribution for such a large axial ratio is well approximated by a very narrow rectangular pulse. It is not practical to obtain such a waveform with one exponential term as in Eq. (78). Therefore, for large axial ratio spheroids, the ramp response derived model should be used. This point is discussed in the next section.

D. Conclusions

It was mentioned earlier in this Chapter that certain of the approaches and procedures followed in attacking the prolate spheroid problem were, with the experience gained herein, not necessarily those recommended either as an approach to future problems or a continuation of the spheroid study. One must remember that the use of transient and impulse response waveform estimates in electromagnetic scattering problems is still an embryonic art. Significant

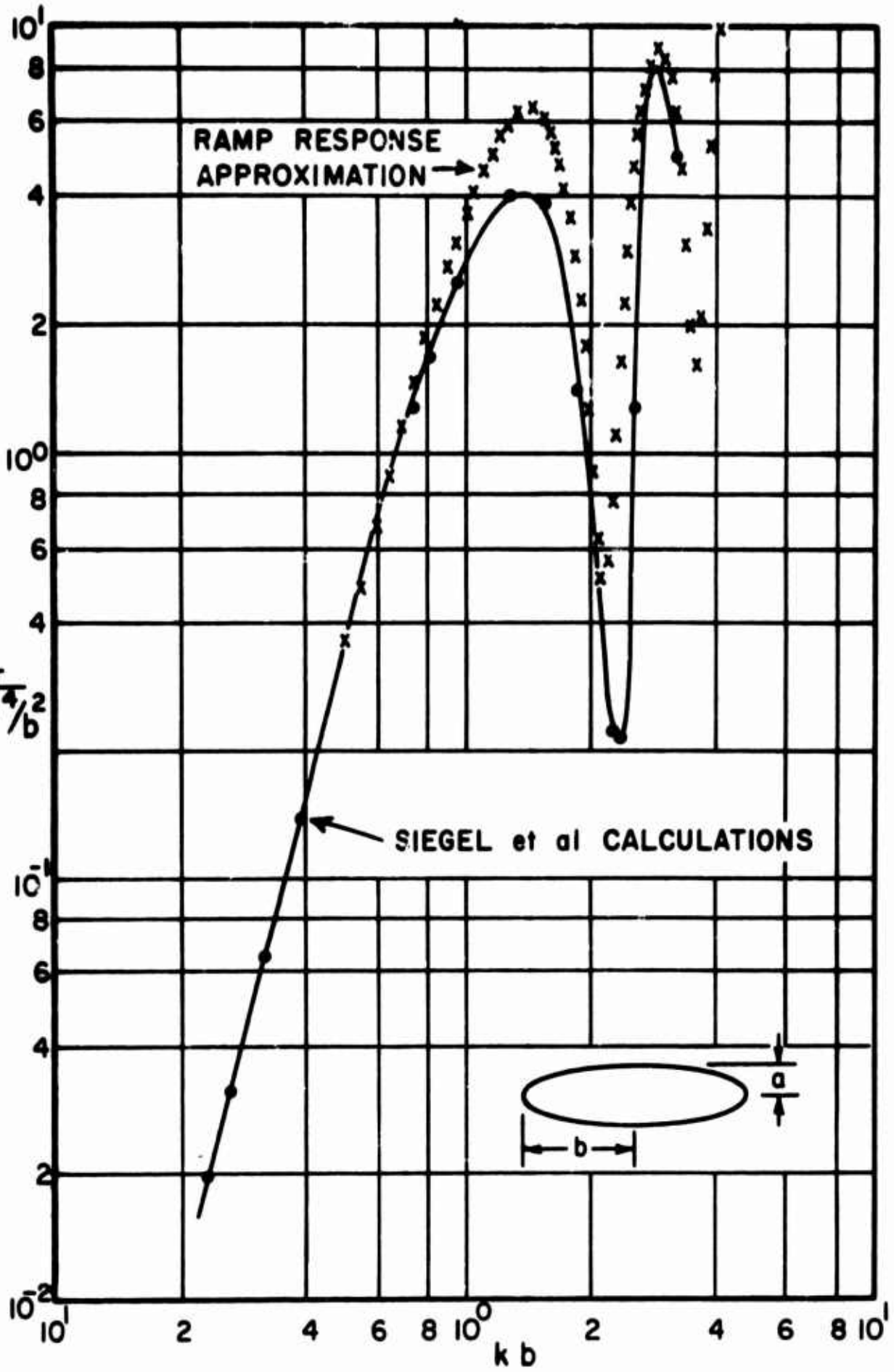

Fig. 38--Axial ($\theta = 0°$) echo area of a 10:1 axial ratio prolate spheroid.

contributions have been made, as cited in Chapter I, both to the solution of new scattering problems, and providing additional insight to the scattering mechanism. In a sense, however, as discussed in Chapter I, these contributions have been made with a limited approach in that a systematic procedure for application of the concepts has not been developed. Unfortunately, these comments hold true for the material reported in this Chapter. A general model has been developed for the electromagnetic backscattering by a perfectly conducting prolate spheroid target for arbitrary linear polarization and arbitrary orientation which has been shown to be in reasonable agreement with measured data for a spheroid of 2:1 axial ratio. But despite this success, the void with regard to a systematic procedure remains. The conclusions from this Chapter therefore are of two types; those pertaining strictly to the spheroid model, its deficiencies, possible improvements, and applicability to other untested axial ratios, and those pertaining to the application of a time domain approach to other problems. In this Section, the discussion will be confined to the former type, i. e., to the specific model developed for the conducting prolate spheroid target. What insight has been gained in developing a systematic approach to the general problem has been incorporated

into Chapter I, primarily into Section C of Chapter I, on the analytical and experimental approximations of transient and impulse response waveforms.

Consider first the deficiencies of the model, and admittedly it has many. These deficiences are primarily in terms of failures to relate the geometrical properties of the spheroid to the corresponding detail of the model. It is certainly clear that the different radii of curvature in the two planes, the changing shadow boundary with respect to the line of sight, and the polarization properties of the spheroid, must, in any complete analysis, materially affect the transient waveform. Some of these effects may have been partially accounted for by the conditions imposed on the model. But these conditions were not explicitly related to the geometrical detail, consequently when rather large changes in the geometry are made, as with a large axial ratio spheroid or a different smooth geometry, there is no assurance that the same conditions will continue to effect adequate compensation. These comments apply both to the illuminated and shadowed side of the spheroid. On the illuminated side, corrections are needed to the physical optics approximation which are related to the geometry. For the conducting sphere, Weston[44] has supplied such an additional term from an asymptotic expansion of the optics field, and asymptotic estimates might be utilized for the spheroid

in a future analysis. Similar comments apply to the creeping wave portion of the model. Despite the success of the comparison with measured data, the exact nature of the creeping wave contribution is still unknown. How the contribution builds to the secondary peak, the slope of the waveform on either side of this peak, and particularly how the geometry of the spheroid is related to these effects is not known. In this regard, the noncausal nature of the creeping wave contribution in the time domain (see Appendix II) predicted by asymptotic estimates and the attendant questions would seem to indicate that a complete understanding of the sphere scattering in all detail has not been attained as yet.

With regard to the estimates of the time domain waveforms, it must be concluded in light of the above remarks that the detailed features of the waveform may bear scant resemblence to the true response. This points out an extremely useful and at the same time frustrating nature of the transient waveforms. Very crude approximations in the time domain lead, in many cases, to estimates of the phasor response which are out of all proportion to the exactness of the approximation. In establishing the correctness of the time domain waveform then, comparisons of the calculated and measured echo area of an object are of limited usefulness. This is particularly true if the measured data are confined to a small portion of the spectrum. It is felt

that the ramp response waveforms predicted by the ramp derived model are a reasonable estimate of the true response. No such confidence is expressed in the ramp and related step and impulse response waveforms of the impulse derived model, however, except in the gross features of the response.

With regard to the utilization of the impulse derived model for other axial ratio spheroids, the following comments are offered. Keller's model for the creeping wave contribution is clearly inadequate since it fails even in the degenerate case of the sphere to predict the correct detail of the waveform. However, with no present alternative, it is suggested that for higher axial ratios the peak of the creeping wave shown in Fig. 13 be utilized after first scaling the results so that they agree, for the degenerate sphere case, with the Fourier synthesis result using the exact solution. Thus for the T. E. polarization a varying magnitude, P, for the creeping wave peak should be used while for the T. M. case it remains fixed by the axial ratio of the spheroid. The predicted ramp response waveform and the magnitude of the correction term remain clues to the estimate. Any radical departure of the form of the ramp waveform, aside from a general stretching, should be suspect as should the magnitude of the correction term. The parameter C should be determined from tests of the impulse response waveform at $\theta = 0°$ and

90°. The basic premise being to retain the gross resemblance of the waveform to that of the sphere. Both Keller's result and simply an examination of the geometry indicate that as the axial ratio of the spheroid increases, the attenuation of the creeping wave should decrease. In the time domain this would indicate that the waveform in the neighborhood of the creeping wave peak should become narrower with increasing axial ratio. As mentioned earlier, the impulse response waveform of a 10:1 axial ratio spheroid given in Reference 3 demonstrated this effect. As the axial ratio of the spheroid increases, the creeping wave contribution apparently approaches a very narrow, high spike, with negligible value except in the immediate vicinity of the creeping wave peak. It is clear that the simple impulse response derived model in Eq. (85) is not practical for large axial ratio spheroids. For example, a value of 1×10^{-3} is required for C to achieve a reasonable waveform for a 10:1 axial ratio spheroid. For such large axial ratios, models such as that given in Reference 3 or the ramp response derived estimate in Section B should be used. For axial ratios greater than 2:1 or 3:1, it will probably not be possible to use a single value for the parameters $\tilde{C}$ and P for all orientations and polarizations. The model loses much of its attractiveness in this case since individual adjustments for each orientation and polarization will be required. The impulse response derived model

has not been tested for axial ratios greater than 2:1. It is evident however that utilization of the model becomes more difficult with increasing axial ratio and is probably prohibitively difficult, without modifications, for axial ratios greater than 5:1.

It is readily apparent that this study in the time domain of the prolate spheroid target has raised more questions than it has answered. A novel result has been obtained; a model predicting the backscattering from the prolate spheroid target for arbitrary orientation, and linear polarization of the incident field has been derived; and the general validity of the model demonstrated for the case of a 2:1 spheroid. In the opinion of the author, this model, with judicious application, may continue to demonstrate reasonable agreement with other measured or calculated data for axial ratios less than 5:1. In fairness both to this study and to the time domain approach in general, one should be cognizant of the numerous frequency domain studies of the spheroid target which have had far less success. However, it is clear than an understanding of the scattering by the spheroid, and consequently an ability to project these results to other shapes, is meager. The most pressing requirement at present is a detailed model for the creeping wave contribution from smooth surfaces in the time domain. The asymptotic high frequency estimates of this response, when transformed to the time domain, offer clues in this

direction, particularly with regard to the behavior of this reponse in the neighborhood of its peak. A feeling persists however that the ultimately most fruitful attack on the problem will be one undertaken in the time domain. Considering the relative simplicity of the real, time-dependent waveforms corresponding to complex frequency-dependent functions; it does not seem unrealistic to suggest that such time-dependent functions may be more intimately and simply related to the geometry of the scattering object. This comment is felt to be pertinent in general, and not restricted to the creeping wave problem.

It is apparent that one could make a number of adjustments on the impulse response derived model to minimize the low frequency corrections required. By examining the ramp and impulse response waveforms and the uncorrected moments as the parameters P and C are varied, an improved model for each aspect and polarization could be obtained. However, as indicated in Chapter I, such an approach does not lead to an "understanding" of the scattering by a prolate spheroid target. It is recommended that future research on this problem begin with improved estimates of the ramp response waveform using measured and calculated low frequency data. The "point matching" solutions mentioned previously appear to offer a convenient and accurate method for securing the necessary phasor response data.

APPENDIX I
RAYLEIGH SCATTERING BY SPHEROIDS

It is well known that for objects sufficiently small in terms of wavelength, the scattering cross section varies as the sixth power of dimension and the fourth power of frequency. The purpose of these notes is to develop explicit expressions for the factor of proportionality for scattering from spheroids. Stevenson[42], in his excellent paper, has provided a general solution for the coefficients in a power series expansion in the wavenumber of the scattered field. We are concerned here with the coefficient of the wavenumber squared or the so-called Rayleigh term for the case of spheroids. We wish to couch our development in terms of electric and magnetic dipoles aligned with the principal axes of the body whose relative strengths are determined by the aspect and polarization of the incident field.

Following Stevenson, let ℓ, m, n be the direction cosines of the direction of propagation of the incident field; ℓ_1, m_1, n_1 be the direction cosines of the incident electric vector; and ℓ_2, m_2, n_2 be the direction cosines of the incident magnetic vector. With $e^{-i\omega t}$ understood the incident field is given by[42]

(101) $$\underline{E}^i = (\ell_1, m_1, n)\ e^{ik(\ell x + my + nz)}$$

and

$$\underline{H}^i = (\ell_2, m_2, n_2)\ e^{ik(\ell x + my + nz)} \quad ,$$

and the scattered fields by[42]

(102) $$E_\theta^s = H_\phi^s = \left[\frac{\partial P}{\partial \theta_s} + \frac{1}{\sin \theta_s}\ \frac{\partial \tilde{P}}{\partial \phi_s}\right]\ \frac{e^{ikR}}{kR}$$

and

$$E_\phi^s = -\ H_\theta^s = \left[\frac{1}{\sin \theta_s}\ \frac{\partial P}{\partial \phi_s}\ -\frac{\partial \tilde{P}}{\partial \theta_s}\right]\ \frac{e^{ikR}}{kR} \quad ,$$

where R, θ_s, ϕ_s are the spherical coordinates of the field point

(103) $$P = (ka)^3\ [K_1 \ell_1 \alpha + K_2 m_1\ \beta + K_3 n_1 \gamma]$$

and

$$\tilde{P} = (ka)^3 [\tilde{K}_1 \ell_2 \alpha + \tilde{K}_2 m_2\ \beta + \tilde{K}_3 n_2\ \gamma] \quad ,$$

where α, β, γ are the direction cosines of the radius vector to the field point. The constants $K_1 . .$, $\tilde{K}_1 . .$, are, respectively, the electric and magnetic coefficients which are a function only of the body and independent of the incident field. Note that in the "a" in Eq. (103) is the principal axis along the x and y coordinates (Fig. 10).

$$(104)\qquad K_1 = \frac{2(\epsilon-1)}{3a^3\left[(\epsilon-1)I_a + \frac{2}{a^2b}\right]}\ ,\ \tilde{K}_1 = \frac{2(\mu-1)}{3a^3\left[(\mu-1)I_a + \frac{2}{a^2b}\right]}\ ;$$

$$K_2 = \frac{2(\epsilon-1)}{3a^3\left[(\epsilon-1)I_a + \frac{2}{a^2b}\right]}\ ,\ \tilde{K}_2 = \frac{2(\mu-1)}{3a^3\left[(\mu-1)I_a + \frac{2}{a^2b}\right]}\ ;$$

and

$$K_3 = \frac{2(\epsilon-1)}{3a^3\left[(\epsilon-1)I_b + \frac{2}{a^2b}\right]}\ ,\ \tilde{K}_3 = \frac{2(\mu-1)}{3a^3\left[(\mu-1)I_b + \frac{2}{a^2b}\right]}\ ,$$

where ϵ and μ are the constitutive parameters of the spheroid. Note that we have altered Stevenson's expressions slightly to conform to our desired dipole development. The expressions I_a, I_b are related by

$$(105)\qquad 2\,I_a + I_b = \frac{2}{a^2b}$$

and

$$2a^2\,I_a + b^2\,I_b = I\ ,$$

where now we must differentiate between two cases. For the prolate spheroid ($a \leq b$)

$$(106)\qquad I = \frac{1}{b\eta}\,\ell n\left[\frac{1+\eta}{1-\eta}\right]\ ,$$

where $\eta = \sqrt{1-(a/b)^2}$. For the oblate spheroid ($a \geq b$)

$$(107) \qquad I = \frac{2}{a\eta} \cos^{-1}\left(\sqrt{1-\eta^2}\right) ,$$

where $\eta = \sqrt{1-(b/a)^2}$. Thus for the prolate spheroid we obtain

$$(108) \quad K_1 = K_2 = \frac{2(\epsilon-1)}{3\left[\frac{(\epsilon-1)}{2\eta^2}\left\{2\sqrt{1-\eta^2} - (1-\eta^2)^{3/2}\,\ell n\left(\frac{1+\eta}{1-\eta}\right)\right\} + 2\sqrt{1-\eta^2}\right]} ,$$

$$K_3 = \frac{2(\epsilon-1)}{3\left[\frac{(\epsilon-1)}{\eta^2}\left\{2\sqrt{1-\eta^2}\,(\eta^2-1) + \frac{(1-\eta^2)^{3/2}}{\eta}\,\ell n\left(\frac{1+\eta}{1-\eta}\right)\right\} + 2\sqrt{1-\eta^2}\right]} ,$$

$$\tilde{K}_1 = \tilde{K}_2 = \frac{2(\mu-1)}{3\left[\frac{\mu-1}{2\eta^2}\left\{2\sqrt{1-\eta^2} - (1-\eta^2)^{3/2}\,\ell n\left(\frac{1+\eta}{1-\eta}\right)\right\} + 2\sqrt{1-\eta^2}\right]} ,$$

and

$$\tilde{K}_3 = \frac{2(\mu-1)}{3\left[\frac{(\mu-1)}{\eta^2}\left\{2\sqrt{1-\eta^2}\,(\eta^2-1) + \frac{(1-\eta^2)^{3/2}}{\eta}\,\ell n\left(\frac{1+\eta}{1-\eta}\right)\right\} + 2\sqrt{1-\eta^2}\right]} .$$

For the perfect conducting case ($|\epsilon| \to \infty$, $\mu \to 0$), the above reduce to

$$(109) \qquad K_1 = K_2 = \frac{4\eta^2}{3\left[2\sqrt{1-\eta^2} - (1-\eta^2)^{3/2}\,\ell n\left(\frac{1+\eta}{1-\eta}\right)\right]} ,$$

$$K_3 = \frac{2\eta}{3\left[2\eta\sqrt{1-\eta^2}\,(\eta^2-1) + (1-\eta^2)^{3/2}\,\ell n\left(\frac{1+\eta}{1-\eta}\right)\right]} .$$

(109 contd.) $$\tilde{K}_1 = \tilde{K} = \frac{-2}{3\left[2\sqrt{1-\eta^2} - \frac{1}{2\eta^2}\left\{2\sqrt{1-\eta^2} - (1-\eta^2)^{3/2}\ \ell n\left(\frac{1+\eta}{1-\eta}\right)\right\}\right]},$$

and

$$\tilde{K}_3 = \frac{-2}{3\left[2\sqrt{1-\eta^2} - \frac{1}{\eta^2}\left\{2\sqrt{1-\eta^2}\ (\eta^2-1) + \frac{(1-\eta^2)^{3/2}}{\eta}\ \ell n\left(\frac{1+\eta}{1-\eta}\right)\right\}\right]}.$$

For the oblate spheroid

(110) $$K_1 = K_2 = \frac{2(\epsilon-1)}{3\left[(\epsilon-1)\left\{\frac{\cos^{-1}(\sqrt{1-\eta^2}) - \eta\sqrt{1-\eta^2}}{\eta^3}\right\} + \frac{2}{\sqrt{1-\eta^2}}\right]},$$

$$K_3 = \frac{2(\epsilon-1)}{3\left[(\epsilon-1)\left\{\frac{2}{\sqrt{1-\eta^2}} - \left(\frac{2\cos^{-1}(\sqrt{1-\eta^2}) - 2\eta\sqrt{1-\eta^2}}{\eta^3}\right)\right\} + \frac{2}{\sqrt{1-\eta^2}}\right]},$$

$$\tilde{K}_1 = \tilde{K}_2 = \frac{2(\mu-1)}{3\left[(\mu-1)\left\{\frac{\cos^{-1}(\sqrt{1-\eta^2}) - \eta\sqrt{1-\eta^2}}{\eta^3}\right\} + \frac{2}{\sqrt{1-\eta^2}}\right]},$$

and

$$\tilde{K}_3 = \frac{2(\mu-1)}{3\left[(\mu-1)\left\{\frac{2}{\sqrt{1-\eta^2}} - \left(\frac{2\cos^{-1}(\sqrt{1-\eta^2}) - 2\eta\sqrt{1-\eta^2}}{\eta^3}\right)\right\} + \frac{2}{\sqrt{1-\eta^2}}\right]}.$$

For a perfect conductor the above become

$$(111)\qquad K_1 = K_2 = \frac{2\eta^3}{3\left[\cos^{-1}\left(\sqrt{1-\eta^2}\right) - \eta\sqrt{1-\eta^2}\right]} ,$$

$$K_3 = \frac{1}{3\left[\frac{1}{\sqrt{1-\eta^2}} - \left(\frac{\cos^{-1}\left(\sqrt{1-\eta^2}\right) - \eta\sqrt{1-\eta^2}}{\eta^3}\right)\right]} ,$$

$$\tilde{K}_1 = \tilde{K}_2 = \frac{-2}{3\left[\frac{2}{\sqrt{1-\eta^2}} - \left(\frac{\cos^{-1}\left(\sqrt{1-\eta^2}\right) - \eta\sqrt{1-\eta^2}}{\eta^3}\right)\right]} ,$$

and

$$\tilde{K}_3 = \frac{-1}{3\left[\frac{1}{\sqrt{1-\eta^2}} - \left\{\frac{1}{\sqrt{1-\eta^2}} - \left(\frac{\cos^{-1}\left(\sqrt{1-\eta^2}\right) - \eta\sqrt{1-\eta^2}}{\eta^3}\right)\right\}\right]} .$$

Now for the general case,

$$(112)\qquad \alpha = \sin\theta_s \cos\phi_s ,$$

$$\beta = \sin\theta_s \sin\phi_s , \text{ and}$$

$$\gamma = \cos\theta_s .$$

Let the coordinates of the source point be R, θ_i, ϕ_i; then

(113) $$\ell = -\sin\theta_i \cos\phi_i ,$$

$$m = -\sin\theta_i \sin\phi_i , \text{ and}$$

$$\eta = -\cos\theta_i \quad .$$

There is no loss of generality if we restrict the direction of incidence to the y, z plane ($\phi_i = \pi/2$) whence

(114) $$\ell = 0,$$

$$m = -\sin\theta_i , \text{ and}$$

$$\eta = -\cos\theta_i \quad .$$

We now consider two particular polarizations of the incident field from which, by superposition, the solution for any arbitrary polarization can be obtained.

T. E. Incident electric vector perpendicular to yz plane.

(115) $$\ell_1 = 1.0 \qquad \ell_2 = 0.0$$

$$m_1 = 0.0 \qquad m_2 = -\cos\theta_i$$

$$\eta_1 = 0.0 \qquad \eta_2 = \sin\theta_i \quad .$$

T. M. Incident electric vector parallel to yz plane.

(116) $$\ell_1 = 0.0 \qquad \ell_2 = -1.0$$

$$m_1 = -\cos\theta_i \qquad m_2 = 0.0$$

$$\eta_1 = \sin\theta_i \qquad \eta_2 = 0.0 \quad .$$

Let us define a normalization such that

$$\frac{\sigma}{\pi a^2} = \left| E_n^s \right|^2 \qquad (117)$$

Then the normalized scattered fields are given by

T. E.

$$E_{\theta\eta} = H_{\phi\eta} = 2(ka)^2 \left[K_1 \cos\theta_s \cos\phi_s - \tilde{K}_2 \cos\theta_i \cos\phi_s\right] \qquad (118)$$

and

$$E_{\phi\eta} = - H_{\theta\eta} = 2(ka)^2\left[-K_1 \sin\phi_s + \tilde{K}_2 \cos\theta_i \cos\theta_s \sin\phi_s + \tilde{K}_3 \sin\theta_i \sin\theta_s\right];$$

T. M.

$$E_{\theta\eta} = H_{\phi\eta} = 2(ka)^2 \left[-K_2 \cos\theta_i \cos\theta_s \sin\phi_s - K_3 \sin\theta_i \sin\theta_s + \tilde{K}_1 \sin\phi_s\right] \qquad (119)$$

and

$$E_{\phi\eta} = - H_{\theta\eta} = 2(ka)^2 \left[-K_2 \cos\theta_i \cos\phi_s + \tilde{K}_1 \cos\theta_s \cos\phi_s\right] .$$

Let us define the Rayleigh coefficient K as

$$E_\eta^s = K(ka)^2 \qquad (120)$$

Then

T. E.

$$K_\theta(\theta_i, \theta_s, \phi_s) = 2[K_1 \cos\theta_s \cos\phi_s - \tilde{K}_2 \cos\theta_i \cos\phi_s] \tag{121}$$

and

$$K_\phi(\theta_i, \theta_s\phi_s) = 2[-K_1 \sin\phi_s + \tilde{K}_2 \cos\theta_i \cos\theta_s \sin\phi_s + \tilde{K}_3 \sin\theta_i \sin\theta_s] ;$$

T. M.

$$K_\theta(\theta_i, \theta_s, \phi_s) = 2[-K_2 \cos\theta_i \cos\theta_s \sin\phi_s - K_3 \sin\theta_i \sin\theta_s + \tilde{K}_1 \sin\phi_s] \tag{122}$$

and

$$K_\phi(\theta_i,\theta_s,\phi_s) = 2[-K_2 \cos\theta_i \cos\phi_s + \tilde{K}_1 \cos\theta_s \cos\phi_s] .$$

For backscatter ($\theta_s = \theta_i$, $\phi_s = \pi/2$)

T. E.

$$K_\phi(\theta) = 2[-K_1 + \tilde{K}_2 \cos^2\theta + \tilde{K}_3 \sin^2\theta] \tag{123}$$

and

T. M.

$$K_\theta(\theta) = 2[-K_2 \cos^2\theta - K_3 \sin^2\theta + \tilde{K}_1] .$$

It is clear from Eqs. (121-123) that a knowledge of the dipole coefficients $K_1 \ldots$, $\tilde{K}_1 \ldots$, suffices to determine the Rayleigh coefficient for any polarization and for any arbitrary orientation of source and receiver.

For the general spheroid, the dipole coefficients may all be obtained from the quantities I_a and I_b, these are plotted in Figs. 39, 40, 41, and 42 as a function of the axial ratio for the prolate and oblate spheroids, respectively. For the perfectly conducting case we note that

$$\tilde{K}_3 = -\frac{1}{2} K_1 \tag{124}$$

and

$$\tilde{K}_1 = -\left[\frac{1}{K_1} + \frac{1}{K_3}\right]^{-1}$$

Thus all the dipole coefficients may be obtained from K_1 and K_3. These quantities are plotted in Figs. 43, 44, 45, and 46 as a function of the axial ratio for the prolate and oblate spheroids, respectively. From the curves in Figs. 39-46, the Rayleigh coefficient for the prolate or oblate spheroid with any combination of constitutive parameters for any polarization and orientation can be quickly obtained.

As an example of the use of these curves, consider a perfectly conducting prolate spheroid with a 2:1 axial ratio. From Figs. 43 and 45, $K_1 \simeq 1.62$ and $K_3 \simeq 3.8$. Then from Eq. (124), $\tilde{K}_1 = -1.13$ and $\tilde{K}_3 = -0.8$. Then from Eq. (123)

$$(125) \qquad \left.\begin{aligned} K_{TE}(\theta) &= 2[-1.62 - 1.13\cos^2\theta - 0.8\sin^2\theta] \\ \text{and} \\ K_{TM}(\theta) &= 2[-1.62\cos^2\theta - 3.8\sin^2\theta - 1.13] \end{aligned}\right\} .$$

In Table V the Rayleigh coefficients are given for perfectly conducting spheroids with axial ratios from 1(1)10 and incidence angles θ from 0(10°)90° for both the T. E. and T. M. polarizations.

TABLE V
RAYLEIGH COEFFICIENTS OF
PERFECTLY CONDUCTING PROLATE SPHEROIDS

Incident Angle θ in Degrees

Prolate Spheroid Axial Ratio, b/a

	0	10	20	30	40	50	60	70	80	90
1TE	3.00	-	-	-	-	-	-	-	-	-
1TM	3.00	-	-	-	-	-	-	-	-	-
2TE	5.50	5.48	5.42	5.34	5.22	5.12	5.00	4.92	4.86	4.84
2TM	5.50	5.64	6.02	6.62	7.34	8.12	8.84	9.44	9.82	9.96
3TE	8.10	8.06	7.94	7.76	7.54	7.30	7.08	6.90	6.78	6.74
3TM	8.10	8.52	9.72	11.58	13.84	16.26	18.52	20.38	21.58	22.00
4TE	10.72	10.66	10.48	10.20	9.88	9.50	9.18	8.90	8.72	8.66
4TM	10.72	11.62	14.18	18.12	22.96	28.10	32.92	36.86	39.44	40.32
5TE	13.38	13.30	13.04	12.68	12.22	11.74	11.28	10.92	10.68	10.60
5TM	13.38	14.96	19.54	26.54	35.14	44.28	52.86	59.86	64.44	66.02
6TE	16.02	15.92	15.62	15.16	14.58	13.98	13.42	12.96	12.64	12.54
6TM	16.02	18.56	25.88	37.08	50.80	65.42	79.16	90.36	97.66	100.20
7TE	18.68	18.56	18.20	17.64	16.96	16.24	15.54	15.00	14.62	14.50
7TM	18.68	22.46	33.34	50.00	70.40	92.14	112.56	129.22	140.08	143.86
8TE	21.36	21.20	20.78	20.12	19.34	18.48	17.68	17.04	16.62	16.46
8TM	21.36	26.68	42.02	65.52	94.34	125.02	153.86	177.36	192.70	198.02
9TE	24.02	23.84	23.36	22.62	21.72	20.74	19.84	19.10	18.60	18.44
9TM	24.02	31.24	52.04	83.92	123.02	164.64	203.74	235.62	256.42	263.66
10TE	26.68	26.48	25.94	25.12	24.08	23.00	21.98	21.14	20.60	20.42
10TM	26.68	36.18	63.52	105.44	156.84	211.54	262.94	304.86	332.20	341.70

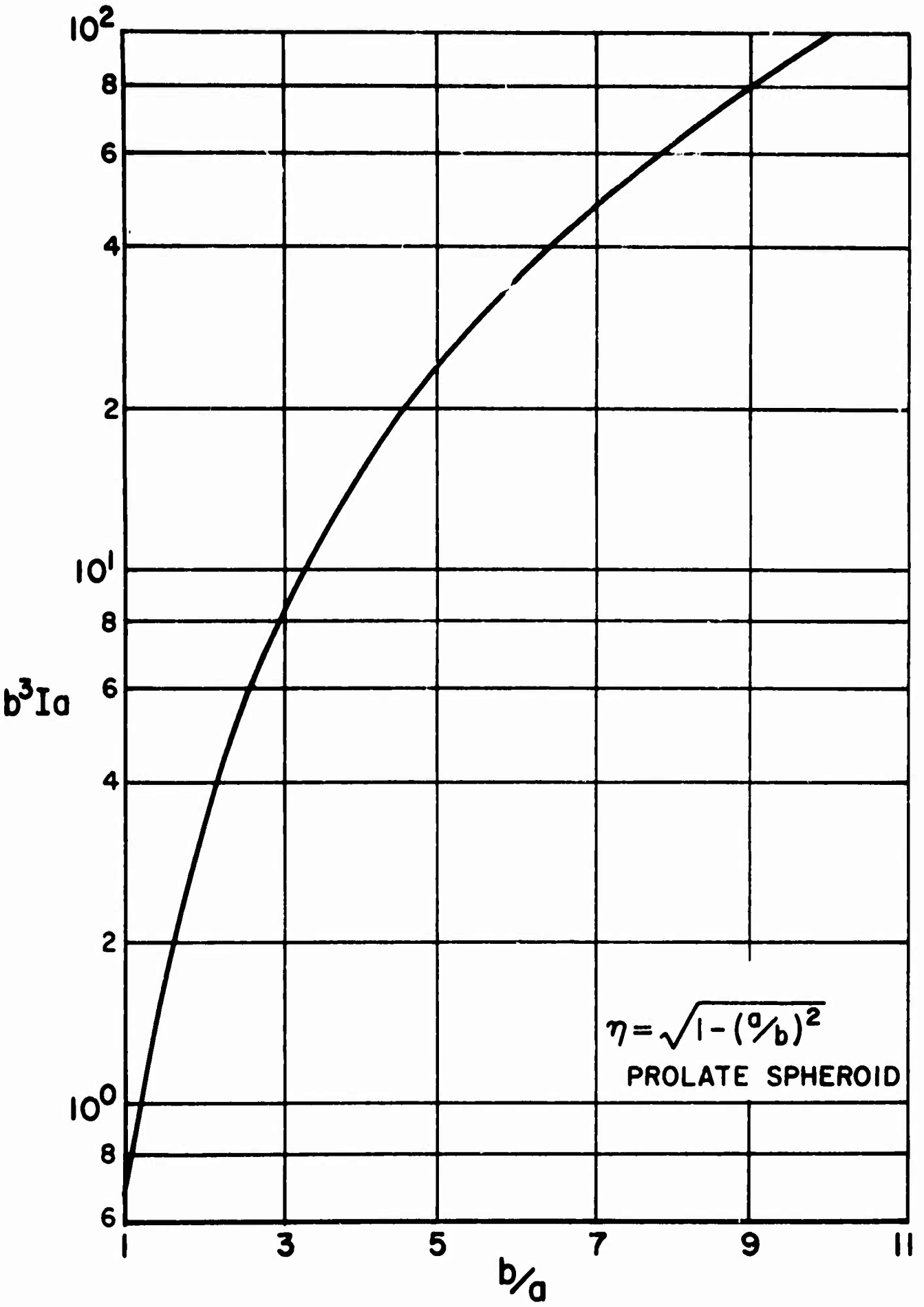

Fig. 39--Dipole coefficient I_a as a function of axial ratio. Prolate spheroid.

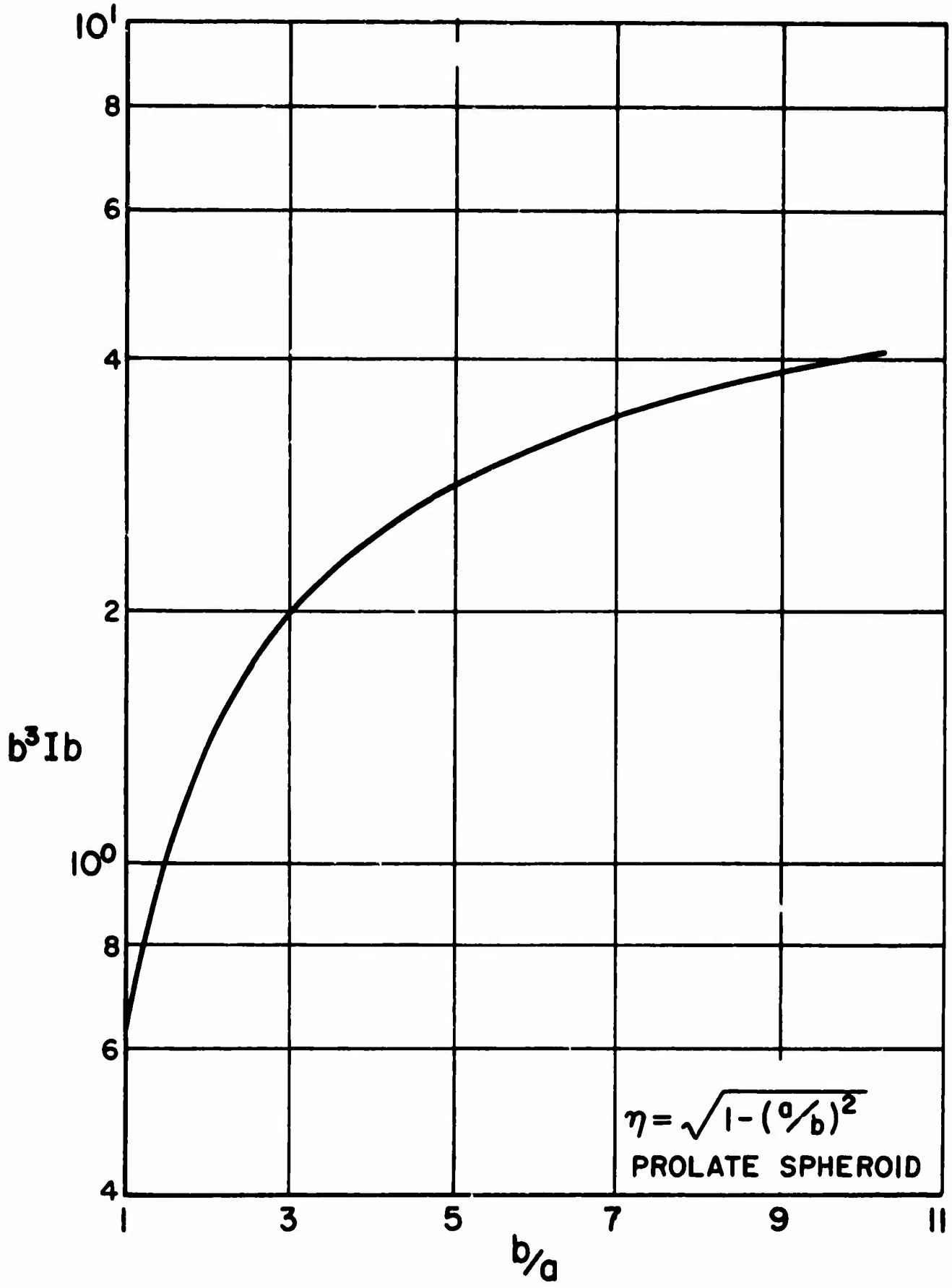

Fig. 40--Dipole coefficient I_b as a function of axial ratio. Prolate spheroid.

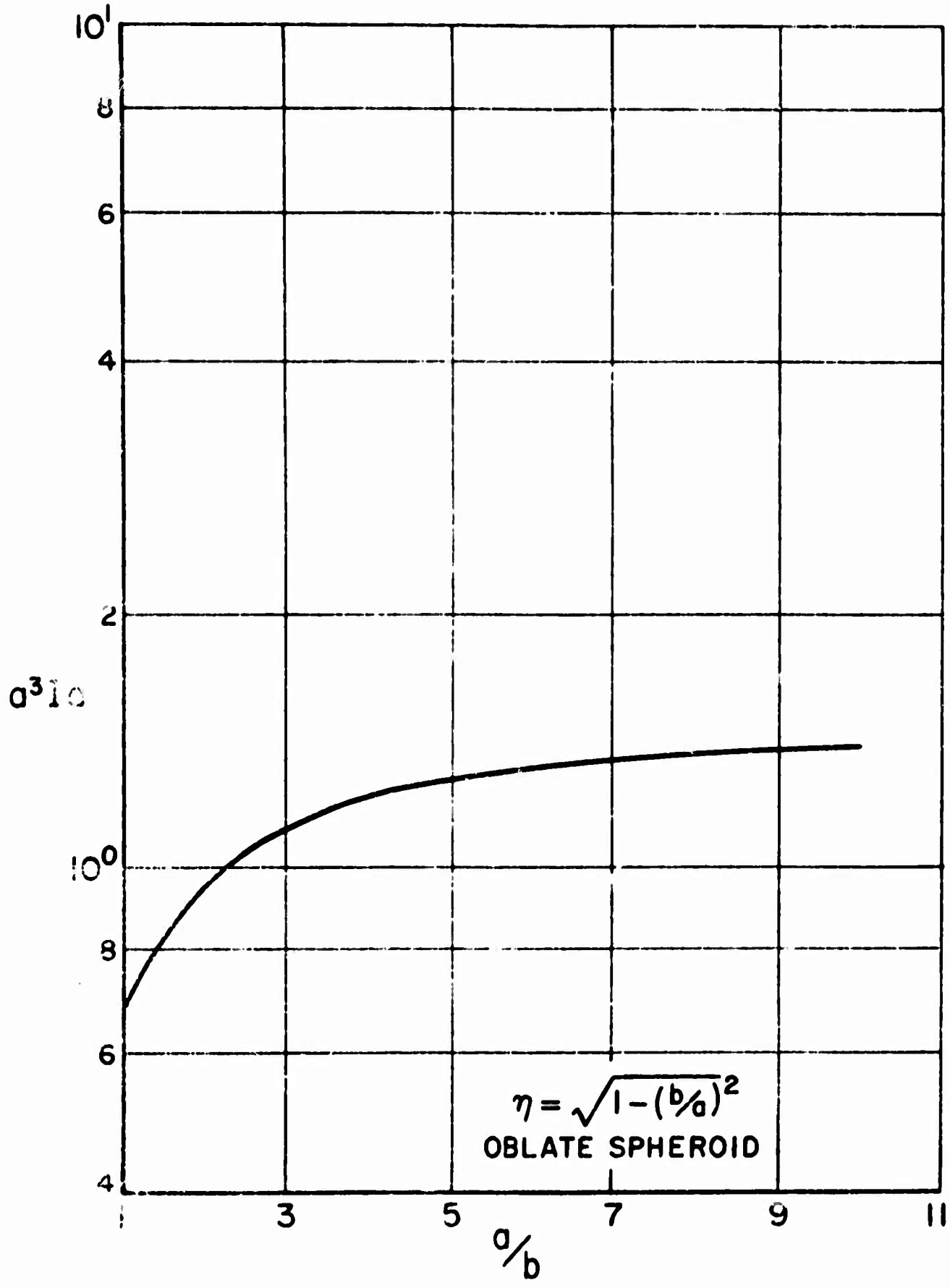

Fig. 41--Dipole coefficient I_a as a function of axial ratio. Oblate spheroid.

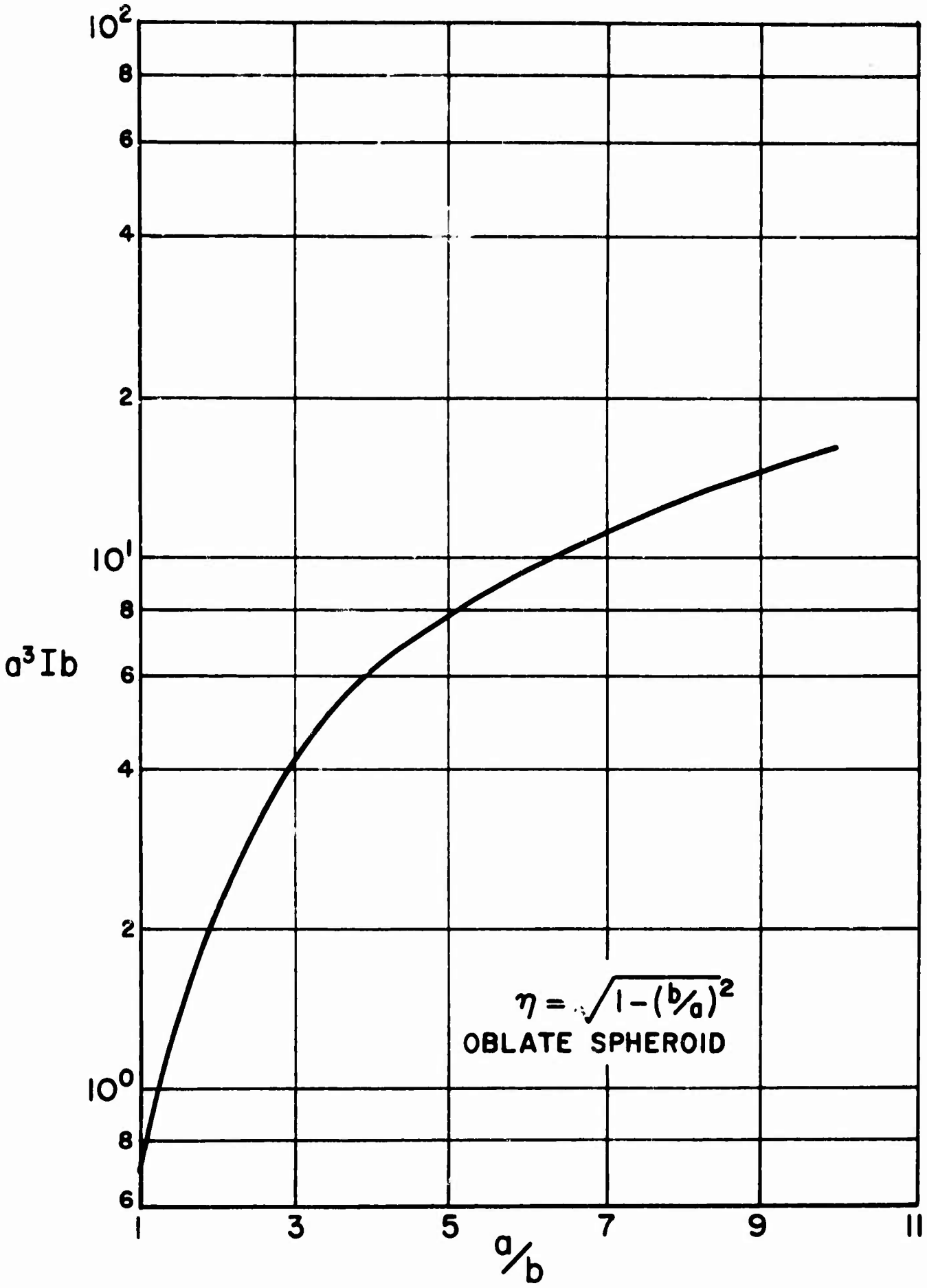

Fig. 42--Dipole coefficient I_b as a function of axial ratio. Oblate spheroid.

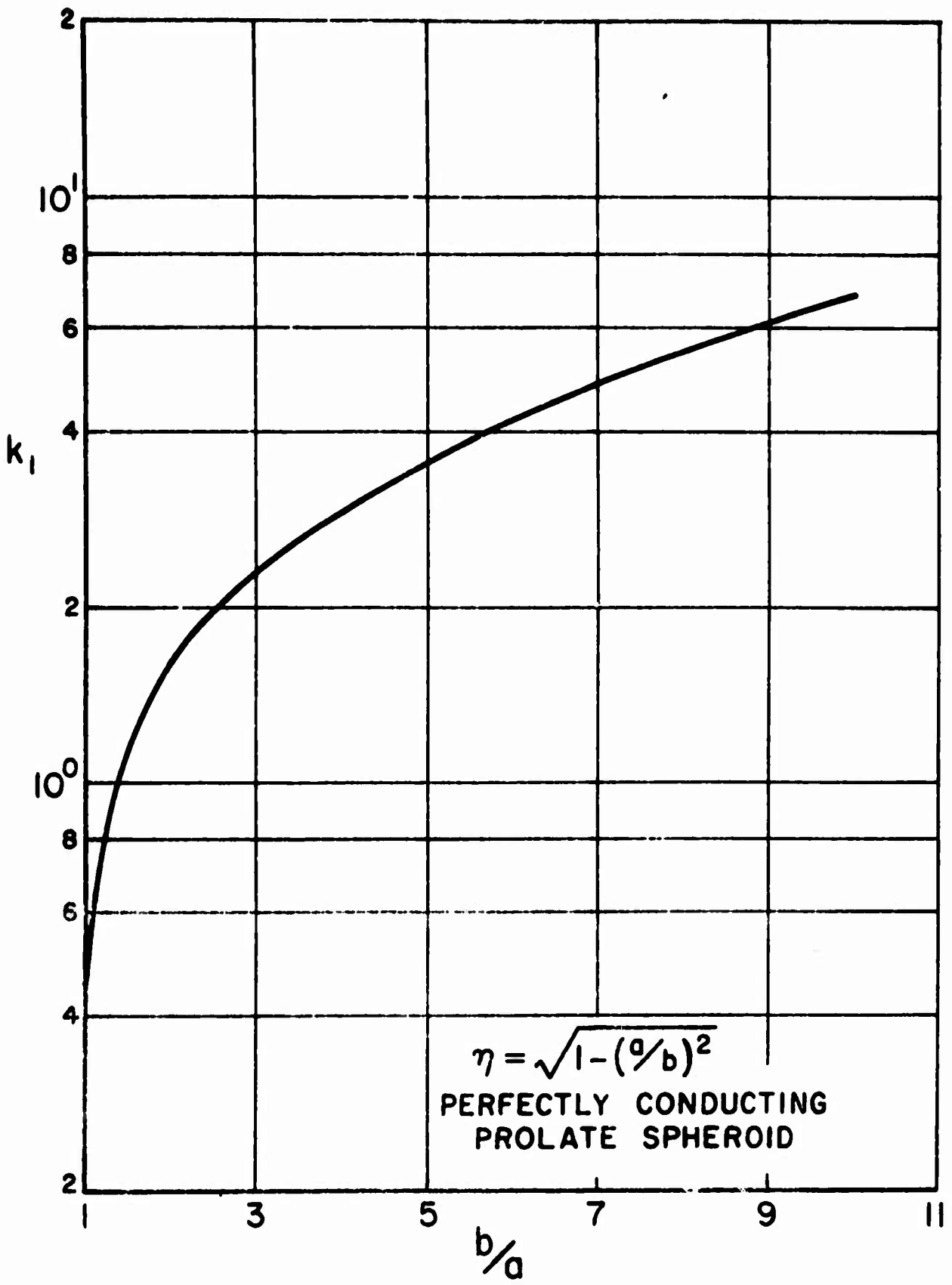

Fig. 43--The quantity K_1 for a perfectly conducting prolate spheroid as a function of axial ratio.

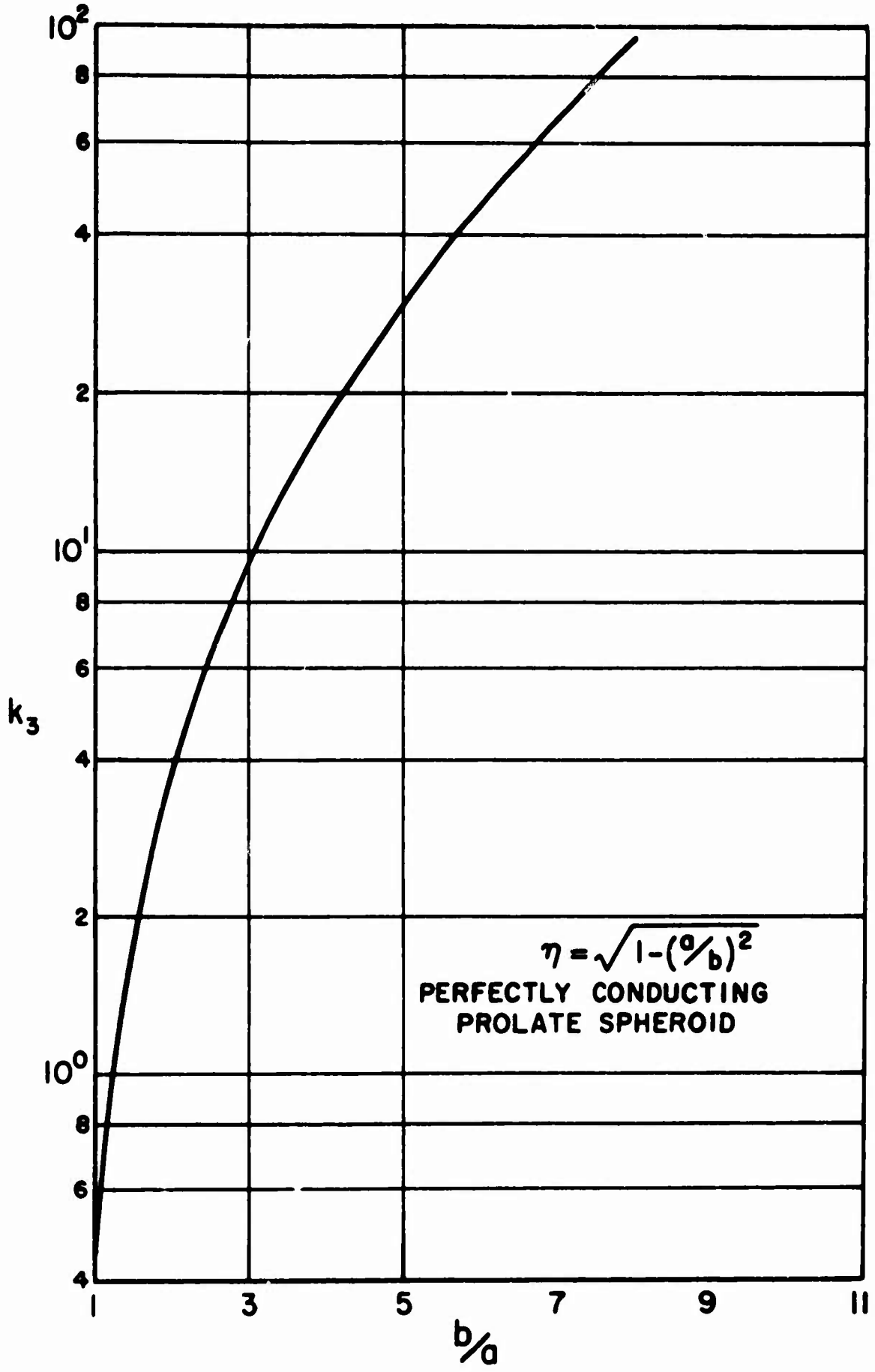

Fig. 44--The quantity K_3 for a perfectly conducting prolate spheroid as a function of axial ratio.

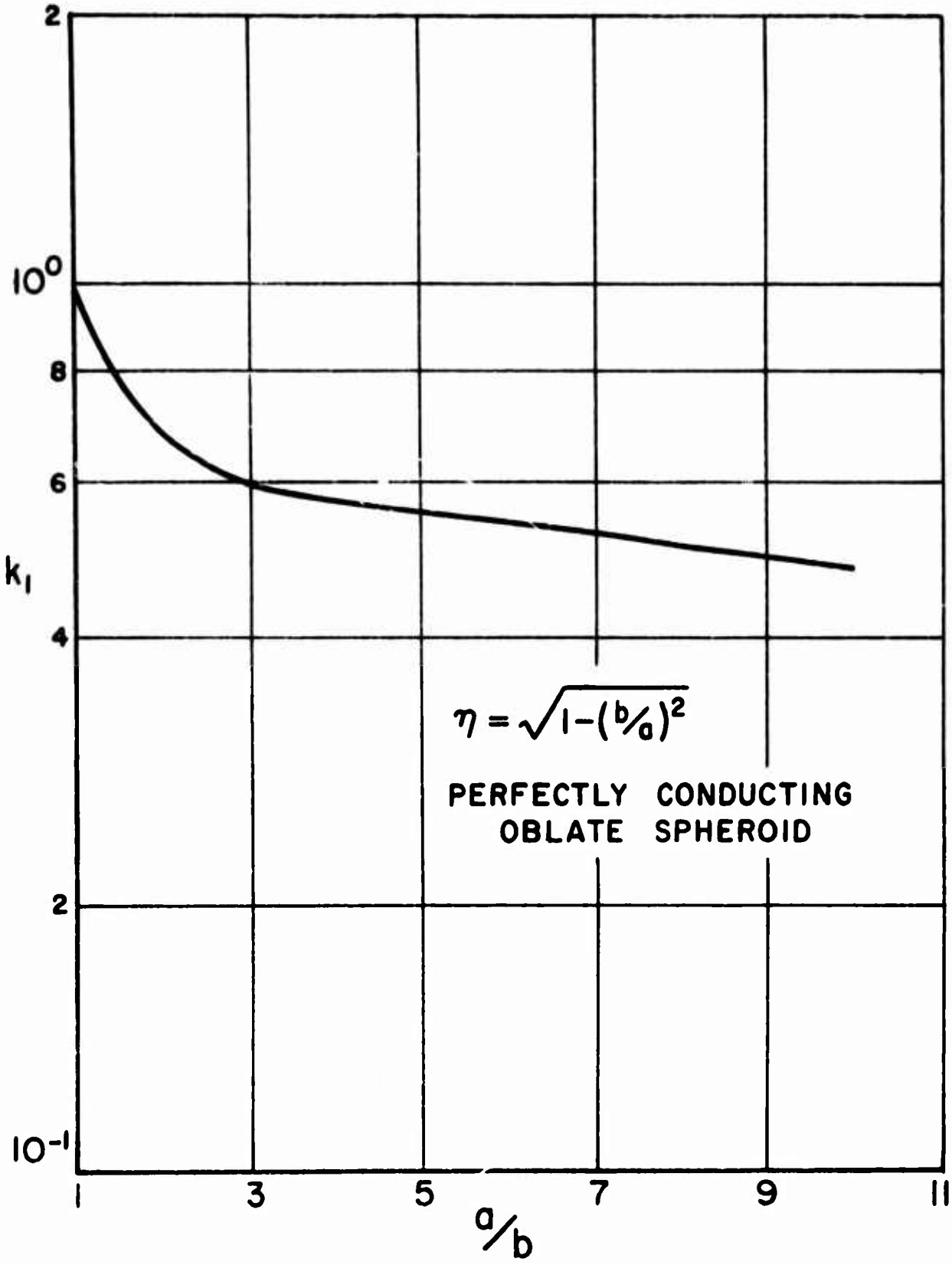

Fig. 45--The quantity K_1 for a perfectly conducting oblate spheroid as a function of axial ratio.

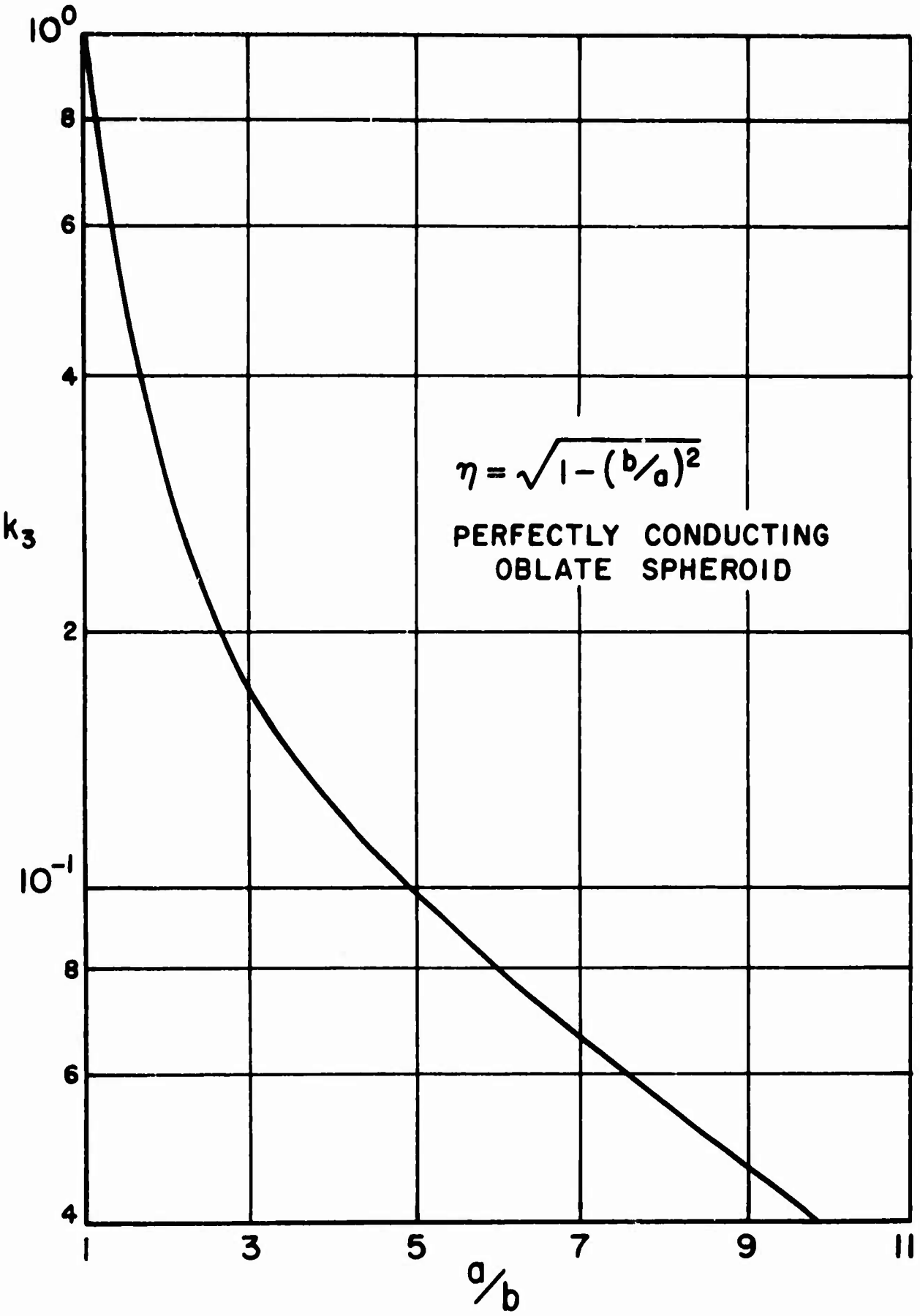

Fig. 46--The quantity K_3 for a perfectly conducting oblate spheroid as a function of axial ratio.

APPENDIX II
ON THE NATURE OF THE CREEPING WAVE

In the derivation of transient and impulse response approximations for smooth curved objects, a model for the creeping wave contribution is an important consideration. High frequency asymptotic solutions have been employed with some success in the prediction of the diffraction from smooth convex curved surfaces. It is of interest to examine certain of these solutions in the time domain, where additional insight both to the scattering mechanism and to the nature of the approximation may possibly be gained. In this Appendix, attention will be given to the perfectly conducting circular cylinder and the perfectly conducting sphere. The geometrical theory of diffraction solutions given by Kouyoumjian[43] and Peters[44] for the cylinder and sphere and by Keller[45] for the sphere* will be examined in addition to Senior's[46] asymptotic expression for the conducting sphere creeping wave.

---

* Keller's result is actually for axial incidence on a spheroid, but considered first is the specialization to the sphere.

A general observation concerning the geometrical diffraction theory can be made. For conducting objects, each surface ray mode according to the theory has associated with it a phase delay of at least $e^{-jk\ell}$, where k is the free space wave number and ℓ the geodesic path length along the surface of the diffracted ray. Thus the geometrical theory expression for the diffracted field, when transformed to the time domain, must have a time delay of at least ℓ/c provided the complete expression is one which leads to a causal time function. As will be seen, there is an essential difference between the geometrical theory expressions for the cylinder and sphere. The geometrical expression for the diffracted field of a cylinder (normal incidence) leads to a causal time function whereas the corresponding expression for the sphere does not. This difference is caused by the presence of a cylindrical caustic for the sphere case, for which a phase jump must be added. If a total caustic correction of other than $\pm n\pi$ radians is dictated by the theory, the resultant expression for the diffracted field apparently leads to a noncausal time function. This is true for edge - as well as surface-diffracted fields. In the frequency domain, the noncausal nature of the inverse transformed diffracted field is of no consequence and in fact the caustic correction is essential for the success of the theory. In the time domain, however, when one attempts to construct a model for the transient or impulse response waveform, the presence of a noncausal time function is not convenient.

Consider the far-field backscattered impulse response waveforms of the conducting sphere and the infinite conducting cylinder for broadside incidence. The sphere waveform is shown in Fig. 47, the cylinder waveforms for parallel polarization (solid) and for perpendicular polarization (dashed) are shown in Fig. 48. These approximate waveforms were obtained from the Fourier synthesis procedure[13] using the exact solutions for the respective scattering problems. For the sphere, 475 harmonics with a fundamental of 0.2512 sphere circumferences in wavelengths were used. For the cylinder, 79 harmonics with

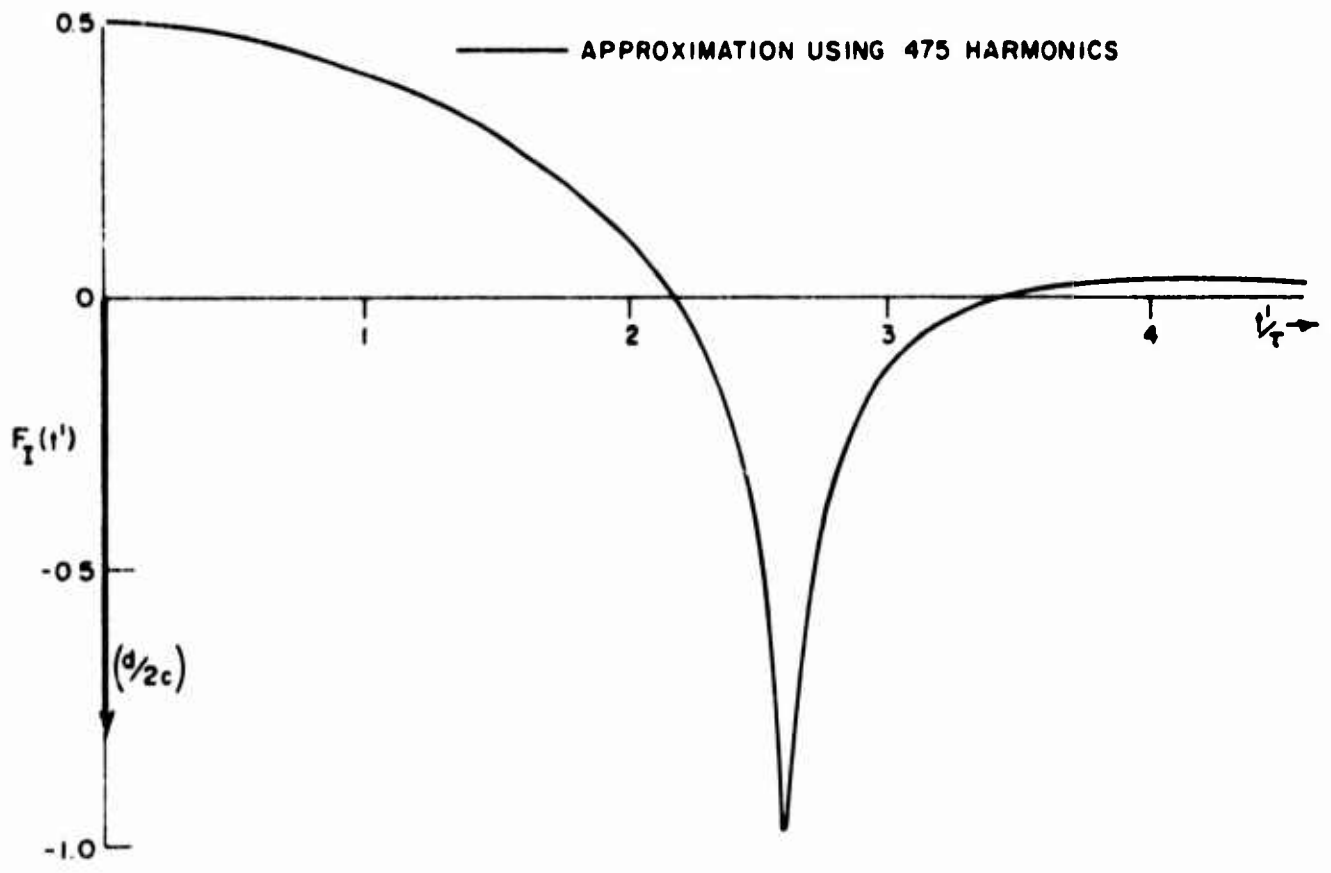

Fig. 47--Approximate impulse response waveform of conducting sphere, backscatter.

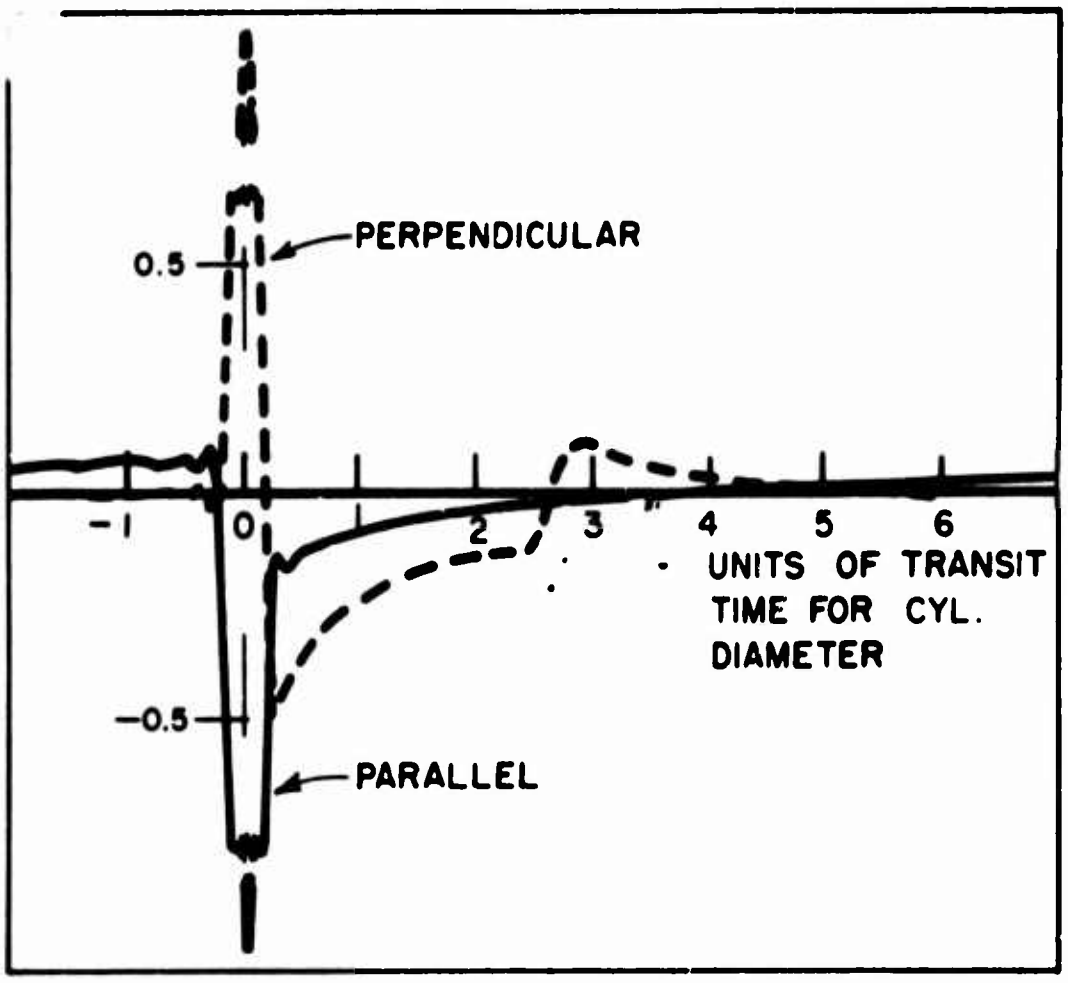

Fig. 48--Approximate impulse response waveform of conducting infinite circular cylinder, backscatter, broadside incidence. Parallel (solid) and perpendicular (dashed) polarization.

a fundamental of 0. 157 cylinder circumferences in wavelengths were used. In both cases, the pulse width and pulse separation of the synthesized incident cosine pulse[13] are sufficient to ensure a reasonably accuracte approximate to the impulse response waveform. * Assuming the progression of creeping wave contributions along

---

* An adequate representation of the sphere impulse waveform can be obtained from as few as 64 harmonics.

geodesic paths, the creeping wave contributions for both the sphere and cylinder should appear first at a time $t' = (1 + \pi/2)\, t_o$. For the sphere (Fig. 47), the creeping wave contribution is a secondary peak occurring at the prescribed time. For parallel polarization on the cylinder (Fig. 48), where the incident electric vector is effectively shorted out at the shadow boundary, there is no evidence of a creeping wave contribution. For perpendicular polarization the contribution begins at the above prescribed time. The distinct difference in the creeping wave contributions for the sphere and cylinder is vividly evident in Figs. 47 and 48.

One should note particularly that the creeping wave contribution for the sphere peaks at $t' = (1 + \pi/2)\, t_o$, whereas the contribution for the cylinder (perpendicular polarization) begins at this same time. With reference to either the sphere or cylinder waveforms, the waveform for $t' > (1 + \pi/2)\, t_o$ might properly be explained by a creeping wave theory, since the creeping wave cannot arrive before this time. Thus one would conclude that a creeping wave theory would be inadequate for the sphere since it could not explain the leading edge of the peak, but adequate for the cylinder. It will be shown, however, that the referenced sphere solutions predict "precursors" in the time domain which agree approximately, in the neighborhood of the peak, with the waveform in Fig. 47.

Consider first the geometrical theory of diffraction solution for the conducting cylinder of radius a for broadside incidence. Both Kouyoumjian[43] and Peters[44] give the result (retaining only one term in the diffraction and attenuation coefficients and neglecting all but the first surface ray mode)

$$(126) \qquad F^{cw}_{(j\omega)} = 0.81\, a^{1/3} \lambda^{1/6}\, e^{-j\frac{\pi}{12}} \cdot e^{-[\,jk\pi a + 1.65 e^{j\frac{\pi}{6}}\, a^{-2/3} \lambda^{-1/3}\, \pi a\,]}\, \frac{e^{-jkR}}{\sqrt{R}} \quad .$$

Using an s notation ($s = j\omega t_o = j2ka$), shifting the phase reference to the specular point of the cylinder, and normalizing such that the echo width predicted for the creeping wave contribution is

$$(127) \qquad \sigma(\omega) = \sqrt{\pi}\, \left| G^{cw}(j\omega) \right|^2 \quad .$$

$$(128) \qquad G^{cw}(j\omega) = \frac{A\, e^{-[\,\alpha s + \beta s^{1/3}\,]}}{s^{1/6}} \quad ,$$

where $A = 0.81 \sqrt{2a}\, (4\pi)^{1/6}$,

$\alpha = (1 + \pi/2)\, t_o$, and

$\beta = \dfrac{1.65 \pi^{2/3}}{4^{1/3}}$.

Friedlander[47] has obtained an approximate general result for the inverse Laplace transform of functions of the type in Eq. (128) using a saddle point technique.

$$(129)\qquad \frac{i}{2\pi j}\int_{\Delta-j\infty}^{\Delta+j\infty} s^{-n}\, e^{[\,Ts\,-\,gs^{1/3}\,]}\, ds = \frac{g^{\left[\frac{3-6n}{4}\right]}\, 3^{\left(\frac{6n-1}{4}\right)}\, T^{\left(\frac{6n-5}{4}\right)}\, e^{-\frac{2g^{3/2}}{3^{3/2}\sqrt{T}}}}{2\sqrt{\pi}}\, u(T)\ ,$$

the result in Eq. (129) holding for T small and $n \geq 0$. Applying Eq. (129) to Eq. (128), the cylinder creeping wave impulse response waveform predicted by the geometrical theory of diffraction is approximately

$$(130)\qquad F_I^{cw}(t') \simeq \frac{0.81\sqrt{a}\,\sqrt{0.825}\; e^{-\left[\frac{\left(\frac{1.65}{3}\right)^{3/2}\pi}{\sqrt{t' - (1+\pi/2)\,t_o}}\right]}}{t' - (1+\pi/2)\,t_o} \cdot u(t' - (1+\pi/2)\,t_o)\ ,$$

where Eq. (130) holds for $t'/t_o - 1 - \pi/2$ small. Note particularly that the geometrical theory has led to a causal time function, i. e., it is identically zero for $t' < (1 + \pi/2)\,t_o$. Equation (130) yields a good estimate of the creeping wave contribution for $t' - (1 + \pi/2)\,t_o$ small.

The impulse response waveforms obtained by Fourier synthesis for the conducting circular cylinder shown in Fig. 48 are felt to be of some interest in their own right, without regard to the comparison to the geometrical theory. To the best of the author's knowledge, such waveforms have not appeared previously in the literature. For parallel polarization it is evident that except at the lowest frequencies, the geometrical optics specular contribution is an excellent approximation. For perpendicular polarization Peters[44] has suggested the combination of the creeping wave component in Eq. (126) and the specular term as an approximation; and demonstrated the validity of this model for cylinder radii greater than 0. 3 wavelengths. Again, it is evident from Fig. 48 that such a model must fail at frequencies somewhat higher than for the specular model for parallel polarization and that the failure of the model is not due to inadequacies of the creeping wave component, but rather to the omission of additional terms for the optical contribution. Finally it is noted that for perpendicular polarization in the neighborhood of $t' = 0+$, the details of the response waveform are somewhat obscured because of the finite width of the incident quasi-impulsive wave and the occurrence of both the specular jump and a second opposite sign discontinuity at the same instant. Details of the response waveform in this region are not germain to the present study, and will not be pursued except to note that the synthesis

procedure could be used to resolve the question by the use of additional harmonics to narrow the incident pulse and by subtracting out the well known specular contribution.

Turning now to the conducting sphere of radius a, it can be shown that the various high frequency asymptotic estimates for the creeping wave reduce to the following, where in each case the phase reference has been shifted to the specular point of the sphere and the expression normalized such that the echo area predicted for the creeping wave is given by

$$\sigma(\omega) = \pi \left| G^{cw}(s) \right|^2 \qquad (131)$$

From Peters[44]

$$G^{cw}(s) = \frac{e^{j\frac{\pi}{4}} A e^{-[\alpha s + \beta s^{1/3}]}}{s^{2/3}} \qquad (132)$$

where $A = 0.54a(4\pi)^{2/3}$,

$\alpha = (1 + \pi/2) t_o$, and

$\beta = \dfrac{0.825\pi^{2/3}}{4^{1/3}}$.

From Keller[45] , specializing the spheroid solution to the sphere case

$$(133) \qquad G^{cw}(s) = -j\,\bar{A}\,s^{1/3}\,e^{-[\alpha s + \bar{\beta} s^{1/3}]} \quad ,$$

where

$$\bar{A} = \frac{a\,\pi^2}{(12)^{1/3}\,q_2 D^2} \quad ,$$

$$\bar{\beta} = \frac{q_2 \pi}{(12)^{1/3}} \quad , \quad q_2 = 1.469354, \quad \text{and}$$

$$D^2 = (1.16680)^2 \quad .$$

It can be shown[48] that when the same number of terms are retained, Kouyoumjian's[43] geometrical theory solution for the creeping wave and Senior's[46] asymptotic high frequency expansion for the creeping wave are identical. Using only the first term, and the acoustically hard component which dominates, there is obtained

$$(134) \qquad G^{cw}(s) = -j\,\bar{\bar{A}}\,s^{1/3}\,e^{-[\alpha s + \bar{\bar{\beta}} s^{1/3} - \gamma s^{-1/3}]}$$

$$-j\,\bar{\bar{B}}\,s^{-1/3}\,e^{-[\alpha s + \bar{\bar{\beta}} s^{1/3} - \gamma s^{-1/3}]} \quad ,$$

where

$$\bar{\bar{A}} = \frac{1}{2^{2/3}\,\bar{q}_o\,(A_i(-\bar{q}_o))^2} \quad ,$$

$$\bar{\bar{B}} = \bar{\bar{A}}\left[\frac{1}{30} \quad \frac{1}{4} \quad \frac{3}{20\,\bar{q}_o^3}\right] \bar{q}_o\,(4)^{2/3} \quad ,$$

$$\bar{\beta} = \frac{\bar{q}_o \pi}{4^{1/3}} \quad ,$$

$$\gamma = \left(\frac{3}{20\, \bar{q}_o^3} - \frac{1}{60} \right) \bar{q}_o^2 \, (4)^{1/3} \pi \quad ,$$

$$\bar{q}_o = 1.01879 \quad .$$

Noting the distinct differences in the various formulas given above, it should be pointed out that each of the results has been shown to yield some degree of agreement, when combined with the optical components, with the well known exact solution for the sphere back-scattering cross section. Keller's expression lacks the correction terms to the diffraction and attenuation coefficients which were included by Kouyoumjian. It was demonstrated indirectly by the author[49] , in a study of the cone-sphere axial cross section, that Keller's result for the sphere creeping wave was incomplete. The purpose here however is not a comparison or criticism of the various results in the frequency domain but an examination of the general type of waveform predicted in the time domain.

Note in the expressions in Eqs. (132), (133), and (134), that they are of the general form

$$(135) \qquad G^{cw}(s) = \pm\, jF(s) \quad ,$$

where F(s) differs for the three formulas. In Peter's case this is one of the two terms obtained when $e^{j\frac{\pi}{4}}$ is expanded. Assuming that F(s) yields a causal time function, which will be shown later, it is seen that the asymptotic estimates of the creeping wave add a constant $\pi/2$ radians phase shift. If F(s) yields a causal time function then $G^{cw}(s)$ is noncausal. To show this,

$$(136) \qquad F_I^{cw}(t') = \frac{1}{2\pi j}\int_{\Delta-j\infty}^{\Delta+j\infty} G^{cw}(s)\, e^{st'}\, ds$$

$$= \frac{1}{\pi}\, Re\left\{\int_0^{\infty} G^{cw}(j\omega)\, e^{j\omega t'} d\omega\right\} \quad ,$$

where $G^{cw}(-s) = G^{cw}(s)^*$ has been utilized. To obtain a real time-dependent waveform, the constant phase shift is assumed to change sign for negative frequencies. From Papoulis[50] ,

$$(137) \qquad \int_0^{\infty} e^{j\omega t'}\, d\omega = \pi\,\delta(t') + j\frac{1}{t'} \quad ,$$

thus

$$(138) \qquad \frac{1}{\pi}\, Re\left\{\mp j\int_0^{\infty} e^{j\omega t'}\, d\omega\right\} = \mp\frac{1}{\pi t'} \quad .$$

If the inverse transform of F(s) is $f_o(t')$, i. e. ,

$$(139) \qquad f_o(t') = \mathcal{L}^{-1}[F(s)] \quad ,$$

then by convolution

$$(140) \qquad F_I^{cw}(t') = \mathcal{L}^{-1}[G^{cw}(s)] = \mp \frac{1}{\pi} \int_{-\infty}^{\infty} \frac{1}{\tau} f_o(t'-\tau)\, d\tau \quad .$$

Turning now to consideration of F(s), for Peter's expression in Eq. (132)

$$(141) \qquad F(s) = \frac{1}{\sqrt{2}} \frac{A\, e^{-[\alpha s + \beta s^{1/3}]}}{s^{2/3}} \quad .$$

From Reference 51,

$$(142) \qquad \mathcal{L}^{-1}\left[\frac{e^{-3s^{1/3}}}{s^{2/3}}\right] = \frac{\sqrt{3}}{\pi\sqrt{t'}} K_{\frac{1}{3}}\left(\frac{2}{\sqrt{t'}}\right) u(t') \quad ,$$

where $K_u(x)$ is the modified Hankel function[52]. Manipulating the result in Eq. (142) and applying convolution,

$$(143) \qquad \mathcal{L}^{-1}\left[\frac{A}{\sqrt{2}} \frac{e^{-[\alpha s + \beta s^{1/3}]}}{s^{2/3}}\right]$$

$$= \frac{A\sqrt{\beta}}{\sqrt{2}\,\pi\sqrt{t'-\alpha}} K_{\frac{1}{3}}\left[\frac{2\beta^{3/2}}{3^{3/2}\sqrt{t'-\alpha}}\right] u(t'-\alpha) \quad .$$

It is interesting to note that for large arguments of the modified Hankel function, i.e., for $t'-\alpha$ small[52],

$$(144) \qquad K_{\frac{1}{3}}\left[\frac{2\beta^{3/2}}{3^{3/2}\sqrt{t'-\alpha}}\right] \simeq \frac{\sqrt{\pi}\, 3^{3/4} (t'-\alpha)^{1/4}}{2\beta^{3/4}} e^{-\frac{2\beta^{3/2}}{3^{3/2}\sqrt{t'-\alpha}}} \quad ,$$

and Eq. (143) reduces to

$$(145)\qquad \mathcal{L}^{-1}\left[\frac{A}{\sqrt{2}}\,\frac{e^{-[\alpha s+\beta s^{1/3}]}}{s^{2/3}}\right] \simeq \frac{A\,3^{3/4}}{2\sqrt{2\pi}\,\beta^{1/4}}\,\frac{e^{-\left[\frac{2\beta^{3/2}}{3^{3/2}\sqrt{t'-\alpha}}\right]}}{(t'-\alpha)^{1/4}}\,u(t'-\alpha)\,,$$

which is exactly the result obtained by using Friedlander's approximate formula (Eq. (129)) in Eq. (141). From Eqs. (142) and (143), the exact expression for Peters' creeping wave in the time domain is

$$(146)\qquad F_I^{cw}(t') = \frac{A\sqrt{\beta}}{\sqrt{2}\,\pi\sqrt{t'-\alpha}}\,K_{\frac{1}{3}}\left[\frac{2\beta^{3/2}}{3^{3/2}\sqrt{t'-\alpha}}\right]u(t'-\alpha)$$

$$-\frac{A\sqrt{\beta}}{\sqrt{2}\,\pi^2}\int_{-\infty}^{\infty}\frac{K_{\frac{1}{3}}\left[\frac{2\beta^{3/2}}{3^{3/2}\sqrt{\tau-\alpha}}\right]u(\tau-\alpha)}{\sqrt{\tau-\alpha}\,(t'-\tau)}\,d\tau\,,$$

and for $t'-\alpha$ small this reduces to

$$(147)\qquad F_I^{cw}(t') \simeq \frac{A\,3^{3/4}}{2\sqrt{2\pi}\,\beta^{1/4}}\,\frac{e^{-\left[\frac{2\beta^{3/2}}{3^{3/2}\sqrt{t'-\alpha}}\right]}}{(t'-\alpha)^{1/4}}\,u(t'-\alpha)$$

$$-\frac{A\,3^{3/4}}{(2\pi)^{3/2}\,\beta^{1/4}}\int_{-\infty}^{\infty}\frac{e^{\frac{2\beta^{3/2}}{3^{3/2}\sqrt{\tau-\alpha}}}}{(\tau-\alpha)^{1/4}\,(t'-\tau)}\,u(\tau-\alpha)\,d\tau\,.$$

For Keller's expression in Eq. (133)

$$(148)\qquad F(s) = \bar{A}\,s^{1/3}\,e^{-[\alpha s+\bar{\beta}s^{1/3}]} = \frac{\bar{A}\,s\,e^{-[\alpha s+\bar{\beta}s^{1/3}]}}{s^{2/3}}\,.$$

From Eq. (142) and the differentiation formula

$$(149)\qquad \mathcal{L}^{-1}\left[\bar{A}\, s^{1/3}\, e^{-[\alpha s + \bar{\beta} s^{1/3}]}\right]$$

$$= -\bar{A}\left\{\frac{\sqrt{\bar{\beta}}}{\pi\sqrt{t'-\alpha}} K_{\frac{1}{3}}'\left(\frac{2\bar{\beta}^{3/2}}{3^{3/2}\sqrt{t'-\alpha}}\right) - \frac{\sqrt{\bar{\beta}}}{2\pi(t'-\alpha)^{3/2}} K_{\frac{1}{3}}\left(\frac{2\bar{\beta}^{3/2}}{3^{3/2}\sqrt{t'-\alpha}}\right)\right\}$$

$$u(t'-\alpha),$$

where the prime indicates differentiation with respect to t'. The exact expression in the time domain for the creeping wave predicted by Keller is

$$(150)\qquad F_I^{cw}(t') = \frac{A\sqrt{\bar{\beta}}}{\pi^2}\int_{-\infty}^{\infty}\left\{\frac{K_{\frac{1}{3}}'\left(\frac{2\bar{\beta}^{3/2}}{3^{3/2}\sqrt{\tau-\alpha}}\right)}{\sqrt{\tau-\alpha}} - \frac{K_{\frac{1}{3}}\left(\frac{2\bar{\beta}^{3/2}}{3^{3/2}\sqrt{\tau-\alpha}}\right)}{2(\tau-\alpha)^{3/2}}\right\}\frac{u(\tau-\alpha)}{(t'-\tau)}\,d\tau\ ,$$

and for $t'-\alpha$ small,

$$(151)\qquad F_I^{cw}(t') \simeq \frac{\bar{A}\, 3^{3/4}}{2\pi\sqrt{\pi}\,\bar{\beta}^{1/4}}\int_{-\infty}^{\infty}\left\{\frac{\beta^{3/2}}{3^{3/2}(\tau-\alpha)^{7/4}} - \frac{1}{4(\tau-\alpha)^{5/4}}\right\} e^{-\frac{2\beta^{3/2}}{3^{3/2}\sqrt{\tau-\alpha}}}\frac{u(\tau-\alpha)}{(t'-\tau)}\,d\tau\ .$$

For the results of Senior (Eq. (134)), F(s) assumes two forms

$$F_1(s) = \overline{\overline{A}}\, s^{1/3}\, e^{-[\alpha s + \overline{\beta} s^{1/3} - \gamma s^{1/3}]} \quad , \tag{152}$$

and

$$F_2(s) = \overline{\overline{B}}\, s^{-1/3}\, e^{-[\alpha s + \overline{\beta} s^{1/3} - \gamma s^{-1/3}]} \quad . \tag{153}$$

Unfortunately, the inverse transform of these functions can only be written in terms of an infinite series. Using Eq. (140), the creeping wave time domain response of the Senior result (Eq. (144)) can be written, but the explicit results are of little interest because of their complexity.

The noncausal nature of the impulse response waveforms predicted for the creeping wave on the sphere is demonstrated in Eqs. (146) and (150), and implicitly from a combination of Eqs. (152) and (153). This is also evident from Eq. (135) alone, once the causal nature of the inverse transform of the frequency-dependent function without the constant phase shift is demonstrated. It is further interesting to note that in the applications of the geometrical theory, i. e., Keller, and Kouyoumjian, this constant phase shift is included because of a caustic correction, and is not a part of the diffraction coefficient obtained from the solution of a canonical problem. However, Senior's expression for the creeping wave also includes the constant

phase shift and in this case results from simply an asymptotic high frequency expansion of the exact solution. In time domain terms, the noncausal nature is that of a network required to yield a $\pi/2$ radians phase shift at all frequencies. The impulse response of such a network would have a "precursor", and the network itself is nonphysical.

Before further comment, the time domain response waveforms predicted by certain of the asymptotic approximations will be calculated. This is done most simply for the results of Senior and Keller, using the Fourier synthesis procedure, since calculations of the frequency-dependent expressions at the requisite harmonics were available.* In both cases, two results are obtained; the causal waveform corresponding to removal of the $\pi/2$ radians phase shift, and the noncausal waveform corresponding to the complete expression. The waveforms for the causal case are shown in Fig. 49. Included in Fig. 49 are calculated results from the analytical expression in Eq. (149) with the simplification of the modified Hankel function for large arguments (Eq. (144)) employed. In Figs. 50 and 51, the corresponding noncausal results for the actual asymptotic high frequency expansions of Keller and

---

* Professor L. Peters, Jr. of The Ohio State University supplied calculated data from Senior's results. Professor E. M. Kennaugh had previously obtained calculated data from Keller's result and had also obtained a portion of the time domain results via Fourier synthesis.

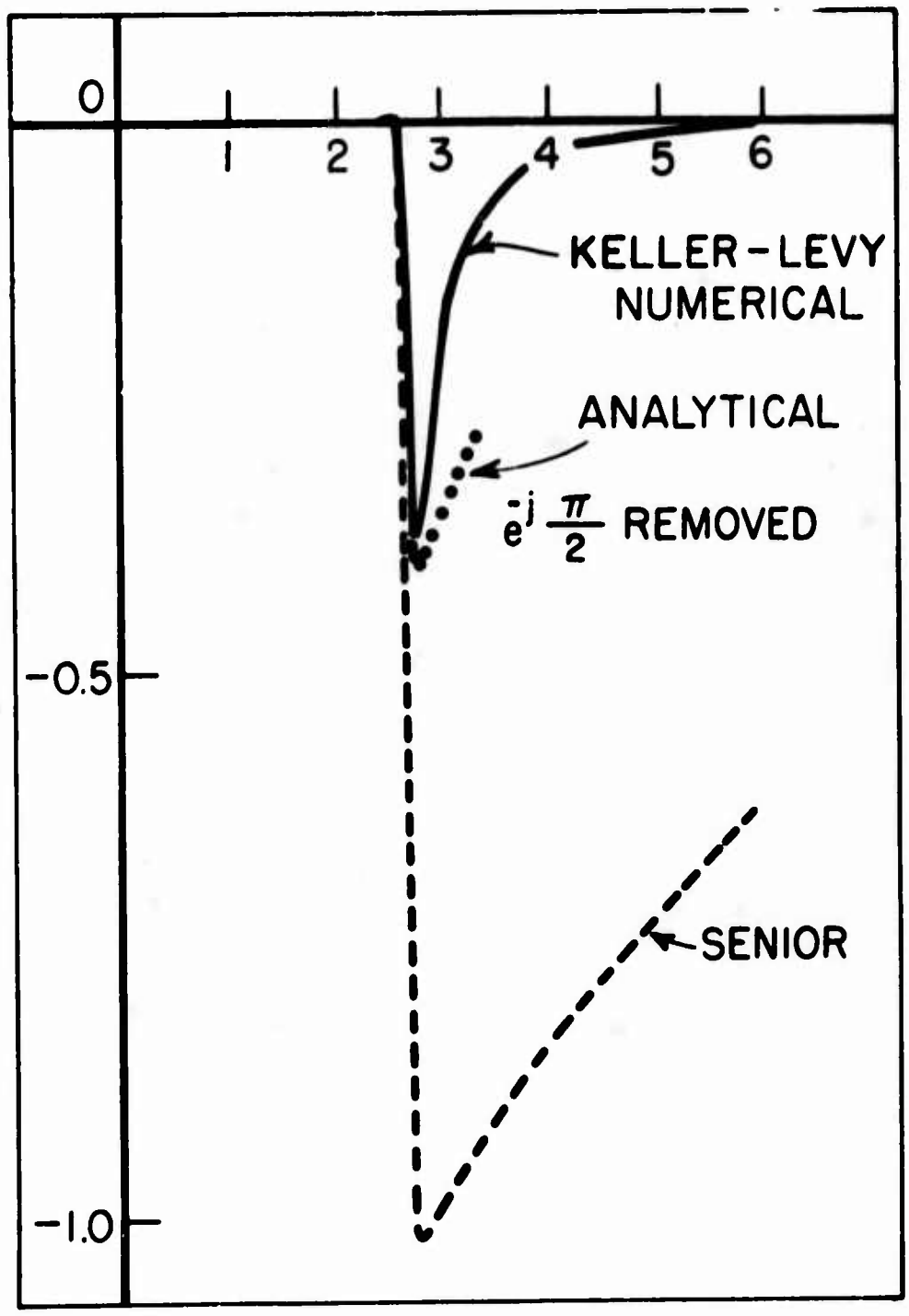

Fig. 49--Time dependent response waveforms predicted by Keller-Levy (solid) and Senior (dashed) asymptotic estimates of creeping wave on conducting sphere when $e^{-j\pi/2}$ phase factor removed. Backscatter.

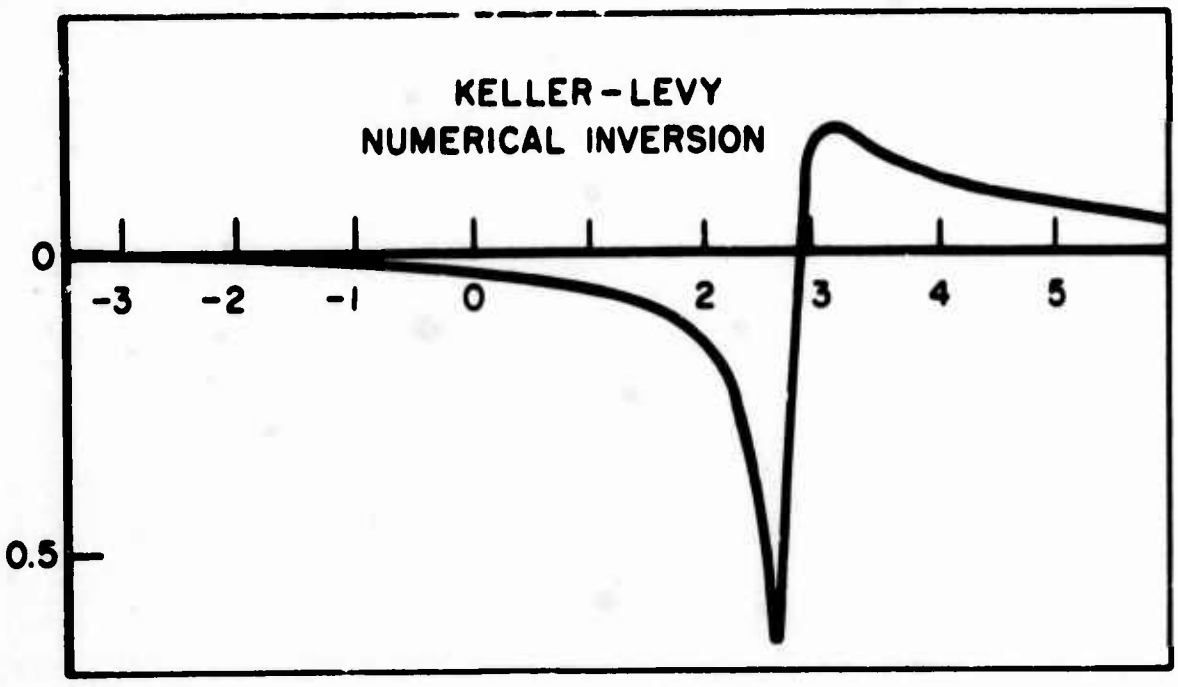

Fig. 50--Time-dependent response waveform predicted by Keller-Levy asymptotic estimate of creeping wave on conducting sphere, backscatter.

Senior respectively are shown. Aside from the demonstrated agreement of the analytical result for short time ($t'-(1+\pi/2)t_o$ small in Fig. 49), the significant result in these figures is that the constant phase shift of $\pi/2$ radians (which amounts to convolution with $1/t'$ in the time domain) has transformed the causal waveforms into noncausal ones in approximate agreement in character with the creeping wave peak shown in Fig. 47. It is apparent that the addition of the optical contributions to the noncausal response waveform in Fig. 51 will yield approximate agreement in form with the sphere impulse response waveform. This comparison is made in Fig. 52. Shown are

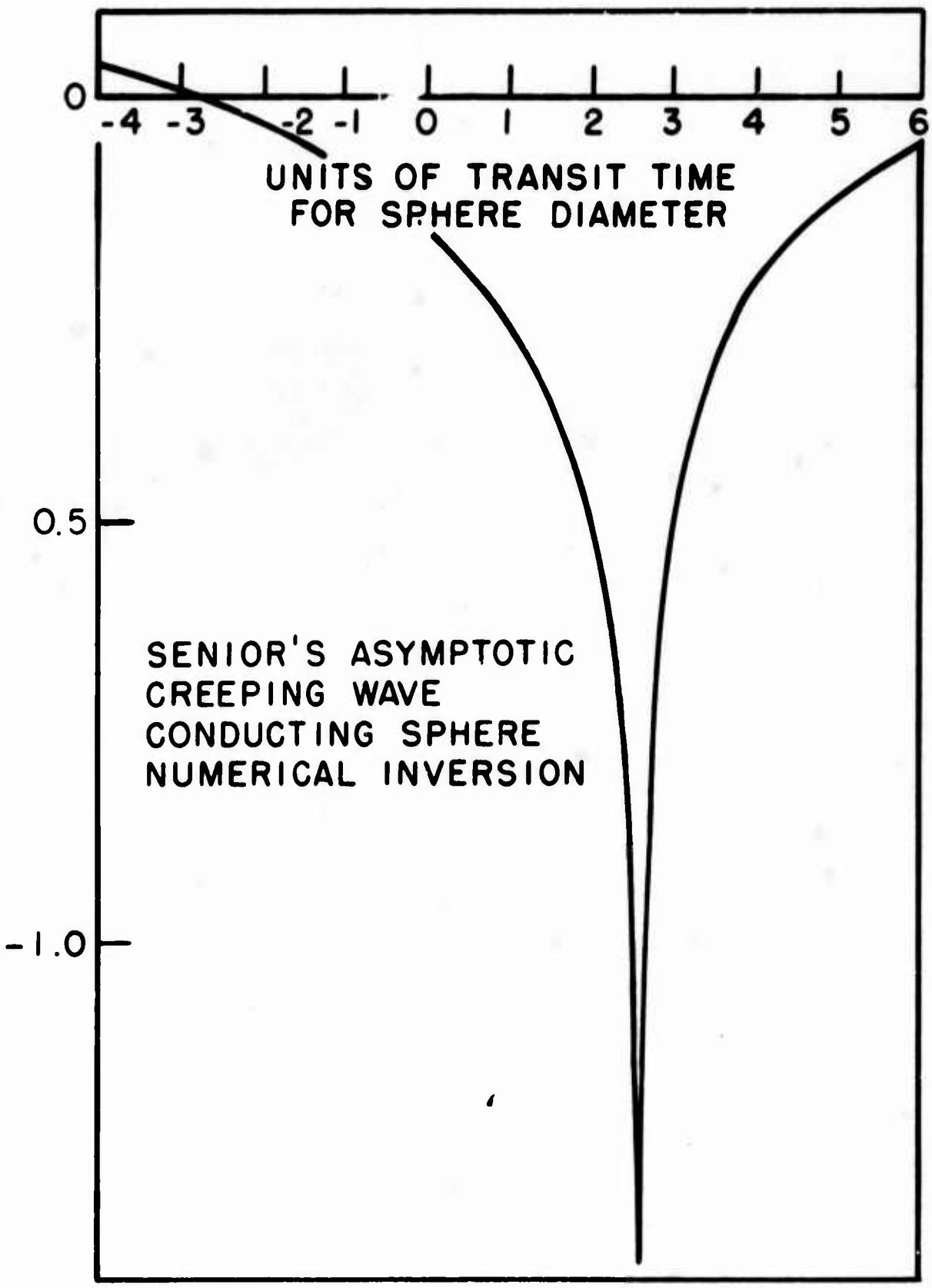

Fig. 51--Time-dependent response waveform predicted by Senior's asymptotic estimate of creeping wave on conducting sphere. Backscatter.

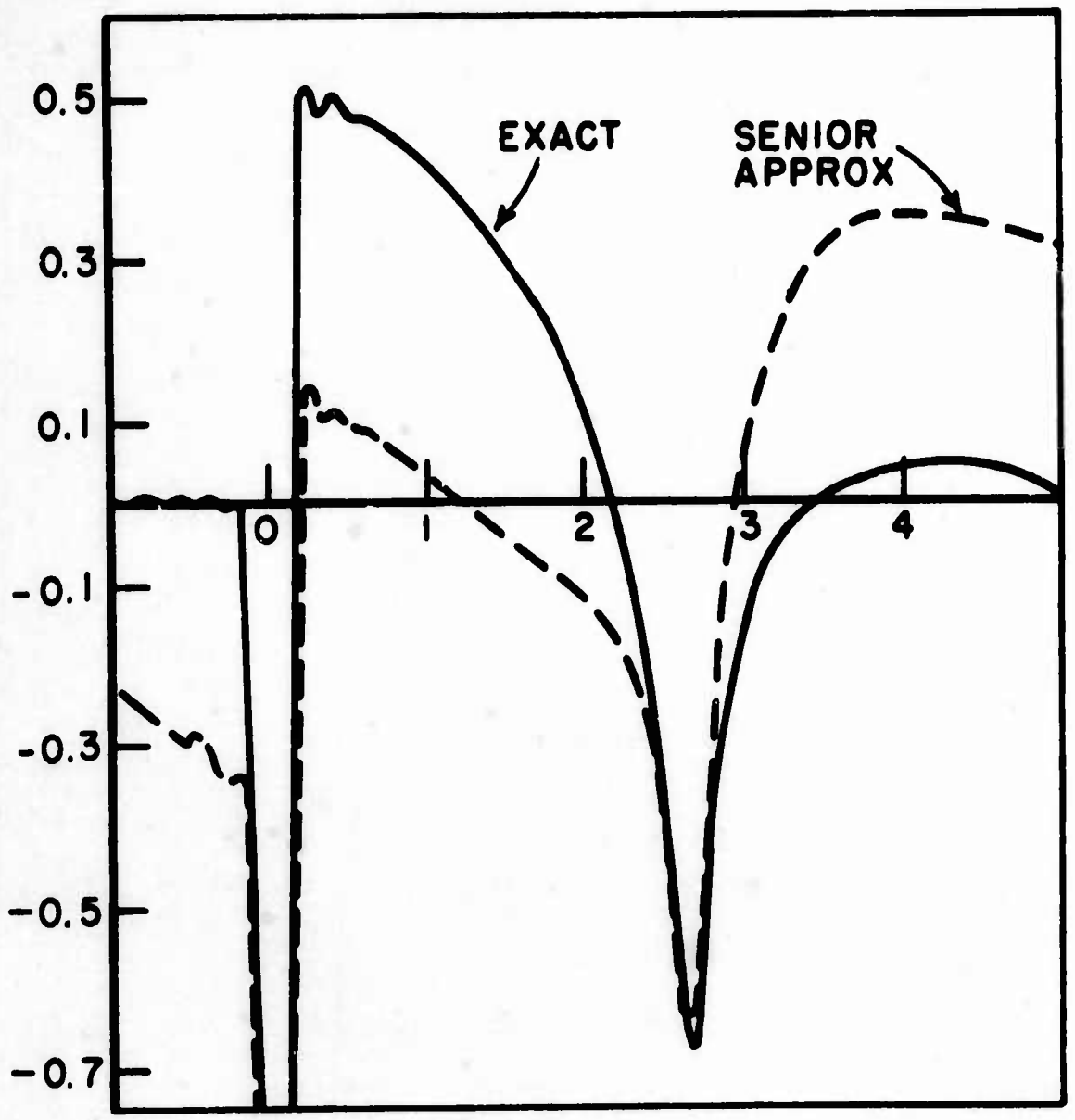

Fig. 52--Impulse response waveform of conducting sphere, backscatter. Solid, Fourier synthesis from Mie Series. Dashed, Fourier synthesis from Senior's creeping wave estimate plus optical terms.

the Fourier synthesis derived waveforms obtained from the exact solution, and from Senior's expression plus the optical terms. It is easily seen from Fig. 52 that the combination of Senior's creeping wave expression with the optical contributions yields a reasonable approximation in the neighborhood of the creeping wave peak to the sphere impulse response waveform.

In one sense, the results in this Appendix undoubtedly are a reiteration of what is already known, namely that asymptotic estimates of the creeping wave, when combined with the optical contributions, yield a fair estimate of the echo area of spheres and cylinders over a range of higher frequencies. From the time domain viewpoint, however, the results explain a paradox which had existed as to how the asymptotic estimates of the creeping wave with the addition of optical terms could possibly yield good cross section data in the resonance region for the sphere. The explanation lies in the noncausal nature of the predicted creeping wave waveform. That is, it was clear that if a response waveform beginning at $t' = (1 + \pi/2)\, t_0$ were added to the optical contributions (a negative delta function and a positive step function), the result would not be a good approximation for the impulse response waveform of the sphere. But the addition of a noncausal waveform can, as has been shown, yield a reasonable approximation.

The time dependent response waveforms predicted by high frequency asymptotic estimates of the creeping waves on spheres and circular cylinders have been demonstrated. For the circular cylinder a closed form expression for the waveform, holding for short times after the arrival of the diffracted front, was obtained. The complexity of the asymptotic expressions precludes such a result for the sphere. In this case a unique tool, the Fourier synthesis technique, was used to demonstrate the character of the response. This same approach can be used to resolve the question of the exact nature of the sphere response in the neighborhood of the secondary peak. That is, with the Fourier synthesis approach it is necessary to use many harmonics to secure a sufficiently narrow pulse width to approximately resolve a jump discontinuity or a cusp type behavior of the waveform. Using the Mie series, it is not economically feasible to secure the requisite harmonics. However, the asymptotic estimates are easily calculated and it is a relatively simple matter to secure the necessary data. Some preliminary work on this question has been done, utilizing up to 1800 harmonics with a fundamental corresponding to a sphere circumference of 0.1 wavelengths. These results represent an order of magnitude decrease in the narrowest pulse width obtained using Mie series calculations. These results are incomplete and will not be detailed. However, it

was concluded that the secondary peak is finite (a previously unsolved question) and that an additional order of magnitude reduction of the pulse width would permit the magnitude of the peak to be determined as well as the slope of the waveform on either side of the peak. It is clear therefore that asymptotic high frequency estimates of diffracted waves can be utilized in the time domain to resolve questions concerning the character of the response waveform at times corresponding to the arrival of the diffracted front. The Fourier synthesis procedure is an indispensible tool in this case since many of the asymptotic estimates are not amenable to an analytical treatment. However, as a device for "understanding" the scattering mechanism of an object, those asymptotic estimates which employ a nonphysical model and predict a noncausal waveform leave a great deal to be desired. For the specific case of the sphere, both time and frequency domain results demonstrate that the estimate of the energy arriving via creeping wave paths is correct. But the interpretation that these paths are confined to great circles is incorrect. Unless one is willing to accept group velocities for the diffracted fields which are greater than the speed of light, the near time build-up of the creeping wave peak can only be explained on the basis of nongreat circle or non-geodesic paths. Note that in terms of geometry, the difference between the cylinder and sphere is that there are no possible shorter

paths on the cylinder (i. e. , shorter than the cylinder circumference) whereas such shorter paths do exist on the sphere. It is concluded therefore that the physical mechanism for creeping waves actually consists of propagation along nongeodesic as well as geodesic paths with the attenuation along the paths increasing with departure from the geodesic. It is suggested that an examination of the time-dependent currents on the shadow side of the sphere when it is illuminated by an incident impulsive wave will reveal the location and relative attenuation of these paths. Some evidence to support this has been found using calculations of the transient currents obtained by Kennaugh[53] . It is estimated that the additional calculations of Mie series and corresponding Fourier synthesis procedure required to produce conclusive evidence of the nongeodesic paths as well as estimates of the attenuation would cost approximately $300. 00 on an IBM 7094 computer.

An alternative approach confined entirely to the frequency domain may also be possible. The asymptotic estimate of the creeping wave derived by Senior is not unique. This suggests that a different asymptotic expansion corresponding to a causal response waveform may be possible. Such an expansion, while of no greater utility than Senior's result in the frequency domain, would be of much greater

use in the time domain. From a philosophical viewpoint, the high-frequency asymptotic estimates of diffracted fields must be considered incomplete, insofar as the time domain picture is concerned, until such estimates can be interpreted in the time domain with a strictly causal relationship between the geometry of the object and specific locations in time of the response waveform. It is hoped that the results in this Appendix may provide the stimulus for future investigations in this direction.

REFERENCES

1. Corriher, H. A. Jr. and B. O. Byron, "A Bibliography of Articles on Radar Reflectivity and Related Subjects: 1957-1964," IEEE Proceedings, Vol. 53, No. 8, August 1965, pp. 1025-1064.

2. Garbacz, R. J., "Modal Expansions for Resonance Scattering Phenomena," IEEE Proceedings, Vol. 53, No. 8, August 1965, pp. 856-863.

3. Kennaugh, E. M. and R. L. Cosgriff, "The Use of Impulse Response in Electromagnetic Scattering Problems," IRE National Convention Record, Part I, 1958, pp. 72-77.

4. Final Engineering Report, "Problems in Electromagnetic Scattering Analysis," Report 1073-4, 1 January 1961, ElectroScience Laboratory, The Ohio State University Research Foundation; prepared under Contract AF 19(604)-6157 with Air Force Cambridge Research Laboratories, L. G. Hanscom Field, Bedford, Massachusetts. AD 255 839

5. Kennaugh, E. M., "The Scattering of Short Electromagnetic Pulses by a Conducting Sphere," IRE Proceedings, Vol. 49, No. 1, January 1961.

6. Moffatt, D. L., "Low Radar Cross Sections, The Cone-Sphere," Report 1223-5, 15 May 1962, ElectroScience Laboratory, The Ohio State University Research Foundation; prepared under Contract AF 33(616)-8039 with Aeronautical Systems Division, Wright-Patterson Air Force Base, Ohio. AD 283 338

7. Kennaugh, E. M. and D. L. Moffatt, "On the Axial Echo Area of the Cone Sphere Shape," IRE Proceedings (Correspondence), Vol. 50, No. 2, February 1962, p. 199.

8. Kennaugh, E. M. and D. L. Moffatt, "Radar Cross Section of a Cone Sphere," IRE Proceedings (Correspondence), Vol. 52, No. 1, January 1963, pp. 231-232.

9. Kennaugh, E. M. and D. L. Moffatt, "The Axial Echo Area of a Perfectly Conducting Prolate Spheroid," Report 1774-1, 15 June 1964, ElectroScience Laboratory, The Ohio State University Research Foundation; prepared under Contract AF 33(615)-1318, Research and Technology Division, Wright-Patterson Air Force Base, Ohio. AD 446 398

10. Moffatt, D. L. and E. M. Kennaugh, "Axial Echo Area of the Prolate Spheroid," IEEE Proceedings, Vol. 52, No. 10, October 1964, pp. 1252-1253.

11. Moffatt, D. L. and E. M. Kennaugh, "The Axial Echo Area of a Perfectly Conducting Prolate Spheroid," IEEE Transactions on Antennas and Propagation, Vol. AP-13, May 1965, pp. 401-409.

12. Moffatt, D. L., "Electromagnetic Scattering by a Perfectly Conducting Prolate Spheroid," Report 1774-11, 10 September 1965, ElectroScience Laboratory, The Ohio State University Research Foundation; prepared under Contract AF 33(615)-1318, Research and Technology Division, Wright-Patterson Air Force Base, Ohio. AD 476 246

13. Kennaugh, E. M. and D. L. Moffatt, "Transient and Impulse Response Approximations," IEEE Proceedings, Vol. 53, No. 8, August 1965, pp. 893-901.

14. Kennaugh, E. M. and D. L. Moffatt, "The Use of Transient and Impulse Response Approximations in Electromagnetic Scattering Problems," Report 1793-3, 28 February 1966, ElectroScience Laboratory, The Ohio State University Research Foundation; prepared under Contract AF

19(628)-4002, Air Force Cambridge Research Laboratories, L. G. Hanscom Field, Bedford, Massachusetts. AD 634 297

15. Makhoul, J. I., "Contour Plots for the Diffraction of a Pulse by a Wedge," Radio Science, Vol. 1 (New Series), No. 5, May 1966, pp. 609-613.

16. Stickler, D. C., "Integral Representation for Maxwell's Equations with Arbitrary Dependence," IEE Proceedings, Vo. 114, No. 1, January 1967, pp. 169-171.

17. Betten, J. R., "A Frequency Domain and S-Plane Analysis of Reflecting Objects," Ph. D. Dissertation, Iowa State University of Science and Technology, Ames, Iowa, 1962.

18. Brown, W. P. Jr., "A Theoretical Study of the Scattering of Electromagnetic Impulses by Finite Obstacles," Antenna Laboratory, California Institute of Technology, Pasadena, California, Technical Report 28, June 1962. AD 282 745

19. Barabanenkov, Yu N., "Scattering of Electromagnetic Delta Pulses by Ideally Conducting Bodies of Finite Dimensions," Radiotekhonika i Elektronika (USSR), Vol. 8, June 1963, pp. 1069-1071. C. C. Translation.

20. Papoulis, A., The Fourier Integral and Its Applications, McGraw-Hill Book Co., Inc., New York, 1962.

21. Stevenson, A. F., "Electromagnetic Scattering by a Spheroid in the Third Approximation," Journal of Applied Physics, Vol. 24, No. 9, September 1953.

22. Van Der Pol, Balth, and H. Bremmer, Operational Calculus Based on the Two-Sided Laplace Integral, Cambridge University Press, London, 1955, pp. 121-123.

23. Kennaugh, E. M., "Interpretation of the Physical Optics Approximation in the Time Domain," Proceedings of Second Symposium on Ground Identification of Satellites, The Mitre Corporation, 2-4 October 1967.

24. Guillemin, E. A., Theory of Linear Physical Systems, John Wiley and Sons, Inc., New York, 1963.

25. Titchmarsh, E. C., The Theory of Functions, Oxford University Press, London, 1939.

26. Franks, L. E., "On the Use of Delay Lines as Network Elements," Ph. D. Dissertation, Stanford University, Palo Alto, California, 1957.

27. Richmond, J. H., "Digital Computer Solutions of the Integral Equations for Scattering Problems," Proceedings of the IEEE, Vol. 53, No. 8, August 1965, pp. 796-804.

28. Horowitz, I. M., Synthesis of Feedback Systems, Academic Press, New York, 1963, p. 661f.

29. Kautz, W. H., "Network Synthesis for Specified Transient Response," Research Laboratory of Electronics, Massachusetts Institute of Technology, Cambridge, Massachusetts, Technical Report No. 209, April 1952, pp. 31-41.

30. Kennaugh, E. M., D. L. Moffatt and R. C. Schafer, Final Report, "Research Into the Scattering of Electromagnetic Theory from Highly Conducting Bodies," Report 1793-4, 24 May 1967, ElectroScience Laboratory, The Ohio State University Research Foundation; prepared under Contract AF 19(628)-4002, Air Force Cambridge Research Laboratories, L. G. Hanscom Field, Bedford, Massachusetts. AD 657 356

31. Courant, R. and D. Hilbert, Methods of Mathematical Physics, Interscience Publishers Inc., New York, 1953, pp. 93-97.

32. Flammer, Carson, Spheroidal Wave Functions, Stanford University Press, Stanford, California, 1957.

33. Sleator, F. B., "Studies in Radar Cross Sections XLIX, Diffraction and Scattering by Regular Bodies. III: The Prolate Spheroid," Report AFCRL-64-138, February 1964, Radiation Laboratory, The University of Michigan, prepared under Contract AF 19(604)-6655, Air Force Cambridge Research Laboratories, L. G. Hanscom Field, Bedford, Massachusetts.

34. Andreason, M. G., "Scattering from Bodies of Revolution," IEEE Transactions on Antennas and Propagation, Vol. AP-13, March 1965, pp. 303-310.

35. Oshiro, F. K., "A Source Distribution Technique for the Solution of General Electromagnetic Scattering Problems," NOR-65-271, Phase 1 Report, Northrop Corporation, Norair Division, prepared under Contract AF 33(615)-3166, Air Force Avionics Laboratory, Wright-Patterson Air Force Base, Ohio, 13 October 1965.

36. Waterman, P. C., "Electromagnetic Scattering by Conducting Spheroids," The Mitre Corporation, prepared under Contract AF 19(628)-5165, Advanced Research Projects Agency, Project Defender, ARPA Order No. 596, February 10, 1967.

37. Schultz, F. V., "Scattering by a Prolate Spheroid," Report No. UMM-42, The University of Michigan Willow Run Research Center, March 1950.

38. Siegel, K. M., F. V. Schultz, B. H. Gere, and F. B. Sleator, "The Theoretical and Numerical Determination of the Radar Cross Section of a Prolate Spheroid," IRE Transactions, AP-4, No. 3, 1956, pp. 266-275.

39. Kennaugh, E. M., Unpublished notes.

40. Abramowitz, M. and L. A. Stegum, Handbook of Mathematical Functions with Formulas, Graphs, and Mathematical Tables, U. S. Department of Commerce, National Bureau of Standards, November 1964, p. 592.

41. Weston, V. H., "Pulse Return from a Sphere," IRE Trans. on Antennas and Propagation, Vol. AP-7, Special Supplement, December 1959.

42. Stevenson, A. F., "Electromagnetic Scattering by an Ellipsoid in the Third Approximation," Journal of Applied Physics, Vol. 24, No. 9, September 1953.

43. Kouyoumjian, R. G., "An Introduction to Geometrical Optics and the Geometrical Theory of Diffraction," Antenna and Scattering Theory: Recent Advances Short Course Notes, The Ohio State University, Columbus, Ohio 1966.

44. Peters, L. Jr., "Modifications of Geometrical Theory of Diffraction for Non-Cylindrical Curved Surfaces," Report 1815-2, 5 March 1965, ElectroScience Laboratory, The Ohio State University Research Foundation; prepared under Subcontract No. 28-5041, Lockheed Missiles and Space Company, Sunnyvale, California.

45. Keller, J. B. and B. R. Levy, "Diffraction by a Spheroid," Research Report No. EM-130, New York University, Institute of Mathematical Sciences, Division of Electromagnetic Research, March 1959.

46. Senior, T. B. A. and R. F. Goodrich, "Scattering by a Sphere," IEE Proceedings, Vol. 111, No. 5, May 1964, pp. 907-916.

47. Friedlander, F. G., Sound Pulses, Cambridge Monographs on Mechanics and Applied Mathematics, Cambridge University Press, London, 1958, pp. 159-160.

48. Private communication with Professor R. G. Kouyoumjian, The Ohio State University, Columbus, Ohio.

49. Moffatt, D. L., op. cit.

50. Papoulis, A., op. cit., pp. 213-214.

51. Roberts, C. E. and H. Kaufman, Tables of Laplace Transforms, W. B. Saunders Company, Philadelphia, Pennsylvania, 1966, p. 249.

52. Stratton, J. A., Electromagnetic Theory, McGraw-Hill Book Co., Inc., New York, 1962, pp. 390-391.

53. Kennaugh, E. M., op. cit.

UNCLASSIFIED

Security Classification

DOCUMENT CONTROL DATA - R&D

(Security classification of title, body of abstract and indexing annotation must be entered when the overall report is classified)

1. ORIGINATING ACTIVITY *(Corporate author)*: ElectroScience Labc atory, Department of Electrical Engineering, The Ohio State University Research Foundation, Columbus, Ohio

2a. REPORT SECURITY CLASSIFICATION: Unclassified

2b. GROUP:

3. REPORT TITLE: INTERPRETATION AND APPLICATION OF TRANSIENT AND IMPULSE RESPONSE APPROXIMATIONS IN ELECTROMAGNETIC SCATTERING PROBLEMS

4. DESCRIPTIVE NOTES *(Type of report and inclusive dates)*: Technical Report

5. AUTHOR(S) *(Last name, first name, initial)*: Moffatt, David L.

6. REPORT DATE	7a. TOTAL NO. OF PAGES	7b. NO. OF REFS
27 March 1968	220	53

8a. CONTRACT OR GRANT NO.: F19628-67-C-0239

b. PROJECT NO.: 5635

c. TASK: 563502

d. Work Unit No. 56350201

9a. ORIGINATOR'S REPORT NUMBER(S): ElectroScience Laboratory 2415-1

9b. OTHER REPORT NO(S) *(Any other numbers that may be assigned this report)*: AFCRL-67-0690

10. AVAILABILITY/LIMITATION NOTICES

Distribution of this document is unlimited. It may be released to the Clearinghouse, Department of Commerce, for sale to the general public.

11. SUPPLEMENTARY NOTES

12. SPONSORING MILITARY ACTIVITY: Air Force Cambridge Research Laboratories (CRD) L. G. Hanscom Field, Bedford, Mass. 01730

13. ABSTRACT

A linear system analysis is applied to electromagnetic scattering problems. The relationship between the incident and scattered fields is reduced to a one-dimensional linear system by suitable restrictions, and modeled as a linear two-port with time-invariant parameters. The two-port is characterized by a real, time-dependent impulse response function and a transform-related complex, frequency-dependent phasor response. Two fundamental approaches for obtaining approximate solutions to electromagnetic scattering problems are seen. Estimates of either the frequency-dependent phasor response or the time-dependent impulse response can be attempted. The material in this study is concerned with the latter approach.

The concept of impulse and transient response approximations in electromagnetic scattering problems and the general properties of such waveforms are reviewed in Chapter I. It is demonstrated that the impulse and transient response waveforms provide a primary conceptual model for electromagnetic scattering which permits the integration of all existing frequency data, calculated or measured, and is simple in form. The model is directly related to the geometrical and physical properties of the scattering object; does not change drastically for small perturbations of parameters; and can be used to predict the response of the object to any type of incident plane wave. Analytical and experimental methods for obtaining estimates of the response waveforms are discussed, and a systematic procedure for securing such estimates is suggested.

Estimates of the impulse and transient response waveforms of a perfectly conducting prolate spheroid are obtained in Chapter II. Two results are derived. The first is restricted to axial incidence and utilizes the geometrical similarity of the sphere and spheroid to obtain the response waveforms of the spheroid. The second result is for arbitrary orientation of the spheroid and arbitrary linear polarization of the incident field. Calculations from both results are compared with measured data on a 2:1 axial ratio spheroid.

Derivation of the response waveforms of the prolate spheroid target requires, as input data, the Rayleigh scattering coefficient of the target. The Rayleigh coefficients of prolate and oblate spheroids for arbitrary orientation, axial ratio, and material properties, and for arbitrary linear polarization of the incident field are given in Appendix I. Time domain interpretations of high frequency asymptotic estimates of the creeping wave on conducting spheres and cylinders are considered in Appendix II. The non-causal nature of creeping wave estimates for the sphere is noted and suggestions for obtaining a causal response waveform are made.

DD FORM 1 JAN 64 1473

UNCLASSIFIED

Security Classification

UNCLASSIFIED

Security Classification

14. KEY WORDS	LINK A		LINK B		LINK C	
	ROLE	WT	ROLE	WT	ROLE	WT
Electromagnetic Scattering Transient Impulse response Prolate spheroid						

INSTRUCTIONS

1. ORIGINATING ACTIVITY: Enter the name and address of the contractor, subcontractor, grantee, Department of Defense activity or other organization *(corporate author)* issuing the report.

2*a*. REPORT SECURITY CLASSIFICATION: Enter the overall security classification of the report. Indicate whether "Restricted Data" is included. Marking is to be in accordance with appropriate security regulations.

2*b*. GROUP: Automatic downgrading is specified in DoD Directive 5200.10 and Armed Forces Industrial Manual. Enter the group number. Also, when applicable, show that optional markings have been used for Group 3 and Group 4 as authorized.

3. REPORT TITLE: Enter the complete report title in all capital letters. Titles in all cases should be unclassified. If a meaningful title cannot be selected without classification, show title classification in all capitals in parenthesis immediately following the title.

4. DESCRIPTIVE NOTES: If appropriate, enter the type of report, e.g., interim, progress, summary, annual, or final. Give the inclusive dates when a specific reporting period is covered.

5. AUTHOR(S): Enter the name(s) of author(s) as shown on or in the report. Enter last name, first name, middle initial. If military, show rank and branch of service. The name of the principal author is an absolute minimum requirement.

6. REPORT DATE: Enter the date of the report as day, month, year, or month, year. If more than one date appears on the report, use date of publication.

7*a*. TOTAL NUMBER OF PAGES: The total page count should follow normal pagination procedures, i.e., enter the number of pages containing information.

7*b*. NUMBER OF REFERENCES: Enter the total number of references cited in the report.

8*a*. CONTRACT OR GRANT NUMBER: If appropriate, enter the applicable number of the contract or grant under which the report was written.

8*b*, 8*c*, & 8*d*. PROJECT NUMBER: Enter the appropriate military department identification, such as project number, subproject number, system numbers, task number, etc.

9*a*. ORIGINATOR'S REPORT NUMBER(S): Enter the official report number by which the document will be identified and controlled by the originating activity. This number must be unique to this report.

9*b*. OTHER REPORT NUMBER(S): If the report has been assigned any other report numbers *(either by the originator or by the sponsor)*, also enter this number(s).

10. AVAILABILITY/LIMITATION NOTICES: Enter any limitations on further dissemination of the report, other than those imposed by security classification, using standard statements such as:

(1) "Qualified requesters may obtain copies of this report from DDC."

(2) "Foreign announcement and dissemination of this report by DDC is not authorized."

(3) "U. S. Government agencies may obtain copies of this report directly from DDC. Other qualified DDC users shall request through

_____."

(4) "U. S. military agencies may obtain copies of this report directly from DDC. Other qualified users shall request through

_____."

(5) "All distribution of this report is controlled. Qualified DDC users shall request through

_____."

If the report has been furnished to the Office of Technical Services, Department of Commerce, for sale to the public, indicate this fact and enter the price, if known.

11. SUPPLEMENTARY NOTES: Use for additional explanatory notes.

12. SPONSORING MILITARY ACTIVITY: Enter the name of the departmental project office or laboratory sponsoring *(paying for)* the research and development. Include address.

13. ABSTRACT: Enter an abstract giving a brief and factual summary of the document indicative of the report, even though it may also appear elsewhere in the body of the technical report. If additional space is required, a continuation sheet shall be attached.

It is highly desirable that the abstract of classified reports be unclassified. Each paragraph of the abstract shall end with an indication of the military security classification of the information in the paragraph, represented as *(TS)*, *(S)*, *(C)*, or *(U)*.

There is no limitation on the length of the abstract. However, the suggested length is from 150 to 225 words.

14. KEY WORDS: Key words are technically meaningful terms or short phrases that characterize a report and may be used as index entries for cataloging the report. Key words must be selected so that no security classification is required. Identifiers, such as equipment model designation, trade name, military project code name, geographic location, may be used as key words but will be followed by an indication of technical context. The assignment of links, rules, and weights is optional.

UNCLASSIFIED

Security Classification